9-1-2021

STRUCTURAL ANALYSIS OF PROTEIN THERAPEUTICS BY HYDROGEN DEUTERIUM EXCHANGE AND COVALENT LABELING MASS SPECTROMETRY

Catherine Yvonne Tremblay
University of Massachusetts Amherst

STRUCTURAL ANALYSIS OF PROTEIN THERAPEUTICS BY HYDROGEN DEUTERIUM EXCHANGE AND COVALENT LABELING MASS SPECTROMETRY

Catherine Yvonne Tremblay

STRUCTURAL ANALYSIS OF PROTEIN THERAPEUTICS BY HYDROGEN DEUTERIUM EXCHANGE AND COVALENT LABELING MASS SPECTROMETRY

A Dissertation Presented

by

CATHERINE TREMBLAY

Submitted to the Graduate School of the
University of Massachusetts Amherst in partial fulfillment
of the requirements for the degree of

DOCTOR OF PHILOSOPHY

September 2021

Department of Chemistry

STRUCTURAL ANALYSIS OF PROTEIN THERAPEUTICS BY HYDROGEN DEUTERIUM EXCHANGE AND COVALENT LABELING MASS SPECTROMETRY

A Dissertation Presented

by

CATHERINE TREMBLAY

Approved as to style and content by:

_____
Prof. Richard W. Vachet, Chair

_____
Prof. Igor A. Kaltashov, Member

_____
Prof. Ricardo Metz, Member

_____
Prof. Stephen J. Eyles, Outside Member
Department of Biochemistry & Molecular Biology

_____
Prof. Ricardo Metz, Department Head
Chemistry

ACKNOWLEDGEMENTS

Completing a PhD is not an easy task. There are times when you feel hopeless, defeated, and like you will never get where you are going. The old adage “it takes a village” comes to mind. I would not be where I am today if it were not for the incredible support system I have behind me. If there are any future students reading this, the advice I would give is to lean on your support systems, those who love you want you to succeed.

First and foremost, I want to acknowledge the most fundamental person to this degree, Prof. Richard Vachet. After my visit weekend to UMass, I knew that the Vachet lab was the lab I wanted to join. I found the way Richard described the research his lab did to be approachable and unassuming. Throughout my graduate career Richard has been nothing but supportive, patient, encouraging, and kind. He is not only a brilliant scientist, but also a brilliant mentor. He wants nothing but success for his students and recognizes that the definition of “success” is as unique as each student is. I cannot thank him enough for his guidance throughout my PhD journey and feel incredibly lucky to have had such an incredible PI.

I also thank my committee members, Prof. Stephen Eyles, Prof. Ricardo Metz, and Prof. Igor Kaltashov. Their perspective and input from my early years of prospectus to the later years of my data defense has always been appreciated. I must acknowledge a question Prof. Metz asked during my prospectus of “I know mass spec is the best technique ever, but have you considered a different method?” and I am sorry to say, after 5 years of study, I still think mass spectrometry is the best

I would also like to thank Prof. Steve Eyles, beyond just serving on my committee. He has been my go-to person for all things mass spec related. He has endless knowledge on how to troubleshoot every instrument in the IALS MS core facility, how to run every piece of data analysis software, and the driest humor of any one I have ever met. I am incredible grateful for the training he has given me throughout my time here, and grateful he never kicked me out of the MS core for breaking too many things.

Additionally, I am grateful for every single Vachet lab member, past and present - Nick, Gokhan, Alyssa, MAC, Tyler, Bo, Meizhe, Tianying, Kristen, Blaise, Kong, Laura, Xiao, Catherine, Stacey, Zack, Dheeraj, Jack, Pablo, Ping, Akaansha, and Max. Every single one of these people contributed to a sense of community and inclusion within the Vachet lab and made the lab a fun place to be. My research specifically would not be anything without Kong, Zack, Stacey, and Xiao. I would have no data to show without the conversations, effort, and time of these four brilliant people. I also thank Ellen who has always been helpful in the skill where I fall short, logistics!

While the Vachet lab is instrumental in my success as a scientist, a would be remiss if I did not acknowledge the rest of the 3rd floor of LSL, and specifically Peter Chien's lab. Every lab on the third floor is welcoming, supportive, and willing to help you find that one chemical you need but your lab is out of. Specially I'd like to thank Nate, Justyne, and Samar in the Chien lab as well as Wes, Afua, and Nicole in the Serio lab. I would also like to acknowledge the chemistry staff that keep the department running, Bob and Ryan, JMS, and Vicki among everyone else. Additionally, I would like to acknowledge the coworkers from my past who continued to support me throughout my

graduate career and helped me on my way to my “adult” career! Those people are Jim Murphy, Mike Fogwill, and Joe Michenzi.

I would like to thank every friend I have made throughout my time in graduate school, and if I listed them all this document would never end. Graduate school can be an incredibly isolating experience, and I have been blessed to create lasting friendships with a number of graduate students I have met during my time here. I have grown friendships with graduate students from a variety of departments ranging from physics, to MCB, to chemical engineering. I would like to thank Scott and Lindley for always being there when I needed them, Shoshie for always being willing to share a beer, Doug for always being there to talk philosophy, and Nat for always being there for a horror movie night.

In acknowledging the graduate student friendships I have made, that thank you goes hand in hand with a thank you to the location where these friendships were built; the Moan and Dove. Approximately 50% of this dissertation was written at this bar, and approximately 50% of my money was also spent at this bar. The Moan and Dove created a sense of community that is unparalleled to any place I have ever patroned before. I thank all of the bartenders I ran into during my time here, Scotti, Molly, Hannah, other Hannah, Nate, Jackson, and Dicap. The Moan and Dove is my happy place, my place to blow off steam, and my place to be productive when my lab desk is too distracting.

I recognize I would not have succeeded through graduate school if I did not have a number of support systems that are outside of academia. I thank my friends from my years in undergrad, Michelle, John, Erin, Pooja, and Andrew. I know you are always just a text away. I found a community in Connecticut that provided me an escape from the stress of graduate school. Through this community I met Svan and Gina, who have been

wonderful people to lean on. A huge thank you to Svan for our weekly phone calls where I get to vent about the “problem of the week”. Svan has always been a source of joy and laughter for me, and I am forever grateful for his patience.

There is one person I met during my time at UMass in particular that deserves a special thank you, and that person is my rock, my anchor, my partner in crime, Jeff. Jeff has been there for me whether it is to write python codes to help process my data, to cook me dinner when I was too busy with my data defense to feed myself, or to support me in every way a person possibly could. Jeff has been my person throughout my time here, and I genuinely do not know how I would have made it through grad school without him. I am forever grateful for his patience, comfort, and love. It is here I will also acknowledge my perfect cat, Newton, who has brought me immense joy and comfort. He somehow knows when I need extra attention. I would highly recommend every graduate student get a cat.

I also have the biggest support system a person could ask for in my hometown in Exeter New Hampshire. I must thank Deb, Mark, Ginny, James, Rachel, and Rich, for their unwavering support for me as if I was their own daughter. I am so incredibly lucky to have such a large group of people who are cheering me on.

Finally, I need to thank my family. This is not a short list, and I recognize that my acknowledgements are getting long. Thank you to Auntie Di, Uncle Jack, Auntie Shell, Cassandra, Harrison, Uncle Bruce, Beth, Brian, Memo, Brittany, Uncle Jim, and Aunt Patty. A special shout out to Mary for being my biggest cheer leader and celebrating my accomplishments as if they were her own. Thank you to Memere and Pepere for the games of cribbage I got to beat you at while I was procrastinating on data analysis. Thank

you to Choo Choo and Chug Chug for your unconditional support. Choo Choo, you may no longer be here physically, but I know your spirit lives on, and you are enjoying one more whoopie pie while you watch me defend my PhD.

Lastly, I need to thank my Mom, Dad, Elizabeth, Jon, and Christopher. My parents deserve the biggest thank you of them all. When I was younger my dad gave me the advice “stay in school as long as you can” and I took that to heart. Thank you for supporting me emotionally, financially, mentally, and physically. I love you and cannot thank you enough for your unconditional love everything you have done for me to help me get to this point.

ABSTRACT

STRUCTURAL ANALYSIS OF PROTEIN THERAPEUTICS BY HYDROGEN DEUTERIUM EXCHANGE AND COVALENT LABELING MASS SPECTROMETRY

SEPTEMBER 2021

CATHERINE Y. TREMBLAY

B.Sc. NORTHEASTERN UNIVERSITY

Ph.D. UNIVERSITY OF MASSACHUSETTS AMHERST

Directed by: Professor Richard W. Vachet

This dissertation focuses on the use of mass spectrometry (MS) to study therapeutic protein higher order structure (HOS) by encoding the structure into the mass of the protein. As therapeutic proteins become more common in the pharmaceutical industry, the need for methods that quickly and accurately determine their HOS has grown. The two methods applied here are hydrogen deuterium exchange (HDX) MS and diethylpyrocarbonate (DEPC) covalent labeling (CL) MS. We demonstrate how these two methods provide complementary, and sometimes synergistic, information about protein HOS. HDX/MS reports on both changes in solvent exposure and changes in protein dynamics, and as a result it can often lead to ambiguous results. DEPC-CL/MS can be used to clarify ambiguous HDX/MS results as a result of its relatively slow (sec-min) intrinsic reaction rate. DEPC-CL/MS does not detect protein dynamics that are

measured by HDX/MS. Thus, it can indicate which HDX decreases are a result of loss of solvent exposure and which are a result of a loss of protein dynamics. Additionally, HDX/MS and DEPC-CL/MS are complementary methods, as HDX reports on backbone dynamics and solvent exposure providing peptide level resolution, while DEPC-CL/MS reports on side chain solvent exposure and microenvironment at the residue level.

In my work, I demonstrate that HDX/MS in parallel with DEPC-CL/MS can provide complementary HOS information about heat stressed monoclonal antibodies (mAbs). Using heat stressed rituximab as a model system, the two methods are used together to provide site-specific information about subtle conformational changes that are undetectable by traditional techniques. DEPC-CL/MS is more sensitive to subtle HOS structural changes occurring at low heat stress while at high heat stress we find that the two methods provide complementary information.

To further exemplify the complementarity between HDX/MS and DEPC-CL/MS, the methods are used to map the epitope in the antigen of a well characterized antibody-antigen system. Using the model system TNFα in complex with a variety of TNFα specific mAbs, we find that DEPC-CL/MS can reveal accurate information about epitopes and subtle structural changes away from epitopes. Moreover, we demonstrate that when HDX/MS is used in parallel with DEPC-CL/MS to study the HOS structural changes of TNFα upon antibody binding, DEPC-CL/MS can clarify ambiguous HDX results. DEPC-CL/MS can help pinpoint which HDX decreases are due to epitope binding and which decreases are due to TNFα stabilization. Our work highlights the effectiveness of these two methods together to study protein systems that are difficult to study by other methods.

TABLE OF CONTENTS

Page

LIST OF TABLES

Table Page

LIST OF FIGURES

CHAPTER 1

1. INTRODUCTION

1.1. Monoclonal Antibody Protein Therapeutics

Antibody based therapeutics are the fastest and largest growing class of protein therapeutics.[1] Since their development as therapeutics in 1980, monoclonal antibodies (mAb) have achieved large clinical and commercial success with over 400 mAbs in clinical development.[1–7] The success of mAbs can be attributed to their superior selectivity, providing substantial advantages over small molecules for treating serious diseases, such as cancer or autoimmune diseases.[3,7–9] It is theoretically possible to develop a mAb therapeutic for any antigen with limited risk of off-target side effects as a result of their extremely high selectivity.[1,2] In fact, epitope mapping, or determining the specific region of the antigen that is recognized by the antibody, is one of the most essential and challenging tasks in the development of novel mAbs. Additionally, unlike small molecules which on average are <500Da, mAbs are large protein molecules (~150KDa) with complex higher order structure (HOS) that dictates function.[10] Unlike small drug molecules which can resist a wide range of storage conditions, due to their complex HOS, mAbs have a significant risk of structural perturbations caused by storage, handling, and transportation.[6,9] Changes in HOS can result in immunogenicity, decreased efficacy, aggregates, or other safety concerns. [11–14] Therefore, detection and characterization of HOS perturbations of mAbs is imperative to development and safety of therapeutic mAbs (**Figure 1.1**).

1.1.1. **Epitope Mapping**

Epitope mapping is one of the most important applications of HOS characterization of mAbs.[15] Epitope mapping is not only critical for the development of novel antibodies, but also for biosimilar development and determining the bioequivalence of a therapeutic.[5,16] Moreover, accurate determination of epitopes can also allow companies to patent different mAbs for the same antigen.[17] While epitope mapping is necessary for the development and patenting of protein therapeutics, vaccine design, and drug discovery it is, however, notoriously difficult.[15,18] Thus, robust techniques for epitope mapping are essential as they guide early protein therapeutic development.[15,17] Currently, high resolution techniques, such as X-ray crystallography, are used to accurately characterize the paratope/epitope binding site.[19] These methods however are not high throughput and have a number of technical limitations.

1.1.2. **Higher Order Structure and Antibody stability**

The HOS of a protein describes its secondary, tertiary, and quaternary structure, or three-dimensional shape of a biomolecule.[20] HOS dictates protein function therefore, the correct HOS of protein therapeutics are essential for therapeutic efficacy and safety. The HOS of mAbs can be perturbed as a result of storage, handling, and transportation.[21] Thus, developing methods to characterize HOS of mAbs quickly and accurately is valuable for the field of protein therapeutics. Additionally, methods for characterizing HOS are useful not only in detecting structural perturbations caused by storage or mishandling, but they may also be useful in determining lot to lot comparability of commercial therapeutics, biosimilarity of "generic versions" of mAbs, or bioequivalence.[22]

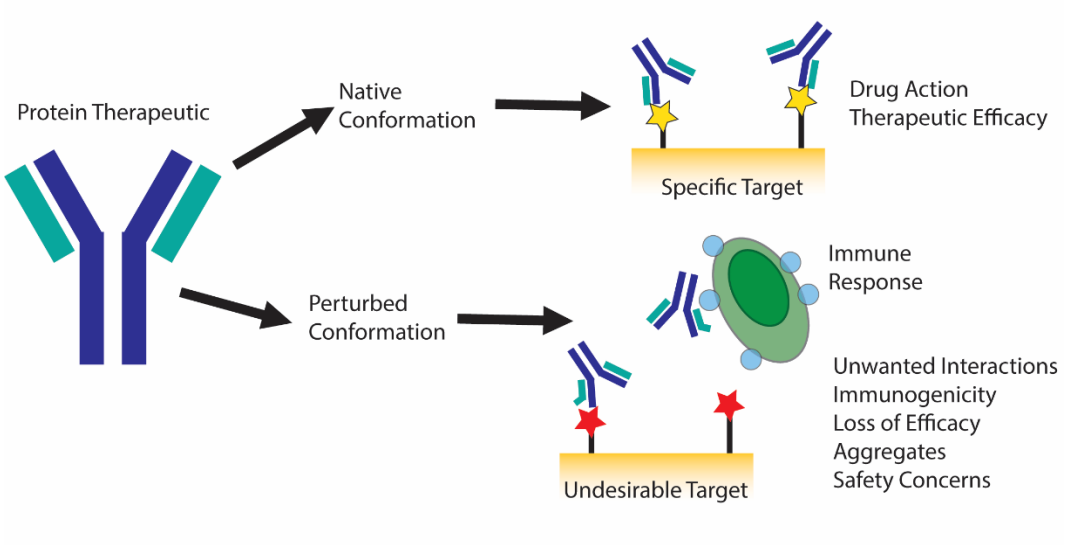

Figure 1.1: Cartoon representation of a monoclonal antibody therapeutic protein. The native conformation leads to the therapeutic effect and targeting of the specific antigen while a perturbed conformation can lead to undesirable results.

1.2. Mass Spectrometry Based Approaches for Protein Structural Characterization

Traditionally, the gold standard of studying protein HOS has been techniques such as nuclear magnetic resonance (NMR) or X-ray crystallography due to the high, atomic-level, resolution of these methods.[23–26] More recently cryo-electron microscopy (cryo-EM) has also emerged as an atomic level resolution tool for studying protein structure.[27,28] However, while X-ray crystallography, NMR, and cryo-EM provide the highest resolution of protein structure, they require a large sample volume, are often time and instrumentation intensive, require highly specialized personnel, and not every protein is compatible with these methods.[29] X-ray crystallography is limited to proteins that can crystalize while NMR is limited on the size of protein that is compatible with this methods. Mass spectrometry (MS) has emerged as a valuable tool for studying protein HOS as it provides moderate to high resolution information on protein structure while

circumventing the technical hurdles of X-ray crystallography, cryo-EM, and NMR.[19,29,30] As a result of the low sample consumption, high throughput, and high specificity and sensitivity of MS, this technique is becoming increasingly popular for studying protein HOS. Other methods to characterize protein structure, such as circular dichroism (CD), dynamic light scattering (DLS), differential scanning calorimetry (DSC), or fluorescence, may not consume high volumes of sample and are relatively quick, but these methods lack the resolution needed to detect subtle HOS changes.[12,20,31] MS is an ideal method for studying protein HOS because it provides a middle ground between the low resolution/high throughput methods, and the high resolution/low throughput methods.

To study protein HOS with MS the structure of the protein must be encoded into the mass of the protein. MS detects the mass-to-charge ratio (m/z) of gas phase ions and while conventional MS techniques, such as bottom up sequencing, can be used to determine primary structure and post-translational modifications, more advanced MS techniques are required to elucidate tertiary structural information.[20,32] Additionally, because MS measurements occur in the gas phase, it is necessary to acquire solution phase structure in an indirect way. There are three methods commonly used to encode structural based information into protein mass, hydrogen deuterium exchange (HDX), covalent labeling (CL), and chemical cross linking.[32,33] Often, methods that encode structure into the mass of the protein are referred to as protein footprinting.[34] This work will investigate HDX and CL in depth and explore the synergy between the two for studying therapeutic protein HOS. The two methods are complementary, and the structural information derived from each will produce a clear picture of HOS of protein therapeutics.

1.2.1. Covalent Labeling Mass Spectrometry

CL is a method in which a small molecule covalently modifies solvent exposed amino acid side chains on a protein.[35] Residues exposed to solvent will react with covalent labeling reagents while buried residues will not.[35] Once a protein is labeled, bottom-up mass spectrometry is typically used to detect a mass shift from covalently modified peptides (Figure 1.2). Tandem MS can then be used to get residue level resolution of modified residues. Labeling extent is calculated using the following equation:

$$\%\ labeling = \frac{\sum_{i=1}^{n}\sum_{z=1}^{m} A_{i,z}^{modi}}{\sum_{i=1}^{n}\sum_{z=1}^{m} A_{i,z}^{modi} + \sum_{i=1}^{n}\sum_{z=1}^{m} A_{i,z}^{unmodi}}$$

Equation 1.1

Where $A_{i,z}^{modi}$ is the peak area of DEPC-modified peptide that contains the modified residue of interest and possessed charge state (z) and $A_{i,z}^{unmodi}$ is the peak area of the DEPC-unmodified peptide that contains the residue of interest and possesses charge state (z).[36]

The majority of CL/MS experiments are comparative studies between two protein states (i.e. unbound protein vs. ligand bound protein, native protein vs. heat stressed protein). Changes in labeling extent from one state to the other will provide data about surface changes to the protein. For instance, differences in labeling extent between a native state and a ligand bound state will indicate the locations where a protein's surface structure has changed as a result of ligand binding.[35]

There are many different reagents that can be used for covalent labeling, some are amino acid specific, while others react with a wide range of amino acid residues. Non-specific labels often rely on reacting proteins with highly reactive radicals such as hydroxy radicals or trifluoromethyl radicals. Hydroxyl radical footprinting (HRF) has been explored in by a number of labs as a CL technique to probe therapeutic protein structure.[18,37,38] Hydroxyl radicals are non-specific and covalently label side chains based on solvent accessible surface area (SASA) on the microsecond time scale.[37,38] Specifically, the Gross group has developed a method of fast photochemical oxidation of proteins (FPOP), which is a type of HRF that utilizes a pulsed KrF laser to create hydroxyl radicals from hydrogen peroxide. This method has been uses to study antibody: antigen interactions, protein aggregation, and protein folding.[39–41] However, FPOP requires specialized facilities and equipment, and interpretation of the resulting data can be complex.[42]

Amino acid specific covalent labeling reagents react with specific residues based on that residue's chemistry. There are a variety of different reagents that can label a variety of specific residues such as dimethyl(2-hydroxy-5- nitrobenzyl)sulfonium bromide (HNSB) which specifically modifies tryptophan residues, 2,3-butanedione which reacts with arginine, or organic acid anhydrides which lead to lysine acetylation, to name a few. While the sequence coverage of residue specific labeling is low, there are a number of valuable applications for residue specific labels. For example, HNSB has been used to study the energy barrier for the pre-amyloid structural change of the protein B-2-microglobulin.[43] The earliest examples of covalent labeling for studying epitopes was lysine acetylation studying the epitope of lysozyme in the late 1990s.[44] This work will

focus on use of diethylpyrocarbonate (DEPC), a pseudo-specific labeling reagent that labels nucleophilic side chains and N-termini.[45,46]

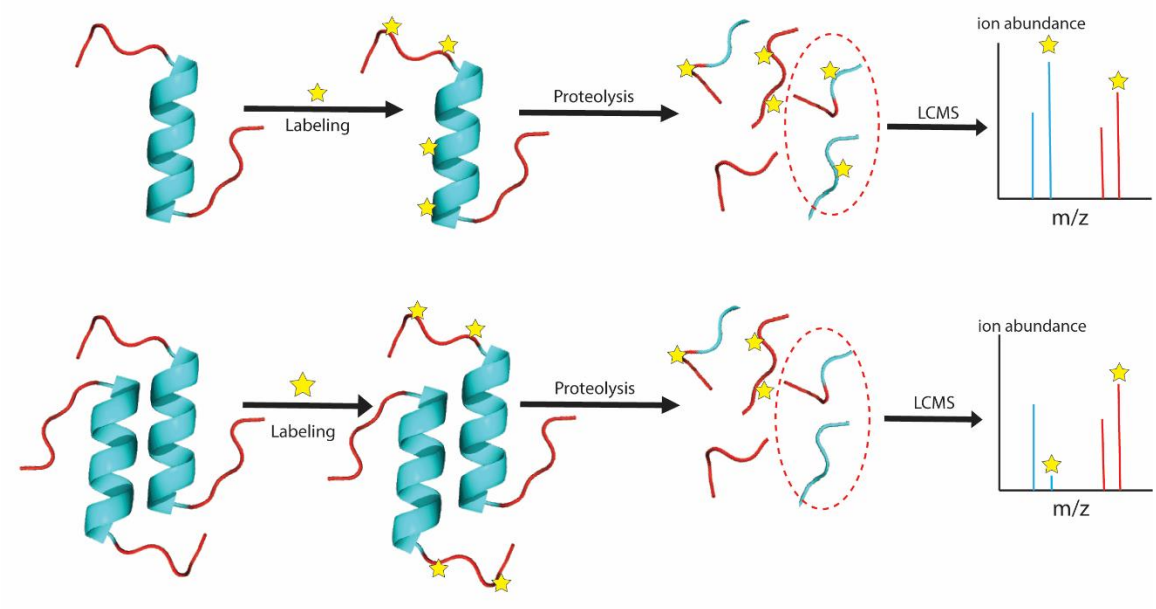

Figure 1.2: Cartoon representation of covalent labeling mechanism. A protein is reacted with the labeling reagent (yellow star) and exposed residues are modified. Protein is then digested, and LC/MS is preformed to detect peptides that have been modified. CL is typically completed in a comparative fashion, if the protein is in a dimer state, there are likely to be residues that are now not exposed to solvent and there for labeled to a lesser extent.

1.2.1.1. DEPC-CL

DEPC is a commercially available covalent labeling reagent that labels nucleophilic residues (histidine, lysine, serine, tyrosine, threonine) and the N-termini (**Figure 1.3**).[46] As a result of the variety of side chains that can react with DEPC, it can probe approximately 30% of an average proteins sequence, providing moderately high HOS resolution.[46] The labeling extents of strongly nucleophilic residues, histidine and lysine, is correlated to solvent accessible surface area (SASA), the more solvent exposed these residues are the higher the extent of labeling is expected to be. For weakly nucleophilic residues, serine, threonine, and tyrosine, labeling extent is dependent on

both solvent exposure and the three dimensional microenvironment surrounding these residues.[36] If ser, thr, or tyr residues are completely buried, they will not be labeled. However, the hydrophobicity of the microenvironment surrounding these residues created by the three-dimensional structure of the protein also influences labeling extent. Previous work has demonstrated that in free peptides, where these residues are entirely solvent exposed and lack 3D structure, the extent of labeling is minimal or nothing.[36] However, if these residues are in solvent accessible hydrophobic pockets, created by nearby hydrophobic residues, they are likely to be labeled. This is presumably due to the fact that DEPC itself is hydrophobic and minimally soluble in aqueous solutions, thus the local effective concentration of DEPC would be higher in hydrophobic pockets of a protein structure.[36]

While DEPC-CL is a relatively simple reaction, there are a number of considerations that must be made to ensure that the solution phase structure is successfully encoded into the mass by DEPC. For instance, DEPC itself could result in perturbation of HOS. Thus, it is important to ensure that the structural integrity of the protein is still intact. Previous work completed by Limipkirati et. al. has investigated this using dose response curves plotting DEPC concentration against reaction rate.[47] It was determined that one label per protein domain seemed to keep native structure intact for mAbs. This work also indicated that for thermally stable proteins it was possible for multiple labels to accurately report on native protein structure.

Further considerations for CL/MS is that the method is semi-quantitative. This is partially a result of the fact that labeling extent is determined using MS peak area as described in equation 1.1. MS peak area is affected by the ionization efficiency of the

analyte in question. Labeled and unlabeled peptides often have significantly different LC retention times, and thus are ionized with different aqueous:organic solvent ratios resulting in different ionization efficiencies. This means the resulting peak area is not perfectly comparable between the unlabeled and labeled peptides. Additionally, the DEPC label itself is known to alter ionization efficiency, thus even if the labeled and unlabeled peptide eluted at the same retention time, there would still be differences in peak area as a result of differences in ionization efficiency.

However, while there are a number of considerations to be made, DEPC is a useful reagent for studying a variety of protein systems. DEPC has been used to stud DEPC-CL has been used previously to study protein-ligand binding sites,[48–50] protein-protein interactions,[51,52] and HOS perturbations of mAbs caused by heat stress.[53–56] This work will furth explore the applications of DEPC in relation to antibody:antigen interactions.

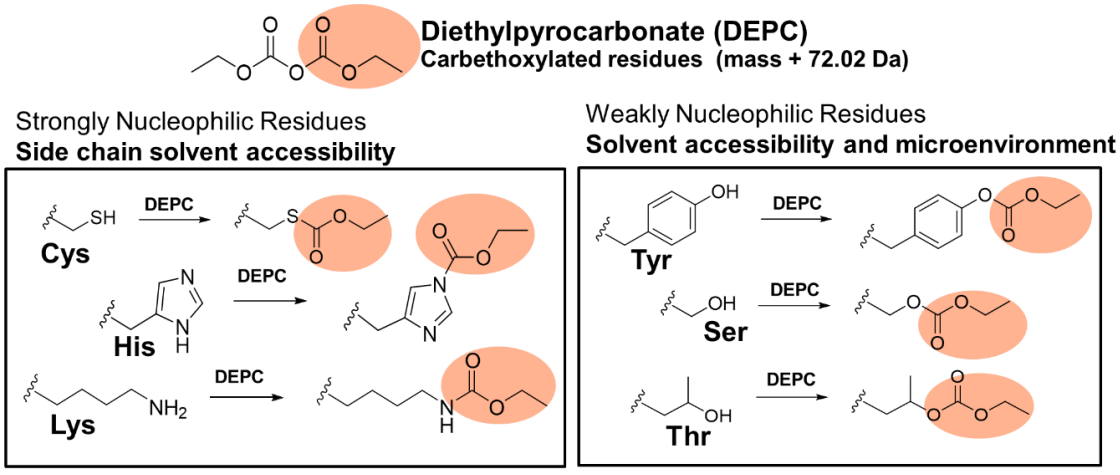

Figure 1.3: Structure of DEPC and the products resulting from reaction with DEPC for each labelable residue.

1.2.2. Hydrogen Deuterium Exchange (HDX)

HDX is a well-established technique for studying the HOS structure and dynamics of proteins.[20,31,57,58] In HDX, a protein of interest is diluted in a solution of D_2O, labile hydrogens will exchange with solvent deuterium. Hydrogens involved in hydrogen bonding and highly structured regions (i.e. beta sheets and alpha helices) exchange slowly while labile hydrogens in solvent exposed loops and dynamic regions of the protein are likely to exchange quickly.[12,19,31,59] Proteins are incubated in deuterium for a predetermined amount of time then the reaction is quenched by dropping the pH to ~2.5 where the lowest rate of exchange of amide hydrogens is observed.[60,61] Bottom-up proteomics analysis can be performed by digesting the analyte with a protease, often pepsin, that functions under acidic quench conditions (**Figure 1.4**).[19] As a result of the back exchange that occurs from deuterium to hydrogen when the reaction is quenched, generally only amide back bone hydrogens are labeled by deuterium. Coupled with liquid chromatography (LC) and electrospray ionization mass spectrometry (ESI/MS), peptides with an increase in mass caused by exchange with deuterium can be separated and detected and a plot of deuterium uptake over time can be generated (**Figure 1.4**). Based on the rate of deuterium uptake over time, conclusions can be made about the HOS surrounding a specific peptide.

The enzyme typically used for HDX analysis, pepsin is a nonspecific protease and therefore, in theory, HDX can provide amino acid level resolution depending on the number of peptides produced, detected, and the nature of overlap of the peptic peptides.[31] In reality, HDX provides peptide to sub-peptide level resolution and methods to improve the spatial resolution of the technique are constantly being investigated. MS

fragmentation techniques such as ETD can be used to pinpoint which residue contains the deuterium however these techniques are not routine as a result of difficult data analysis and the likelihood of labeling scrambling.[62] Additionally methods using multiple different enzymes or coupling HDX with molecular modeling have also been employed.

HDX has been used to study protein-protein interactions, conformational changes, stability, ligand binding sites, among other structural variations.[17,63–71] HDX for mAb characterization has been investigated and optimized extensively by the Engen lab.[72–74] Houde et. al. demonstrated that HDX is a valuable tool for comparability studies using the protein interferon-β-1a[75] while Wei et. al. has shown HDX can be used to study conformational changes the result from PEGylation.[73]

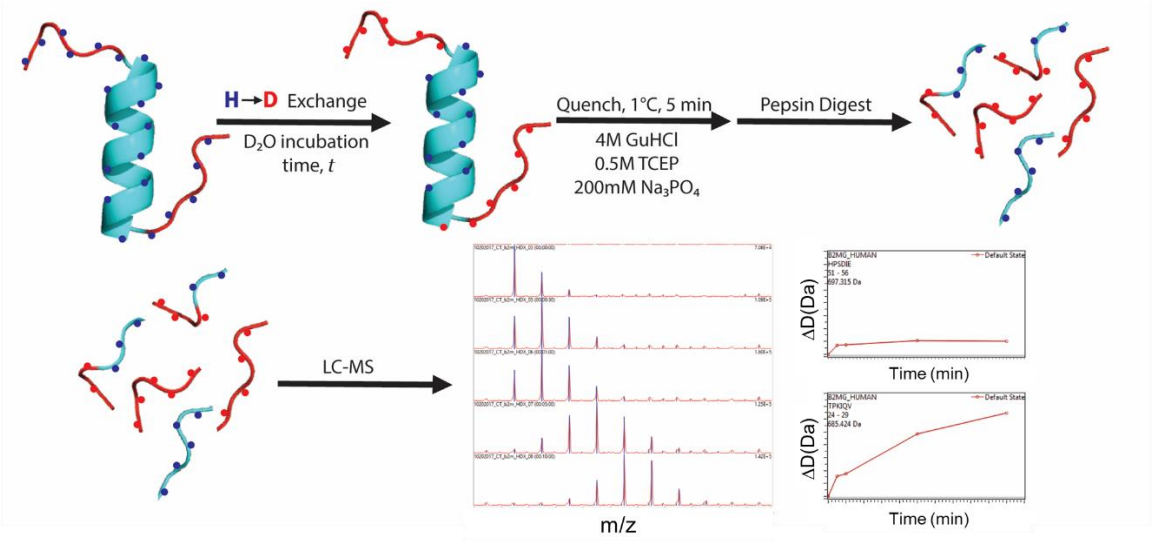

Figure 1.4: Cartoon depiction of HDX mechanism. Protein is incubated in deuterium; exposed hydrogens will exchange with deuterium in solution. The reaction will be quenched and digested, and LC/MS will be completed on resulting peptides. The change in deuterium over time can be plotted on a deuterium uptake plot.

1.3. Synergistic information from HDX and DEPC-CL

Due to the increasing complexity of protein therapeutic development, it is necessary to investigate multiple orthogonal techniques for characterizing protein HOS. HDX and CL are orthogonal techniques for describing overall HOS changes. CL reports on side chain structure while HDX reports on backbone amide hydrogen structure and dynamics. We propose that because CL reports on side chain solvent accessibility and is not typically completed at different time points, it is superior in detecting ligand binding sites and protein-protein interaction faces. HDX, however, provides information concerning allosteric and dynamic structural perturbations, as well as changes in solvent exposure. As a result of the fact that HDX is not limited in the same way as CL and can detect both protein dynamics and changes in solvent exposure, HDX data can be ambiguous as a result of its sensitivity. It can be difficult to determine which changes in HDX are a result of changes in protein dynamics and which are changes due to changes in solvent exposure. Thus, by taking advantage of the synergy between the two techniques, CL and HDX, and applying them in parallel, a greater depth of structural information can be achieved.

While this work will focus specifically on DEPC-CL, the use of CL and HDX together to study protein systems has been investigated previously. HRF and the related technique FPOP have been implemented in parallel with HDX to study protein systems.[18,38,39,41,76,77] For example, Cornwell et. al. used FPOP in combination with HDX to investigate the conformational dynamics of the protein β-2-microglobulin and its mutant D76N. Their conclusions demonstrated that by using the two techniques in parallel a confident conclusion about changes in dynamics as a result of the mutation

could be made.[39] The Gross group has used FPOP in combination with HDX to study protein small molecule ligand interactions. This work demonstrated that FPOP had a higher sensitivity than HDX for determining the location ligand binding. HDX alone was incapable of mapping the ligand binding site.[76] While these studies highlight the ability for CL and HDX to provide complementary information, there are a number of draw backs to FPOP as a protein foot-printing method. FPOP requires highly specialize equipment, data analysis is complicated and time consuming, and FPOP take place on the order of microsecond, meaning that unlike DEPC-CL it is sensitive to changes in dynamics. Thus, FPOP can suffer from the same ambiguous data problems that plague HDX data.

DEPC-CL and HDX provide a unique synergism for studying protein systems. DEPC reactions take place on the order of seconds to minutes and is thus, blind to protein dynamics. The synergy between these two methods has been demonstrated in the context of ligand binding by Liu et. al. By employing both DEPC-CL and HDX to study small molecule ligand binding with β-2-microglobulin, it was demonstrated that as a result of the different time scales, the ligand binding site could be definitively determined.[48]

DEPC-CL and HDX experiments on proteins are typically conducted using different sample preparation conditions, therefore some protocol optimization and standardization of sample preparation is necessary to appropriately compare the data from each technique. Unlike CL, HDX is reversible, so HDX analysis must happen immediately after labeling while CL samples can undergo other cleanup, such as buffer exchange or reconcentration, before analysis. Two major conditions that may affect comparability of the two methods for mAbs specifically, are the presence of formulation

additives and exchange/labeling temperature. Therapeutic mAbs are kept in a formulation for stability, removal of the tween in formulation is suggested for LC/MS runs as the tween will cause interference in collected data. Additionally, some formulation additives may react with DEPC and need to be corrected for. However, neither of these considerations are relevant for HDX runs, it is prohibitively difficult to remove the tween after labeling without causing an unacceptable amount of back exchange. The temperature of exchange is also important to consider when relating DEPC to HDX. DEPC labeling is typically carried out at 37°C. However, the rate of deuterium uptake is dependent on temperature, with exchange happening 10 times faster at 22°C than at 0°C.[20,21] The difference in temperatures could affect protein structure and should be considered when comparing data.

1.3.1 HDX and CL for epitope mapping and antibody therapeutics

The binding to an epitope can cause HOS changes in areas not directly involved with binding, or allosteric effects.[17] Mapping allosteric effects caused by ligand binding is just as important to the field of protein therapeutics as mapping paratopes.[78,79] HDX is an ideal method of detection of allosteric changes, as these changes influence hydrogen bonding interactions and thus backbone structure.[17] Paradoxically, allosteric perturbations are one of the largest problems for HDX analysis of paratopes or ligand binding sites.[17,20,79] It is impossible to distinguish if changes in deuterium uptake are a result of binding site-induced hydrogen solvent accessibility changes or dynamic allosteric changes.[17] In contrast, CL by DEPC, or other reagent, is transparent to dynamics and should clearly indicate binding site without interference from allosteric effects. Therefore, it will be possible to take advantage of CL insensitivity to dynamic changes in

combination with the sensitivity of HDX to accurately describe overall HOS structural perturbations and binding sites.

Prior work investigating these two methods for epitope mapping by the Gross group investigated the relationship between FPOP-CL and HDX in the context of epitope mapping of an antibody/interlukin-3 interaction.[18] This study utilized a combination of HDX/MS, FPOP/MS, computational surface residue analysis, alanine shave mutagenesis, and binding analytics techniques to identify the epitope binding site, ultimately demonstrating the need for orthogonal techniques for epitope mapping.[18] HDX and FPOP identified four overlapping epitope regions involved in binding. However, HDX identified a peptide involved with binding where no corresponding oxidative products were detected by FPOP, while FPOP indicated a region of peptide protection that was not observed by HDX. They hypothesize that these inconsistencies are a result of the differences in labeling methods.[18] Huang et. al. has also employed FPOP and HDX for epitope mapping for the NKG2A/CD94 protein complex with the Anti-NKG2A antibody where they concluded that the two methods orthogonally were necessary to characterize the complex protein system.[80]

1.4. Summary

In this chapter, we have described the scientific significance of protein therapeutics, explored methods for studying their higher order structure, and laid out a case for utilizing DEPC-CL/MS alone as well as both HDX/MS and DEPC-CL/MS together to characterize the HOS or therapeutic proteins. Characterizing the HOS of proteins is a necessity in the field of protein therapeutics for development of new drugs, biosimilar drugs, stability studies, and quality assurance, yet presents several challenges.

Characterizing the HOS of mAbs specifically can be difficult as a result of the multidomain nature and size of these proteins. Additionally, epitope mapping is a difficult but lucrative field of study. This dissertation focuses on the use of MS based methods, HDX and DEPC-CL, for studying a variety of protein therapeutic systems. We utilize DEPC-CL alone to investigate antigen antibody interactions and we propose that DEPC-CL can clarify ambiguous HDX results. We will to demonstrate that the two methods provide complementary information as a result of the fact that HDX detects changes in backbone amide hydrogen structure and CL reports on changes in SASA of side chains. When used in combination, the two techniques will give a comprehensive description of overall structural effects. Robust methods of protein therapeutic characterization will be developed through a deeper understanding of the relationship between HDX and CL.

In **Chapter 2**, we demonstrated that CL/MS coupled with HDX/MS can provide complementary information about structural perturbations of therapeutic mAb caused by heat stress. Using Rituximab as a model system we demonstrate that DEPC-CL is superior in detecting subtle HOS changes at low heat stress conditions but that at higher heat stress conditions considering the data given by each method gives a clearer picture of the HOS that take place in rituximab upon heat stress. The combination of these two methods gives insight into what regions of the protein are likely responsible for aggregation.

In **Chapter 3**, we investigated DEPC-CL/MS for the study of antigen-antibody interactions. We choose to use tumor necrosis factor α (TNFα) in complex with three different mAbs all with different epitopes as a model system for this work. We

demonstrate that while DEPC-CL/MS cannot be used for epitope mapping, it can provide valuable HOS information about TNFα upon binding with therapeutic mAbs.

In **Chapter 4,** we apply the methods from chapter 2, namely DEPC-CL and HDX, to the protein system in chapter 3, TNFα in complex with three different mAbs. This chapter demonstrates the utility of using the two methods together to study protein: protein interactions. We show that by using HDX/MS and DEPC-CL/MS to investigate antigen: antibody interactions we can more confidently determine what HDX decreases are a result of loss of solvent exposure due to mAb binding and what changes are due to changes in dynamics. This in turn leads to higher confidence of the exact epitope. We also suggest that these methods can also provide information about quaternary structure of TNFα. The TNFα homotrimer is stabilized by the mAbs and HDX in parallel with DEPC-CL can reveal that stabilization.

Finally, **Chapter 5** presents conclusions and future directions of this work.

1.5. References

(1) Ecker, D. M.; Jones, S. D.; Levine, H. L. The Therapeutic Monoclonal Antibody Market. MAbs 2015, 7 (1), 9–14. https://doi.org/http://dx.doi.org/10.4161/19420862.2015.989042.

(2) Nelson, A. L.; Dhimolea, E.; Reichert, J. M. Development Trends for Human Monoclonal Antibody Therapeutics. Nat. Rev. Drug Discov. 2010, 9, 767–774. https://doi.org/10.1038/nrd3229.

(3) Weiner, L. M.; Surana, R.; Wang, S. Monoclonal Antibodies : Versatile Platforms for Cancer Immunotherapy. Nat. Publ. Gr. 2010, 10 (5), 317–327. https://doi.org/10.1038/nri2744.

(4) Reichert, J. M. Monoclonal Antibodies as Innovative Therapeutics. Curr. Pharm. Biotechnol. 2008, 423–430.

(5) Elgundi, Z.; Reslan, M.; Cruz, E.; Sifniotis, V.; Kayser, V. The State-of-Play and Future of Antibody Therapeutics. Adv. Drug Deliv. Rev. 2017, 122, 2–19. https://doi.org/10.1016/j.addr.2016.11.004.

(6) Mark, R.; Aitken, M. L.; Berndt, E. R. Characterizing Markets for Biopharmaceutical Innovations : Do Biologics Differ from Small Molecules ? Forum Health Econ. Policy 2010, 13 (1).

(7) Reichert, J. M.; Valge-archer, V. E. Development Trends for Monoclonal Antibody Cancer Therapeutics. Nat. Rev. 2007, 6 (May), 349–356.

(8) Trikha, M.; Yan, L.; Nakada, M. T. Monoclonal Antibodies as Therapeutics in Oncology. Curr. Opin. Biotechnol. 2002, 609–614.

(9) Leader, B.; Baca, Q. J.; Golan, D. E. Protein Therapeutics: A Summary and Pharmacological Classification. Nat. Rev. 2008, 7 (january), 21–39.

(10) Beneta, L. Z.; Hoseya, C. M.; Ursub, O.; Opreab, T. I. BDDCS, the Rule of 5 and Drugability Leslie. Adv. Drug Deliv. Rev. 2016, 101, 89–98. https://doi.org/10.1016/j.addr.2016.05.007.BDDCS.

(11) Beck, A.; Goetsch, L.; Dumontet, C.; Corvaïa, N. Strategies and Challenges for the next Generation of Antibody–Drug Conjugates. Nat. Publ. Gr. 2017, 16 (5), 315–337. https://doi.org/10.1038/nrd.2016.268.

(12) Majumdar, R.; Middaugh, C. R.; Weis, D. D.; Volkin, D. B. Hydrogen – Deuterium Exchange Mass Spectrometry as an Emerging Analytical Tool for Stabilization and Formulation Development of Therapeutic Monoclonal Antibodies. J. Pharm. Sci. 2015, 104 (2), 327–345. https://doi.org/10.1002/jps.24224.

(13) Manikwar, P.; Majumdar, R.; Hickey, J. M.; Thakkar, S. V; Samra, H. S.; Sathish, H. A.; Bishop, S. M.; Middaugh, C. R.; Weis, D. D.; Volkin, D. B. Correlating Excipient

Effects on Conformational and Storage Stability of an IgG1 Monoclonal Antibody with Local Dynamics as Measured by Hydrogen / Deuterium-Exchange Mass. J. Pharm. Sci. 2013, 102 (7), 2136–2151. https://doi.org/10.1002/jps.23543.

(14) Hawe, A.; Christina, J.; Friess, W.; Jiskoot, W. Structural Properties of Monoclonal Antibody Aggregates Induced by Freeze – Thawing and Thermal Stress. Eur. J. Pharm. Sci. 2009, 38, 79–87. https://doi.org/10.1016/j.ejps.2009.06.001.

(15) Pettersson, I. Methods of Epitope Mapping. Mol. Biol. Rep. 1992, 149–150.

(16) Berkowitz, S. A.; Engen, J. R.; Mazzeo, J. R.; Jones, G. B. Analytical Tools for Characterizing Biopharmaceuticals and the Implications for Biosimilars. Nature 2012, 11, 527–540. https://doi.org/10.1038/nrd3746.

(17) Deng, B.; Zhu, S.; Macklin, A. M.; Xu, J.; Lento, C.; Sljoka, A.; Wilson, D. J. Suppressing Allostery in Epitope Mapping Experiments Using Millisecond Hydrogen / Deuterium Exchange Mass Spectrometry. MAbs 2017, 0862. https://doi.org/10.1080/19420862.2017.1379641.

(18) Li, J.; Wei, H.; Krystek, S. R.; Bond, D.; Brender, T. M.; Cohen, D.; Feiner, J.; Hamacher, N.; Harshman, J.; Huang, R. Y.; Julien, S. H.; Lin, Z.; Moore, K.; Mueller, L.; Noriega, C.; Sejwal, P.; Sheppard, P.; Stevens, B.; Chen, G.; Tymiak, A. A.; Gross, M. L.; Schneeweis, L. A. Mapping the Energetic Epitope of an Antibody/Interleukin-23 Interaction with Hydrogen/Deuterium Exchange, Fast Photochemical Oxidation of Proteins Mass Spectrometry, and Alanine Shave Mutagenesis. Anal. Chem. 2017. https://doi.org/10.1021/acs.analchem.6b03058.

(19) Deng, B.; Lento, C.; Wilson, D. J. Hydrogen Deuterium Exchange Mass Spectrometry in Biopharmaceutical Discovery and Developm .... Anal. Chim. Acta 2016, 940 (October 2017), 8–20. https://doi.org/10.1016/j.aca.2016.08.006.

(20) Wei, H.; Mo, J.; Tao, L.; Russell, R. J.; Tymiak, A. A.; Chen, G.; Iacob, R. E.; Engen, J. R. Hydrogen / Deuterium Exchange Mass Spectrometry for Probing Higher Order Structure of Protein Therapeutics : Methodology and Applications. Drug Discov. Today 2014, 19 (1), 95–102. https://doi.org/10.1016/j.drudis.2013.07.019.

(21) Hageman, T. S.; Weis, D. D. Reliable Identification of Significant Differences in Differential Hydrogen Exchange-Mass Spectrometry Measurements Using a Hybrid Significance Testing Approach. Anal. Chem. 2019, 91 (13), 8008–8016. https://doi.org/10.1021/acs.analchem.9b01325.

(22) Pisupati, K.; Tian, Y.; Okbazghi, S.; Benet, A.; Ackermann, R.; Ford, M.; Saveliev, S.; Hos, C. M.; Urh, M.; Carlson, E.; Becker, C.; Tolbert, T. J.; Schwendeman, S. P.; Ruotolo, B. T.; Schwendeman, A. A Multidimensional Analytical Comparison of Remicade and the Biosimilar Remsima. Anal. Chem. 2017. https://doi.org/10.1021/acs.analchem.6b04436.

(23) Abbott, W. M.; Damschroder, M. M.; Lowe, D. C. Current Approaches to Fine Mapping of Antigen-Antibody Interactions. Immunology 2014, 142 (4), 526–535. https://doi.org/10.1111/imm.12284.

(24) Chen, K.; Long, D. S.; Lute, S. C.; Levy, M. J.; Brorson, K. A.; Keire, D. A. Simple NMR Methods for Evaluating Higher Order Structures of Monoclonal Antibody Therapeutics with Quinary Structure. J. Pharm. Biomed. Anal. 2016, 128, 398–407. https://doi.org/10.1016/j.jpba.2016.06.007.

(25) Lewis, E. Protein Dynamics from NMR. Biochem. Cell Biol. 1998.

(26) Rousseau, F.; Schymkowitz, J.; Serrano, L. Protein Aggregation and Amyloidosis: Confusion of the Kinds? Curr. Opin. Struct. Biol. 2006, 16 (1), 118–126. https://doi.org/10.1016/j.sbi.2006.01.011.

(27) Fei, X.; Bell, T. A.; Jenni, S.; Stinson, B. M.; Baker, T. A.; Harrison, S. C.; Sauer, R. T. Structures of the ATP-Fueled ClpXP Proteolytic Machine Bound to Protein Substrate. Elife 2020, 9, 1–22. https://doi.org/10.7554/eLife.52774.

(28) Yip, K. M.; Fischer, N.; Paknia, E.; Chari, A.; Stark, H. Atomic-Resolution Protein Structure Determination by Cryo-EM. Nature 2020, 587 (7832), 157–161. https://doi.org/10.1038/s41586-020-2833-4.

(29) Pan, J.; Zhang, S.; Chou, A.; Borchers, C. H. Higher-Order Structural Interrogation of Antibodies Using Middle-down Hydrogen/Deuterium Exchange Mass Spectrometry. Chem. Sci. 2016, 7 (2), 1480–1486. https://doi.org/10.1039/c5sc03420e.

(30) Dass, C. Mass Spectrometry : Structure Determination of Proteins and Peptides; 2010.

(31) Houde, D.; Arndt, J.; Domeier, W.; Berkowitz, S.; Engen, J. R. Characterization of IgG1 Conformation and Conformational Dynamics by Hydrogen / Deuterium Exchange Mass Spectrometry. Anal. Chem. 2009, 81 (7), 2644–2651. https://doi.org/10.1021/ac802575y.

(32) Biemann, K. Contributions of Mass Spectrometry to Peptide and Protein Structure. Biomed. Environ. Mass Spectrom. 1988, 16, 99–111.

(33) Leitner, A. Cross-Linking and Other Structural Proteomics Techniques : How Chemistry Is Enabling Mass Spectrometry Applications in Structural Biology. Chem. Sci. 2016, 7, 4792–4803. https://doi.org/10.1039/C5SC04196A.

(34) Narang, D.; James, D. A.; Balmer, M. T.; Wilson, D. J. Protein Footprinting, Conformational Dynamics, and Core Interface-Adjacent Neutralization “Hotspots” in the SARS-CoV-2 Spike Protein Receptor Binding Domain/Human ACE2 Interaction. J. Am. Soc. Mass Spectrom. 2021. https://doi.org/10.1021/jasms.0c00465.

(35) Mendoza, V. L.; Vachet, R. W. Probing Protein Structure by Amino Acid-Specific Covalent Labeling and Mass Spectrometry. Mass Spectrom. Rev. 2010, 28 (5), 785–815. https://doi.org/10.1002/mas.20203.Probing.

(36) Limpikirati, P.; Pan, X.; Vachet, R. W. Covalent Labeling with Diethylpyrocarbonate: Sensitive to the Residue Microenvironment, Providing Improved Analysis of Protein Higher Order Structure by Mass Spectrometry. Anal. Chem. 2019, 91 (13), 8516–8523. https://doi.org/10.1021/acs.analchem.9b01732.

(37) Deperalta, G.; Alvarez, M.; Bechtel, C.; Dong, K.; Mcdonald, R.; Ling, V. Structural Analysis of a Therapeutic Monoclonal Antibody Dimer by Hydroxyl Radical Footprinting. MAbs 2013, 5 (1), 86–101.

(38) Li, K. S.; Shi, L.; Gross, M. L. Mass Spectrometry-Based Fast Photochemical Oxidation of Proteins (FPOP) for Higher Order Structure Characterization. Acc. Chem. Res. 2018, 51, 736–744. https://doi.org/10.1021/acs.accounts.7b00593.

(39) Cornwell, O.; Ault, J. R.; Bond, N. J.; Radford, S. E.; Ashcroft, A. E. Investigation of D76N β 2 - Microglobulin Using Protein Footprinting and Structural Mass Spectrometry. J Am Soc Mass Spectrom 2021. https://doi.org/10.1021/jasms.0c00438.

(40) Lisa M. Jones; Sperry, J.; Carroll, J.; Gross, M. L. Fast Photochemical Oxidation of Proteins (FPOP) for Epitope Mapping. Anal. Chem. 2011, 83 (20), 7657–7661. https://doi.org/10.1021/ac2007366.Fast.

(41) Cornwell, O.; Radford, S. E.; Ashcroft, A. E.; Ault, J. R. Comparing Hydrogen Deuterium Exchange and Fast Photochemical Oxidation of Proteins: A Structural Characterisation of Wild-Type and ΔN6 B2-Microglobulin. J. Am. Soc. Mass Spectrom. 2018, 29, 2413–2426. https://doi.org/10.1007/s13361-018-2067-y.

(42) Kaur, P.; Tomechko, S. E.; Kiselar, J.; Shi, W.; Deperalta, G.; Wecksler, A. T.; Gokulrangan, G.; Ling, V.; Chance, M. R. Characterizing Monoclonal Antibody Structure by Carboxyl Group Footprinting. MAbs 2015, 7 (3), 540–552.

(43) Arden, B. G.; Borotto, N. B.; Burant, B.; Warren, W.; Akiki, C.; Vachet, R. W. Measuring the Energy Barrier of the Structural Change That Initiates Amyloid Formation. Anal. Chem. 2020, 92 (7), 4731–4735. https://doi.org/10.1021/acs.analchem.0c00368.

(44) Fiedler, W.; Borchers, C.; Macht, M.; Deininger, S. O.; Przybylski, M. Molecular Characterization of a Conformational Epitope of Hen Egg White Lysozyme by Differential Chemical Modification of Immune Complexes and Mass Spectrometric Peptide Mapping. Bioconjug. Chem. 1998, 9 (2), 236–241. https://doi.org/10.1021/bc970148g.

(45) Borotto, N. B.; Zhou, Y.; Hollingsworth, S. R.; Hale, J. E.; Graban, E. M.; Vaughan, R. C.; Vachet, R. W. Investigating Therapeutic Protein Structure with

Diethylpyrocarbonate Labeling and Mass Spectrometry. Anal. Chem. 2015. https://doi.org/10.1021/acs.analchem.5b03180.

(46) Mendoza, V. L.; Vachet, R. W. Protein Surface Mapping Using Diethylpyrocarbonate with Mass Spectrometric Detection. Anal. Chem. 2008, 80 (8), 2895–2904. https://doi.org/10.1021/ac701999b.

(47) Limpikirati, P. K.; Zhao, B.; Pan, X.; Eyles, S. J.; Vachet, R. W. Covalent Labeling/Mass Spectrometry of Monoclonal Antibodies with Diethylpyrocarbonate: Reaction Kinetics for Ensuring Protein Structural Integrity. J. Am. Soc. Mass Spectrom. 2020, 31 (6), 1223–1232. https://doi.org/10.1021/jasms.0c00067.

(48) Liu, T.; Limpikirati, P.; Vachet, R. W. Synergistic Structural Information from Covalent Labeling and Hydrogen − Deuterium Exchange Mass Spectrometry for Protein − Ligand Interactions. Anal. Chem. 2019, 91, 15248–15254. https://doi.org/10.1021/acs.analchem.9b04257.

(49) Glocker, M. O.; Kalkum, M.; Yamamoto, R.; Schreurs, J. Selective Biochemical Modification of Functional Residues in Recombinant Human Macrophage Colony-Stimulating Factor β (RhM-CSF β): Identification by Mass Spectrometry†. Biochemistry 1996, 35 (46), 14625–14633. https://doi.org/10.1021/bi961199o.

(50) Hondal, R. J.; Ma, S.; Caprioli, R. M.; Hill, K. E.; Burk, R. F. Heparin-Binding Histidine and Lysine Residues of Rat Selenoprotein P. J. Biol. Chem. 2001, 276 (19), 15823–15831. https://doi.org/10.1074/jbc.M010405200.

(51) Blanco, C.; Vachet, R. W.; Mendoza, V. L.; Antwi, K.; Baron-rodriguez, M. A. Structure of the Preamyloid Dimer of β -2-Microglobulin from Covalent Labeling And. Biochemistry 2010, 1522–1532. https://doi.org/10.1021/bi901748h.

(52) Mendoza, V. L.; Baro, M. A.; Blanco, C.; Vachet, R. W. Structural Insights into the Pre-Amyloid Tetramer of β -2- Microglobulin from Covalent Labeling and Mass Spectrometry ‡´. Biochemistry 2011.

(53) Limpikirati, P.; Hale, J. E.; Hazelbaker, M.; Huang, Y.; Jia, Z.; Yazdania, M.; Grabanb, E. M.; Vaughan, R. C.; Vachet, R. W. Covalent Labeling and Mass Spectrometry Reveal Subtle Higher Order Structural Changes for Antibody Therapeutics. MAbs 2019, 11 (3), 463–476. https://doi.org/10.1080/19420862.2019.1565748.

(54) Tremblay, C. Y.; Limpikirati, P.; Vachet, R. W. Complementary Structural Information for Stressed Antibodies from Hydrogen − Deuterium Exchange and Covalent Labeling Mass Spectrometry. 2021. https://doi.org/10.1021/jasms.1c00072.

(55) Liu, T.; Marcinko, T. M.; Kiefer, P. A.; Vachet, R. W. Using Covalent Labeling and Mass Spectrometry To Study Protein Binding Sites of Amyloid Inhibiting Molecules. Anal. Chem. 2017, 89, 11583–11591. https://doi.org/10.1021/acs.analchem.7b02915.

(56) Wilson, D. J.; Brown, K. A. Bottom-up Hydrogen Deuterium exchange Mass Spectrometry: Data Analysis and Interpretation. R. Soc. Chem. 2017, 2874–2886. https://doi.org/10.1039/c7an00662d.

(57) Huang, R. Y.; Chen, G. Higher Order Structure Characterization of Protein Therapeutics by Hydrogen/Deuterium Exchange Mass Spectrometry. Anal Bioanal Chem 2014, 406, 6541–6558. https://doi.org/10.1007/s00216-014-7924-3.

(58) Pan, J.; Zhang, S.; Chou, A.; Hardie, D. B.; Borchers, C. H. Fast Comparative Structural Characterization of Intact Therapeutic Antibodies Using Hydrogen − Deuterium Exchange and Electron Transfer Dissociation. Anal. Chem. 2015. https://doi.org/10.1021/ac504809r.

(59) FINUCANE, M. D.; JARDETZKY, O. The PH Dependence of Hydrogen-Deuterium Exchange in Trp Repressor: The Exchange Rate of Amide Protons in Proteins Reflects Tertiary Interactions, Not Only Secondary Structure. Protein Sci. 1996, 653–662.

(60) Englander, S. W.; Sosnickt, T. R.; Englander, J. J.; Maynet, L. Mechanisms and Uses of Hydrogen Exchange. Curr. Opin. Struct. Biol. 1996.

(61) Engen, J. R.; Botzanowski, T.; Peterle, D.; Georgescauld, F.; Wales, T. E. Developments in Hydrogen/Deuterium Exchange Mass Spectrometry. Anal. Chem. 2021, 93 (1), 567–582. https://doi.org/10.1021/acs.analchem.0c04281.

(62) Kattat, V.; Chit, B. T. Hydrogen / Deuterium Exchange Electrospray Ionization Mass Spectrometry : A Method for Probing Protein Conformational Changes in Solution. J. Am. Chem. Soc. 1993, No. 13, 4–8. https://doi.org/10.1021/ja00067a054.

(63) Hamuro, Y.; Coales, S. J.; Southern, M. R.; Nemeth-Cawley, J. F.; Stranz, D. D.; Griffin, P. R. Rapid Analysis of Protein Structure and Dynamics by Hydrogen/Deuterium Exchange Mass Spectrometry. J. Biomol. Tech. 2003, 14 (3), 171–182.

(64) Fast, C. S.; Vahidi, S.; Konermann, L. Changes in Enzyme Structural Dynamics Studied by Hydrogen Exchange-Mass Spectrometry: Ligand Binding E Ff Ects or Catalytically Relevant Motions? Anal. Chem. 2017. https://doi.org/10.1021/acs.analchem.7b03506.

(65) Trabjerg, E.; Nazari, Z. E.; Rand, K. D. Conformational Analysis of Complex Protein States by Hydrogen/Deuterium Exchange Mass Spectrometry (HDX/MS): Challenges and Emerging Solutions. TrAC - Trends Anal. Chem. 2018, 106, 125–138. https://doi.org/10.1016/j.trac.2018.06.008.

(66) Marciano, D. P.; Dharmarajan, V.; Griffin, P. R. HDX/MS Guided Drug Discovery: Small Molecules and Biopharmaceuticals. Curr. Opin. Struct. Biol. 2014, 28, 105–111. https://doi.org/10.1016/j.sbi.2014.08.007.

(67) Edgeworth, M. J.; Phillips, J. J.; Lowe, D. C.; Kippen, A. D.; Higazi, D. R.; Scrivens, J. H. Global and Local Conformation of Human IgG Antibody Variants Rationalizes Loss of Thermodynamic Stability. Angew. Chemie - Int. Ed. 2015, 54 (50), 15156–15159. https://doi.org/10.1002/anie.201507223.

(68) Tian, Y.; Huang, L.; Ruotolo, B. T.; Wang, N. Hydrogen/Deuterium Exchange-Mass Spectrometry Analysis of High Concentration Biotherapeutics: Application to Phase-Separated Antibody Formulations. MAbs 2019, 11 (4), 779–788. https://doi.org/10.1080/19420862.2019.1589850.

(69) Marcsisin, S. R.; Engen, J. R. Hydrogen Exchange Mass Spectrometry: What Is It and What Can It Tell Us? Sean. Anal Bioanal Chem 2011, 397 (3), 967–972. https://doi.org/10.1007/s00216-010-3556-4.Hydrogen.

(70) Schmidt, C.; Robinson, C. V. Dynamic Protein Ligand Interactions - Insights from MS. FEBS J. 2014, 281 (8), 1950–1964. https://doi.org/10.1111/febs.12707.

(71) Wei, H.; Mo, J.; Tao, L.; Russell, R. J.; Tymiak, A. A.; Chen, G.; Iacob, R. E.; Engen, J. R. Hydrogen/Deuterium Exchange Mass Spectrometry for Probing Higher Order Structure of Protein Therapeutics: Methodology and Applications. Drug Discov. Today 2015, 19 (1), 95–102. https://doi.org/10.1016/j.drudis.2013.07.019.Hydrogen/Deuterium.

(72) Wei, H.; Ahn, J.; Yu, Y. Q.; Tymiak, A.; Engen, J. R.; Chen, G. Using Hydrogen/Deuterium Exchange Mass Spectrometry to Study Conformational Changes in Granulocyte Colony Stimulating Factor upon PEGylation Hui. J Am Soc Mass Spectrom 2012, 23 (3), 498–504. https://doi.org/10.1007/s13361-011-0310-x.

(73) Houde, D.; Berkowitz, S. A.; Engen, J. R. The Utility of Hydrogen/Deuterium Exchange Mass Spectrometry in Biopharmaceutical Comparability Studies. J. Pharm. Sci. 2011, 100 (6), 2071–2086. https://doi.org/10.1002/jps.22432.

(74) Houde, D.; Berkowitz, S. A.; Engen, J. R. The Utility of Hydrogen / Deuterium Exchange Mass Spectrometry in Biopharmaceutical Comparability Studies. J. Pharm. Sci. 2011, 100 (6), 2071–2086. https://doi.org/10.1002/jps.22432.

(75) Li, K. S.; Schaper Bergman, E. T.; Beno, B. R.; Huang, R. Y. C.; Deyanova, E.; Chen, G.; Gross, M. L. Hydrogen-Deuterium Exchange and Hydroxyl Radical Footprinting for Mapping Hydrophobic Interactions of Human Bromodomain with a Small Molecule Inhibitor. J. Am. Soc. Mass Spectrom. 2019, 30 (12), 2795–2804. https://doi.org/10.1007/s13361-019-02316-1.

(76) Saleem, R.; Cantin, G.; Wikström, M.; Bolton, G.; Kuhns, S.; McBride, H. J.; Liu, J. Analytical and Functional Similarity Assessment of ABP 710, a Biosimilar to Infliximab Reference Product. Pharm. Res. 2020, 37 (6). https://doi.org/10.1007/s11095-020-02816-w.

(77) Sowole, M. A.; Simpson, S.; Skovpen, Y. V; Palmer, D. R. J.; Konermann, L. Evidence of Allosteric Enzyme Regulation via Changes in Conformational Dynamics: A Hydrogen/Deuterium Exchange Investigation of Dihydrodipicolinate Synthase. Biochemistry 2016. https://doi.org/10.1021/acs.biochem.6b00764.

(78) Konermann, L. Heavy Lessons in Protein Allostery. Nat. Publ. Gr. 2016, 23 (6), 511–512. https://doi.org/10.1038/nsmb.3234.

(79) Huang, R. Y. C.; Wang, Y.; Jhatakia, A. D.; Deng, A. X.; Bee, C.; Deshpande, S.; Rangan, V. S.; Bezman, N.; Gudmundsson, O.; Chen, G. Higher-Order Structure Characterization of NKG2A/CD94 Protein Complex and Anti-NKG2A Antibody Binding Epitopes by Mass Spectrometry-Based Protein Footprinting Strategies. J. Am. Soc. Mass Spectrom. 2021. https://doi.org/10.1021/jasms.0c00399.

CHAPTER 2

2. COMPLEMENTARY STRUCTURAL INFORMATION FOR STRESSED ANTIBODIES FROM HYDROGEN−DEUTERIUM EXCHANGE AND COVALENT LABELING MASS SPECTROMETRY

This chapter is part of a research article published as: Tremblay, C. Y.; Limpikirati, P.; and Vachet, R. W., Complementary Structural Information for Stressed Antibodies from Hydrogen−Deuterium Exchange and Covalent Labeling Mass Spectrometry. JASMS 2021, 32 (5), 1237-1248.

2.1. Introduction

The market for monoclonal antibodies (mAbs) has grown tremendously in the past 25 years and is estimated to be a $300 billion market in 2025.[1-4] As the mAb market is growing, there is an increasing need to characterize their higher order structure (HOS) quickly and effectively. Unlike small molecules, mAb structure is complex, and changes in HOS resulting from mishandling or storage can lead to reduced stability, loss of efficacy, or possible immunogenicity.[5,6] In addition to monitoring changes in HOS, general structural information is useful for biologics license applications as it is necessary to demonstrate lot-to-lot comparability and stability.[7] Methods to assess HOS are also essential in biosimilar development as comparability of a biosimilar to an approved drug is necessary for FDA approval.[8]

Detecting mAb HOS changes is difficult due to their complexity and multidomain nature. High resolution methods such as nuclear magnetic resonance (NMR) or X-ray crystallography can provide atomic-level resolution; however, these techniques require large amounts of sample, have difficulty with heterogeneous proteins (e.g. multiple glycoforms), and/or are incapable of analyzing high molecular weight mAbs. Conversely,

low-resolution techniques such as differential scanning calorimetry, dynamic light scattering, fluorescence spectroscopy, infrared spectroscopy, and circular dichroism spectroscopy are relatively fast and have low sample consumption, but they do not provide site-specific information about localized conformational changes. As a result, there is a need for methods that are rapid, low on sample consumption, and provide high enough resolution to detect site-specific HOS changes.

Mass spectrometry (MS) is a powerful tool for protein analysis and has some advantages over other structural characterization techniques. MS-based methods have the benefits of limited sample consumption, essentially no molecular weight limitation, and the ability to analyze complex protein mixtures. MS is emerging as a method that can examine protein HOS.[7,9] To characterize protein HOS, protein structural information must be encoded into the protein's mass. One commonly used method to achieve this is hydrogen deuterium exchange (HDX). HDX/MS is well established in industry for detecting protein dynamics, protein/protein interactions, and protein-ligand binding, including for mAbs.[10-18] In HDX/MS the exchange of backbone amide hydrogens with deuterium is measured, and the extent of exchange depends on solvent accessibility, H-bonding, and dynamics, resulting in an increase in mass that can be detected and localized to peptide fragments using MS after proteolytic digestion.

Covalent labeling (CL) with MS detection has also been used increasingly to characterize protein HOS such as protein-ligand binding sites and protein/protein interactions,[19,20] and recently the method has been applied for structural analysis and epitope-paratope mapping of antibodies.[19,21-25] In CL a reagent is used to covalently modify solvent exposed amino acid side chains, resulting in a mass shift that can be

detected with MS. When used with bottom-up tandem MS (MS/MS), residue-level resolution can be obtained, which contrasts with typical HDX measurements that are limited to peptide-level information. CL/MS methods have the additional advantage of being permanent modifications that are typically not lost during analysis, as can happen to deuterium labels during HDX/MS.

HDX/MS and CL/MS are complementary methods as HDX provides protein backbone information while CL reports on side chains. The complementarity of the two techniques has recently been used to gain deeper structural information about a variety of protein systems.[22,26-28] For example, Gross and coworkers have used fast photochemical oxidation of proteins (FPOP), which is a CL/MS method, and HDX/MS to investigate the conformational changes that take place in the interleukin-6 receptor when it binds with different adnectins. The same group also used FPOP and HDX/MS to structurally characterize antibodies, finding that the two methods provide overlapping results, while FPOP was able to identify potential residues within the epitope.[26] An important aspect of FPOP is the hydroxyl radicals that are used react on the μs to ms timescale, which is similar to the intrinsic (or chemical) exchange rate of HDX. Our group recently demonstrated other CL reagents, such as diethylpyrocarbonate (DEPC), which react on a slower time scale (i.e. s) can be combined with HDX/MS data to provide synergistic structural information about protein-ligand interactions.[29] DEPC reacts with nucleophilic residues, including Cys, Lys, His, Thr, Ser, and Tyr, labeling around 30% of the surface exposed residues on the average protein. HDX/MS measures both changes in solvent exposure and dynamics, which can lead to uncertainty when studying protein interactions, while CL/MS with DEPC is primarily sensitive to changes in solvent

exposure because of the relatively slow-reacting nature of the reagent. Moreover, unlike typical HDX experiments that are done at different time points (e.g. 10 s to 24 h), CL experiments are typically conducted at a single reaction time point (e.g. 5 min), and thus lack the kinetic information that might report on dynamics. Together, the two techniques can provide greater insight into binding sites and binding-induced structural or dynamical changes.

Here, we demonstrate HDX/MS and DEPC-based CL/MS can be used to provide complementary and synergistic HOS information about heat-stressed therapeutic mAbs, using rituximab as a model system. Three levels of heat stress were chosen to induce different extents of structural changes to compare the information provided by these two techniques. Under low and moderate heat stress (i.e. 45 °C and 55 °C), the two methods provide complementary information about regions of rituximab that undergo subtle structural changes. By using high heat stress conditions, just below the melting temperature of the protein, we demonstrate that the two techniques together more clearly differentiate structural changes resulting from changes in protein dynamics from those resulting from decreases in solvent exposure due to aggregation. The techniques provide greater confidence in the aggregation sites by using CL data to clarify ambiguous HDX results. Together, DEPC-based CL/MS and HDX/MS provide a more comprehensive picture of the structural changes that take place in a heat-stressed mAb.

2.2. Experimental section

2.2.1. Materials

Rituximab formulation (Rituxan® 100 mg/10 mL vial, lot# 3209283, Genentech) was purchased from Myoderm. Diethylpyrocarbonate (DEPC) (#D5758), imidazole

(#I5513), iodoacetamide (#I6125), tris(2-carboxyethyl)phosphine (TCEP) (#C4706), deuterium oxide (D2O) (#151882), Guanidine hydrochloride (GnHCl) (#G3272), sodium chloride (#S5886), and trypsin (#T1426) were obtained from Sigma-Aldrich. Urea (#AC424581000) was purchased from Acros Organics. Sodium phosphate monobasic monohydrate (#S0710-1) was obtained from EM Science. Sodium phosphate dibasic anhydrous (#S374-500), LC/MS-grade formic acid (#A117-50), acetonitrile (#A998-4), and water (#W7-4) were purchased from Fisher Scientific.

2.2.2. Heat Treatment

Formulated rituximab was used in all experiments. The formulation consists of 10 mg/mL (69.5 μM) rituximab, 0.7 mg/mL polysorbate 80, 7.35 mg/mL sodium citrate dihydrate and 9 mg/mL sodium chloride in water at pH 6.5. Samples were aliquoted from a rituximab formulation stored at 4 °C. Control samples were incubated at 37 °C for 5 min, and heat-stressed samples were incubated at 45 °C, 55 °C, and 65 °C for 4 h in a water bath prior to cooling to an appropriate temperature for DEPC labeling or HDX experiments.

2.2.3. DEPC labeling and proteolytic digestion

DEPC stock solutions were prepared in acetonitrile and further diluted in water in order to have acetonitrile levels that are less than 1% v/v in the final samples. The DEPC labeling reaction was done on the rituximab formulation (5 μL aliquot) with only a small dilution (to 58 μM) due to the addition of DEPC. Labeling was conducted at a DEPC:protein molar ratio of 4:1 at 37 °C for 5 min. We have found that a 5-min reaction a 4:1 molar ratio leads to sufficient labeling of antibodies without perturbing the protein's structure.[3047] Imidazole was then added at a 1:50 DEPC:imidazole molar ratio to quench

the reaction. For each stress conditions, at least three replicates were performed on the rituximab samples.

The quenched reaction mixtures were subsequently added into a urea-containing microtube and diluted in 50 mM phosphate buffer (pH 7.4). Protein denaturation was conducted in an 8 M urea solution. To reduce the disulfide bonds and alkylate the reduced Cys residues, TCEP and iodoacetamide were both added at final concentrations of 25 mM. The samples were kept in the dark for 20 min at room temperature to prevent photodegradation of iodoacetamide. DetergentOUT™ Tween® Micro spin columns (#786–214, G-Biosciences) were then used to remove polysorbate 80 from the samples. Subsequently, samples were diluted 4-fold with phosphate buffer to ensure less than 2 M urea was present during the digestion. Proteolytic digestion was performed using trypsin at a 1:10 (w/w) enzyme to substrate, and the protein was digested overnight at 37 °C. To remove trypsin and collect the resulting peptides after the digestion, the samples were filtered through an Amicon® centrifugal filter with a 10 kDa molecular weight cutoff (#UFC501096, Millipore). The filtrate was collected, flash-frozen in liquid nitrogen, and stored at −20 °C until LC/MS/MS analysis.

2.2.4. LC/MS of CL samples

For online LC/MS/MS analyses, a sample containing approximately 2 μg of rituximab peptides was loaded on an Easy-NanoLC 1000 system (Thermo Scientific). The flow rate was set at 300 nL/min. An Acclaim PepMap C18 trap column (2 cm × 75 μm, 3 μm, Thermo Scientific) was used for sample trapping and desalting. The separation of peptides was then performed using a FortisBIO C18 nanocolumn (15 cm x 75 μm, 1.7 μm; Fortis Technologies). LC/MS-grade water (solvent A) and acetonitrile (solvent B),

each containing 0.1% formic acid, were used as mobile phases. A linear gradient of solvent B was increased from 0% B to 50% B over 90 min. A nanoelectrospray ionization was used as an ion source at a needle voltage of 2100 V (positive mode). Mass spectra were acquired on a Thermo Scientific Orbitrap Fusion mass spectrometer. Tandem mass spectrometry (MS/MS) was conducted using collision-induced dissociation (CID) on a linear quadrupole ion trap.

2.2.5. CL/MS data analysis

Details about a custom software pipeline designed specifically for protein DEPC CL/MS experiments were described previously.[3145] Briefly, CID tandem mass spectra were searched against the sequence database to achieve peptide mapping with labeled site identification. The search parameters were set as follows: a precursor mass tolerance of 10 ppm, a product ion tolerance of 0.5 Da, carbamidomethylation of Cys and DEPC modification of His, Lys, Ser, Thr, Tyr, and N-terminus (mass addition of 72.0211 Da) as variable modifications. For semi-quantitation of modification extent, peak areas of labeled and unlabeled species obtained from reconstructed ion chromatograms of each species are used to calculate percent labeling at each labeled site.

2.2.6. HDX procedure

Samples were aliquoted (15 μL) from a rituximab formulation stored at 4 °C and then were incubated at 45 °C, 55 °C, or 65 °C for 4 h in a temperature-controlled water bath. After incubation, samples were diluted to 3 mg/mL and cooled to 10 °C for 15 min prior to HDX. Control samples were diluted to 3 mg/mL, and then cooled to 10 °C for 15 min prior to HDX.

D_2O was prepared in a 10 mM phosphate buffer. The pD was adjusted via a pH meter corrected by the following relationship: pD = pH reading + 0.41.[81] HDX experiments were conducted using the Leap HDX Automation Manager as part of the Waters nanoACQUITY UPLC system (Waters Corporation, Milford, MA, USA). The HDX procedure, including the exchange reaction, quench, proteolytic digestion, LC separation, and MS conditions are detailed in the SI.

A 3.0 µL aliquot of native or stressed rituximab sample was diluted into 57.0 µL D_2O buffer and allowed to exchange for various lengths of time ranging from 10 s to 24 h at 10 °C. At the end of each exchange period, the reaction was quenched by mixing the sample with a quenching buffer (1:1, v/v) that contained 4 M GnHCl, 0.5 M TCEP, and 200 mM Na_2PO_4 in water (pH = 2.5) at 1 °C for 5 min. After the quench step, the sample was transferred and injected into the Waters ACQUITY UPLC System.

2.2.7. LC/MS of HDX samples

Online digestion was performed using a Waters ENZYMATE immobilized pepsin column (ID: 2.1 length: 30 mm) at high pressure (~11000 psi) and 10 °C. The proteolytic peptides were collected by a trap column (HSS T3 pre-column, 100 Å, 1.8 µm, 2.1 mm X 5 mm, Waters) for 4.5 min at 0 °C. Then, trapped peptides were eluted into a Waters ACQUITY C18 column (2.1 x 50 mm, 1.8 µm). The LC separation was conducted using binary solvent system; solvent A was water with 0.1% formic acid at pH 2.5, and solvent B was acetonitrile with 0.1% formic acid. The separation was carried out at 0 °C with a linear gradient that was increased from 5% B to 35% B over 7 min. The column was then washed by increasing from 35% B to 85% B in 1 min at a flow rate of 40 µL/min. The

eluent was then directed into a Waters SYNAPT G2Si mass spectrometer for analysis in MS^E mode over the m/z range of 50-2000.

2.2.8. HDX Data Analysis

The deuterium uptake level of each measured peptide at different exchange time points was automatically calculated using the Waters DynamX 3.0 software. Each peptide was manually inspected. Sequence coverage is >80% for all conditions. Averaged values from triplicate experiments with propagated error are reported. The reported deuterium uptake values are not corrected for back-exchange. Back exchange experiments were performed as described previously, and back exchange ranged from 30 to 50% for the measured peptides.[33] The relatively long quench times (i.e. 5 min) and high pressure digestion conditions facilitate protein digestion at the expense of higher back exchange. However, back exchange was still within an acceptable range.[33] Differences in exchange at the peptide level comparing native and heat stressed states were calculated in Excel for peptides that had 4 or more time points in at least 2 trials. Peptides were found to be statistically different if they were 3σ outside of the average of all differences for all time points and for all peptides. For the 45 °C samples, the ΔD that indicated significant difference was found to be 0.21 Da. For 55 °C, the value was 0.30 Da, and for 65 °C it was 0.46 Da. Peptides were further validated as significant by calculating their deuterium uptake change on a per residue basis (ΔD / # of exchangeable residues in peptide), with peptides being considered significantly different if they were 3σ outside the average of the per residue change. The peptides that were significantly different by absolute difference in deuterium uptake and per residue difference in deuterium uptake were consistent with each other for 45 °C and 55 °C; however, for the

65 °C data, some peptides that were found to be different by absolute value were not significantly different on a per residue basis. These peptides were still considered different, as no peptide was significantly different on only a per residue basis. The ion intensities of the peptides that exhibited two different exchange distributions were exported to the program Origin, and multiple peak fitting was used to fit separate Gaussians to each distribution so that the exchange rates could be determined.

2.2.9. Circular Dichroism (CD) Spectroscopy

Far-UV CD analyses were performed on a Jasco J-1500 spectropolarimeter. 200-μL of 1 μM rituximab in 50 mM phosphate buffer at pH 7.4 were transferred to a quartz cuvette. Heated samples were cooled to 37 °C prior to analysis. CD spectra were recorded over a scan range of 250 to 195 nm at room temperature. A scan resolution of 0.5 nm, scan rate of 20 nm/min, band width of 2 nm, and digital integration time of 1 s were used. Measurements were performed in triplicate for each sample. Raw CD outputs (θ, degree) were converted into mean residue ellipticity using the following equation.

$$[\theta]^{\mathrm{MR}}(\text{degree cm}^2\text{dmol}^{-1}) = \frac{100 \times \theta\ (\text{millidegree})}{\mathrm{C}(\text{mol L}^{-1} \times \mathrm{N} \times \mathrm{l}(\text{cm})}$$

where $[\theta]^{MR}$ is mean residue ellipticity in deg cm^2 $dmol^{-1}$, θ is raw signal output in mdeg, C is rituximab concentration in molarity, N is the number of amino acid residues, and l is path length of the cuvette in cm.

2.2.10. Dynamic Light Scattering (DLS)

Hydrodynamic radii of native and stressed rituximab were measured using a Malvern Zetasizer ZSP DLS system. 1 mL of a 1 μM rituximab sample in 50 mM phosphate buffer, at pH 7.4, and room temperature was placed in a plastic cuvette. Back scattering was detected at a measurement angle of 173^{O}, and volume particle size distribution of the sample was recorded. Measurements were performed in quintuplicate at room temperature. Measurement duration was set to automatic mode.

2.2.11. Size-Exclusion Chromatography (SEC)

SEC separation of rituximab after heating was performed at room temperature on an Agilent 1260 Infinity HPLC system using a TSKgel SuperSW3000 column (30 cm x 7.8 mm ID, 5 μm particle size; Tosoh Bioscience LLC). 50 μg of rituximab diluted to 1 mg/mL in 50 mM phosphate buffer at pH 8.0 was loaded on the SEC column. The mobile phase used was 50 mM sodium phosphate, 400 mM sodium perchlorate, and 10% isopropanol, at pH 6.5. An isocratic flow rate of 0.5 mL/min was used. The variable wavelength UV detector was set at 280 nm for detection.

2.2.12. Alamar Blue Assay

Rituximab samples were incubated at the desired temperatures prior to analysis. The conditions used for this assay were derived from Zhang et al. [34] In brief, Raji cells (ATCC CLL-86) were grown in a T75 flask using RPMI media supplemented with fetal bovine serum. Once confluent, cells were washed with phosphate-buffered saline (PBS) and diluted to 1 x 10^6 cells/mL in RPMI media. 10 μL of control or heat-treated rituximab (4 ng/mL) in RPMI media was added to 90 μL of cells in a 96-well plate.

Plates were incubated for 30 min at 37 °C, then each well was supplemented with 10% Invitrogen™ normal human serum (#31876, Thermo Fisher Scientific). Plates were returned to 37 °C for 4 h. Then 11 µL of Invitrogen™ Alamar Blue reagent (#DAL1025, Thermo Fisher Scientific) were added and fluorescence signals were read after 1 h using an excitation wavelength of 560 nm and emission of 590 nm. Data were collected using a Synergy H1 microplate reader (BioTek) and exported to Microsoft Excel for analysis. Triplicate measurements were performed on each sample, and independently generated to confirm trends were the same.

2.2.13. Rituximab bridging ELISA

Custom rituximab ELISA plates were generated as previously described in Cragg et al.[35] and Hampson et al.[36] with some alterations. In brief, antihuman capture antibody (clone SB2H2 recognizing the Fc region of human antibody, #MCA2531, Biorad) was diluted 1 to 1000 in coating buffer (15 mM sodium carbonate, 28.5 mM sodium bicarbonate, pH 9.6), and 100 µL was added to each well of a 96-well NUNC MaxiSorp flat-bottom plate (#44-2404-21, Thermo Fisher Scientific). Plates were incubated at 4 °C overnight, then blocked with 200 µL of 1% bovine serum albumin in PBS for 2 h. Prior to use plates were washed three times with PBS containing Tween® 20 (PBST). For the rituximab standard curve generation and quantitation, samples were diluted in PBST at the concentrations indicated (1 to 500 ng/mL rituximab). 10 ng/mL rituximab was used for the binding assay. Prior to an analysis, rituximab samples were incubated at different temperatures. 100 µL of sample was added to each well and incubated at room temperature for 1 h. Wells were then washed with PBST five times. Horseradish peroxidase (HRP)-labeled anti-rituximab detection antibody (clone MB2A4 anti-idiotypic

antibody, #MCA2260P, Bio-Rad) was added at a 1:60,000 dilution in blocking buffer. Samples were incubated for 90 minutes, then washed with PBST five times. Plates were then developed for 45 min using 100 μL of HRP substrate, and the developing was stopped with the addition of 50 μL of 3 M sulfuric acid. Data was collected on a Synergy H1 microplate reader (BioTex) measuring absorbance at 450 nm and normalized against the absorbance at 630 nm to correct for background signal. The results were exported to Microsoft Excel for analysis. Each sample was generated in triplicate independently.

2.2.14. Raji Cell Pull-Down Assay

Rituximab samples were preheated at the desired temperatures. Control and heat-treated rituximab were diluted to 200 ng/mL in PBS and mixed 1:1 with either Raji cells (1 x 106 cells/mL) in PBS or PBS alone as a control for a final concentration of 100 ng/mL. Free rituximab was quantified using the ELISA plates and normalized against the control wells. Absolute quantitation was performed using standard curves generated from each heat-treated sample independently to confirm quantitation was in the linear part of the standard curve.

2.3. Results

2.3.1. Heat stress at 45°C for 4 h

HDX and DEPC-CL with MS detection were used to identify any HOS changes experienced by rituximab after heat stress. Each heavy chain/light chain dimer of rituximab contains 236 total His, Lys, Tyr, Thr, and Ser residues that can be labeled by DEPC (**Table B.1**). After heating the protein at 45 °C for 4 h and then reacting it with DEPC, we find 154 residues are labeled, but only 17 undergo a significant change in

labeling extent in comparison to the unheated (i.e. 37 °C) state (**Table 2.1**). These 17 residues are scattered throughout the protein and do not cluster in any one location (**Figure 2.1A**). Moreover, 12 of these 17 residues are Ser, Thr, and Tyr, whose CL reactivity with DEPC is influenced by the microenvironment around these residues,[24] suggesting the changes in reactivity are primarily due to the re-orientation of these side chains. The majority of the remaining five Lys and His residues that undergo changes are found to increase in labeling, which is consistent with mild heating leading to minor structural changes in some protein molecules that cause higher solvent exposure of these residues. These minor structural changes, however, do not cause any significant changes in HDX between the 45 °C heated and native states (**Figure 2.1B** and **Figure *2.2*).** Importantly, three of the 87 peptides used for the HDX/MS analysis exhibit two exchange distributions in both the stressed and the native state, indicating that at least two different conformations of rituximab exist in solution (**Figure 2.3**). However, these three peptides do not show any significant difference between the 45 °C stressed and native conditions. Additionally, activity and biophysical assays show no significant change in rituximab upon heating at 45 °C for 4 h (**Figure 2.4Figure 2.5**). Overall, it appears that the structure of rituximab is not significantly altered after 4 h of heat stress at 45 °C.

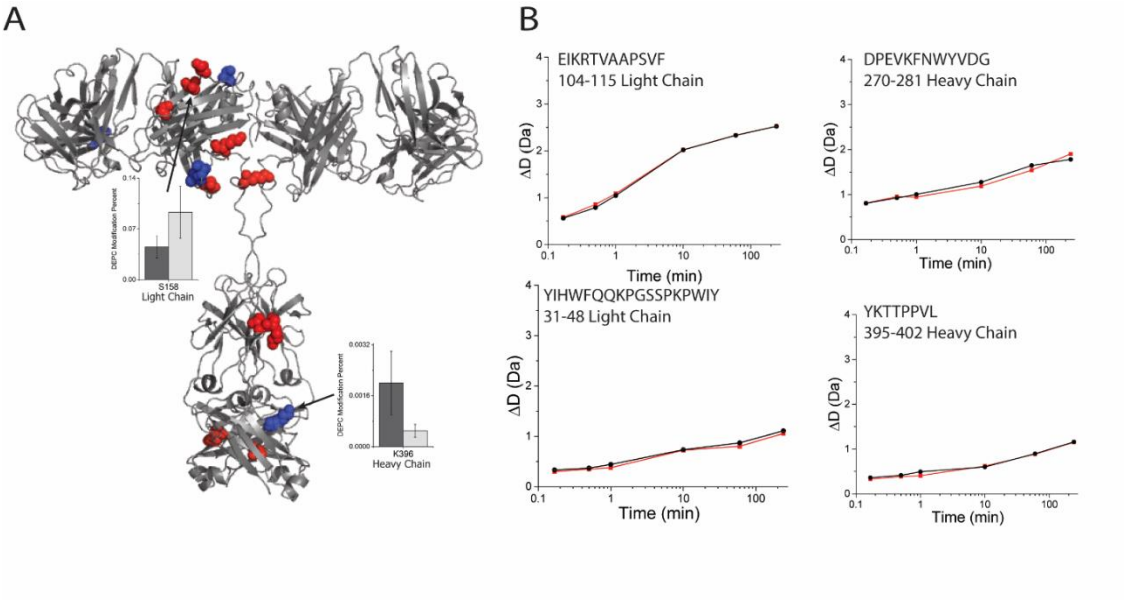

Figure 2.1: DEPC CL/MS and HDX/MS results of heat stressed (4 h at 45 °C) rituximab. (A) DEPC CL changes. Residues depicted in red represent increases in CL extent while residues in blue represent decreases in CL extent. Representative plots of change in labeling extent are shown for residues Ser158 and Lys396. Dark gray indicates the native state while the light gray indicates the heat stressed state. Changes are scattered throughout the entire protein with no clustering, which indicates a lack of substantial HOS changes. Atomic coordinates of an existing IgG1 F_{ab} crystal structure (PDB 1FC2) and a generic IgG1 F_c crystal structure (PDB 2IG2) were used as templates to generate the rituximab structure, with the hinge region theoretically modeled.[37] The F_c (PDB 4W4N) and F_{ab} (PDB 4KAQ) structures of rituximab were then aligned to the template, using the molecular visualization system PyMOL. For clarity, CL on only one light chain and one heavy chain are indicated. (B) Representative deuterium uptake plots from HDX/MS of rituximab after heating at 45 °C. The unheated state is shown in black, and the heat-stressed state is shown in red. No measurable difference in deuterium uptake is observed.

Light Chain

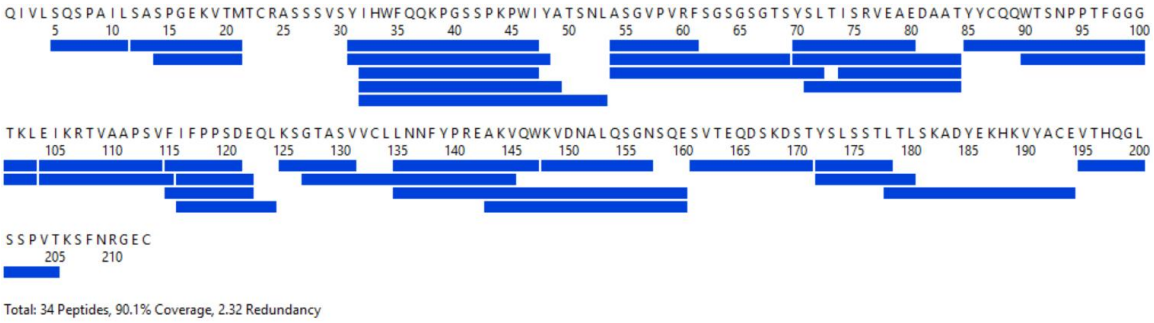

Heavy Chain

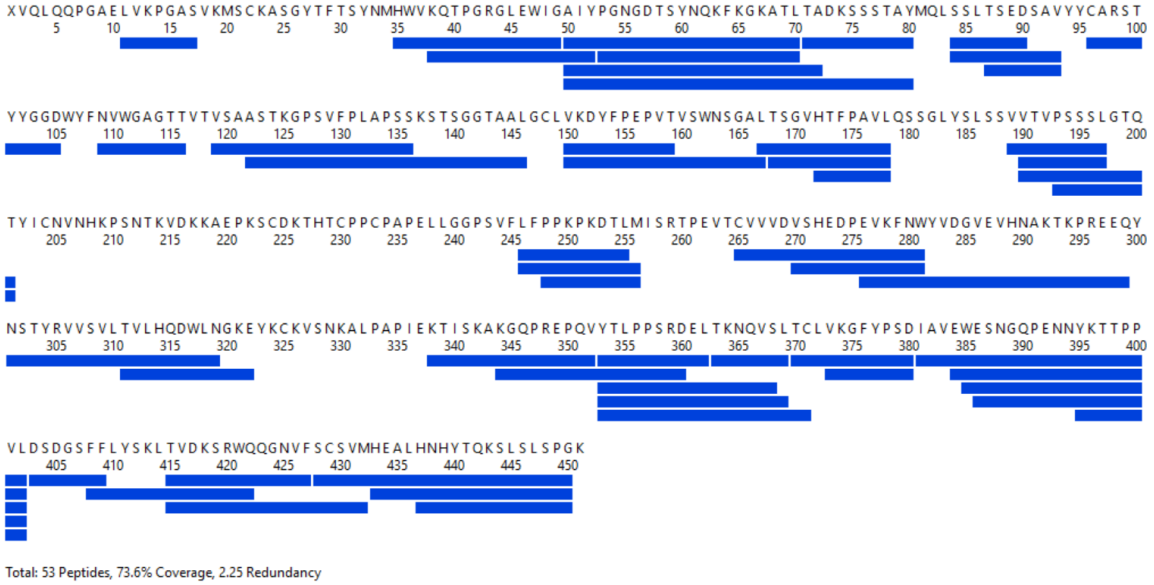

Figure 2.2: Sequence coverage for HDX/MS analysis at 45 °C heat stress. Peptides included in our analysis appear in both stressed and native samples in at least two of three trials that were conducted. Coverage for trials 1, 2, and 3, were 91.5%, 90.1% and 93.5% for the light chain, and 81.8%, 78.0%, and 79.5% for the heavy chain, respectively. Region 202-245 in the heavy chain lacks coverage. This region spans the hinge region of the antibody and contains two disulfide bonds which could result in lower digestion efficiency. However, since there was no detectable difference in any peptide from the 45 °C stress condition to the native condition, we do not believe this region would have provided any more insight into our HDX data interpretation.

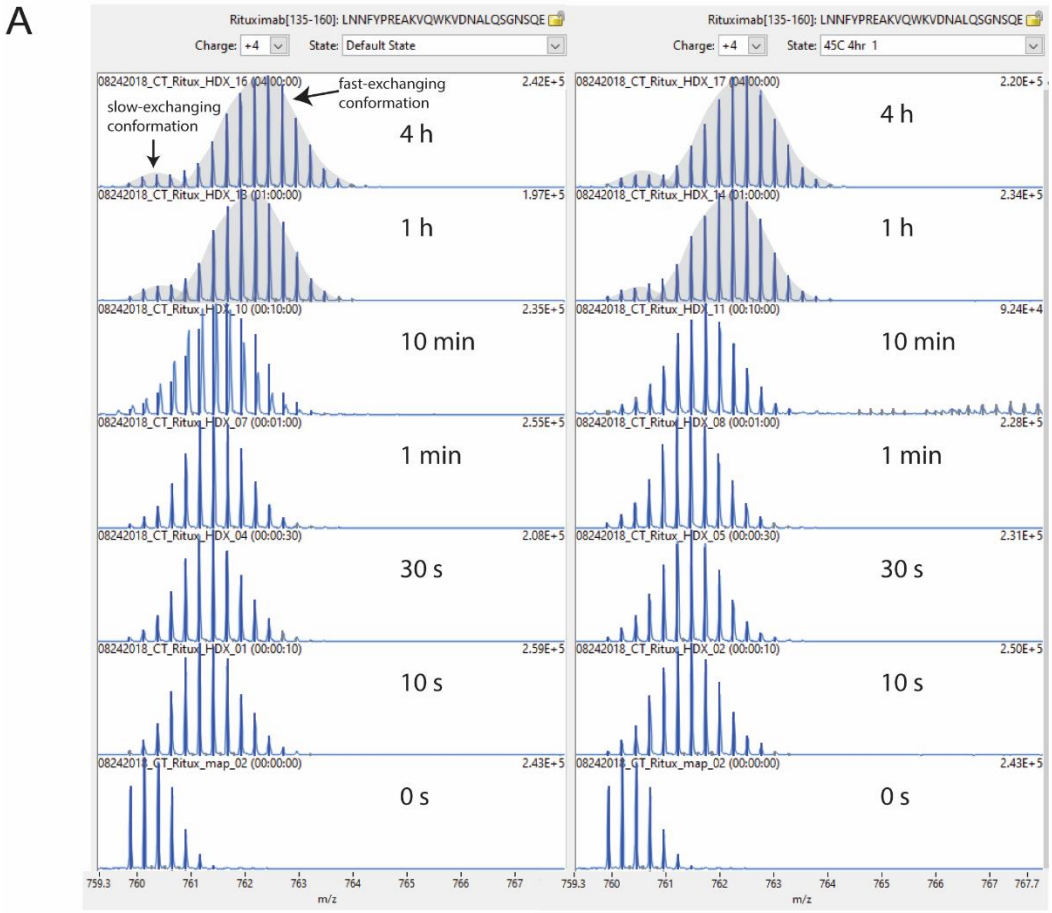

Figure 2.3: Mass spectra for the HDX over time of the peptide 135-160 after heating rituximab to 45 °C. (A) Stacked spectral plots of the +4 charge state with the native condition on the left and the heat-stressed condition on the right. The 1- and 4-h time points demonstrate two distinct exchange distributions, one a fast-exchanging conformation and the other a slow-exchanging conformation.

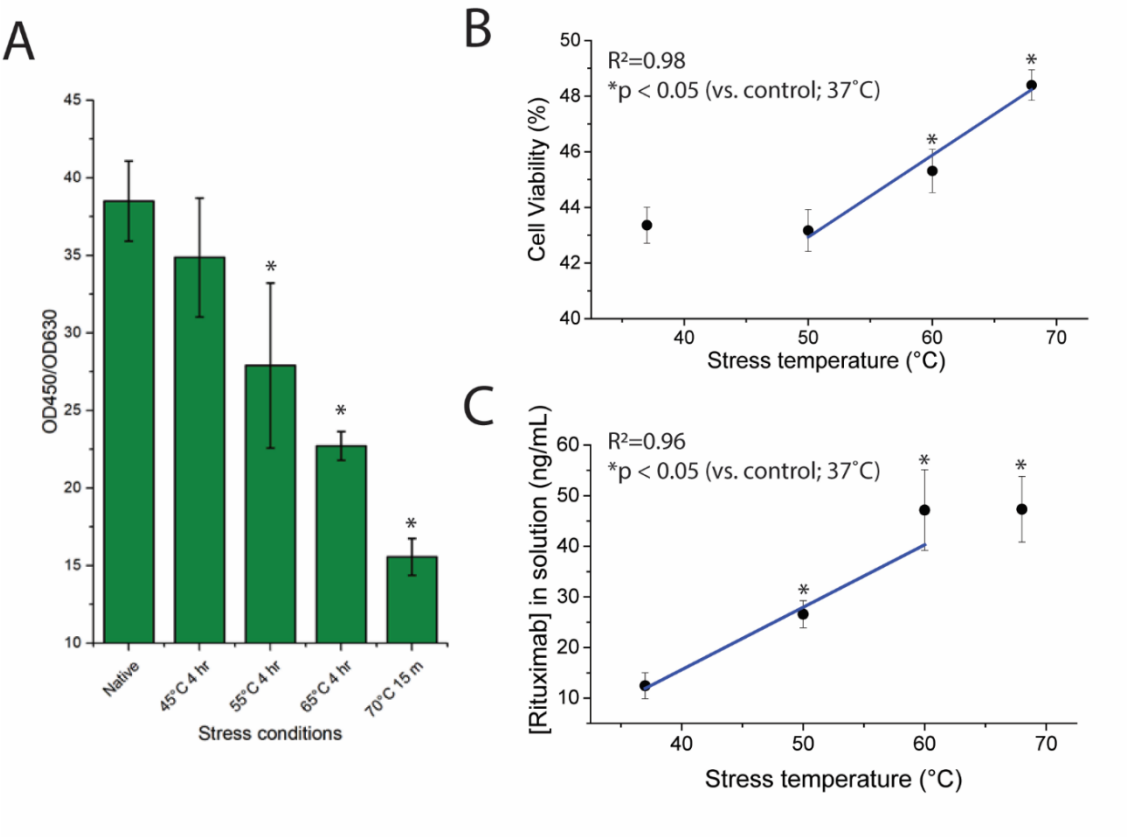

Figure 2.4: Activity assay data for heat stressed rituximab. Structural perturbations in the F_c region are assessed by (A) a bridging ELISA that measures rituximab F_c binding to a capture antibody and (B) an Alamar blue assay that measures complement dependent cytotoxicity (CDC), thereby revealing structural changes in the F_c. Structural integrity of F_{ab} is investigated with (C) a Raji cell pull-down assay that measures F_{ab} binding to CD-20 antigen on B cells. Each assay was performed in triplicate (n=3). The means of the stressed vs. controlled were compared for each heat stress condition using student t-test at 95% confidence level.

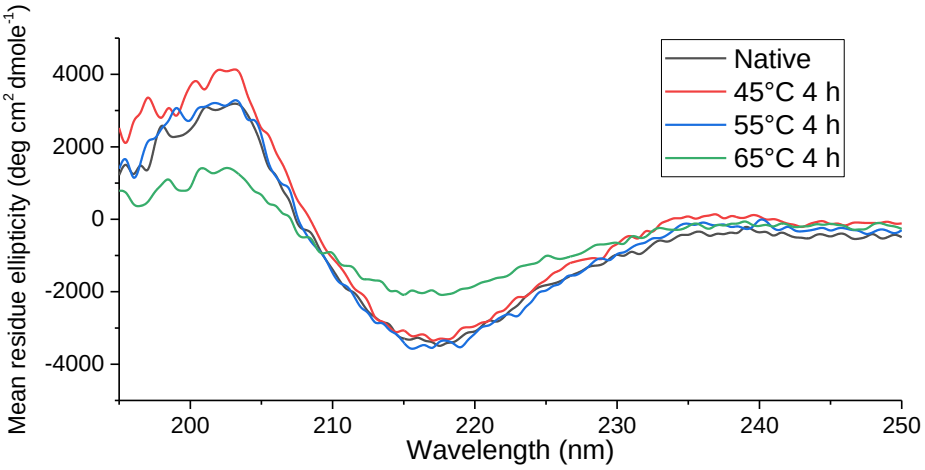

Figure 2.5: Far-UV circular dichroism (CD) spectroscopy characterization of rituximab at 37°C (native, black) and thermally-stressed conditions, after incubation of the rituximab formulation at 45°C for 4 h (red), 55°C for 4 h (blue), and 65°C for 4 h (green). The nearly identical overlap of the spectra of the native and 45°C and 55°C heat-stressed samples indicate that CD is insensitive to any structural changes in rituximab upon heating at the lower temperatures. CD is able to detect structural changes at 65°C; however, CD cannot localize where these changes take place.

Table 2.1: Table of significant changes in DEPC labeling extent under different heat-stress conditions.

Residue	Native	Stressed
45 °C for 4 h		
Light chain		
Ser155	5 ± 2%	9 ± 4%
Ser158	5 ± 2%	9 ± 4%
Ser161	5 ± 2%	9 ± 4%
Ser181	1.0 ± 0.5%	0.31 ± 0.06%
Heavy chain		
Ser76	26 ± 7%	6 ± 4%
Ser77	14 ± 4%	2 ± 2%
Lys137	0.05 ± 0.02%	0.2 ± 0.1%
Ser140	0.3 ± 0.2%	0.06 ± 0.03%
Thr143	0.3 ± 0.2%	0.07 ± 0.04%
Ser194	0.04 ± 0.02%	0.2 ± 0.1%
Lys226	40 ± 10%	73 ± 20%
Thr293	7 ± 3%	20 ± 10%
Lys294	7 ± 3%	20 ± 10%
Thr370	8 ± 1%	14 ± 4%
Lys374	8 ± 1%	14 ± 4%
Lys396	0.2 ± 0.1%	0.05 ± 0.02%
Ser448	17 ± 2%	26 ± 4%
55 °C for 4 h		
Residue	**Native**	**Stressed**
Light chain		
Thr20	17 ± 4%	8 ± 2%
His33	0.08 ± 0.02%	0.20 ± 0.02%
Lys44	0.06 ± 0.02%	0.15 ± 0.01%
Thr73	50 ± 10%	86 ± 3%
Ser75	50 ± 10%	86 ± 3%
Thr84	1.3 ± 0.2%	2.6 ± 0.5%
Tyr85	1.3 ± 0.2%	2.6 ± 0.5%
Thr91	0.03 ± 0.02%	0.10 ± 0.01%
Thr128	5 ± 1%	3.1 ± 0.3%
Ser130	5 ± 1%	3.1 ± 0.3%
Tyr185	23.5 ± 0.3%	27 ± 2%
His188	55 ± 2%	64 ± 3%
Heavy Chain		
Lys13	2.7 ± 0.5%	3.7 ± 0.3%
Ser21	24 ± 4%	11 ± 4%
His35	23 ± 3%	4 ± 1%
Lys38	30 ± 2%	22 ± 3%
Lys74	79 ± 4%	87 ± 1%

Ser76	2.4 ± 0.2%	1.5 ± 0.2%
Thr118	71 ± 3%	59 ± 7%
Ser120	84 ± 2%	70 ± 7%
Ser164	0.002 ± 0.001%	0.016 ± 0.005%
Lys226	33 ± 7%	72 ± 5%
Thr293	38 ± 6%	85 ± 8%
Ser302	38 ± 3%	16 ± 6%
Tyr353	0.4 ± 0.6%	14 ± 2%
Thr363	0.006 ± 0.002%	0.012 ± 0.003%
Ser368	0.02 ± 0.02%	0.18 ± 0.01%
Ser407	15 ± 4%	30 ± 6%
Tyr411	7 ± 5%	20 ± 4%
Ser448	70 ± 10%	92 ± 4%
Lys451	40 ± 30%	79 ± 7%
65 °C for 4 h		
Residue	**Native**	**Stressed**
Light chain		
Ser5	0.03 ± 0.01%	0.01 ± 0.01%
Tyr70	14 ± 5%	2 ± 2 %
Thr101	0.18 ± 0.01%	0.07 ± 0.05%
His197	0.11 ± 0.03%	0.6 ± 0.2%
Heavy Chain		
His35	23 ± 3%	11 ± 3%
Lys67	23 ± 7%	70 ± 20%
Lys74	79 ± 4%	52 ± 8%
Ser77	0.01 ± 0.01%	0.03 ± 0.01%
Thr118	71 ± 3%	55 ± 5%
Ser120	84 ± 2%	69 ± 4%
Ser161	1.8 ± 0.2%	1.2 ± 0.2%
Ser196	0.01 ± 0.00%	0.08 ± 0.02%
Thr199	0.01 ± 0.00%	0.05 ± 0.02%
His208	0 ± 0%	0.04 ± 0.01%
Ser211	0 ± 0%	0.21 ± 0.02%
Ser258	5 ± 2%	1 ± 1%
Ser302	38 ± 3%	10 ± 10%
Thr363	0.006 ± 0.002%	0.002 ± 0.001%
Ser428	0.86 ± 0.08%	0.4 ± 0.2%
His439	5.4 ± 0.9%	2.5 ± 0.3%
Tyr440	0.02 ± 0.01%	0.01 ± 0.01%
Lys451	40 ± 20%	5 ± 5%

2.3.2. Heat stress at 55 °C for 4 h

After heating rituximab at 55 °C for 4 h, changes in DEPC CL (

Table *B.2*) are primarily clustered in the F_{ab} region, with scattered CL increases in the F_c region (**Figure 2.6A**). Out of the 236 labelable residues, 133 are labeled, while 31 undergo a significant change in labeling extent upon heat stress. Like the 45 °C heat stress condition, the majority (70%) of residues that undergo CL changes are Ser, Thr, and Tyr residues (

Table *B.2*). Most of the remaining His and Lys residues that change in labeling undergo increased CL, which one would expect upon heating, as some protein molecules partially unfold and have increased side chain solvent accessibility. The His and Lys residues that have increased CL mostly reside in the F_{ab} and hinge regions. HDX/MS data show that one region of the protein, 148-171, in the C_L domain undergoes increased deuterium uptake (**Figure 2.2B andFigure *2.7***). The differences in deuterium uptake of this peptide disappears after 24 h of exchange. Identical deuterium exchange after 24 h, while having differential uptake at shorter exchange times (i.e. 1 and 4 h), is consistent with increases in protein dynamics, which likely occur upon protein heating.

Closer inspection of the HDX data reveals that eight out of the 80 peptides are found to have two exchange distributions, again suggesting two conformations in solution. Three of these peptides come from the C-terminal end of the light chain, four come from the C-terminal end of the heavy chain, and one is from the middle of the C_{H1} domain. These two distributions can be separated into "slow exchangers" and "fast exchangers" (**Figure 2.8Figure 2.9**), yet we find no significant differences between the slow and fast exchangers for these peptides upon comparing the native and 55 °C stress states. So, even if new protein conformations are populated in these regions upon heating at 55 °C, they are not readily resolvable by HDX/MS. Only the region spanned by 148-171 in the C_L domain undergoes a significant change in exchange. The change in HDX in this one location and the changes in DEPC labeling extent are supported by activity assays that show significant changes in F_{ab} activity. The activity assay results for the F_c region are somewhat ambiguous (**Figure 2.4**), and circular dichroism spectroscopy is insensitive to these changes at 55 °C (**Figure 2.5**).

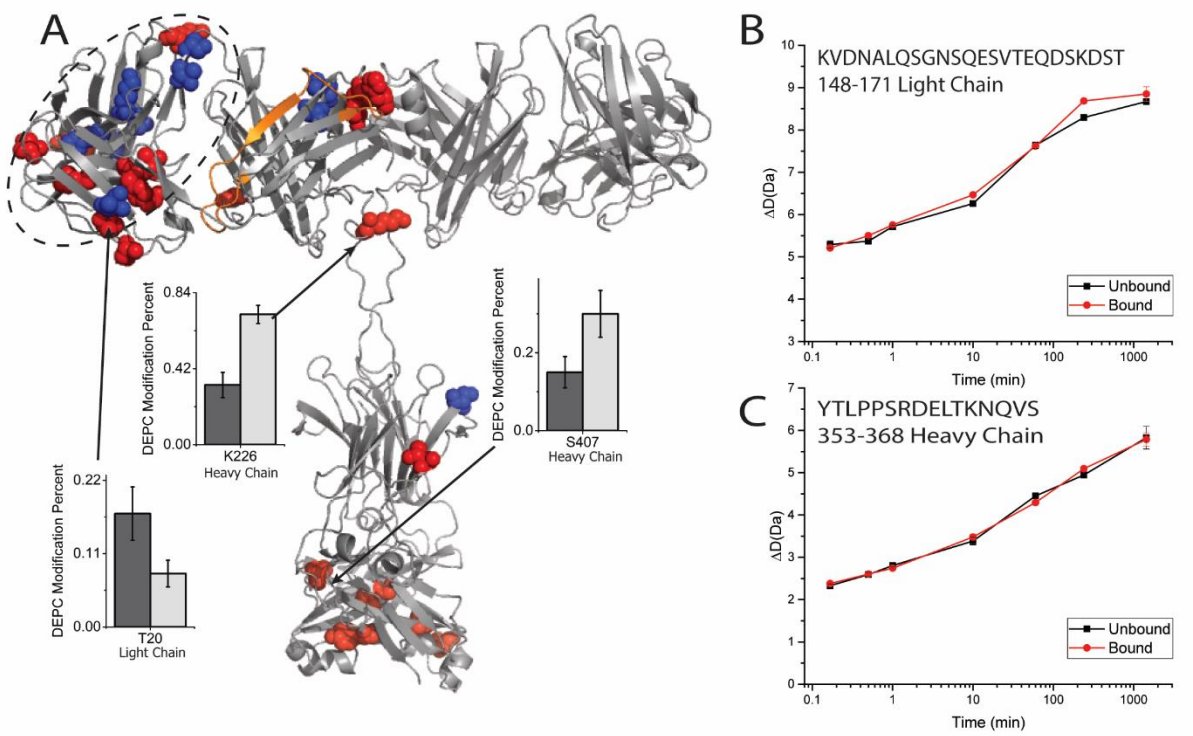

Figure 2.6: DEPC CL/MS and HDX/MS of heat stressed (4 h at 55 °C) rituximab. (A) DEPC CL and HDX changes. Residues depicted in red represent increases in CL extent while residues in blue represent decreases in CL extent. Residues that undergo changes in CL extent are clustered in the F_{ab} (circled with a dotted black line). Representative plots of CL/MS changes in labeling extent are shown for residues Lys226, Thr20, and Ser407. Dark gray indicates the native state while the light gray indicates the heat stressed state. Highlighted in orange on the structure is the peptide that undergoes increased HDX. Details of the molecular model of rituximab are found in the Figure 2.1 caption. For clarity, only labeling on one heavy chain and one light chain is shown. (B) Deuterium uptake plot from HDX/MS of rituximab after heating at 55 °C for peptide 148-171 that experiences a significant change in uptake. The unheated state is in black, and the heat-stressed state is shown in red. (C) Representative deuterium uptake plot from HDX/MS of rituximab after heating at 55 °C for peptide 353-368 that does not experience a significant change in uptake. The unheated state is in black, and the heat-stressed state is shown in red. Peptides were found to be statistically different if they were 3σ outside of the average of all differences for all time points and for all peptides.

Light chain

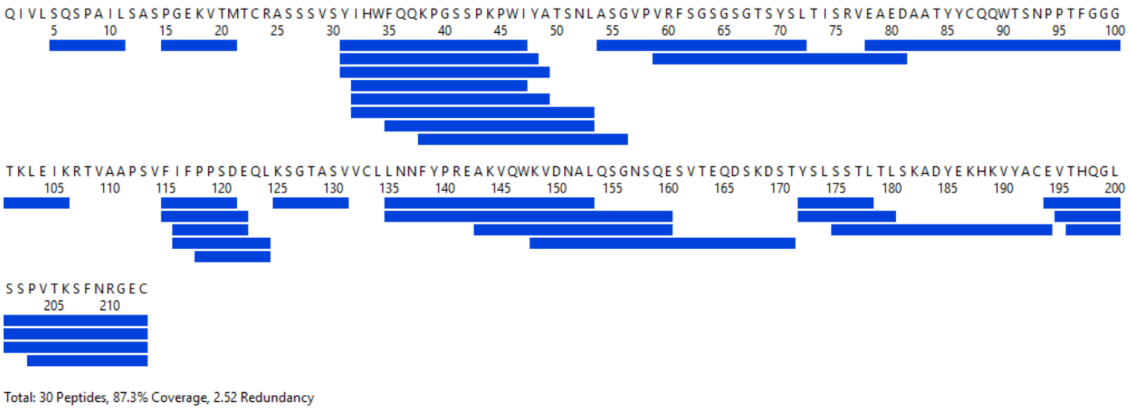

Heavy chain

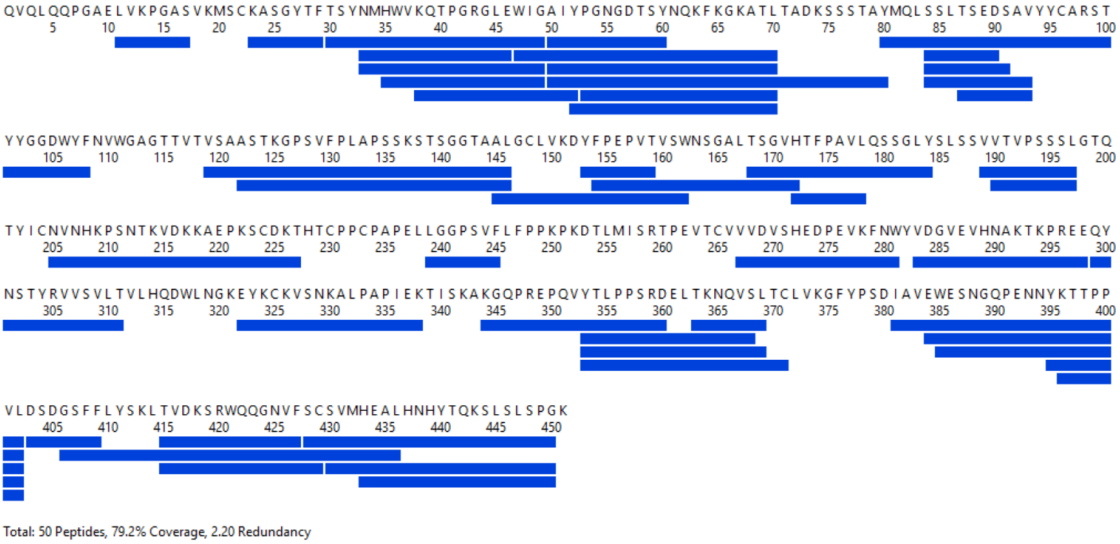

Figure 2.7: Sequence coverage for HDX/MS analysis at 55 °C heat stress. Peptides included in our analysis appear in both stressed and native samples in at least two of three trials that were conducted. Coverage for trials 1, 2, and 3, were 96.2%, 90.6% and 89.7% for the light chain, and 77.3%%, 89.6%, and 91.4% for the heavy chain, respectively.

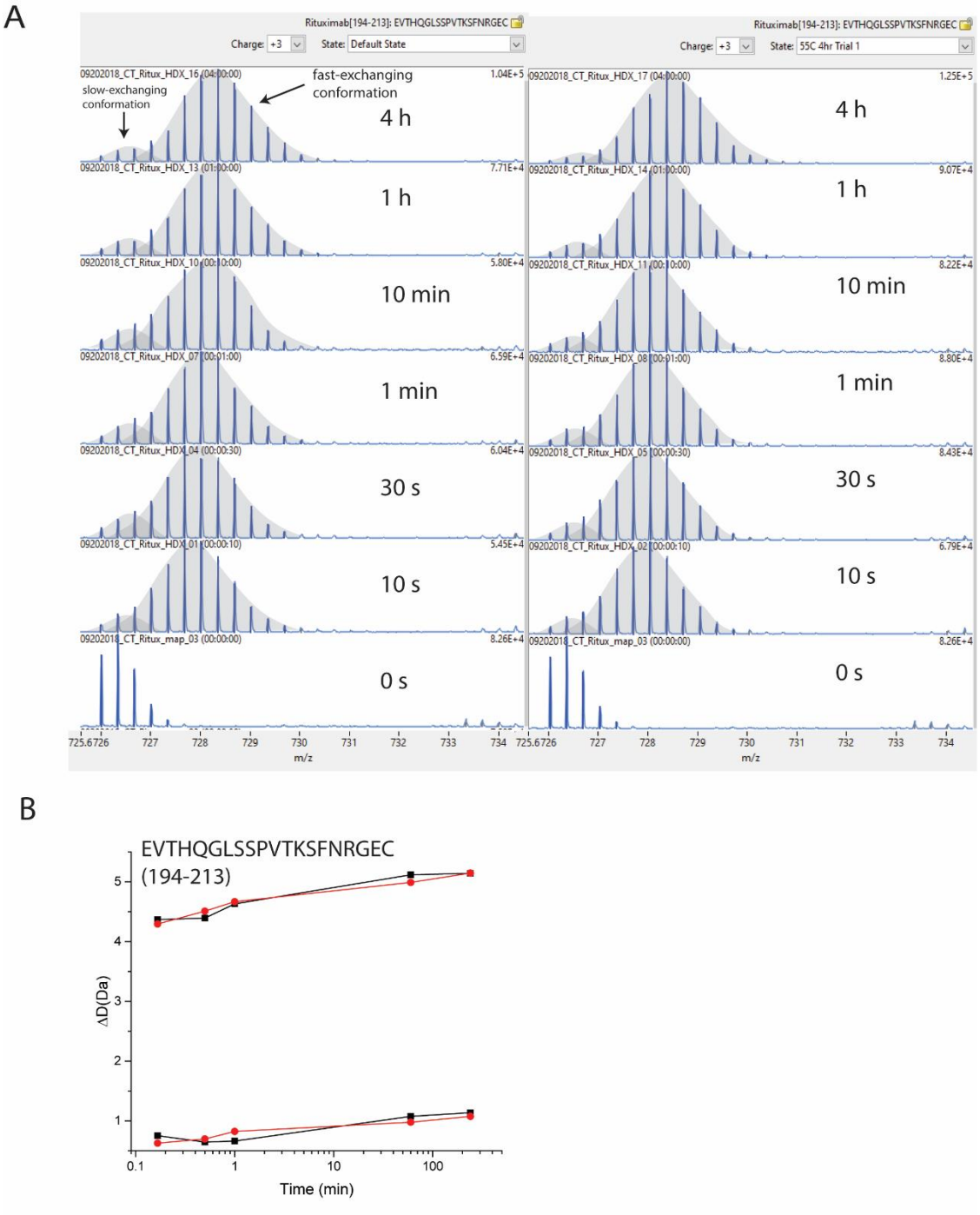

Figure 2.8: Mass spectra for the HDX over time of peptide 194-213 after heating rituximab to 55 °C. (A) Stacked spectral plots for +3 charge state of C-terminal peptide 194-213 with the native condition on the left and heat-stressed state on the right. All time points have two distinct exchange distributions, one a fast-exchanging conformation and the other a slow-exchanging conformation. In this case the fast-exchanging conformation is significantly more intense than the slow-exchanging conformation (B) Deuterium uptake plot for fast and slow exchanging conformations. The stressed state is depicted in red and the native state in black.

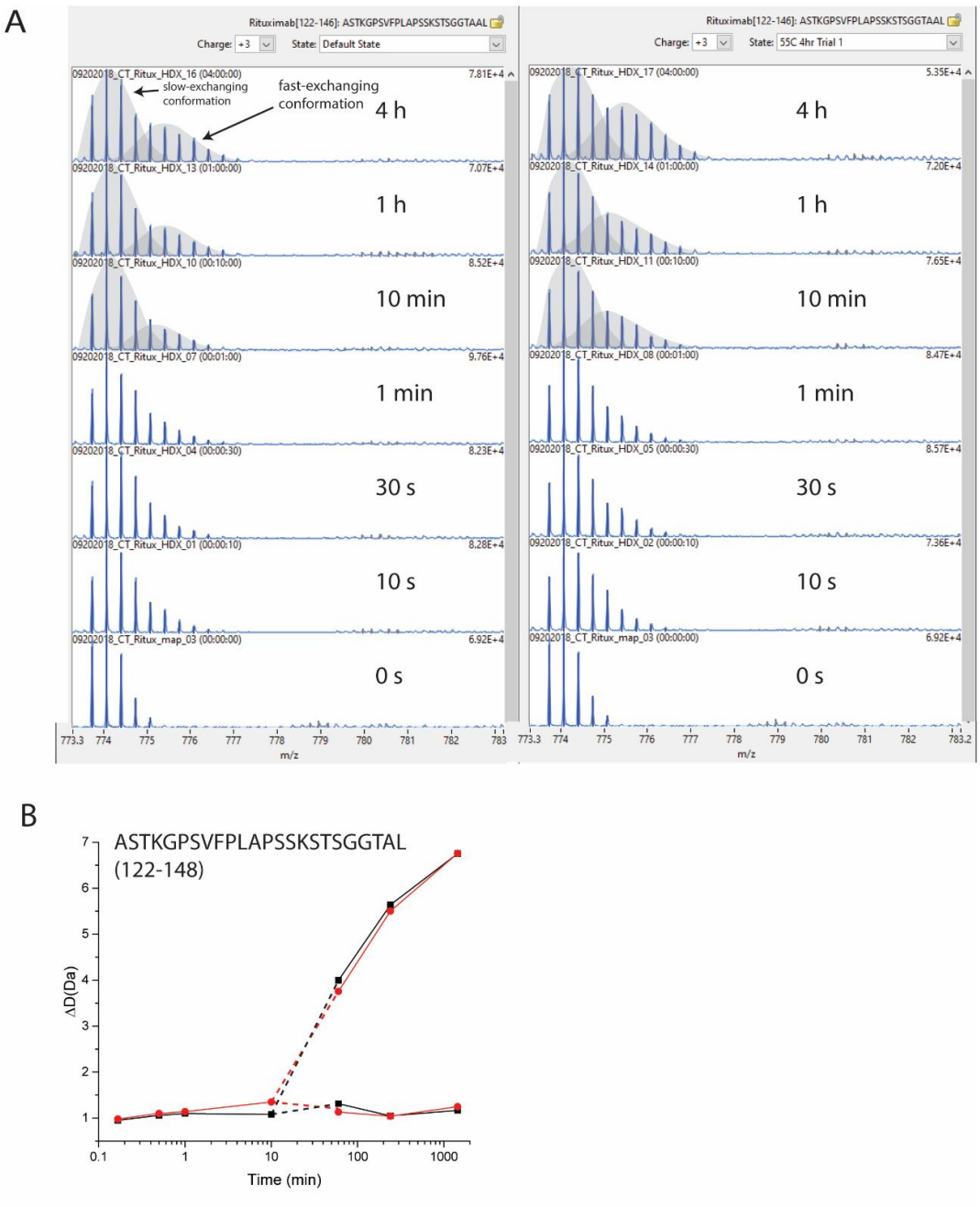

Figure 2.9: Mass spectra for the HDX over time of peptide 122-148 after heating rituximab to 55 °C. (A) Stacked spectral plots for +3 charge state of peptide 122-148 with the native condition on the left and heat- stressed condition on the right. In this case the slow-exchanging conformation is significantly more intense than the fast-exchanging conformation (B) Deuterium uptake plot for fast and slow exchanging conformations. The stressed state is depicted in red and the native state in black. The two different distributions are indistinguishable until 1 h of incubation time, and thus, time points 10 s, 30 s, 1 min, and 10 min are a combined for both conformations with a bias towards the slow-exchanging conformation as that conformation is more abundant.

2.3.3. Heat stress at 65 °C for 4 h

After heating rituximab at 65 °C for 4 h, significant structural changes are apparent from both DEPC CL/MS (**Table B.3**) and HDX/MS results. Visually, the solution becomes cloudy, which is indicative of protein aggregation, but this cloudiness mostly disappears upon dilution for the labeling experiments. Moreover, dynamic light scattering and size-exclusion chromatography experiments reveal the existence of larger molecules in solution, further confirming aggregation (**Figure 2.11**). Because the measured sequence coverage is comparable for the 45 °C, 55 °C, and 65 °C experiments, we do not feel that the observed aggregation has affected our results significantly.

While 65 °C is below the melting temperature of rituximab, the protein was heated at this temperature for 4 h to cause significant structural changes that we expected to be measurable by the two MS techniques.[3882] Significant changes in CL extent are observed for 22 residues, and six peptides are found to undergo significant changes in deuterium uptake. Of the 22 residues, seven increase and 15 decrease in CL, while two of the six peptides increase in HDX and four decrease (**Figure 2.10**). Notably, one of the two peptides that increases in exchange is the same peptide (i.e. 148-171) that increases in exchange when heated at 55 °C, suggesting this part of the protein is prone to unfolding or increased dynamics after heating (**Figure 2.12**).

Additionally, seven of the 128 peptides considered in the HDX analysis have two exchange distributions, indicating multiple conformations (**Figure 2.13Figure 2.14, Figure 2.15**). In two of the seven peptides that display multiple conformations, the slow-exchanging conformation becomes more abundant after heating, which is consistent with these sites becoming buried due to aggregation in a fraction of the protein molecules.

Considering the data overall, the results from CL/MS and HDX/MS are generally consistent with each other (**Table 2.2**). The relatively few increases in CL and deuterium uptake occur in the F_{ab} region, while decreases are measured throughout the protein (**Figure 2.10A and B**). The prevalence of decreased labeling and exchange is expected due to the protein aggregation that occurs at this temperature.

While the CL/MS and HDX/MS results are mostly consistent, a closer inspection of the 65 °C data provides a useful comparison of the information provided by the two techniques. Residues that undergo changes in DEPC labeling are located within regions that have either (i) no coverage by HDX, (ii) no change in HDX, (iii) the opposite change as HDX, or (iv) the same change as HDX (**Table 2.2**). While we have excellent protein sequence coverage (> 80%) in our HDX/MS experiments (**Figure 2.16**), two of the 22 residues that undergo changes in CL are in regions lacking coverage by HDX/MS, making it difficult to compare the data for these residues. Fifteen of the residues that undergo CL changes are in regions with no change in deuterium uptake, with five having increased CL and the other 10 undergoing decreased labeling. The CL decreases are mostly for Ser, Thr, or Tyr residues, which are sensitive to changes in the side chain microenvironment. This inherent sensitivity to changes in microenvironment may explain why CL changes are observed and HDX changes are not. The CL reactivity of Ser, Thr, and Tyr residues is exquisitely sensitive to changes in microenvironment, as is seen in the 45 °C data, whereas more substantial structural changes are necessary to result in measurable changes in HDX/MS.[39]

Table 2.2: Comparison of HDX and CL changes

Covalently labeled residues that fall within peptides that have:	**Sites of CL Increases**		**Sites of CL Decreases**	
	Light Chain	Heavy Chain	Light Chain	Heavy Chain
No Change in HDX	His197	Lys 67, Ser196, Thr199, His208	Ser5, Tyr70,	His35, Lys74, Thr118, Ser120, Ser161, Ser258, Ser302, Thr363
Opposite change as HDX	None		Thr101	None
Same change as HDX	None		None	Ser428, His439, Tyr440, Lys451
No HDX coverage	None	Ser77, Ser211	None	

Only one residue, Thr101, undergoes a change in CL that appears to be the opposite of the HDX results. Thr101 undergoes decreased CL and is located in a peptide (94-103) in the heavy chain that increases in deuterium uptake after heating. Two other residues in the protein region spanned by this peptide are also covalently labeled, but their CL changes are statistically insignificant (i.e. Thr96 [2.0 ± 0.6% to 4 ± 2%] and Lys102 [0.08 ± 0.02% to 0.04 ± 0.02%], see **Table B.3**). The CL increase for Thr96 might be consistent with the HDX increase in this protein region, but the poor measurement precision for this residue does not allow us to draw this conclusion with confidence.

Finally, four residues undergo CL changes that are consistent with the HDX results. Ser428, His439, Tyr440, and Lys451 undergo a decrease in CL after heating at 65 °C, and a peptide measured by HDX/MS that spans this region of the heavy chain (428-450) also undergoes a decrease in deuterium uptake. This peptide exhibits both slow and fast-exchanging distributions in the native and heat-stressed states. Interestingly, only the slow-exchanging distribution decreases in exchange in the stressed state, while the fast-exchanging distribution increases in exchange in the stressed state. Furthermore, this 28-

residue region of the protein contains nine residues that are covalently labeled (**Table B.3**). Unlike Ser428, His439, Tyr440, and Lys451, five residues (Ser430, His433, His437, Lys443, and Ser448) do not undergo statistically significant changes in labeling. These observations point to a mixture of conformations and some complex structural changes to this region of the protein.

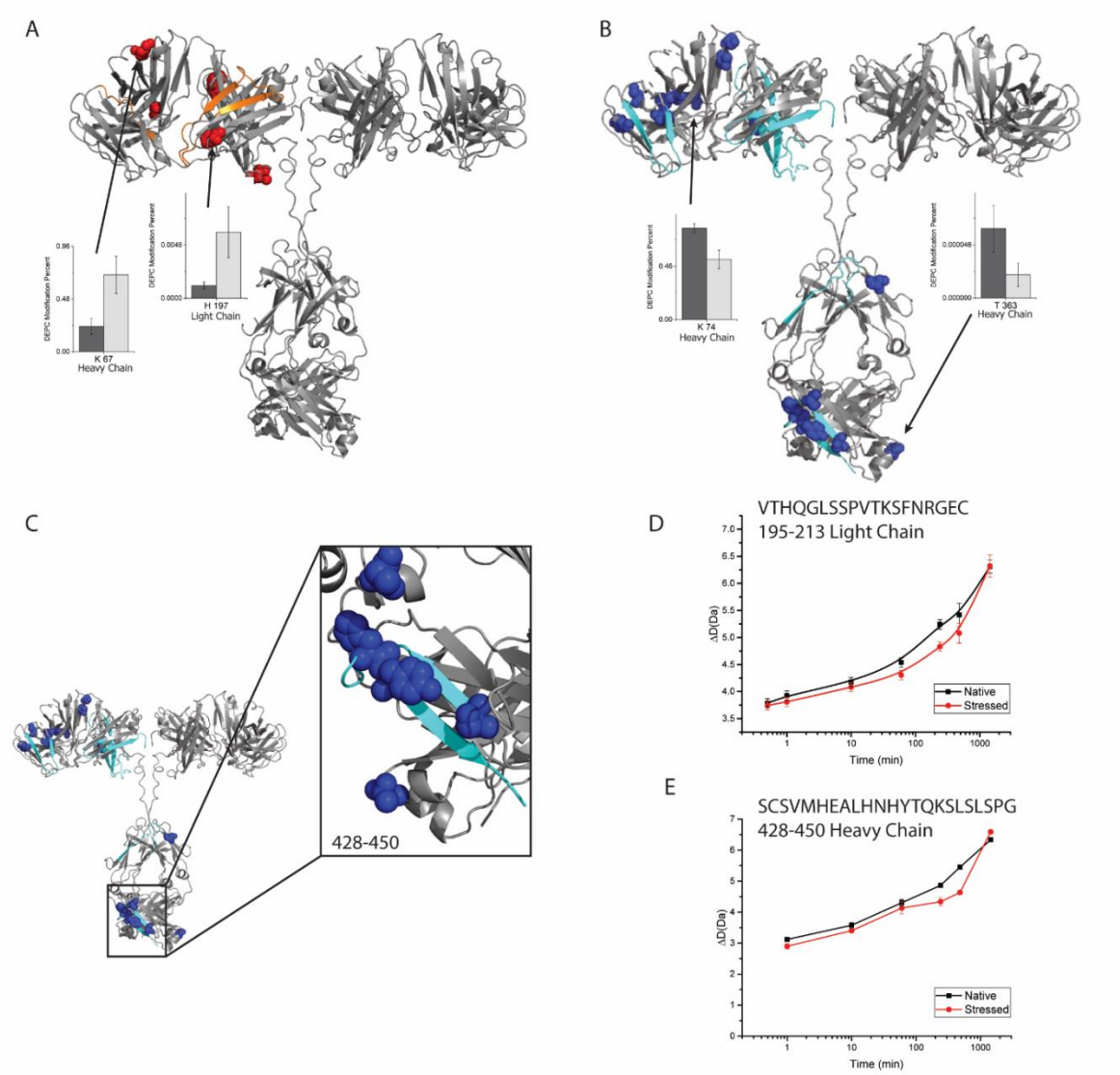

Figure 2.10: DEPC CL/MS and HDX/MS of heat stressed (4 h at 65 °C) rituximab. (A) Increases in DEPC CL extent and HDX uptake. Residues depicted in red represent increases in CL extent while peptides highlighted in orange represent increases in deuterium uptake. Representative plots of change in labeling extent are shown for residues Lys67 and His197. Dark gray indicates the native state while the light gray indicates the heat stressed state. (B) DEPC CL/MS and HDX/MS decreases. Residues depicted in blue represent increases in CL extent while peptides highlighted in cyan represent increases in deuterium uptake. Representative plots of change in labeling extent are shown for residues Lys74 and Thr363. Dark gray indicates the native state while the light gray indicates the heat stressed state. (C) Expanded view of the C_{H3} region where decreases overlap from both methods. (D, E) Representative deuterium uptake plots from HDX/MS of rituximab after heating at 65 °C. The unheated state is shown in black, and the heat-stressed state is shown in red. Peptides were found to be statistically different if they were 3σ outside of the average of all differences for all time points and for all peptides.

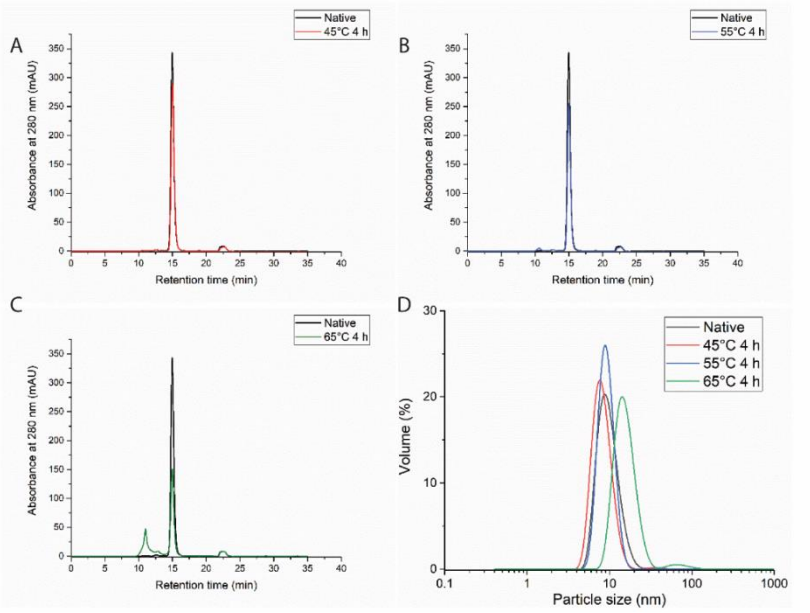

Figure 2.11: Biophysical characterization to confirm aggregation of heat stressed rituximab. Size exclusion chromatography (SEC) of rituximab at 37 °C (native, black) and thermally stressed conditions (A) 45°C for 4 h, (B) 55°C for 4 h, (C) and 65°C for 4 h. The existence of large molecular weight entities in the 65 °C heat-stressed samples indicates aggregation. (D) Dynamic light scattering shows an increase in particle size after 65 °C heat stress (green); however, no significant changes at 45°C (red) or 55°C (blue) are observed, indicating aggregation does not occur at the lower temperatures.

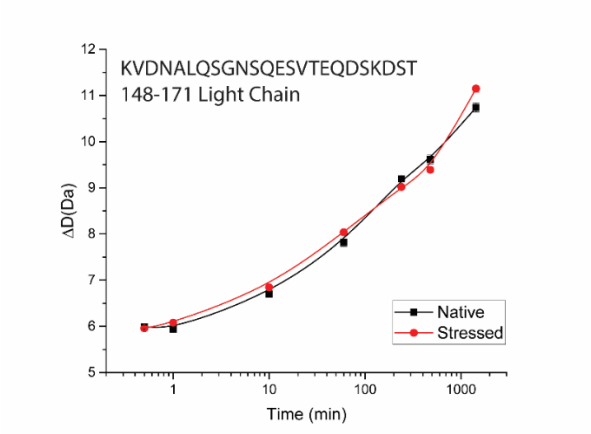

Figure 2.12: Representative deuterium uptake plot from HDX/MS of rituximab after heating at 65 °C for peptide 148-171 that experiences a significant change in uptake at 24 hours. The unheated state is in black, and the heat-stressed state is shown in red. Peptides were found to be statistically different if they were 3σ outside of the average of all differences for all time points and for all peptides.

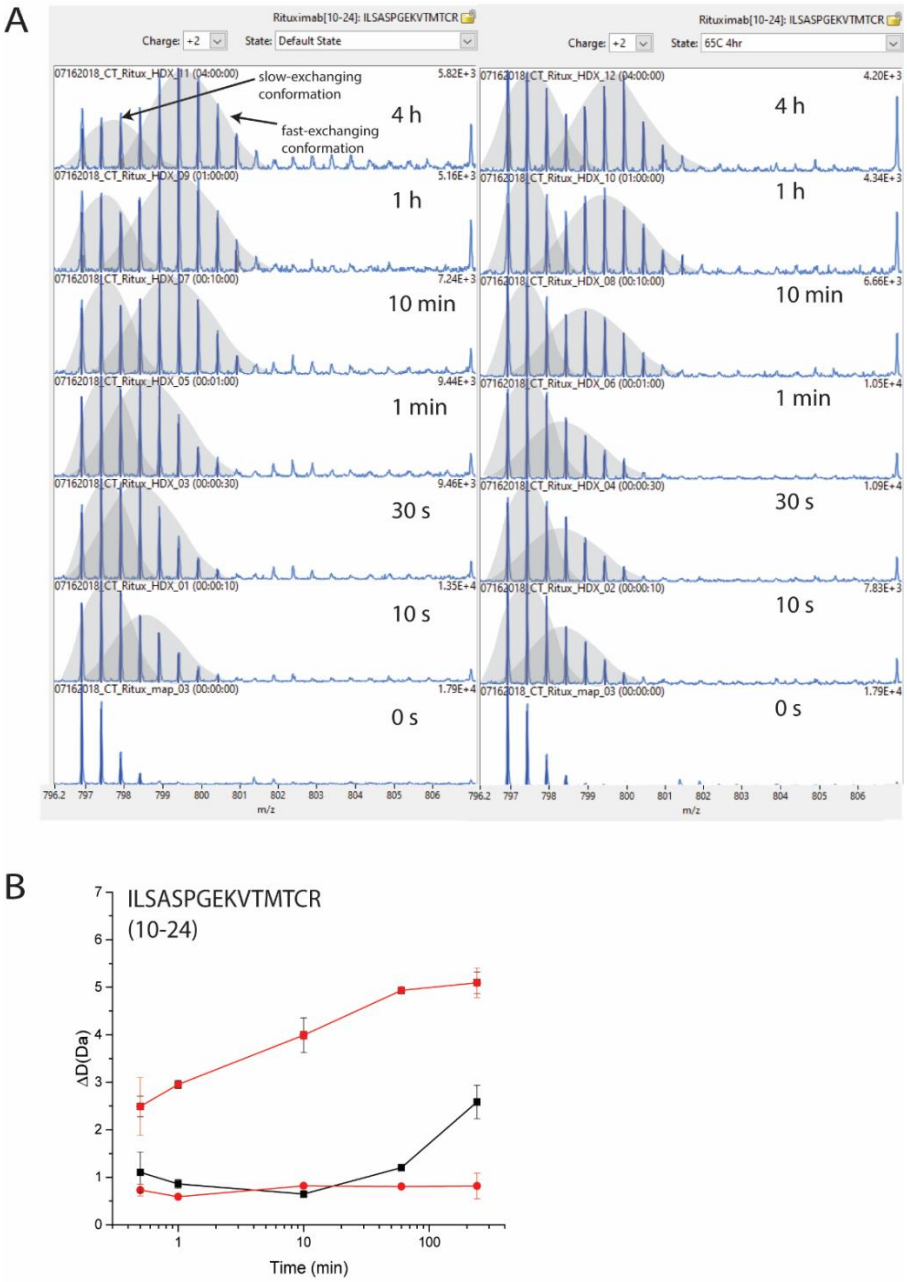

Figure 2.13: Mass spectra for the HDX over time of peptide 10-24 after heating rituximab to 65 °C. (A) Stacked spectral plots for +2 charge state of peptide 10-24 with the native condition on the left and heat-stressed state on the right. All time points have two distinct exchange distributions, one a fast-exchanging conformation and the other a slow-exchanging conformation. (B) Deuterium uptake plot for fast and slow exchanging conformations. The stressed state is depicted in red and the native state in black. The fast-exchanging conformation shows no difference between the stressed and native conditions while the slow-exchanging conformation indicates a decrease in exchange in the stressed condition.

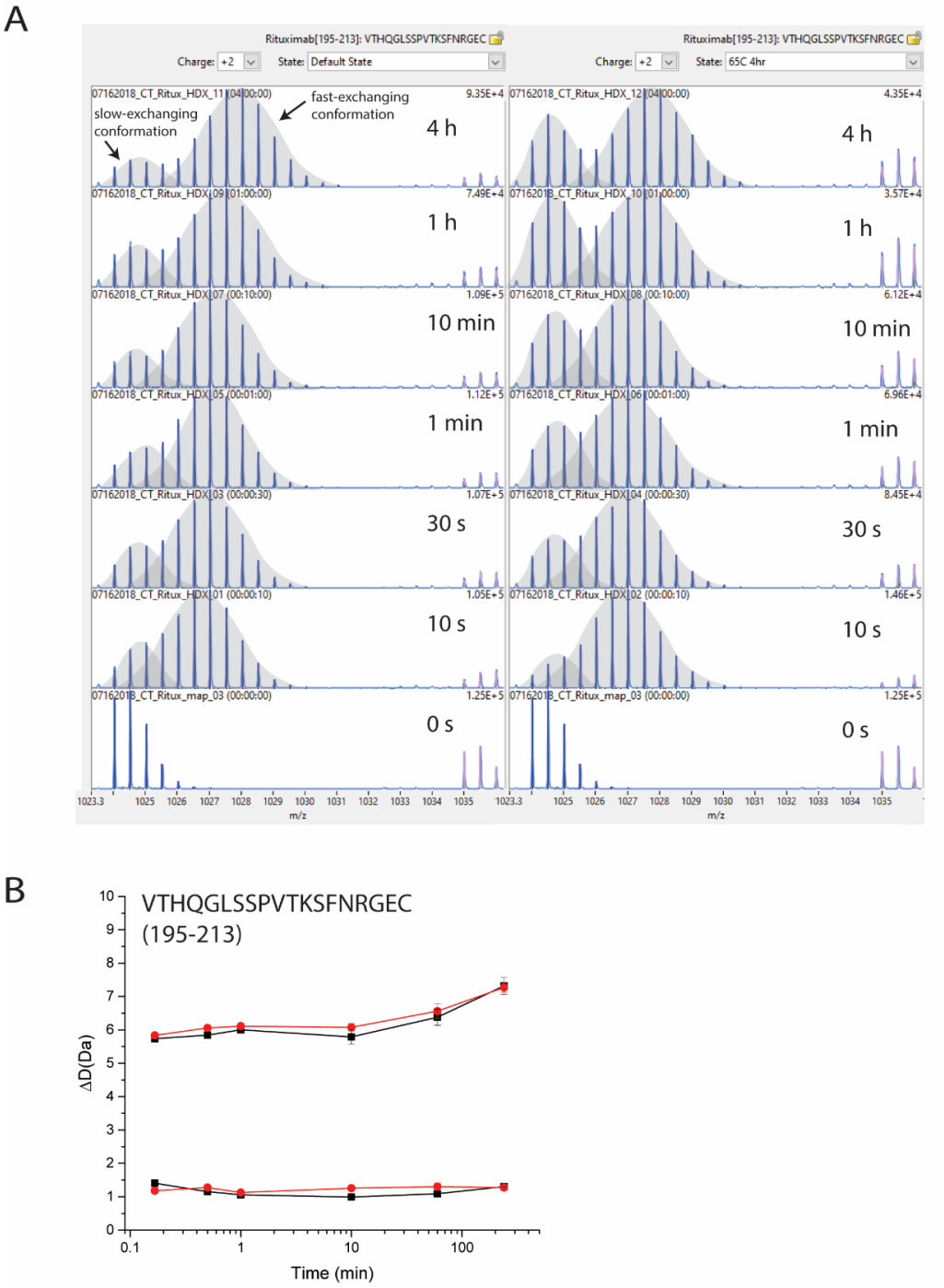

Figure 2.14: Mass spectra for the HDX over time of peptide 195-213 after heating rituximab to 65 °C (A) Stacked spectral plots for +3 charge state of C-terminal peptide 195-213 with the native condition on the left and heat-stressed state on the right. All time points have two distinct exchange distributions, one a fast-exchanging conformation and the other a slow-exchanging conformation. (B) Deuterium uptake plot for fast and slow exchanging conformations. The stressed state is depicted in red and the native state in black. There is no significant difference between the stressed and native states.

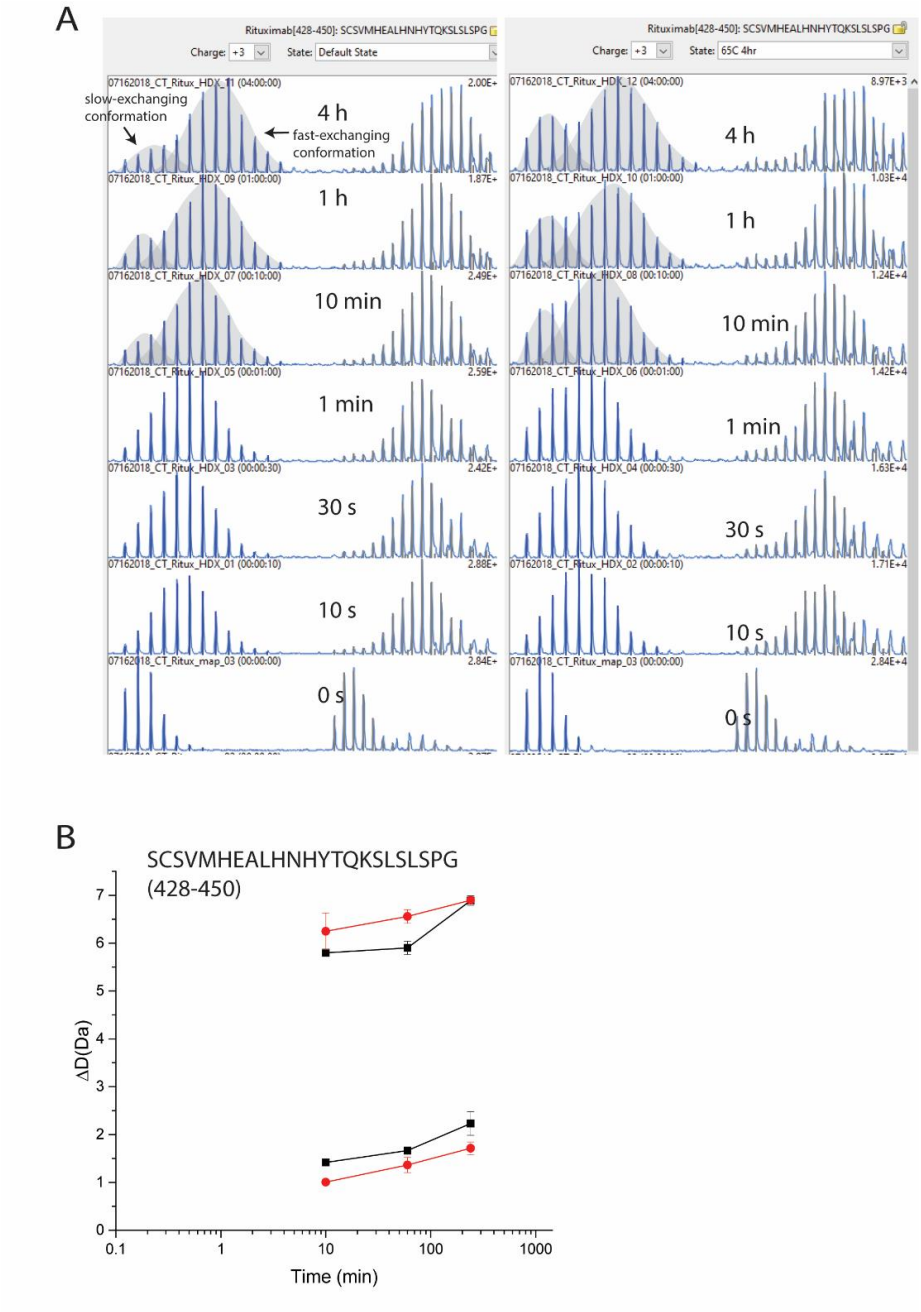

Figure 2.15: Mass spectra for the HDX over time of peptide 428-450 after heating rituximab to 65 °C (E) Stacked spectral plots for +3 charge state of C-terminal peptide 428-450 with the native condition on the left and heat-stressed state on the right. (F) Deuterium uptake plot for fast and slow exchanging conformations. The stressed state is depicted in red and the native state in black. The two different distributions are indistinguishable for time points 10 s, 30 s, 1 min, and 24 h, and thus these points are not shown. There is a significant decrease in exchange in the stressed state in the slow-exchanging conformation and a significant increase in exchange in the stressed state in the fast-exchanging conformation.

Light Chain

Heavy Chain

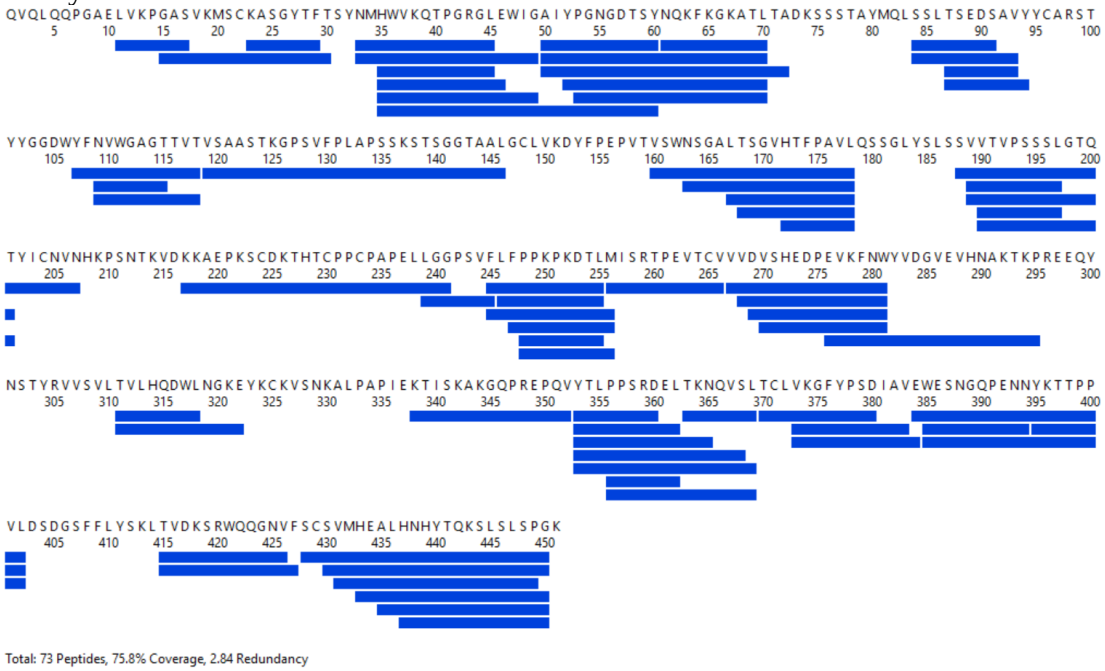

Figure 2.16: Sequence coverage for HDX/MS analysis at 65 °C heat stress. Peptides included in our analysis appear in both stressed and native samples in at least two of four trials that were conducted. Coverage for trials 1, 2, 3, and 4 were 100%, 95.3%, 94.8% and 92.0% for the light chain, and 67.8%, 64.2%, 79.6%, and 69.4% for the heavy chain, respectively.

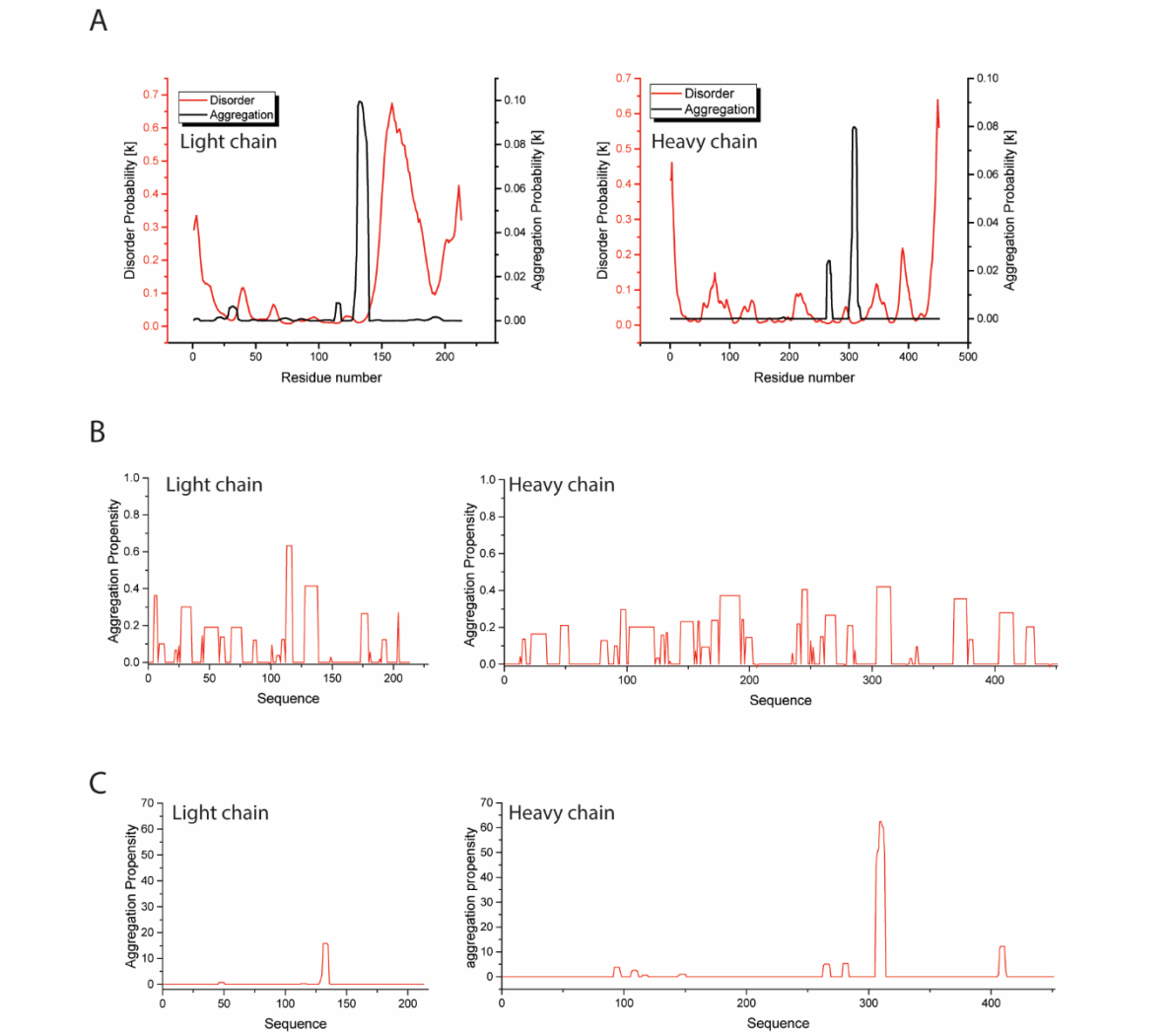

Figure 2.17: Predicted aggregation hotspots of rituximab using (A) PASTA, (B) AGGRESCAN, and (C) TANGO. The primary sequence is used in all three algorithms to predict aggregation. PASTA and TANGO predict the stability of beta-sheet structures toward aggregation while AGGRESCAN predicts aggregation propensity for each residue and locates aggregation prone stretches of residues. All three methods indicate the C_{H2} domain as a likely hot sport of aggregation, consistent with thermal stability data that normally attributes the first thermal transition to the unfolding of the C_{H2} domain.[17] PASTA analysis indicates a significantly disordered region predicted in the C_{H3} domain where our data indicates aggregation. AGGRESCAN predicts a hot spot at residues 426-432 which overlap with the C_{H3} domain where HDX and CL indicate aggregation. Our data suggest that the C_{H2} domain is not a likely location of aggregation as it contains only one peptide that decreases in HDX and one residue that decreases in DEPC-CL extent (S302).

2.4. Discussion

The work described here is one of the first studies that has used CL/MS and HDX/MS together to examine the same heat-stressed mAb. While a few other studies have reported oxidative labeling (e.g. FPOP)[22,40] together with HDX/MS to analyze mAb structure and interactions, the use of DEPC as the labeling agent in this study provides a unique set of information for stressed mAbs because of the rate at which the reagent reacts with residue side chains. Our results support the idea that DEPC CL/MS can be more sensitive to subtle structural changes than HDX/MS. In addition, we demonstrate that the methods are complementary, as might be expected, but they also provide some synergistic information, yielding new insight not available from either technique alone.

2.4.1. CL is more sensitive than HDX

The CL/MS results for rituximab at 45 and 55 °C indicate that DEPC-CL is more sensitive to subtle HOS changes than HDX. After heating at 45 °C, no significant changes in HDX are detected, while 17 residues undergo changes in CL extent. About 70% of the changes in DEPC-CL are residues that are weakly nucleophilic, namely Ser, Thr, and Tyr. The sensitivity of DEPC CL/MS to subtle structural changes is primarily due to how the reactivity of weakly nucleophilic Ser, Thr, and Tyr residues are influenced by small changes in their microenvironment. Previous studies have demonstrated that unlike the more highly nucleophilic residues, His and Lys, the reactivity of Ser, Thr, and Tyr are not dictated primarily by their solvent exposure.[3936] Instead, a partially exposed hydrophobic microenvironment increases the reactivity of these weakly nucleophilic

residues by increasing the local concentration of hydrophobic DEPC. If the microenvironment around a Ser, Thr, or Tyr becomes more hydrophilic because of side chain rearrangements or other HOS changes, the reactivity of the residue will decrease, thus leading to a lower extent of labeling even though the residue might have similar solvent exposure. Measurable changes in deuterium uptake in HDX require making or breaking of H-bonds along the backbone to bury or expose amide hydrogens. Such changes require more energy than simple side chain reorientations, explaining why no HDX changes are observed upon heating at only 45 °C. Together the HDX/MS and CL/MS data suggest structural changes at 45 °C are likely a result of some side chain orientation changes and not large-scale structural or dynamic changes. None of the structural changes is sufficient to cause any measurable change in rituximab activity (**Figure 2.4**) or circular dichroism signal (**Figure 2.5**).

The DEPC CL/MS and HDX/MS data after heating at 55 °C further demonstrate the greater sensitivity of DEPC CL/MS to rituximab structural changes. Only one peptide has increased exchange in HDX, while CL changes are clustered in the antigen-binding region of the protein and scattered in the F_c region. The CL/MS, and not the HDX/MS data, is consistent with the Raji cell pull-down activity assay at 55 °C (**Figure 2.4C**), which indicates a significant change in the F_{ab} region. Two other F_c-specific activity assays, the rituximab bridging ELISA and the Alamar blue assays, are somewhat ambiguous in whether significant changes are occurring in the F_c region. A small, but statistically significant change is detected in F_c binding from the bridging ELISA assay near 55 °C (**Figure 2.4A**), but the Alamar blue assay shows no significant change in the activity of the F_c region (**Figure 2.4B**). This discrepancy may reflect the scattered

changes in labeling extent in the CL/MS data from F_c region. The increase in HDX at 55 °C is not reflected in the activity assays, as no significant changes in deuterium uptake are measured in the antigen-binding or F_c regions. This observation indicates that HDX is not sensitive to the structural changes that influence activity, in the same way CL/MS is. It may be that most of the changes detected by HDX/MS are changes in backbone dynamics that have little effect on the activity assays. The idea that HDX/MS is reporting on backbone dynamics is further supported by the fact that changes in deuterium uptake upon heating at 55 °C are no longer apparent after 24 h of exchange. After 24 h of exchange, regions that are less dynamic under native conditions can exchange fully, adding deuterium to the same extent as a region made more dynamic upon heating. The different responses of the two MS-based methods can perhaps be understood by appreciating that DEPC-based CL/MS is better at reporting on changes in side chain orientations, interactions, and solvent accessibility, whereas HDX/MS better measures backbone dynamics and backbone solvent accessibility. Since binding in the F_{ab} region, as reported by the activity assays, is mostly mediated by side chain interactions, it is perhaps not surprising that DEPC-CL more sensitively detects these sorts of changes.

2.4.2. Methods are complementary

HDX/MS and CL/MS are complementary methods because HDX provides information about the backbone and CL monitors side chains. The full scope of the methods' complementarity is especially apparent in the 65 °C heat-stress data. Overall, the structural information obtained from both methods is consistent, in that increases take place only in the F_{ab}, while decreases take place throughout the protein, yet each method fills in gaps of information for the other. For example, locations where HDX/MS cannot

detect changes, but CL/MS can, is a good demonstration of complementarity. Upon heating at 65 °C, the V_H domain undergoes no significant changes in HDX, but there are six residues (His35, Lys67, Lys74, Ser77, Thr118, and Ser120) that undergo significant changes in CL. The Raji cell pull-down assay shows substantial changes in F_{ab} binding upon heating at 65 °C heat stress, which is consistent with the changes in CL in the V_H domain. The lack of changes in the HDX/MS data in this region might indicate that changes in activity assay are entirely the result of side chain re-orientations and not significant backbone changes in this domain, which would undoubtedly lead to HDX changes. These data illustrate the advantage of using both methods to detect HOS changes. Clearly, if only HDX/MS had been used, structural changes in V_H domain would not have been detected, even though they are substantial enough to affect the activity of rituximab.

Locations where one method indicates an increase in labeling or exchange, while the other indicates a decrease in labeling or exchange could seem contradictory. However, these particular data demonstrate the complementarity of CL/MS and HDX/MS. Our data contain one example of apparently contradictory HDX/MS and CL/MS results. In the V_L domain (**Figure 2.10**), there is a peptide that increases (94-103) in HDX, one that decreases (10-24) in HDX, and three residues that decrease in CL (Ser5, Tyr70, and Thr101). The apparent contradiction involves Thr101, which undergoes a CL decrease, while the relatively short peptide that spans this residue undergoes an increase in HDX. It is likely that the V_L domain partially unfolds at 65 °C, leading to an increase in solvent exposure at peptide 94-103 and a decrease in solvent exposure around peptide 10-24 that is caused by aggregation or repacking of the hydrophobic core. The HDX data reveal that

residues 10-24 are in a region of conformational heterogeneity as there are two exchange distributions. The decreased deuterium uptake after heating is only observed in the slow-exchanging conformation of the peptide, while the fast-exchanging conformation shows no difference in the stressed and native states (**Figure 2.13**). The differences in deuterium uptake for the peptide 10-24 persists even after 24 h of exchange, suggesting the HOS changes that take place might not be caused by changes in protein dynamics. The increase in solvent exposure at peptide 94-103 likely eliminates hydrophobic contacts with Thr101, creating a more hydrophilic microenvironment that decreases the CL of this residue.[39] Structural changes that affect the microenvironment around Thr101 likely affect the positioning of residues Tyr70 and Ser5 as well. These residues undergo significant decreases in CL and are directly adjacent in 3D space to peptide 10-24, which also decreases in deuterium uptake (**Figure 2.18**). The decreases in both methods could be a result of a repacking of the hydrophobic core involving residues Leu11 and Ile10. By interpreting the complex changes detected in the V_L domain by each method, we conclude that significant structural changes are taking place here upon heat stress. Data from both methods thus provide complementary information that yield a more complete picture.

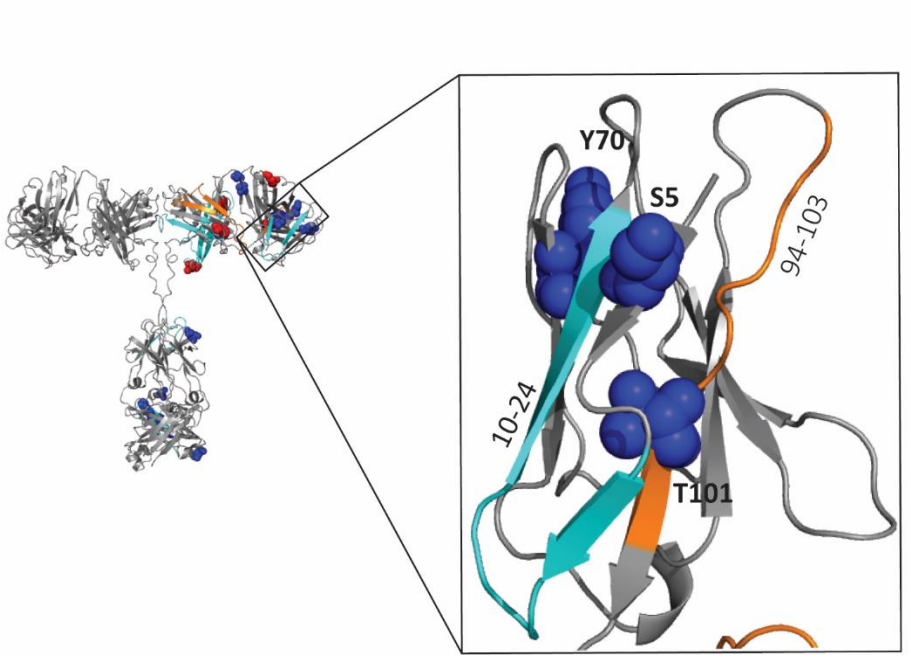

Figure 2.18: Expanded view of the V_L domain of rituximab and the CL/MS and HDX/MS changes that occur in this region upon heat stress at 65 °C for 4 h. Residues indicated in blue spheres undergo decreased CL upon heating. The strands in orange and cyan represent peptides that undergo increased or decreased HDX, respectively, upon heating. The peptide 10-24 becomes more solvent exposed, eliminating the hydrophobic microenvironment around Thr101, while peptide 94-103 experiences a decrease in solvent exposure as a result of aggregation or repacking of the hydrophobic core.

2.4.3. Methods are synergistic

When used together CL/MS can clarify ambiguous HDX/MS data, providing new information that neither method can provide alone. This synergism is a result of the differences in intrinsic reactions rates of each method. The intrinsic or chemical exchange rate of HDX is on the order of ms, which means HDX is sensitive to protein dynamic changes. In contrast, the intrinsic reaction rate of DEPC-CL is on the order of s to min and is not used in a time course, making DEPC-CL essentially blind to protein dynamics.[29] Because of the differences in intrinsic reaction rates, DEPC-CL can clarify ambiguous HDX data, thus providing insight not accessible from HDX/MS. HDX/MS

data can sometimes be ambiguous because decreases in exchange can be the result of changes in dynamics or solvent accessibility. DEPC-CL/MS can be used to help determine which of these changes is taking place.

After heating at 65 °C, HDX decreases are measured throughout protein (**Figure 2.10**), yet few regions show overlapping decreases in both CL and HDX. As previously discussed, many of the labeling and exchange results provide complementary information (e.g. V_H domain data), so positive correlations for the two methods yield additional information. One such region is the C_{H3} domain in which the peptide 428-450 undergoes significant HDX changes, and several residues in or near this region also undergo decreased CL. As indicated in the Results section, the protein region spanned by residues 428-450 exists in two conformations, with the slow-exchanging conformation decreasing in deuterium uptake after heating and the fast-exchanging conformation increasing in uptake after heating (**Figure 2.15**). The decreased exchange in the slow-exchanging conformation together with the decrease in CL in this protein region and sample cloudiness upon heating at 65 °C suggests that protein aggregation is occurring in this domain. The conformational heterogeneity revealed by the HDX data indicates additional unique behavior for this protein region. The increased exchange of the fast-exchanging conformation suggest that some protein molecules unfold in the F_c region instead of aggregate.

In the absence of other experimental data to confirm protein aggregation in the F_c region, we used several aggregation prediction algorithms to identify possible aggregation "hot spots" in rituximab. Aggregation hotspots that are identified by the algorithms PASTA, AGGRESCAN, and TANGO include regions of the C_{H2} domain, the

C_L domain, and the C_{H3} domain (**Figure 2.9**).[41-45] Our experimental results are only somewhat consistent with these theoretical predictions. The C_{H2} region is predicted to have the highest likelihood of aggregation, yet we only observe one peptide (268-281) that decreases in HDX and one residue (Ser302) that decreases in CL in this domain upon heating at 65 °C. A larger cluster of HDX/MS and CL/MS decreases would be expected if the C_{H2} domain were an aggregation site. It should be noted that PASTA and TANGO, which most definitively predict aggregation in the C_{H2} domain, are algorithms primarily used to predict amyloid-like aggregation. Thus, these algorithms may not be well suited for predicting mAb aggregation upon heating. Our HDX/MS and CL/MS data do not support the predicted aggregation in the C_L domain. The region in the C_L domain that is predicted to aggregate by AGGRESCAN and TANGO undergoes an increase in HDX upon heating at both the 55 and 65 °C (i.e. peptide 148-171). Moreover, The C_L domain contains 18 labeled residues; however, only one has a significant change in labeling, and it is an increase in labeling (His196).

AGGRESCAN and TANGO also indicate that there are aggregation "hot spots" in the C_{H3} domain. There is a cluster of residues in this domain that undergo decreased CL (Ser428, His439, Tyr440, Lys451) within a region that also undergoes decreased HDX (428-450), suggesting aggregation does occur at this site. HDX/MS data by itself might suggest the C_{H3} region as an aggregation site, but it would also indicate the C_{H2} domain as an aggregation site because the residues 268-281 in this domain undergo a significant decrease in exchange as well. However, there are three DEPC labelable residues in the span from 268 to 281, and none of them undergo a significant decrease in CL upon heating. Based on the reaction timescales of the two methods, a decrease in HDX that

does not coincide with a decrease in CL suggests reduced backbone dynamics, rather than a site of aggregation. Drawing this conclusion from the HDX/MS data alone would be difficult, although using much longer exchange times (≥ 24 h) can sometimes distinguish between decreased protein dynamics and aggregation. However, if the aggregated protein molecules are in equilibrium with un-aggregated protein molecules, as the multiple exchange distributions observed in the HDX data suggest, even longer exchange times might not accurately distinguish between aggregated sites and decreased protein dynamics. Additionally, it is possible that soluble aggregates become insoluble at longer times, rendering them undetectable by HDX at longer exchange times (>24 h). When considered together, the HDX/MS and CL/MS data indicate that predicted aggregation in the C_{H2} and C_L domains is not observed experimentally, but the predicted aggregation in the C_{H3} domain is. Overall, the differences in intrinsic reaction rates of HDX and CL allow us to obtain clearer information about the structural and dynamic changes caused by heat stress to rituximab.

2.5. Conclusions

We have demonstrated here that HDX and DEPC-CL provide complementary, and sometimes synergistic, information about structural perturbations undergone by mAbs upon exposure to heat stress. We find that DEPC-CL uniquely detects subtle shifts in side chain orientation, as demonstrated by heating rituximab at 45 °C for 4 h. Upon this mild heating, changes in DEPC-CL/MS were detected throughout the protein, while no significant changes in HDX were measured. Under higher heat-stress conditions, results from the two methods complement one another. CL/MS can reveal changes in side chain orientation and solvent exposure that are not accompanied by changes in backbone

solvent exposure or dynamics. On the other hand, HDX/MS is sensitive to changes in backbone dynamics that are not accompanied by changes in side chain orientation or solvent exposure. This capability is exemplified by changes that are observed in the V_L domain upon heating at 65 °C. Finally, under conditions that lead to aggregation, the two techniques work synergistically to identify likely aggregation sites. This synergy is a result of differences in the intrinsic reactions rates. The intrinsic reaction rate of HDX is fast enough for HDX/MS to report on changes in protein dynamics, while the slower intrinsic reaction rate of DEPC-CL and the way we apply it means this method is blind to changes in dynamics. Due to differences in their intrinsic reactions rates, DEPC-CL can be used to clarify ambiguous HDX/MS data, as demonstrated by changes in labeling and exchange in the C_{H3} and C_{H2} domain upon heating at 65 °C. Both domains contain peptides that undergo decreased HDX after heat stress, but only the C_{H3} domain also undergoes decreased DEPC-CL, indicating this region as a likely aggregation site. Given the complementarity of the two methods, HDX/MS and CL/MS together should be amenable for studies of the HOS perturbations of other protein therapeutics. Moreover, these methods should be applicable to epitope and paratope mapping studies and biosimilar evaluation, while providing deeper structural insight that could improve protein therapeutic design.

2.6. References

(1) Ecker, D. M.; Jones, S. D.; Levine, H. L. The Therapeutic Monoclonal Antibody Market. MAbs 2015, 7 (1), 9–14. https://doi.org/http://dx.doi.org/10.4161/19420862.2015.989042.

(2) Nelson, A. L.; Dhimolea, E.; Reichert, J. M. Development Trends for Human Monoclonal Antibody Therapeutics. Nat. Rev. Drug Discov. 2010, 9, 767–774. https://doi.org/10.1038/nrd3229.

(3) Elgundi, Z.; Reslan, M.; Cruz, E.; Sifniotis, V.; Kayser, V. The State-of-Play and Future of Antibody Therapeutics. Adv. Drug Deliv. Rev. 2017, 122, 2–19. https://doi.org/10.1016/j.addr.2016.11.004.

(4) Lu, R.; Hwang, Y.; Liu, I.; Lee, C.; Tsai, H.; Li, H.; Wu, H. Development of Therapeutic Antibodies for the Treatment of Diseases. J. Biomed. Sci. 2020, 27 (1), 1–30. https://doi.org/https://doi.org/10.1186/s12929-019-0592-z.

(5) Frokjaer, S.; Otzen, D. Protein Drug Stability: A Formulation Challenge. Nat. Rev. Drug Discov. 2005, 4 (May), 298–306. https://doi.org/10.1038/nrd1695.

(6) Berkowitz, S. A.; Engen, J. R.; Mazzeo, J. R.; Jones, G. B. Analytical Tools for Characterizing Biopharmaceuticals and the Implications for Biosimilars. Nat. Rev. Drug Discov. 2012, 11, 527–540. https://doi.org/10.1038/nrd3746.

(7) Rogstad, S.; Faustino, A.; Ruth, A.; Keire, D.; Boyne, M.; Park, J. Retrospective Evaluation of the Use of Mass Spectrometry in FDA Biologics License Applications. Am. Soc. Mass Spectrom. 2017, 28, 786–794. https://doi.org/10.1007/s13361-016-1531-9.

(8) Beck, A.; Sanglier-Cianférani, S.; Van Dorsselaer, A. Biosimilar, Biobetter, and Next Generation Antibody Characterization by Mass Spectrometry. Anal. Chem. 2012, 84 (11), 4637–4646. https://doi.org/10.1021/ac3002885.

(9) Artigues, A.; Nadeau, O. W.; Rimmer, M. A.; Villar, M. T.; Du, X.; Fenton, A. W.; Carlson, G. M. Protein Structural Analysis via Mass Spectrometry-Based Proteomics. Adv. Exp. Med. Biol. 2016, 919, 397–431. https://doi.org/10.1007/978-3-319-41448-5.

(10) Pan, J.; Zhang, S.; Chou, A.; Borchers, C. H. Higher-Order Structural Interrogation of Antibodies Using Middle-down Hydrogen/Deuterium Exchange Mass Spectrometry. Chem. Sci. 2016, 7 (2), 1480–1486. https://doi.org/10.1039/c5sc03420e.

(11) Huang, R. Y.; Chen, G. Higher Order Structure Characterization of Protein Therapeutics by Hydrogen/Deuterium Exchange Mass Spectrometry. Anal Bioanal Chem 2014, 406, 6541–6558. https://doi.org/10.1007/s00216-014-7924-3.

(12) Marciano, D. P.; Dharmarajan, V.; Griffin, P. R. HDX/MS Guided Drug Discovery: Small Molecules and Biopharmaceuticals. Curr. Opin. Struct. Biol. 2014, 28, 105–111. https://doi.org/10.1016/j.sbi.2014.08.007.

(13) Wei, H.; Mo, J.; Tao, L.; Russell, R. J.; Tymiak, A. A.; Chen, G.; Iacob, R. E.; Engen, J. R. Hydrogen/Deuterium Exchange Mass Spectrometry for Probing Higher Order Structure of Protein Therapeutics: Methodology and Applications. Drug Discov. Today 2015, 19 (1), 95–102. https://doi.org/10.1016/j.drudis.2013.07.019.Hydrogen/Deuterium.

(14) Edgeworth, M. J.; Phillips, J. J.; Lowe, D. C.; Kippen, A. D.; Higazi, D. R.; Scrivens, J. H. Global and Local Conformation of Human IgG Antibody Variants Rationalizes Loss of Thermodynamic Stability. Angew. Chemie - Int. Ed. 2015, 54 (50), 15156–15159. https://doi.org/10.1002/anie.201507223.

(15) Konermann, L.; Pan, J.; Liu, Y.-H. Hydrogen Exchange Mass Spectrometry for Studying Protein Structure and Dynamics. R. Soc. Chem. 2011, 1224–1234. https://doi.org/10.1039/c0cs00113a.

(16) Zhang, M. M.; Huang, R. Y. C.; Beno, B. R.; Deyanova, E. G.; Li, J.; Chen, G.; Gross, M. L. Epitope and Paratope Mapping of PD-1/Nivolumab by Mass Spectrometry-Based Hydrogen-Deuterium Exchange, Cross-Linking, and Molecular Docking. Anal. Chem. 2020, 92 (13), 9086–9094. https://doi.org/10.1021/acs.analchem.0c01291.

(17) Iacob, R. E.; Bou-assaf, G. M.; Makowski, L. E. E.; Engen, J. R.; Berkowitz, S. A.; Houde, D. Investigating Monoclonal Antibody Aggregation Using a Combination of H / DX/MS and Other Biophysical Measurements. J. Pharm. Sci. 2013, 102, 4315–4329. https://doi.org/10.1002/jps.23754.

(18) Huang, R. Y. C.; Krystek, S. R.; Felix, N.; Graziano, R. F.; Srinivasan, M.; Pashine, A.; Chen, G. Hydrogen/Deuterium Exchange Mass Spectrometry and Computational Modeling Reveal a Discontinuous Epitope of an Antibody/TL1A Interaction. MAbs 2018, 10 (1), 95–103. https://doi.org/10.1080/19420862.2017.1393595.

(19) Liu, T.; Marcinko, T. M.; Kiefer, P. A.; Vachet, R. W. Using Covalent Labeling and Mass Spectrometry To Study Protein Binding Sites of Amyloid Inhibiting Molecules. Anal. Chem. 2017, 89, 11583–11591. https://doi.org/10.1021/acs.analchem.7b02915.

(20) Liu, X. R.; Zhang, M. M.; Gross, M. L. Mass Spectrometry-Based Protein Footprinting for Higher-Order Structure Analysis: Fundamentals and Applications. Chem. Rev. 2020, 120, 4355–4454. https://doi.org/10.1021/acs.chemrev.9b00815.

(21) Li, K. S.; Shi, L.; Gross, M. L. Mass Spectrometry-Based Fast Photochemical Oxidation of Proteins (FPOP) for Higher Order Structure Characterization. Acc. Chem. Res. 2018, 51, 736–744. https://doi.org/10.1021/acs.accounts.7b00593.

(22) Cornwell, O.; Radford, S. E.; Ashcroft, A. E.; Ault, J. R. Comparing Hydrogen Deuterium Exchange and Fast Photochemical Oxidation of Proteins: A Structural Characterisation of Wild-Type and ΔN6 B2-Microglobulin. J. Am. Soc. Mass Spectrom. 2018, 29, 2413–2426. https://doi.org/10.1007/s13361-018-2067-y.

(23) Kaur, P.; Tomechko, S. E.; Kiselar, J.; Shi, W.; Deperalta, G.; Wecksler, A. T.; Gokulrangan, G.; Ling, V.; Chance, M. R. Characterizing Monoclonal Antibody Structure by Carboxyl Group Footprinting. MAbs 2015, 7 (3), 540–552.

(24) Limpikirati, P.; Hale, J. E.; Hazelbaker, M.; Huang, Y.; Jia, Z.; Yazdania, M.; Grabanb, E. M.; Vaughan, R. C.; Vachet, R. W. Covalent Labeling and Mass Spectrometry Reveal Subtle Higher Order Structural Changes for Antibody Therapeutics. MAbs 2019, 11 (3), 463–476. https://doi.org/10.1080/19420862.2019.1565748.

(25) Limpikirati, P.; Liu, T.; Vachet, R. W. Covalent Labeling-Mass Spectrometry with Non-Specific Reagents for Studying Protein Structure and Interactions. Methods 2018, 144, 79–93. https://doi.org/10.1016/j.ymeth.2018.04.002.

(26) Li, K. S.; Chen, G.; Mo, J.; Huang, R. Y.; Deyanova, E. G.; Beno, B. R.; O'Neil, S. R.; Tymiak, A. A.; Gross, M. L. Orthogonal Mass Spectrometry-Based Footprinting for Epitope Mapping and Structural Characterization: The IL-6 Receptor upon Binding of Protein Therapeutics. Anal. Chem. 2017, 89, 7742–7749. https://doi.org/10.1021/acs.analchem.7b01748.

(27) Pan, Y.; Piyadasa, H.; O'Neil, J. D.; Konermann, L. Conformational Dynamics of a Membrane Transport Protein Probed by H/D Exchange and Covalent Labeling: The Glycerol Facilitator. J. Mol. Biol. 2012, 416 (3), 400–413. https://doi.org/10.1016/j.jmb.2011.12.052.

(28) Zheng, X.; Wintrode, P. L.; Chance, M. R. Complementary Structural Mass Spectrometry Techniques Reveal Local Dynamics in Functionally Important Regions of a Metastable Serpin. Cell Press 2008, 16 (January), 38–51. https://doi.org/10.1016/j.str.2007.10.019.

(29) Liu, T.; Limpikirati, P.; Vachet, R. W. Synergistic Structural Information from Covalent Labeling and Hydrogen − Deuterium Exchange Mass Spectrometry for Protein − Ligand Interactions. Anal. Chem. 2019, 91, 15248–15254. https://doi.org/10.1021/acs.analchem.9b04257.

(30) Limpikirati, P. K.; Zhao, B.; Pan, X.; Eyles, S. J.; Vachet, R. W. Covalent Labeling/Mass Spectrometry of Monoclonal Antibodies with Diethylpyrocarbonate: Reaction Kinetics for Ensuring Protein Structural Integrity. J. Am. Soc. Mass Spectrom. 2020, 31 (6), 1223–1232. https://doi.org/10.1021/jasms.0c00067.

(31) Borotto, N. B.; Zhou, Y.; Hollingsworth, S. R.; Hale, J. E.; Graban, E. M.; Vaughan, R. C.; Vachet, R. W. Investigating Therapeutic Protein Structure with Diethylpyrocarbonate Labeling and Mass Spectrometry. Anal. Chem. 2015. https://doi.org/10.1021/acs.analchem.5b03180.

(32) Krezel, A.; Bal, W. A Formula for Correlating PKa Values Determined in D2O and H2O. J. Inorg. Biochem. 2004, 98, 161–166. https://doi.org/10.1016/j.jinorgbio.2003.10.001.

(33) Masson, G. R.; Burke, J. E.; Ahn, N. G.; Anand, G. S.; Borchers, C.; Brier, S.; Bou-assaf, G. M.; Engen, J. R.; Englander, S. W.; Faber, J.; Garlish, R.; Griffin, P. R.; Gross, M. L.; Guttman, M.; Hamuro, Y.; Heck16, A. J. R.; Houde, D.; Iacob, R. E.; Jørgensen, T. J. D.; Kaltashov, I. A.; Klinman, J. P.; Konermann, L.; Man, P.; Mayne, L.; Pascal, B. D.; Reichmann, D.; Skehel, M.; Snijder, J.; Strutzenberg, T. S.; Underbakke, E. S.; Wagner, C.; Wales, T. E.; Walters, B. T.; Weis, D. D.; Wilson, D. J.; Wintrode, P.

L.; Zhang, Z.; Zheng, J.; Schriemer, D. C.; Rand, K. D. Recommendations for Performing, Interpreting and Reporting Hydrogen Deuterium Exchange Mass Spectrometry (HDX/MS) Experiments. Nat. Methods 2019, 16 (July), 595–602. https://doi.org/10.1038/s41592-019-0459-y.

(34) Zhang, H.; Song, L.; Ye, H.; Hu, L.; Liang, W.; Liu, D. Characterization of a Novel Humanized Anti-CD20 Antibody with Potent Anti-Tumor Activity against Non-Hodgkin's Lymphoma. Cell. Physiol. Biochem. 2013, 32 (3), 645–654. https://doi.org/10.1159/000354468.

(35) Cragg, M. S.; Bayne, M. B.; Tutt, A. L.; French, R. R.; Beers, S.; Glennie, M. J.; Illidge, T. M. A New Anti-Idiotype Antibody Capable of Binding Rituximab on the Surface of Lymphoma Cells. Blood 2004, 104 (8), 2540–2542. https://doi.org/10.1182/blood-2004-05-1733.

(36) Hampson, G.; Ward, T. H.; Cummings, J.; Bayne, M.; Tutt, A. L.; Cragg, M. S.; Dive, C.; Illidge, T. M. Validation of an ELISA for the Determination of Rituximab Pharmacokinetics in Clinical Trials Subjects. J. Immunol. Methods 2010, 360 (1–2), 30–38. https://doi.org/10.1016/j.jim.2010.05.009.

(37) Padlan, E. A. Anatomy of the Antibody Molecule. Mol. Immunol. 1994, 31 (3), 169–217.

(38) Andersen, C. B.; Manno, M.; Rischel, C.; Thorolfsson, M.; Martorana, V. Aggregation of a Multidomain Protein : A Coagulation Mechanism Governs Aggregation of a Model IgG1 Antibody under Weak Thermal Stress. Protein Sci. 2010, 19, 279–290. https://doi.org/10.1002/pro.309.

(39) Limpikirati, P.; Pan, X.; Vachet, R. W. Covalent Labeling with Diethylpyrocarbonate: Sensitive to the Residue Microenvironment, Providing Improved Analysis of Protein Higher Order Structure by Mass Spectrometry. Anal. Chem. 2019, 91 (13), 8516–8523. https://doi.org/10.1021/acs.analchem.9b01732.

(40) Li, J.; Wei, H.; Krystek, S. R.; Bond, D.; Brender, T. M.; Cohen, D.; Feiner, J.; Hamacher, N.; Harshman, J.; Huang, R. Y.; Julien, S. H.; Lin, Z.; Moore, K.; Mueller, L.; Noriega, C.; Sejwal, P.; Sheppard, P.; Stevens, B.; Chen, G.; Tymiak, A. A.; Gross, M. L.; Schneeweis, L. A. Mapping the Energetic Epitope of an Antibody/Interleukin-23 Interaction with Hydrogen/Deuterium Exchange, Fast Photochemical Oxidation of Proteins Mass Spectrometry, and Alanine Shave Mutagenesis. Anal. Chem. 2017. https://doi.org/10.1021/acs.analchem.6b03058.

(41) Linding, R.; Schymkowitz, J.; Rousseau, F.; Diella, F.; Serrano, L. A Comparative Study of the Relationship between Protein Structure and β-Aggregation in Globular and Intrinsically Disordered Proteins. J. Mol. Biol. 2004, 342 (1), 345–353. https://doi.org/10.1016/j.jmb.2004.06.088.

(42) Kant, R. Van Der; Karow-zwick, A. R.; Durme, J. Van; Blech, M.; Gallardo, R.; Seeliger, D.; Aßfalg, K.; Baatsen, P.; Compernolle, G.; Gils, A.; Studts, J. M.; Schulz, P.; Garidel, P.; Schymkowitz, J.; Rousseau, F. Prediction and Reduction of the Aggregation

of Monoclonal Antibodies. J. Mol. Biol. 2017, 429 (8), 1244–1261. https://doi.org/10.1016/j.jmb.2017.03.014.

(43) Fernandez-Escamilla, A. M.; Rousseau, F.; Schymkowitz, J.; Serrano, L. Prediction of Sequence-Dependent and Mutational Effects on the Aggregation of Peptides and Proteins. Nat. Biotechnol. 2004, 22 (10), 1302–1306. https://doi.org/10.1038/nbt1012.

(44) Conchillo-Solé, O.; de Groot, N. S.; Avilés, F. X.; Vendrell, J.; Daura, X.; Ventura, S. AGGRESCAN: A Server for the Prediction and Evaluation of "Hot Spots" of Aggregation in Polypeptides. BMC Bioinformatics 2007, 8. https://doi.org/10.1186/1471-2105-8-65.

(45) Walsh, I.; Seno, F.; Tosatto, S. C. E.; Trovato, A. PASTA 2.0: An Improved Server for Protein Aggregation Prediction. Nucleic Acids Res. 2014, 42 (W1), 301–307. https://doi.org/10.1093/nar/gku399.

CHAPTER 3

3. COVALENT LABELING MASS SPECTROMETRY WITH DIETHYLPYROCARBONATE FOR INVESTIGATING ANTIBODY/ANTIGEN INTERACTIONS

3.1. Introduction

Monoclonal antibody (mAb) based therapeutics are successful because of the high specificity and affinity between an antibody and its antigen. Epitope mapping, which involves identifying the antigen residues that are recognized by the mAb, is vital for understanding binding mechanisms and helping design future therapeutics and vaccines.[1] Identifying the bound residues in the antigen and the features of the antigen's higher order structure (HOS) that are necessary for specific binding are essential not only for understanding the mechanism of binding but also can be useful for intellectual property protection.

Mass spectrometry (MS) has emerged as a promising tool for epitope mapping because of limitations in traditional tools, especially when studying intact antibody-antigen complexes. Traditionally, X-ray crystallography and/or nuclear magnetic resonance (NMR) have been used to study protein-protein interactions due to their atomic-level resolution. However, X-ray crystallography is limited to proteins that can crystalize, requires lots of sample, and can be time-consuming, thereby limiting its throughput. NMR on high molecular weight protein complexes can be challenging, limiting its applicability for the routine analysis of mAb-antigen complexes. MS, on the other hand, requires low sample amounts, does not seem to be limited by molecular weight, and offers higher throughput analysis than either NMR or X-ray crystallography.

Various mass spectrometry tools have been developed for this purpose such as epitope excision and epitope extraction, hydrogen deuterium exchange (HDX) MS, and covalent labeling (CL) MS.[2–7] Epitope excision and extraction methods are historically the most frequently used methods for MS based epitope mapping. In these methods, proteolytic digestion of the antigen is carried out either before (epitope extraction) or after (epitope excision) complexation with an antibody. In epitope extraction methods, specific recognition peptide(s) that are created by proteolytic digestion are then isolated by immunoaffinity methods and detected by MS.[4,8] Epitope excision relies on digestion in the presence of the bound antibody, which prevents proteolysis on the parts of the antigen that are buried in the binding pocket thereby allowing conformational epitopes to be identified when combined with MS.[4] However, epitope excision and extraction techniques are limited in their resolution, usually providing only peptide level resolution. Moreover, while these methods are capable of finding linear epitopes, they are not as useful at finding discontinuous epitopes.

More recently, HDX/MS has been used to study antibody-antigen interactions, as it can provide more precise mapping of the contact sites.[3,9–11] In HDX, proteins are incubated in D_2O, which results in exchange of hydrogens on heteroatoms for deuterium in solution. Proteolytic digestion at low pH, followed by LC/MS detection allows the exchange of backbone amide hydrogens to be detected. The different rates at which deuterium labels the backbone can be used to analyze solvent accessibility and higher order structure. By completing comparative studies of antigen alone vs. antigen in complex with antibody, epitope regions can often be identified.[5,12] However, HDX/MS suffers from some limitations. Protein digestion and separation of the resulting peptide

can lead to label loss due to back exchange, which lowers the sensitivity and resolution of the method. In addition, changes in protein dynamics at sites distant from the epitope also result in reduced HDX, and this decreased exchange can sometimes be difficult to distinguish from reduced exchange at the epitope. Lastly, while HDX/MS is higher throughput than methods such as NMR and X-ray crystallography, data analysis is time intensive and specialized robotic equipment is often needed to facilitate the experiments.

Covalent labeling (CL) has emerged as a promising complementary technique because of its advantages over other MS based epitope-mapping approaches. CL can provide residue level resolution and is relatively high throughput. CL methods typically do not suffer from label loss like HDX, and depending on the reagent, sample preparation is simple with no specialized equipment needed. A number of CL techniques such as fast photochemical oxidation of proteins (FPOP),[13] carboxyl group footprinting,[14] lysine acetylation,[15,16] and diethylpyrocarbonate (DEPC) labeling[17–20] have been used to study antibodies. For example, FPOP has been used alone or with HDX to characterize epitopes and even paratopes in protein therapeutics.[9,13,21] Carboxyl group footprinting with glycine ethyl ester (GEE) has been used to determine the residues involved in the interface between vascular endothelial growth factor and it binding mAbs.[22] One of the earliest examples of CL for studying epitopes was with lysine acetylation in studies of the epitope of lysozyme.[15]

DEPC is a promising CL reagent because it can label numerous nucleophilic residues, including lysine, histidine, serine, threonine, tyrosine, and the N-terminus, allowing about 30% of the residues in the average protein to be probed.[23] The labeling extents of histidine and lysine residues are correlated with their solvent accessible surface area

(SASA), while the labeling of serine, threonine and tyrosine are sensitive to their microenvironment, particularly the presence of nearby hydrophobic residues.[19] DEPC-CL/MS has been used previously to study protein-ligand binding sites,[24–26] protein-protein interactions,[27,28] and HOS perturbations of mAbs caused by heat stress.[17,18,29,30] Despite the proven value of DEPC-CL/MS for studying protein interactions, there are no reports, to our knowledge, that demonstrate its use for studying antibody-antigen interactions.

To evaluate DEPC-CL/MS for studying antibody-antigen interactions, we chose to use tumor necrosis factor-α (TNFα) as a model system. TNFα is a pro inflammatory cytokine that mediates inflammation. At physiological pH and concentration, it is a homotrimer that reversibly dissociates to an inactive monomer.[31–34] Neutralizing TNFα is an effective treatment against a number of diseases such as rheumatoid arthritis, Crohn's disease, and psoriasis. As a result, numerous TNFα neutralizing protein therapeutics have been developed. Each of these therapeutic proteins has a slightly different epitope,[35] making this protein and its associated antibodies a good system for evaluating the effectiveness of DEPC-CL/MS for epitope mapping. In this work, three model mAbs were investigated – adalimumab, infliximab, and golimumab – each of which has a different epitope and stabilizes the TNFα trimer to different extents (**Figure 3.1**).[33,35,36] Of particular interest in this study was elucidating the DEPC labeling behavior of residues both near the epitope and distant from the epitope. Our results show that histidine and lysine residues in the epitope undergo dramatic decreases in labeling, while serine, threonine, and tyrosine residues at the edges of the epitope can undergo unexpected increases in labeling due to the creation of nearby hydrophobic pockets. In

addition, we find that most residues that are distant from the epitope do not undergo labeling changes, but a few residues do change, presumably due to side chain reorganizations that occur upon antibody-TNFα binding.

3.2.Materials and Methods

3.2.1. Materials

Golimumab formulation (Simponi® 12.5mg/mL vial, batch#HJS1V01, Janssen), adalimumab formulation (Humira® 50mg/mL vial, lot#1088193, Abbvie), and infliximab formulation (Remicade®, lyophilized powder, lot#01184, Janssen) were purchased from Millipore Sigma, and rituximab formulation (Rituxan® 100 mg/10 mL vial, lot# 320928 3, Genentech) was purchased from Myoderm. Bovine serum albumin (#A2394), diethylpyrocarbonate (DEPC) (#D5758), imidazole (#I5513), iodoacetamide (#I6125), tris(2-carboxyethyl) phosphine (TCEP) (#C4706), guanidine hydrochloride (GnHCl) (#G3272), and sodium chloride (#S5886) were obtained from Sigma-Aldrich. Sodium phosphate monobasic monohydrate (#S0710-1) was obtained from EM Science. Immobilized trypsin (#20230), sodium phosphate dibasic anhydrous (#S374-500), LC/MS-grade formic acid (#A117-50), acetonitrile (#A998-4), and water (#W7-4) were purchased from Fisher Scientific.

3.2.2. DEPC labeling and proteolytic digestion

DEPC stock solutions were prepared in acetonitrile, and final acetonitrile concentrations in reacted protein samples were less than 1% v/v. The DEPC labeling reaction was completed in 500 µL total volume in MOPS buffer, with antibody:antigen concentrations of 1 µM mAb:1.2 µM TNFα monomer. Because TNFα is a trimer, a molar

excess of the mAb was used to ensure ~100% complexation of the trimer. Labeling was conducted at a DEPC:protein molar ratio of 1000:1 at 37 °C for 5 min. The DEPC concentration was chosen based on predictions of proper reagent concentration to avoid over labeling.[37] After 5 minutes of reaction time, imidazole was added to quench the reaction at a 1:50 DEPC:imidazole molar ratio. At least three replicate DEPC analyses were performed for each mAb-TNFα complex.

After the reaction, mixtures were quenched with imidazole, 50 µL of acetonitrile were added, and samples were heated at 50 °C for 45 min to denature the proteins. Prior to denaturation, the disulfide bonds were reduced with TCEP at 25 mM for 5 minutes and then alkylated with iodoacetamide at 25 mM for 20 minutes in the dark. Finally, proteolytic digestion was performed using 50 µL of immobilized trypsin, and the protein was digested overnight at 37 °C. To remove trypsin and collect the resulting peptides after the digestion, the samples were centrifuged at 14,000 rpm, and the supernatant was collected. The supernatant was then concentrated using a speed vacuum from 500 µL to 100 µL. Samples were analyzed immediately after concentration.

3.2.3. LC/MS/MS of CL samples

For online LC/MS/MS analyses, 5 µL was injected into a Dionex UltiMate 3000 RSLC capillary LC system (Thermo Scientific). The flow rate was set at 400 nL/min. Peptides were separated with an Acclaim Pepmap RSLC column (300 µm x 15 cm, C18, 2 µM, Thermo Scientific) with LC/MS grade water and 0.1% formic acid as solvent A and acetonitrile as solvent B. A linear gradient from 5% B to 50% B over 55 minutes with a final wash of 95% B for 15 minutes was used. An electrospray ionization source

was used in positive mode with a needle voltage of 2100 V. Mass spectra were acquired on a Thermo Scientific Orbitrap Fusion mass spectrometer. Tandem mass spectrometry (MS/MS) was conducted using collision-induced dissociation (CID) on a linear quadrupole ion trap. An inclusion list of possible labeled and unlabeled TNFα tryptic peptides was used to ensure these ions would be fragmented while an exclusion list of antibody peptides was used. The inclusion was used to guarantee detection and fragmentation of TNFα peptides for determining their covalent labeling sites and extents.

3.2.4. CL/MS data analysis

A custom software pipeline designed specifically for protein DEPC-CL/MS experiments was used as described previously.[38] Briefly, tandem mass spectra were searched against a database consisting of TNFα and the common repository of adventitious proteins ((http://www.thegpm.org/crap/index.html) for identifying peptides and their labeled sites. The search parameters used were a precursor mass tolerance of 10 ppm, a product ion tolerance of 0.5 Da, carbamidomethylation of Cys and DEPC modification of His, Lys, Ser, Thr, Tyr, and N-terminus (mass addition of 72.0211 Da) as variable modifications. For determining modification extents, peak areas of labeled and unlabeled ions obtained from reconstructed ion chromatograms of each species were used to calculate percent labeling at each labeled site.

3.2.5. SEC and SEC-MALS

SEC separation of TNFα and mAbs was performed at room temperature on an Agilent 1260 Infinity HPLC system using a TSKgel SuperSW3000 column (30 cm x 7.8 mm ID, 5 μm particle size; Tosoh Bioscience LLC). 100 μL of 1 μM TNFα and/or 1.2

μM mAb in 50 mM phosphate buffer at pH 7.0 was loaded on the SEC column. The mobile phase used was 50 mM sodium phosphate at pH 6.8. A flow rate of 0.35 mL/min was used. The variable wavelength UV detector was set at 280 nm for detection. The TSKgel SuperSW3000 is able to separate TNFα trimer from mAb, but the TNFα:mAb complexes all elute at the exclusion limit. Thus, the TSKgel Super3000 column confirmed that TNFα and mAbs were in complex with each other but gave no information as to the binding stoichiometry of the complex. Therefore, SEC-MALS was also performed with a Sepax SRT SED-500 column (30 cm x 4.6. mm ID, 5 μm particle size; Sepax Technologies), which has a larger molecular weight exclusion limit, to resolve large molecular weight species.

For SEC-MALS measurements, separations were performed at room temperature on an Agilent 1260 Infinity HPLC system using the Sepax SRT SED-500 column. 100 μL of 1 μM TNFα and/or 1.2 μM mAb in 50 mM phosphate buffer at pH 7.0 was loaded on the SEC column. The mobile phase used was 50 mM sodium phosphate at pH 6.8. An flow rate of 0.35 mL/min was used. The variable wavelength UV detector was set at 280 nm for detection. An 18-angle light scattering detector (DAWN HELEOS-II) and a refractive index detector (Optilab T-rEX) (Wyatt Technology) were used, and data were collected every second. The software ASTRA (Wyatt Technology) was used for the data analysis and bovine serum albumin was used for calibration and quality control. Measurements were taken at room temperature. The light scattering data were collected across the entire chromatographic peak to ensure a representative distribution of molecular weights.

3.3. Results and Discussion

3.3.1. DEPC-CL labeling considerations for antibody-antigen interactions

TNFα is a 157-residue protein with 35 residues that can be labeled by DEPC. DEPC labeling of TNFα alone reveals that 34 of these residues can be modified, thereby providing adequate structural coverage of the protein (**Table 3.1**). DEPC-CL/MS experiments typically compare labeling of the free protein to the complexed protein to identify binding sites. However, for antibody-antigen interactions, it is challenging to directly compare free TNFα to TNFα in complex with a mAb due to the excess protein load contributed by the antibody. The labeling extent of residues on TNFα alone versus in complex is different due to the high concentration of labelable residues when the mAb is present. To correct for this increased number of labelable residues, control experiments were conducted on TNFα in solution with the non-binding mAb rituximab. Rituximab has an equivalent number of labelable residues to the mAbs that bind TNFα, providing a means of correcting for any labeling changes causes by the presence of the large antibody. Labeling experiments in the presence of rituximab reveal that there are a few residues that are labeled when TNFα is alone that are not labeled in the presence of rituximab. This observation indicates that while these residues may be labeled to a small extent in TNFα alone, their labeling levels likely drop below the detection limit when extra protein is present. Thus, the labeling data from the free TNFα experiments are simply used as indicators of residues that can be labeled in the protein, rather than being used quantitatively.

A comparison of the labeling of TNFα with rituximab vs. TNFα with a binding mAb reveals three different outcomes for the labeled residues (**Figure 3.2**). First, there

are residues that undergo no significant change in labeling extent, indicating that the given residue experiences no change in its microenvironment or its accessibility to DEPC. Second, there is an increase in the labeling extent in the presence of the binding mAb due to either an increase in solvent accessibility, especially for histidine and lysine residues, and/or changes in microenvironment, especially for serine, threonine, and tyrosine residues. In recent work, we have found that a more hydrophobic microenvironment around accessible serine, threonine, and tyrosine residues causes these weakly nucleophilic residues to react more extensively due to increased local concentrations of DEPC.[17-19] Third, there is a decrease in labeling in the presence of the binding mAb due to the loss of solvent exposure of a given residue or possibly a decreased hydrophobic microenvironment for serine, threonine, and tyrosine residues.

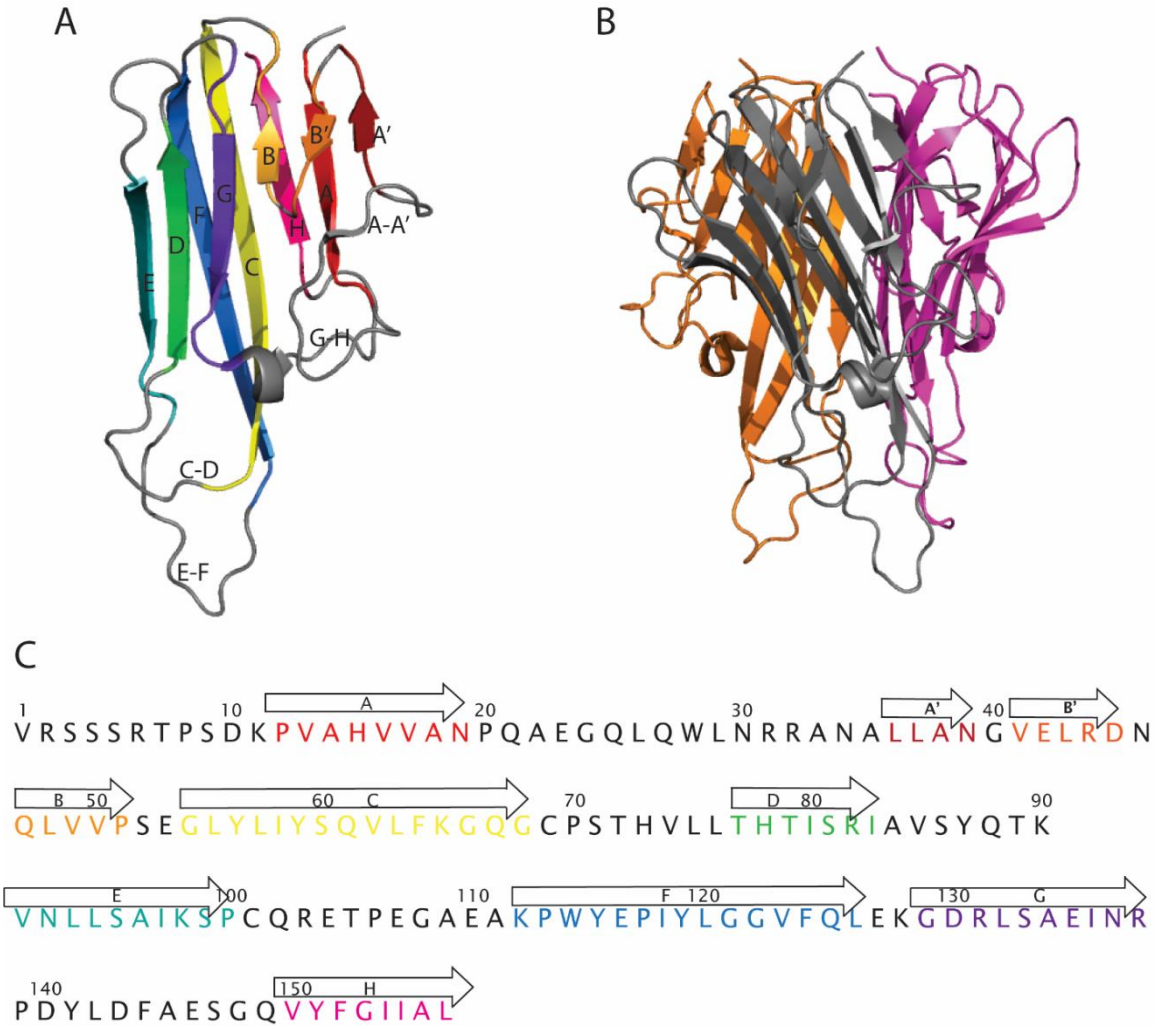

Figure 3.1: TNFα structure (A) Crystal structure with each β-strand indicated in a different color, and relevant loops indicated by the β strands they connect. (B) TNFα homotrimer structure with each monomer a different color. (C) TNFα amino acid sequence, color coded for each β-strand.

Table 3.1: DEPC Labeling Extent of TNFα alone

Residues	Labeling extent
Ser3/4/5	4% ± 4%
Thr7	3.3% ± 0.9%
Ser9	1.1% ± 0.3%
Lys11	12% ± 4%
His15	3% ± 0.7%
Ser52	14% ± 6%
Tyr56	14% ± 6%
Ser60	1% ± 1%
Lys65	3% ± 4%
Ser71	50% ± 6%
Thr72	0.7% ± 0.4%
His73	14% ± 10%
Thr77	17% ± 5%
Thr79	0 % ± 0%
Ser81	21% ± 3%
Ser86	13% ± 7%
Tyr87	10% ± 7%
Thr89	9% ± 7%
Lys90	20% ± 7%
Ser95	2% ± 1%
Lys98	0.18% ± 0.01%
Ser99	31% ± 7%
Thr105	12% ± 6%
Lys112	3.2% ± 0.4%
Tyr115	3.3% ± 0.6%
Tyr119	3.3% ± 0.6%
Lys128	3.9% ± 0.9%
Ser133	13% ± 5%
Tyr141	2.1% ± 0.1%
Ser147	10% ± 4%
Tyr151	1.3% ± 0.4%

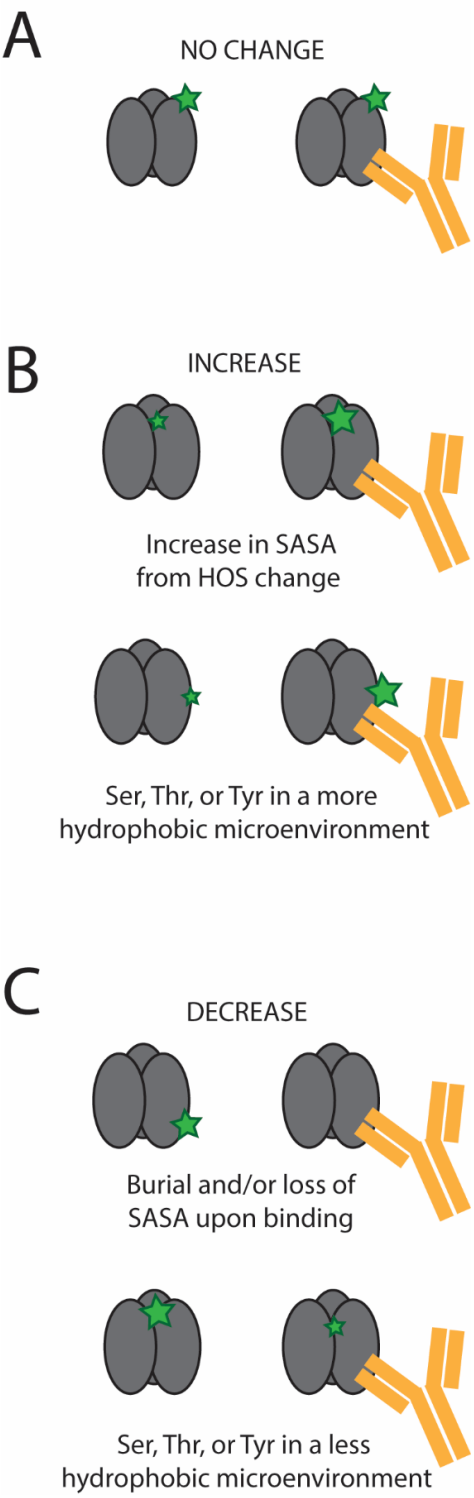

Figure 3.2: Cartoon representation of possible changes in labeling extent upon mAb binding. The TNFα trimer is depicted in gray; the antibody is depicted in yellow; and labeling is indicated by the green star, with the size of the star being proportional to the labeling extent. Results corresponding to (A) no change, (B) increases in labeling extent and (C) decreases in labeling extent are shown.

3.3.2. DEPC-CL of TNFα in complex with adalimumab

Adalimumab has the largest epitope of the three mAbs studied. The epitope is made up of two protomers of the TNFα homotrimer (**Figure 3.3**A and B), and is comprised of residues in the A-A', E-F, D-E, and G-H loops, as well as residues in the A and D β strands (**Figure 3.1**).[31,35] The epitope contains 11 labelable residues, eight of which are labeled in the control (i.e. rituximab-containing sample) and/or in the presence of adalimumab (**Table *3.2***). The remaining three, His78, His73, and Lys65, are not labeled in either the rituximab or adalimumab conditions, but they are labeled in free TNFα. His73 is part of the trimer interface, and Lys65 and His78 are largely buried. The labeling of these residues in free TNFα might occur due to a small extent of trimer dissociation, which is not expected when adalimumab is present, as this mAb strongly stabilizes the trimer. In any case, the lack of labeling of these residues in the control and mAb samples makes it difficult to definitively conclude anything about these residues.

The remaining eight epitope residues undergo changes in labeling extent upon comparing the control and mAb samples (**Figure 3.3**C and **Table *3.2***). Five of the eight residues decrease in labeling, including Tyr141, Lys112, Lys90, Thr72, and Ser71, as a result of burial due to adalimumab binding (**Figure 3.3**E). Labeling of all these residues, except Lys90 and Ser71, is completely prevented upon binding to adalimumab. Interestingly, three of the epitope residues (Thr77, Ser81, and Ser147) become labeled upon adalimumab binding, even though they were not labeled in the presence of non-binding rituximab (**Figure 3.3**F). The increased labeling of Thr77 may result from an increased hydrophobic microenvironment upon adalimumab binding from proximity to Trp53 on the heavy chain of adalimumab (**Figure 3.5**A). While Ser81 does not make

contact with adalimumab it is considered part of the epitope due to its location buried behind Lys90 and Glu135, which are both epitope residues (**Figure 3.5**B). Ser81 becomes partially exposed upon binding, causing labeling to occur. Ser147 also becomes labeled, likely due to a more hydrophobic environment resulting from nearby adalimumab residues (**Figure 3.5**C). Overall, DEPC labeling changes occur for all modifiable residues in the TNFα epitope, but the changes for Thr and Ser residues that are at the edges of the epitope actually undergo increased labeling. These counterintuitive changes in labeling reflect the unique sensitivity that DEPC labeling has to hydrophobic microenvironments for these weakly nucleophilic residues.[17-19]

Outside of the epitope, 21 residues are labeled, and most of these (11/21) do not change in labeling extent, indicating that these residues do not experience significant changes in SASA or microenvironment. One residue, Ser86, decreases in labeling extent. Ser86 resides in the D-E loop and is repositioned upon adalimumab binding. It is likely that the hydrophobic pocket around Ser86 changes upon adalimumab binding, causing a decrease in labeling (**Figure 3.3**D). Interestingly, the labeling of adjacent Tyr87 also changes (**Figure 3.3**D), although the large error bars associated with the measurement of this residue cause this change to be insignificant according to a t-test. Nine residues outside of the epitope increase in labeling extent. Most (7/9) of these residues are serines, threonines, or tyrosines, whose DEPC reactivity are very sensitive to microenvironment changes.[17–19] Two residues, Thr89 and Thr105, are not labeled in the control (**Figure 3.3**D), but upon adalimumab binding, their microenvironment becomes more hydrophobic, likely as a result of their close proximity to the epitope, explaining their increased labeling extent (**Figure 3.5**E). The labeling increases for Ser9, Tyr56, Tyr119,

and Tyr151 are more difficult to explain. A common feature of these residues is that they face the trimer interface in TNFα (**Figure 3.5**F). It is possible that the stabilization of the trimer that occurs upon adalimumab binding changes the microenvironment of these residues in a way that increases their labeling extent. Two of these residues (i.e. Tyr56, and Tyr151) are completely unlabeled in the control and become labeled in the complex, making their behavior similar to the Ser and Thr residues at the edges of the epitope.

The two other non-epitope residues that increase in labeling extent are His15 and Lys128. Previous work with DEPC labeling indicates that changes in the labeling of histidine and lysine residues occurs with changes in SASA;[23–28] however, the crystal structure of the F_{ab} of adalimumab with the TNFα trimer does not indicate any significant change in the SASA of His15 or Lys128. One possible explanation is that there are more complex changes to the adalimumab/TNFα complex that are not reflected in the crystal structure because the complete antibody is not present, as is the case in our CL/MS experiments. Indeed, SEC experiments (**Figure 3.4**A and B) indicate that complexes larger than 3:1 complexes (**Figure 3.3**A) are formed under the concentrations used in our experiments. Large protein complexes consisting of multiple TNFα trimers and more than three adalimumab molecules are measured, which are consistent with previous reports that postulated polymeric-like complexes at high concentrations, such as those found in formulations[39] and used in our studies. It is possible that these higher-order complexes influence the SASA of His15 and Lys128 that are both far from the epitope and the trimer interface of TNFα.

Table 3.2: DEPC Modification percentages of each residue in complex with adalimumab. Residues with an asterisk (*) are part of the epitope.

Residue	TNFα and rituximab	TNFα and adalimumab	Significant?	Change
Ser3/4/5	8% ± 2%	7% ± 3%	No	
Thr7	3% ± 1%	2% ± 0%	No	
Ser9	0.4% ± 0.2%	1.6% ± 0.3%	Yes	Increase
Lys11	22% ± 6%	25% ± 9%	No	
His15	0.7% ± 0.3%	24% ± 9%	Yes	Increase
Ser52	0.3% ± 0.4%	0 % ± 0%	No	
Tyr56	0 % ± 0%	3% ± 2%	Yes	Increase
Ser60	0 % ± 0%	3% ± 2%	Yes	Increase
Ser71*	21% ± 9%	6% ± 2%	Yes	Decrease
Thr72*	5% ± 4%	0 % ± 0%	Yes	Decrease
Thr77*	0 % ± 0%	7% ± 5%	No	
Ser81*	0 % ± 0%	30% ± 10%	Yes	Increase
Ser86	14% ± 6%	4% ± 2%	Yes	Decrease
Tyr87	41% ± 10%	21% ± 10%	No	
Thr89	0% ± 0%	8% ± 3%	Yes	Increase
Lys90*	33% ± 3%	3% ± 2%	Yes	Decrease
Ser95	17% ± 4%	19.2% ± 0.7%	No	
Lys98	30% ± 6%	25% ± 3%	No	
Thr105	0 % ± 0%	5% ± 3%	Yes	Increase
Lys112*	9 % ± 3%	0.7% ± 0.8%	Yes	Decrease
Tyr115	3% ± 1%	1.51% ± 0.05%	No	
Tyr119	7% ± 1%	60% ± 10%	Yes	Increase
Lys128	14% ± 4%	76% ± 7%	Yes	Increase
Ser133	4% ± 3%	0 % ± 0%	No	
Tyr141*	0.3% ± 0.1%	0 % ± 0%	Yes	Decrease
Ser147*	0.3% ± 0.1%	14% ± 8%	Yes	Increase
Tyr151	0 % ± 0 %	12% ± 8%	Yes	Increase

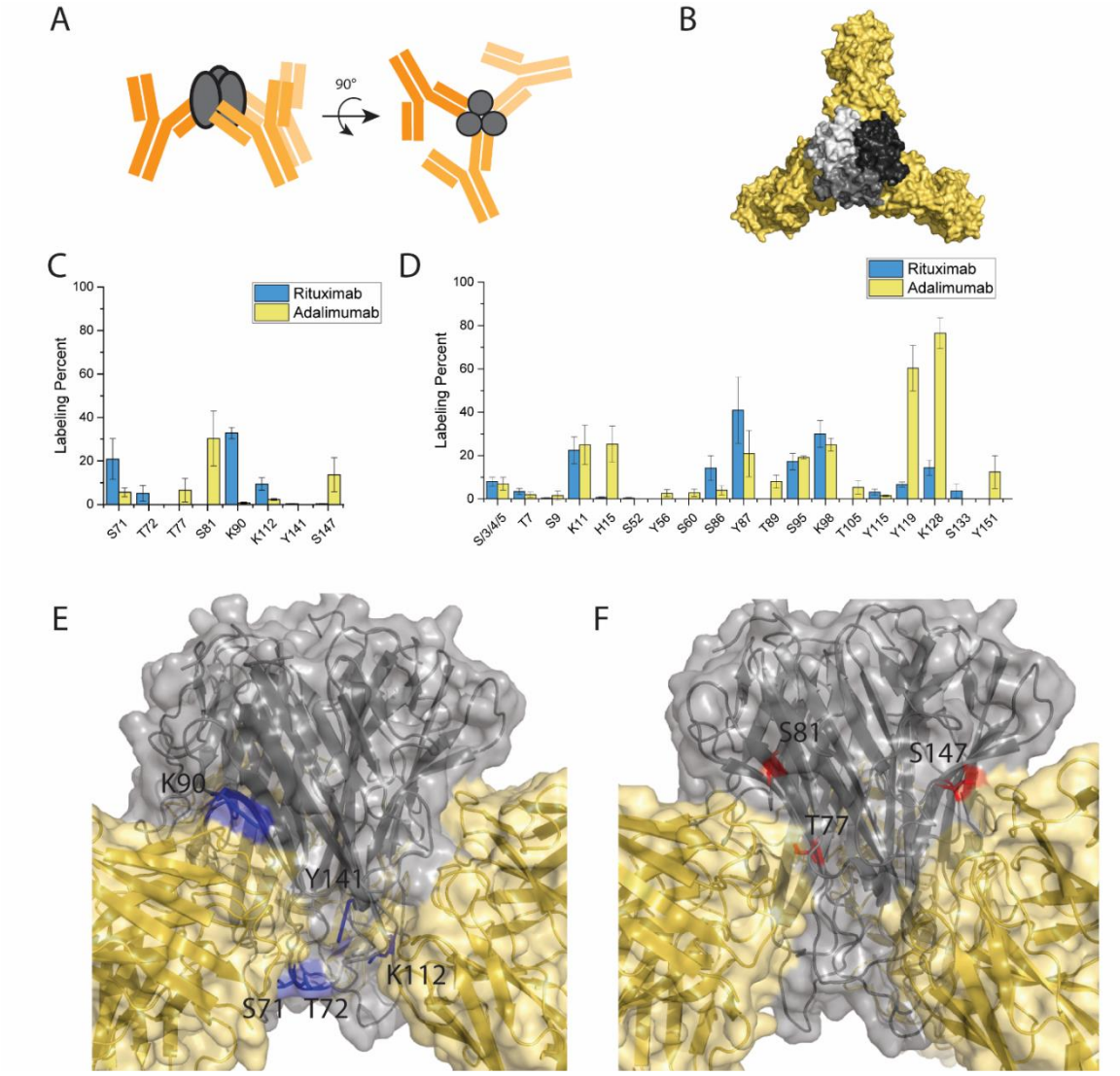

Figure 3.3: Structure and DEPC labeling residues for TNFα in complex with adalimumab. (A) Cartoon representation of adalimumab in complex with the TNFα trimer. Adalimumab binds in the trimer groove to two protomers of the TNFα trimer. (B) Surface structure representation of the F_{ab} of adalimumab in complex with the TNFα trimer (PDB ID: 3WD5). (C) DEPC labeling extents for the epitope residues in TNFα with and without adalimumab. (D) DEPC labeling extents for the non-epitope residues in TNFα with and without adalimumab. (E) Epitope residues that decrease in labeling (blue) upon adalimumab binding, mapped on the TNFα trimer. Adalimumab is shown in yellow and TNFα trimer is shown in gray. (F) Epitope residues that increase in labeling (red) upon adalimumab binding, mapped on the TNFα trimer.

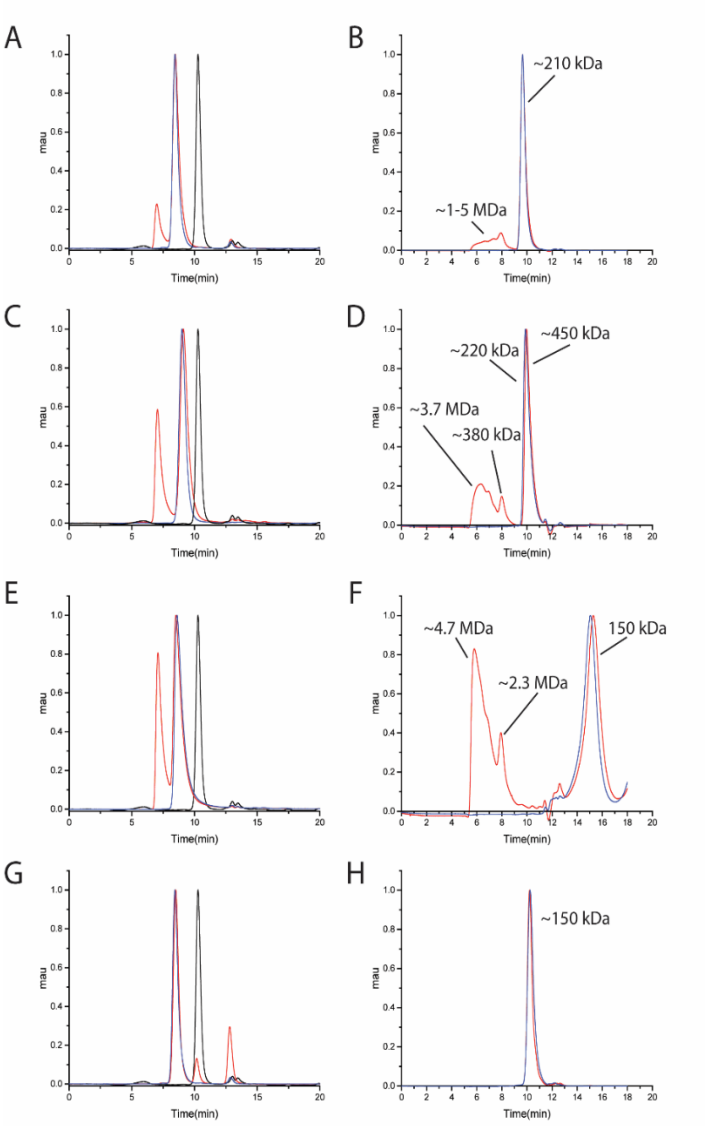

Figure 3.4: SEC data of TNFα in solution with (A, B) adalimumab, (C, D) infliximab, (E, F) golimumab, and (G, H) rituximab. The chromatograms in A, C, E, and G separate the proteins using the TSKgel SuperSW3000 column with a dynamic range of 15 kDa to 500 kDa, which allow TNFα to be separated from the mAb and TNFα/mAb complex. The chromatogram for TNFα alone is plotted in black, the mAb alone is plotted in blue, and the mixture is plotted in red. The chromatograms in B, D, F, and H separate the proteins using the Sepax SRT SED-500 column with a dynamic range of 15 kDa to 5 MDa, which cannot resolve free TNFα from free mAb but can provide further insight into the molecular weights of the complexes that are formed. The separations shown in B, D, F, and H were analyzed with a MALS detector, and the measured masses are indicated on the plot. It should be noted that golimumab interacted with this column, leading to an unexpectedly high retention time. MALS of free infliximab indicates the existence of a species with molecular weights of 150 kDa and 450 kDa, presumably due to the known quinary structure of free infliximab that has been reported previously.[40]

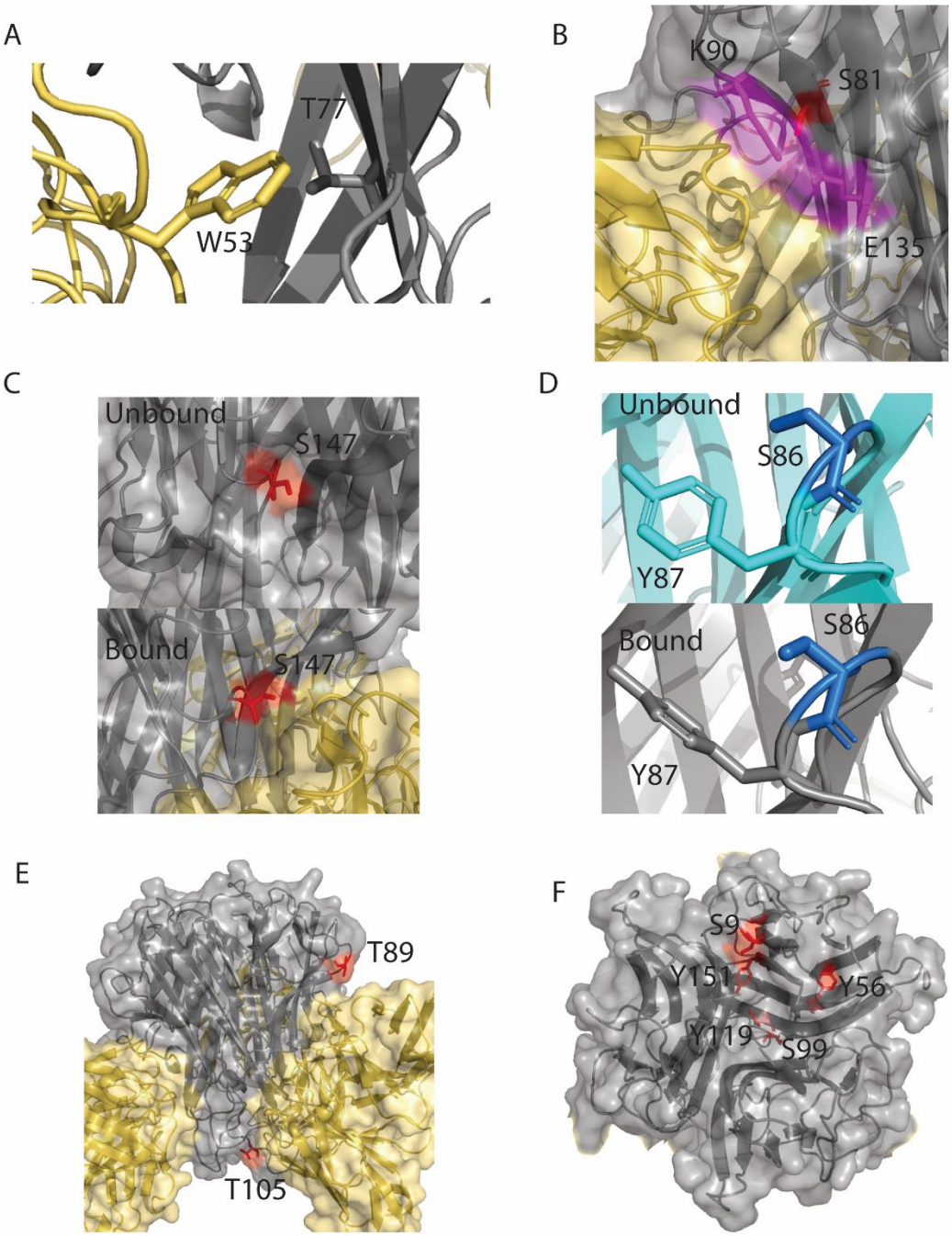

Figure 3.5: Representative changes to TNFα residues upon binding of adalimumab
(A) The microenvironment of Thr77 increases in hydrophobicity as a result of its proximity to Trp53 in adalimumab. (B) Ser81 is buried by epitope residues Lys90 and Glu135, but becomes partially exposed upon adalimumab binding, causing its DEPC reactivity to increase. (C) In unbound TNFα, Ser147 is entirely exposed to solvent, however, in the presence of adalimumab, this residue is located in a more hydrophobic microenvironment. (D) The microenvironment of Ser86 becomes less hydrophobic in the bound state (gray) due to its decreased proximity to Tyr87. (E) Thr89 and Thr105 increase in labeling due to their proximity to adalimumab. (F) Ser9, Tyr151, Tyr119, and Tyr56 all increase in labeling extent and are far from the epitope, but these residues are near the trimer interface.

3.3.3. DEPC-CL of TNFα in complex with infliximab

The infliximab epitope is smaller than the adalimumab epitope and is made up primarily of residues on the C-D and E-F loops and a few residues in the C and D β-strands. The residues Tyr141, Thr72, Ser71, and His73 are common to both the adalimumab and infliximab epitopes. Importantly, crystallographic data indicates that a large conformation change in the E-F loops occurs upon infliximab binding.[41] While infliximab only binds to one protomer of the TNFα homotrimer, it stabilizes the trimer to a similar extent as adalimumab.[31,35] The infliximab epitope has five labelable residues, but only four are labeled in the control or infliximab-bound state. As was seen in the adalimumab experiments, His73 is not labeled. Of the other four labeled epitope residues, three of them (Tyr141, Thr72, and Ser71) decrease in labeling (**Figure 3.6**A), as was observed upon adalimumab binding. These decreases are consistent with a burial of these residues upon infliximab binding (**Figure 3.6**C). Thr105, on the other hand, increases in labeling extent (**Figure 3.6**A) even though it is considered part of the epitope. Thr105 is on a very solvent exposed loop in free TNFα, but upon infliximab binding, this residue becomes partially buried, thereby creating a more hydrophobic environment that increases its reactivity (**Figure 3.6**D). Thr105 labeling also increased upon adalimumab binding because of a more hydrophobic environment, but infliximab binding creates an even bigger hydrophobic pocket near Thr105, causing its DEPC reactivity to increase even more. Again, like was seen with adalimumab, most of the epitope residues undergoes decreases in labeling, but Thr residues at the edge of the epitope undergo an increase in labeling due to the hydrophobic microenvironment that is created upon binding.

In addition to the four labeled residues in the epitope, there are 22 residues that are not considered part of the epitope that are labeled by DEPC with and without infliximab. As with adalimumab, most of these residues (12/22) do not change in labeling extent; however, six residues decrease in labeling extent and three increase (**Figure 3.6**B). One of these residues, Lys112, decreases due to its proximity to the epitope, which causes it to be partially buried upon binding (**Figure 3.7**A). Lys98, Tyr119, and Ser95 also decrease in labeling. Each of these residues faces toward the TNFα trimer interface (**Figure 3.7**B), and their decreased labeling is due to structural changes that occur upon stabilization of the trimer, as was observed with adalimumab. Interestingly, upon adalimumab binding, Y119 labeling increases, while Lys98 and Ser95 do not change, suggesting that the structural changes associated with trimer stabilization are different for these two mAbs. These structural differences in stabilization are perhaps not surprising as adalimumab binds two promoters of TNFα while infliximab only binds one. Lastly, Ser147 and Tyr87 also decrease in labeling, but they are not near the trimer interface or the epitope. It is possible that the higher order molecular weight complexes that are detected by SEC are responsible for the decreases observed at these residues (**Figure 3.4**C and D).

Three residues that are not part of the epitope increase in DEPC labeling upon infliximab binding: Ser99, Thr89, and Lys128. Ser99 is near the epitope, and therefore in a more hydrophobic environment as a result of the presence of infliximab (**Figure 3.7**C). Ser99 is positioned close to Phe28 in the heavy chain of infliximab and Tyr115 in the adjacent TNFα monomer to create a hydrophobic pocket without completely burying this residue, which leads to an increase in labeling. Such a microenvironment is not created upon adalimumab binding, so Ser99 is not found to be labeled upon binding that mAb.

The increase in labeling of Lys128 and Thr89 is difficult to explain, but as with adalimumab binding, the formation of higher-order complexes may explain their labeling behavior.

Table 3.3: DEPC Modification percentages of each residue for TNFα in complex with infliximab. Residues with an asterisk are part of the epitope.

Residue	TNFα and rituximab	TNFα and infliximab	Significant?	Change
Ser3/4/5	8% ± 2%	6% ± 5%	No	
Thr7	3% ± 1%	13% ± 7%	No	
Ser9	0.4% ± 0.2%	1.4% ± 0.7%	No	
Lys11	22% ± 6%	30% ± 7%	No	
His15	0.7% ± 0.3%	1.2% ± 0.3%	No	
Ser52	0.3% ± 0.4%	3% ± 2%	No	
Ser71*	21% ± 9%	0 % ± 0%	Yes	Decrease
Thr72*	5% ± 4%	0 % ± 0%	Yes	Decrease
Ser86	14% ± 6%	12% ± 5%	No	
Tyr87	41% ± 10%	0 % ± 0%	Yes	Decrease
Thr89	0 % ± 0%	5.9% ± 0.7%	Yes	Increase
Lys90	33% ± 3%	24% ± 7%	No	
Ser95	17% ± 4%	2 % ± 1%	Yes	Decrease
Lys98	30% ± 6%	13% ± 7%	Yes	Decrease
Ser99	0 % ± 0%	46% ± 10%	Yes	Increase
Thr105*	0 % ± 0%	21% ± 3%	Yes	Increase
Lys112	9% ± 3%	4% ± 2%	Yes	Decrease
Tyr115	3% ± 1%	1.3% ± 0.8%	No	
Tyr119	7% ± 1%	0.9% ± 0.3%	Yes	Decrease
Lys128	14% ± 4%	39% ± 7%	Yes	Increase
Ser133	4% ± 3%	0.3% ± 0.2%	No	
Tyr141*	0.3% ± 0.1%	0 % ± 0%	Yes	Decrease
Ser147	0.3% ± 0.1%	0 % ± 0%	Yes	Decrease

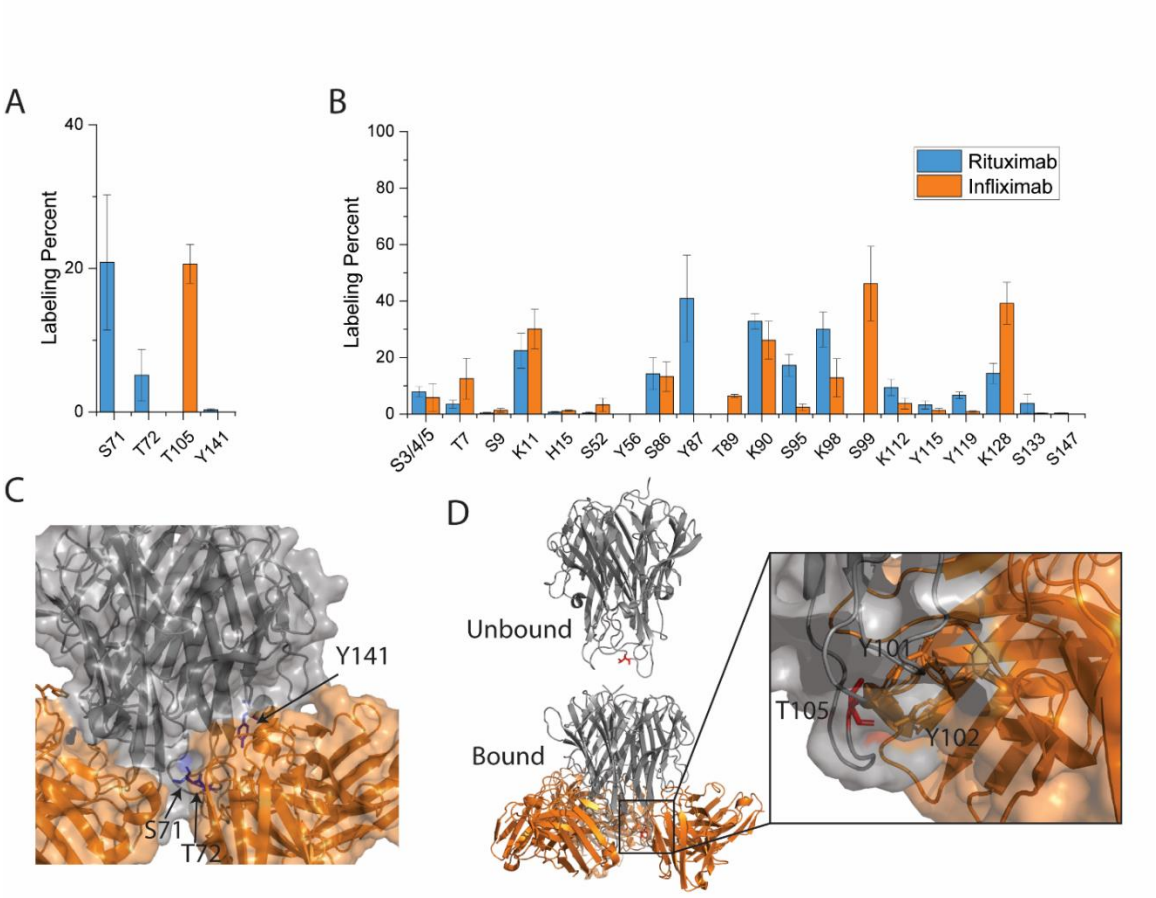

Figure 3.6: Structure and DEPC labeling residues for TNFα in complex with infliximab. (A) DEPC labeling extents for the epitope residues in TNFα with and without infliximab. (B) DEPC labeling extents for the non-epitope residues in TNFα with and without infliximab. (C) Epitope residues that decrease in labeling (blue) upon infliximab binding, mapped on the TNFα trimer. Infliximab is shown in orange and TNFα trimer is shown in gray (PDB 4G3Y). (D) Epitope residues that increase in labeling (red) upon infliximab binding, mapped on the TNFα trimer.

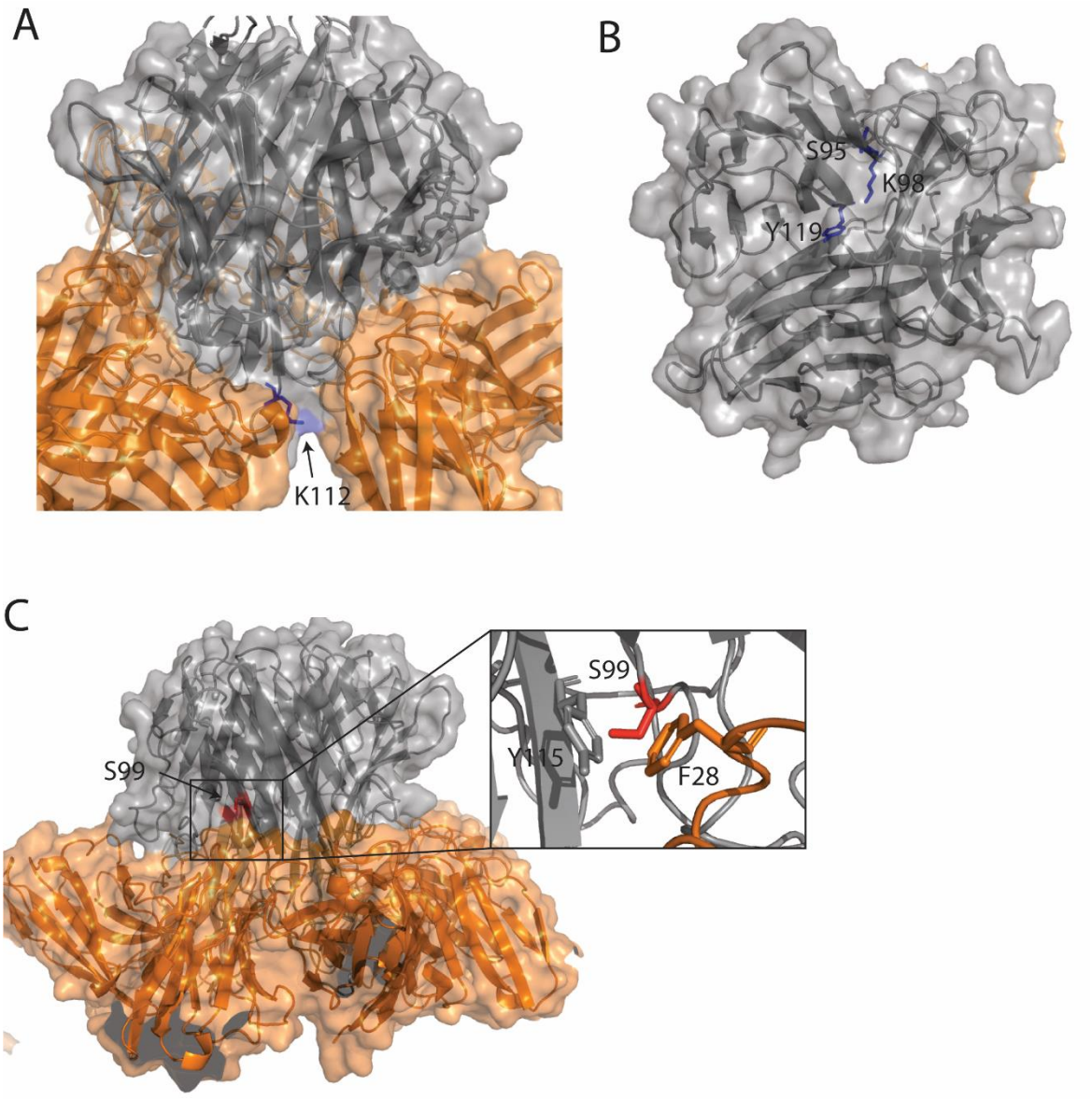

Figure 3.7: Representative changes to TNFα residues upon binding infliximab. (A) Lys112, represented in blue, is partially buried upon infliximab (orange) binding. (B) Tyr119, Ser95, and Lys98 (blue) face into the trimer interface, and decrease in labeling upon infliximab binding, presumably due to structural changes associated with trimer stabilization. (C) The microenvironment of Ser99 becomes more hydrophobic as a result of the increased proximity to hydrophobic residues Tyr119 on TNFα and Phe28 on infliximab, causing it to undergo increased DEPC labeling.

3.3.4. DEPC-CL of TNFα in complex with golimumab

Golimumab has the smallest epitope of the three mAbs studied yet has the highest binding affinity.[42] Golimumab only binds one promoter of the trimer and stabilizes the trimer the least out of the three mAbs studied (**Figure 3.8**A).[31,35] The golimumab epitope is made up of residues in the A-A', C-D, G-H, and E-F loops. Similar to infliximab and adalimumab, the E-F loop is a key component of antibody binding, whereas the G-H loop and C-D loop are less important for golimumab binding. The residues Tyr141, Thr72, and Ser71 are involved in all three epitopes studied, while residue Thr105 is important for both golimumab and infliximab, but not adalimumab.

The golimumab epitope has five labelable residues, of which four are experimentally found to be labeled. The one epitope residue that is not labeled in either the control or upon golimumab binding is Lys65. The other four epitope residues, Tyr141, Thr105, Thr72, and Ser71 are the same four epitope residues in infliximab. These four residues have the same labeling behavior as was seen upon infliximab binding. Tyr141, Thr72, and Ser71 all decrease in labeling (**Figure 3.8**A) due to burial (**Figure 3.8**C), while Thr105 experiences an increase in labeling due to its increased hydrophobic environment caused by the proximity of Ile102 in the heavy chain of golimumab (**Figure 3.8**D).

There are 19 residues labeled by DEPC that are not considered part of the epitope (**Figure 3.8**B). Eight do not change in labeling extent, eight decrease, and four increase. Of the eight decreases, Lys98, His15, Tyr119, and Ser95 are all part of the trimer interface, and thus their decreased labeling is perhaps due to trimer stabilization (**Figure 3.9**A),[43] as was observed for infliximab and adalimumab. Interestingly, both golimumab

and infliximab bind one protomer and have similar patterns of changes to residues in the trimer interface, while adalimumab binds two promoters and different residues undergo changes in labeling. These data suggest that the structural changes associated with trimer stabilization are similar for golimumab and infliximab. The other four residues that are distant from the epitope and decrease in labeling, Tyr87, Ser86, Thr7 and Ser147, are also distant from the trimer interface (**Figure 3.9**B). Ser86 and Tyr87 are in the D-E loop, and the crystal structure of the TNFα/golimumab complex indicates structural changes in the D-E loop upon binding (**Figure 3.9**D), which cause a change in the microenvironment around these residues. Labeling changes to Thr7 and Ser147 are more difficult to explain, but the complicated mixture of higher order complexes that are observed by SEC (**Figure 3.4**E and F) upon golimumab binding could be the cause of these labeling changes. The labeling increases that are observed for Lys128, Thr89, Thr77, and Ser9 might also be caused by the same complicated mix of complexes. All four of these residues are distant from the epitope and are not involved in the trimer interface (**Figure 3.9**C), although it should be noted that Ser9 is not resolved in the crystal structure of the complex.

Table 3.4: DEPC Modification percentages of each residue upong binding with golimumab. Residues with an asterisk (*) are part of the epitope.

Residue	TNFα and rituximab	TNFα and golimumab	Significant?	Change
Ser3/4/5	8% ± 2%	7% ± 6%	No	
Thr7	3% ± 1%	0 % ± 0%	Yes	Decrease
Ser9	0.4% ± 0.2%	18% ± 8%	Yes	Increase
Lys11	22% ± 6%	13% ± 4%	No	
His15	0.7% ± 0.3%	0 % ± 0%	Yes	Decrease
Ser71*	21% ± 9%	6% ± 3%	Yes	Decrease
Thr72*	5% ± 4%	0 % ± 0%	Yes	Decrease
Thr77	0 % ± 0%	21% ± 2%	Yes	Increase
His78	0 % ± 0%	1.2% ± 0.3%	Yes	Decrease
Ser86	14% ± 6%	0 % ± 0%	Yes	Decrease
Tyr87	41 % ± 10%	0 % ± 0%	Yes	Decrease
Thr89	0 % ± 0%	9% ± 1%	Yes	Increase
Lys90	33% ± 3%	37% ± 5%	No	
Ser95	17% ± 4%	2.3% ± 0.4%	Yes	Decrease
Lys98	30% ± 6%	3% ± 1%	Yes	Decrease
Thr105*	0 % ± 0%	20% ± 4%	Yes	Increase
Lys112	9% ± 3%	11% ± 3%	No	
Tyr115	3% ± 1%	1.7% ± 0.5%	No	
Tyr119	7% ± 1%	0 % ± 0%	Yes	Decrease
Lys128	14% ± 4%	25% ± 3%	Yes	Increase
Ser133	4% ± 3%	0 % ± 0%	No	
Tyr141*	0.3% ± 0.1%	0 % ± 0%	Yes	Decrease
Ser147	0.3% ± 0.1%	0 % ± 0%	Yes	Decrease

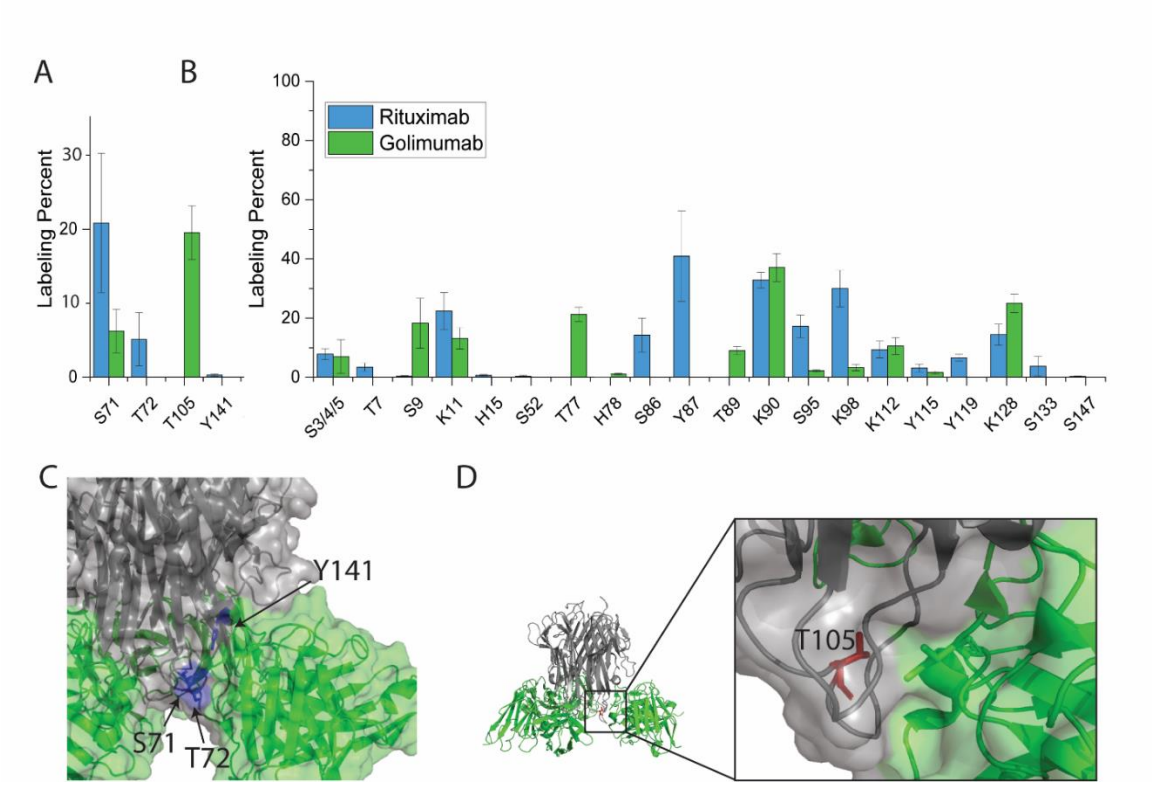

Figure 3.8: Structure and DEPC labeling residues for TNFα in complex with golimumab. (A) DEPC labeling extents for the epitope residues in TNFα with and without golimumab. (B) DEPC labeling extents for the non-epitope residues in TNFα with and without golimumab. (C) Epitope residues that decrease in labeling (blue) upon golimumab binding, mapped on the TNFα trimer. Golimumab is shown in green and TNFα trimer is shown in gray (PDB 5YOY). (D) Epitope residues that increase in labeling (red) upon golimumab binding, mapped on the TNFα trimer.

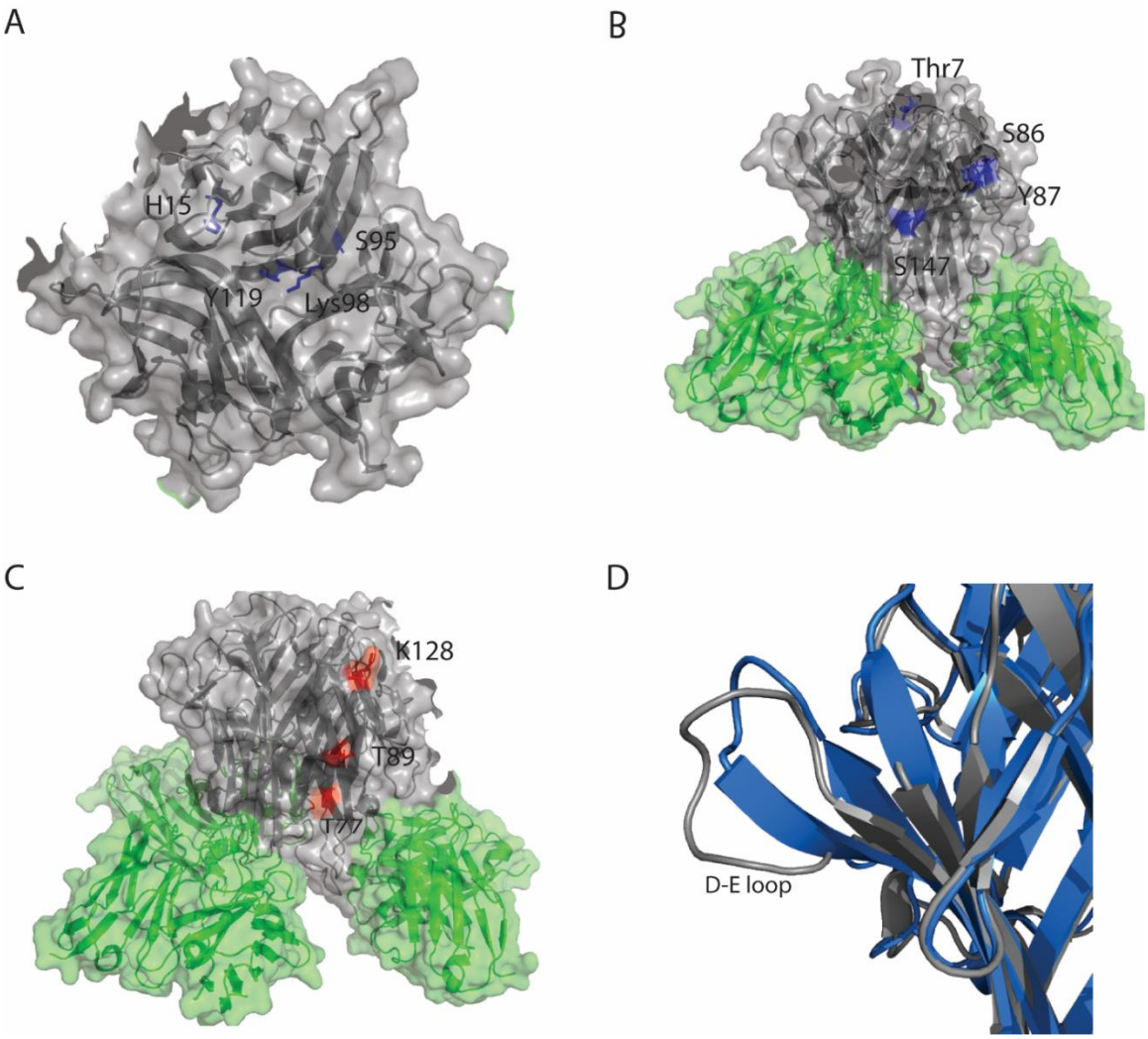

Figure 3.9: Representative changes to TNFα labelable residues upon binding golimumab (A) His15, Tyr119, Ser95, and Lys98 (blue) face into the trimer interface and decrease in labeling upon golimumab binding, presumably due to the structural changes associated with trimer stabilization. (B) Thr7, Ser147, Ser86 and Tyr87 (blue) decrease upon golimumab binding but are far from the epitope and trimer interface. (C) Lys128, Thr89, and Thr77 (red) increase upon golimumab binding but are far from the epitope and trimer interface. These residues possibly increase in labeling due to the formation of higher-order complexes as observed in SEC measurements. (D) Conformational change of D-E loop from unbound TNFα (blue) to bound TNFα (gray).

3.4. Conclusion

Using three different mAbs that bind their antigen TNFα in a well-characterized manner, we demonstrate that DEPC-CL/MS can reveal accurate information about epitopes and subtle structural changes away from epitopes. To get reliable epitope mapping results, control experiments involving a non-binding mAb are required to account for labeling changes that are caused by the presence of a large number of labelable residues in the mAb. Our data show that residues in the epitope that become completely buried upon binding decrease in labeling extent. Interestingly, weakly nucleophilic residues (i.e. Ser, Thr, Tyr) that are in or near the epitope, but are not completely buried upon binding, undergo an increase in labeling extent due to an increased hydrophobic microenvironment that is created by nearby mAb residues. This effect is consistent with our previous work and is likely explained by increased local concentrations of DEPC, which is a somewhat hydrophobic molecule.[17–19] An excellent example of this effect is the increased labeling of Thr105 upon binding to all three mAbs. In free TNFα, Thr105 is on an unstructured loop and is fully solvent exposed; however, upon mAb binding, residues from the antibodies create a hydrophobic microenvironment around this residue without fully burying it, causing an increase in labeling. A more significant hydrophobic microenvironment is created upon infliximab and golimumab binding, and Thr105 labeling is found to increase to the greatest extent when these antibodies are bound to TNFα. Most residues that are distant from the epitope do not undergo any significant changes in labeling extent, although some residues do change. The residues that do change primarily fall into three categories. The first category includes residues that are not part of the epitope but are in close proximity to the epitope and thus experience a change in labeling extent due to partial burial. Second, there are

residues at the TNFα trimer interface that undergo changes in labeling that reflect structural changes caused by trimer stabilization when the antibody binds. The third category includes primarily Ser, Thr, and Tyr residues that experience changes in microenvironment due to higher-order structural changes that occur upon antibody binding. These changes can be either increases or decreases in labeling and reflect more or less hydrophobic environments being created around these residues that are the result of structural changes or the formation of complexes with large mAb/TNFα stoichiometries that are present in solution but not in the crystal structures. Overall, DEPC labeling can provide insight into antibody-antigen epitopes, although the resulting labeling changes depend on the extent to which a residue is buried and how the microenvironment around the residue changes upon binding. In the latter case, we again see that the reactivity of Ser, Thr, and Tyr residues are very sensitive to the hydrophobic microenvironment of these residues, making them very sensitive probes of binding and structural changes throughout the protein.

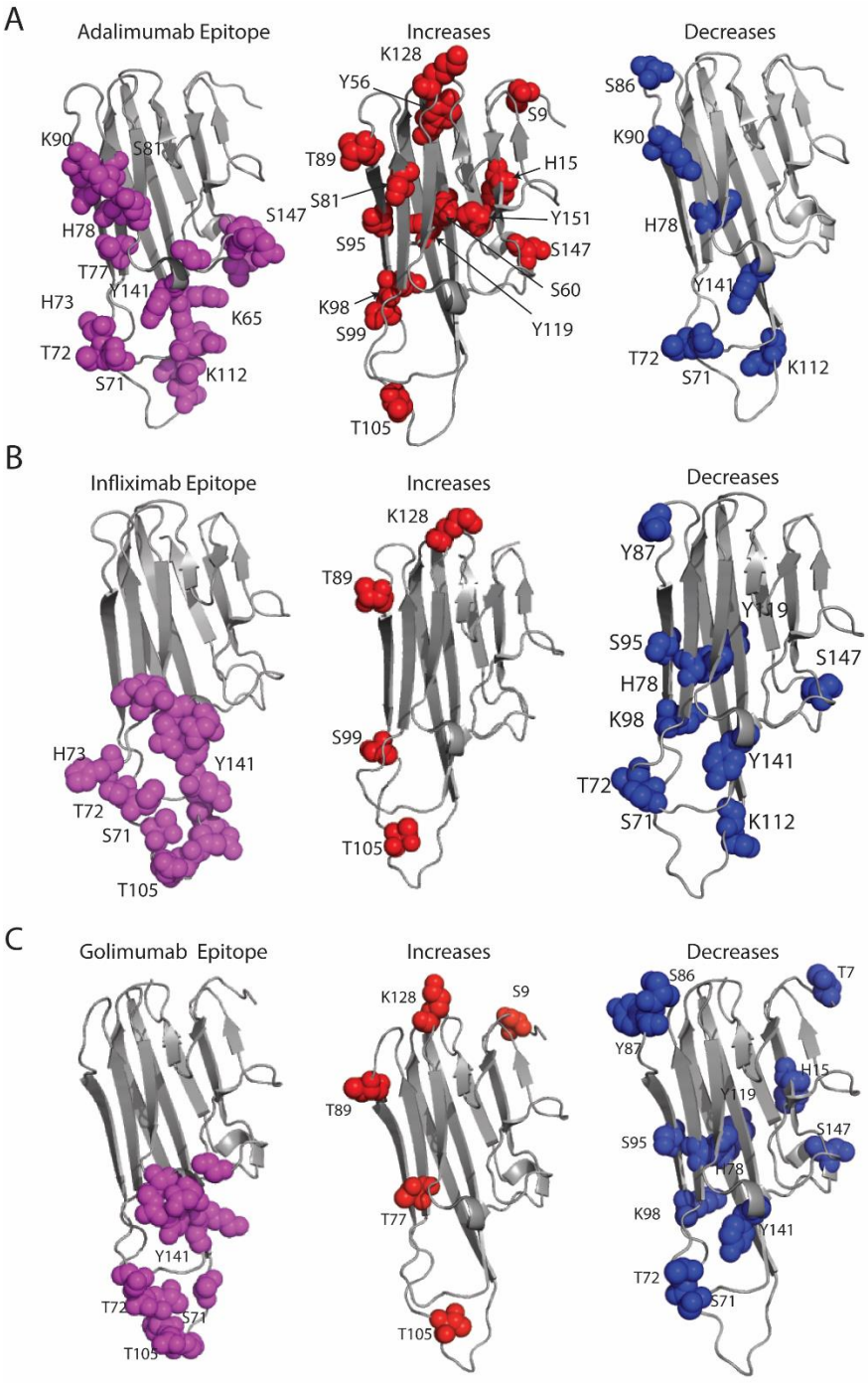

Figure 3.10: Monomeric TNFα with epitope, DEPC increases, and DEPC decreases mapped on to structure (PDB: 1TNF). The epitope is mapped in magenta, increases in DEPC-CL labeling extent in red, and decreases in blue for (A) adalimumab (B) infliximab (C) golimumab.

3.5. References

(1) Pettersson, I. Methods of Epitope Mapping. Mol. Biol. Rep. 1992, 16, 149–153.

(2) Abbott, W. M.; Damschroder, M. M.; Lowe, D. C. Current Approaches to Fine Mapping of Antigen-Antibody Interactions. Immunology 2014, 142 (4), 526–535. https://doi.org/10.1111/imm.12284.

(3) Huang, R. Y. C.; Iacob, R. E.; Sankaranarayanan, S.; Yang, L.; Ahlijanian, M.; Tao, L.; Tymiak, A. A.; Chen, G. Probing Conformational Dynamics of Tau Protein by Hydrogen/Deuterium Exchange Mass Spectrometry. J. Am. Soc. Mass Spectrom. 2018, 29 (1), 174–182. https://doi.org/10.1007/s13361-017-1815-8.

(4) Hager-Braun, C.; Tomer, K. B. Determination of Protein-Derived Epitopes by Mass Spectrometry. Expert Rev. Proteomics 2005, 2 (5), 745–756. https://doi.org/10.1586/14789450.2.5.745.

(5) Sun, H.; Ma, L.; Wang, L.; Xiao, P.; Li, H.; Zhou, M.; Song, D. Research Advances in Hydrogen–Deuterium Exchange Mass Spectrometry for Protein Epitope Mapping. Anal. Bioanal. Chem. 2021, 413 (9), 2345–2359. https://doi.org/10.1007/s00216-020-03091-9.

(6) Li, K. S.; Chen, G.; Mo, J.; Huang, R. Y.; Deyanova, E. G.; Beno, B. R.; O'Neil, S. R.; Tymiak, A. A.; Gross, M. L. Orthogonal Mass Spectrometry-Based Footprinting for Epitope Mapping and Structural Characterization: The IL-6 Receptor upon Binding of Protein Therapeutics. Anal. Chem. 2017, 89, 7742–7749. https://doi.org/10.1021/acs.analchem.7b01748.

(7) Opuni, K. F. M.; Al-Majdoub, M.; Yefremova, Y.; El-Kased, R. F.; Koy, C.; Glocker, M. O. Mass Spectrometric Epitope Mapping. Mass Spectrom. Rev. 2018, 37 (2), 229–241. https://doi.org/10.1002/mas.21516.

(8) Suckau, D.; Köhl, J.; Karwath, G.; Schneider, K.; Casaretto, M.; Bitter-Suermann, D.; Przybylski, M. Molecular Epitope Identification by Limited Proteolysis of an Immobilized Antigen-Antibody Complex and Mass Spectrometric Peptide Mapping. Proc. Natl. Acad. Sci. U. S. A. 1990, 87 (24), 9848–9852. https://doi.org/10.1073/pnas.87.24.9848.

(9) Zhang, M. M.; Huang, R. Y. C.; Beno, B. R.; Deyanova, E. G.; Li, J.; Chen, G.; Gross, M. L. Epitope and Paratope Mapping of PD-1/Nivolumab by Mass Spectrometry-Based Hydrogen-Deuterium Exchange, Cross-Linking, and Molecular Docking. Anal. Chem. 2020, 92 (13), 9086–9094. https://doi.org/10.1021/acs.analchem.0c01291.

(10) Gramlich, M.; Hays, H. C. W.; Crichton, S.; Kaiser, P. D.; Heine, A.; Schneiderhan-Marra, N.; Rothbauer, U.; Stoll, D.; Maier, S.; Zeck, A. Hdx-Ms for Epitope Characterization of a Therapeutic Antibody Candidate on the Calcium-Binding

Protein Annexin-A1. Antibodies 2021, 10 (11), 1–12. https://doi.org/10.3390/antib10010011.

(11) Zhang, Q.; Yang, J.; Bautista, J.; Badithe, A.; Olson, W.; Liu, Y. Epitope Mapping by HDX-MS Elucidates the Surface Coverage of Antigens Associated with High Blocking Efficiency of Antibodies to Birch Pollen Allergen. Anal. Chem. 2018, 90 (19), 11315–11323. https://doi.org/10.1021/acs.analchem.8b01864.

(12) Baerga-Ortiz, A.; Hughes, C. A.; Mandell, J. G.; Komives, E. A. Epitope Mapping of a Monoclonal Antibody against Human Thrombin by H/D-Exchange Mass Spectrometry Reveals Selection of a Diverse Sequence in a Highly Conserved Protein. Protein Sci. 2002, 11 (6), 1300–1308. https://doi.org/10.1110/ps.4670102.

(13) Jones, L. M.; Sperry, J.; Carroll, J.; Gross, M. L. Fast Photochemical Oxidation of Proteins (FPOP) for Epitope Mapping. Anal. Chem. 2011, 83 (20), 7657–7661. https://doi.org/10.1021/ac2007366.Fast.

(14) Pan, L. Y.; Salas-Solano, O.; Valliere-Douglass, J. F. Localized Conformational Interrogation of Antibody and Antibody-Drug Conjugates by Site- Specific Carboxyl Group Footprinting. MAbs 2017, 9 (2), 307–318. https://doi.org/10.1080/19420862.2016.1268306.

(15) Fiedler, W.; Borchers, C.; Macht, M.; Deininger, S. O.; Przybylski, M. Molecular Characterization of a Conformational Epitope of Hen Egg White Lysozyme by Differential Chemical Modification of Immune Complexes and Mass Spectrometric Peptide Mapping. Bioconjug. Chem. 1998, 9 (2), 236–241. https://doi.org/10.1021/bc970148g.

(16) Glocker, M. O.; Nock, S.; Sprinzl, M.; Przybylski, M. Characterization of Surface Topology and Binding Area in Complexes of the Elongation Factor Proteins EF-Ts and EF-Tu·GDP from Thermus Thermophilus: A Study by Protein Chemical Modification and Mass Spectrometry. Chem. - A Eur. J. 1998, 4 (4), 707–715.

(17) Tremblay, C. Y.; Limpikirati, P.; Vachet, R. W. Complementary Structural Information for Stressed Antibodies from Hydrogen − Deuterium Exchange and Covalent Labeling Mass Spectrometry. 2021, 32 (5), 1237–1248. https://doi.org/10.1021/jasms.1c00072.

(18) Limpikirati, P.; Hale, J. E.; Hazelbaker, M.; Huang, Y.; Jia, Z.; Yazdania, M.; Grabanb, E. M.; Vaughan, R. C.; Vachet, R. W. Covalent Labeling and Mass Spectrometry Reveal Subtle Higher Order Structural Changes for Antibody Therapeutics. MAbs 2019, 11 (3), 463–476. https://doi.org/10.1080/19420862.2019.1565748.

(19) Limpikirati, P.; Pan, X.; Vachet, R. W. Covalent Labeling with Diethylpyrocarbonate: Sensitive to the Residue Microenvironment, Providing Improved Analysis of Protein Higher Order Structure by Mass Spectrometry. Anal. Chem. 2019, 91 (13), 8516–8523. https://doi.org/10.1021/acs.analchem.9b01732.

(20) Limpikirati, P. K.; Zhao, B.; Pan, X.; Eyles, S. J.; Vachet, R. W. Covalent Labeling/Mass Spectrometry of Monoclonal Antibodies with Diethylpyrocarbonate: Reaction Kinetics for Ensuring Protein Structural Integrity. J. Am. Soc. Mass Spectrom. 2020, 31 (6), 1223–1232. https://doi.org/10.1021/jasms.0c00067.

(21) Li, J.; Wei, H.; Krystek, S. R.; Bond, D.; Brender, T. M.; Cohen, D.; Feiner, J.; Hamacher, N.; Harshman, J.; Huang, R. Y.; Julien, S. H.; Lin, Z.; Moore, K.; Mueller, L.; Noriega, C.; Sejwal, P.; Sheppard, P.; Stevens, B.; Chen, G.; Tymiak, A. A.; Gross, M. L.; Schneeweis, L. A. Mapping the Energetic Epitope of an Antibody/Interleukin-23 Interaction with Hydrogen/Deuterium Exchange, Fast Photochemical Oxidation of Proteins Mass Spectrometry, and Alanine Shave Mutagenesis. 2017. https://doi.org/10.1021/acs.analchem.6b03058.

(22) Wecksler, A. T.; Kalo, M. S.; Deperalta, G. Mapping of Fab-1:VEGF Interface Using Carboxyl Group Footprinting Mass Spectrometry. J. Am. Soc. Mass Spectrom. 2015, 26 (12), 2077–2080. https://doi.org/10.1007/s13361-015-1273-0.

(23) Mendoza, V. L.; Vachet, R. W. Protein Surface Mapping Using Diethylpyrocarbonate with Mass Spectrometric Detection. Anal. Chem. 2008, 80 (8), 2895–2904. https://doi.org/10.1021/ac701999b.

(24) Liu, T.; Limpikirati, P.; Vachet, R. W. Synergistic Structural Information from Covalent Labeling and Hydrogen − Deuterium Exchange Mass Spectrometry for Protein − Ligand Interactions. Anal. Chem. 2019, 91, 15248–15254. https://doi.org/10.1021/acs.analchem.9b04257.

(25) Glocker, M. O.; Kalkum, M.; Yamamoto, R.; Schreurs, J. Selective Biochemical Modification of Functional Residues in Recombinant Human Macrophage Colony-Stimulating Factor β (RhM-CSF β): Identification by Mass Spectrometry. Biochemistry 1996, 35 (46), 14625–14633. https://doi.org/10.1021/bi961199o.

(26) Hondal, R. J.; Ma, S.; Caprioli, R. M.; Hill, K. E.; Burk, R. F. Heparin-Binding Histidine and Lysine Residues of Rat Selenoprotein P. J. Biol. Chem. 2001, 276 (19), 15823–15831. https://doi.org/10.1074/jbc.M010405200.

(27) Mendoza, V. L.; Antwi, K.; Baron-Rodriguez, M. A.; Blanco, C.; Vachet, R. W. Structure of the Preamyloid Dimer of β-2-Microglobulin from Covalent Labeling and Mass Spectrometry. Biochemistry 2010, 49, 1522–1532. https://doi.org/10.1021/bi901748h.

(28) Mendoza, V. L.; Baro, M. A.; Blanco, C.; Vachet, R. W. Structural Insights into the Pre-Amyloid Tetramer of β -2- Microglobulin from Covalent Labeling and Mass Spectrometry. Biochemistry 2011, 50, 6711–6722.

(29) Borotto, N. B.; Zhou, Y.; Hollingsworth, S. R.; Hale, J. E.; Graban, E. M.; Vaughan, R. C.; Vachet, R. W. Investigating Therapeutic Protein Structure with

Diethylpyrocarbonate Labeling and Mass Spectrometry. Anal. Chem. 2015, 87, 10627–10634. https://doi.org/10.1021/acs.analchem.5b03180.

(30) Liu, T.; Marcinko, T. M.; Kiefer, P. A.; Vachet, R. W. Using Covalent Labeling and Mass Spectrometry To Study Protein Binding Sites of Amyloid Inhibiting Molecules. Anal. Chem. 2017, 89, 11583–11591. https://doi.org/10.1021/acs.analchem.7b02915.

(31) Van Schie, K. A.; Ooijevaar-De Heer, P.; Dijk, L.; Kruithof, S.; Wolbink, G.; Rispens, T. Therapeutic TNF Inhibitors Can Differentially Stabilize Trimeric TNF by Inhibiting Monomer Exchange. Sci. Rep. 2016, 6, 32747. https://doi.org/10.1038/srep32747.

(32) Corti, A.; Fassina, G.; Marcucci, F.; Barbanti, E.; Cassani, G. Oligomeric Tumour Necrosis Factor α Slowly Converts into Inactive Forms at Bioactive Levels. Biochem. J. 1992, 284 (3), 905–910. https://doi.org/10.1042/bj2840905.

(33) Daub, H.; Traxler, L.; Ismajli, F.; Groitl, B.; Itzen, A.; Rant, U. The Trimer to Monomer Transition of Tumor Necrosis Factor-Alpha Is a Dynamic Process That Is Significantly Altered by Therapeutic Antibodies. Sci. Rep. 2020, 10 (9265), 1–10. https://doi.org/10.1038/s41598-020-66123-5.

(34) Ono, M.; Horita, S.; Sato, Y.; Nomura, Y.; Iwata, S.; Nomura, N. Structural Basis for Tumor Necrosis Factor Blockade with the Therapeutic Antibody Golimumab. Protein Sci. 2018, 27 (6), 1038–1046. https://doi.org/10.1002/pro.3407.

(35) Hu, S.; Liang, S.; Guo, H.; Zhang, D.; Li, H.; Wang, X.; Yang, W.; Qian, W.; Hou, S.; Wang, H.; Guo, Y.; Lou, Z. Comparison of the Inhibition Mechanisms of Adalimumab and Infliximab in Treating Tumor Necrosis Factor α-Associated Diseases from a Molecular View. J. Biol. Chem. 2013, 288 (38), 27059–27067. https://doi.org/10.1074/jbc.M113.491530.

(36) Mitoma, H.; Horiuchi, T.; Tsukamoto, H.; Ueda, N. Molecular Mechanisms of Action of Anti-TNF-α Agents – Comparison among Therapeutic TNF-α Antagonists. Cytokine 2018, 101, 56–63. https://doi.org/https://doi.org/10.1016/j.cyto.2016.08.014.

(37) Pan, X.; Limpikirati, P.; Chen, H.; Liu, T.; Vachet, R. W. Higher-Order Structure Influences the Kinetics of Diethylpyrocarbonate Covalent Labeling of Proteins. J. Am. Soc. Mass Spectrom. 2020, 31 (3), 658–665. https://doi.org/10.1021/jasms.9b00132.

(38) Borotto, N. B.; Zhou, Y.; Hollingsworth, S. R.; Hale, J. E.; Graban, E. M.; Vaughan, R. C.; Vachet, R. W. Investigating Therapeutic Protein Structure with Diethylpyrocarbonate Labeling and Mass Spectrometry. Anal. Chem. 2015. https://doi.org/10.1021/acs.analchem.5b03180.

(39) Contreras, M. A.; Macaya, L.; Neira, P.; Camacho, F.; González, A.; Acosta, J.; Montesino, R.; Toledo, J. R.; Sánchez, O. New Insights on the Interaction Mechanism of RhTNFα with Its Antagonists Adalimumab and Etanercept. bioRxiv Prepr. 2020. https://doi.org/10.1101/2020.06.21.163824.

(40) Chen, K.; Long, D. S.; Lute, S. C.; Levy, M. J.; Brorson, K. A.; Keire, D. A. Simple NMR Methods for Evaluating Higher Order Structures of Monoclonal Antibody Therapeutics with Quinary Structure. J. Pharm. Biomed. Anal. 2016, 128, 398–407. https://doi.org/10.1016/j.jpba.2016.06.007.

(41) Liang, S.; Dai, J.; Hou, S.; Su, L.; Zhang, D.; Guo, H.; Hu, S.; Wang, H.; Rao, Z.; Guo, Y.; Lou, Z. Structural Basis for Treating Tumor Necrosis Factor α (TNFα)-Associated Diseases with the Therapeutic Antibody Infliximab. J. Biol. Chem. 2013, 288 (19), 13799–13807. https://doi.org/10.1074/jbc.M112.433961.

(42) Kim, M. S.; Lee, S. H.; Song, M. Y.; Yoo, T. H.; Lee, B. K.; Kim, Y. S. Comparative Analyses of Complex Formation and Binding Sites between Human Tumor Necrosis Factor-Alpha and Its Three Antagonists Elucidate Their Different Neutralizing Mechanisms. J. Mol. Biol. 2007, 374 (5), 1374–1388. https://doi.org/10.1016/j.jmb.2007.10.034.

(43) Krissinel, E.; Henrick, K. Inference of Macromolecular Assemblies from Crystalline State. J. Mol. Biol. 2007, 372 (3), 774–797. https://doi.org/10.1016/j.jmb.2007.05.022.

CHAPTER 4

4. SYNERGISTIC STRUCTURAL INFORMATION FROM HYDROGEN DEUTERIUM EXCHANGE AND COVALENT LABELING MASS SPECTROMETRY FOR STUDYING ANTIBODY/ANTIGEN INTERACTIONS

4.1. Introduction

The increasing importance of monoclonal antibody (mAb) therapeutics for treatment of disease has increased the necessity for robust methods of higher order structure characterization. Specifically, characterizing antibody-antigen interactions and understanding the epitopes responsible for these interactions is of upmost importance to the development of these drugs.[1,2] Epitope mapping is incredibly valuable for developing future therapeutic mAbs, understanding mechanisms of action, and patenting new drug molecules.[1,3] Traditionally, high resolution methods such as X-ray crystallography and NMR are the gold standards for epitope mapping or higher order structure (HOS) characterization of protein therapeutics, however these methods suffer from a number of drawbacks.[4] For instance, not every protein system can be crystallized for X-ray crystallography, large volumes of protein sample are needed, and throughput is very low.[5,6] NMR is limited in the size of protein that can be characterized. Both NMR and X-ray crystallography can be expensive and time intensive measurements.

Mass spectrometry (MS) has emerged as a promising tool for epitope mapping and HOS characterization because of limitations in traditional tools, especially when studying interactions involving the complete antibody and antigen.[3,7,8] In order to study HOS by mass spectrometry, the structure of the protein must be encoded into the mass. Multiple MS methods have been developed to achieve this such as chemical crosslinking, covalent labeling (CL), and hydrogen deuterium exchange (HDX). Chemical crosslinking is a method by which two amino acids that are in close spatial proximity to each other are covalently linked with a crosslinking reagent. Epitope mapping by chemical crosslinking has proven useful, as residues in the antigen are crosslinked to antibody residues, providing insight into which residues are important for antibody-antigen binding. For example, Pimenova et al. have used chemical crosslinking to determine the epitope of bovine prion protein.[9] However, chemical crosslinking data analysis can be laborious and time intensive due to its complexity, and residues buried in the epitope may not be accessible for cross-linking.

HDX is a well-established method for protein HOS characterization and is often used in industrial settings for characterizing bio-therapeutics, examining protein-protein interactions, and epitope mapping.[10] HDX/MS involves incubating a protein in a solution of deuterated water for varying lengths of time to allow labile hydrogens on the protein to exchange with deuterium in a structurally dependent manner. Deuteration sites can then be identified by digesting the protein and separating the resulting peptide fragments at low pH to minimize back exchange. The mass shift caused by deuterium uptake is then measured by MS, and the rates at which deuterium labels backbone sites can be obtained. These rate measurements indicate a protein region's solvent accessibility and backbone

dynamics. Comparing a native protein state to an experimental state (e.g. free antigen vs. antigen:antibody complex) reveals changes in solvent exposure due to antigen binding and/or changes in dynamics due to structural changes distant from the epitope. Previous work with HDX has demonstrated its utility for investigating mAb structure as well as for epitope mapping.[8,11,12] Most often, HDX/MS provides peptide-level resolution, but when combined with MS/MS via electron transfer dissociation, for example, residue-level information can be obtained.[13–15] One challenge with HDX/MS, however, is that it can sometimes be difficult to distinguish decreases in deuterium uptake due to antigen binding from decreases caused by changes in backbone dynamics due to protein stabilization.

CL/MS is a complementary method to HDX/MS. In CL a reagent reacts with solvent exposed amino acid side chains, covalently modifying them and causing a mass shift that can then be detected using MS. Because the modification results in the formation of a covalent bond, standard proteomics methods based on digestion and LC/MS/MS analysis can be used to pinpoint which residues are modified. Residue side chains that are solvent exposed tend to be labeled, while buried residues are not, making it a valuable approach for epitope mapping. Because CL/MS reports on side chain solvent accessibility while HDX/MS provides information about backbone dynamics and solvent accessibility, the two methods provide complementary information. Several recent studies have combined HDX/MS and CL/MS to study antibody:antigen interactions. These studies have primarily employed fast photochemical oxidization of proteins (FPOP) to oxidize exposed amino acid side chains. For example, FPOP and HDX/MS have been used together to study antibody/interleukin-23 interactions, providing orthogonal structural

information due to HDX/MS's ability to measure structural stability combined with FPOP's ability to report on rapid changes in solvent accessibility of side chains.[16] While FPOP and HDX/MS together provide complementary structural information, the inherent chemistry of both techniques occurs on the millisecond and sub-millisecond time scale, making both methods similarly sensitive to the same types of changes in protein dynamics.[17,18]

Another CL reagent that has been used extensively to study protein interactions is diethylpyrocarbonate (DEPC).[19–22] Unlike FPOP, which requires a special experiment setup, DEPC can simply be added to solution whereupon it labels nucleophilic residues such as Cys, Lys, His, Ser, Thr, and Tyr. DEPC reacts with protein side chains on the seconds to minutes timescale and is therefore affected by protein dynamics in a very different manner than FPOP. In recent work, we have demonstrated that the slow reaction timescale of DEPC labeling can be used in a complementary and synergistic fashion with HDX/MS to readily distinguish protein interactions from changes in protein dynamics in the context of heat stressed mAbs[23] and small molecule ligand-protein binding.[24] In essence, the slower reaction rate of DEPC-CL makes it mostly 'blind' to common changes in protein dynamics that are detectable by HDX/MS.

Because protein interactions with antibodies typically involve the burial of significant surface area and result in substantial protein stabilization, we were interested in assessing the degree of complementarity that exists when DEPC-CL/MS and HDX/MS are both used to study antibody-antigen binding. As a model system for these studies, we have chosen tumor necrosis factor α (TNFα) in complex with three different therapeutic

antibodies: adalimumab, infliximab, and golimumab. The epitopes on TNFα for each of the antibodies differs in size and location, and each antibody stabilizes the TNFα homotrimer to a different extent.[25–30] The features of these antibody-antigen interactions allow us to further assess the extent to which DEPC-CL/MS is sensitive to changes in protein dynamics and the complementarity that exists between this CL/MS technique and HDX/MS. We generally find that epitope sites result in labeling decreases in both HDX/MS and CL/MS, whereas DEPC-CL/MS often clarifies other decreases in HDX/MS as due to protein stabilization. Additionally, we demonstrate that DEPC-CL/MS can often provide improved spatial resolution as compared to HDX/MS.

4.2. Materials and Methods

4.2.1. Materials

Golimumab formulation (Simponi® 12.5mg/mL vial, batch#HJS1V01, Janssen), adalimumab formulation (Humira® 50mg/mL vial, lot#1088193, Abbvie), and infliximab formulation (Remicade®, lyophilized powder, lot#01184, Janssen) were purchased from Millipore Sigma, and rituximab formulation (Rituxan® 100 mg/10 mL vial, lot# 320928 3, Genentech) was purchased from Myoderm. Diethylpyrocarbonate (DEPC) (#D5758), imidazole (#I5513), iodoacetamide (#I6125), tris(2-carboxyethyl) phosphine (TCEP) (#C4706), guanidine hydrochloride (GnHCl) (#G3272), and sodium chloride (#S5886) were obtained from Sigma-Aldrich. Sodium phosphate monobasic monohydrate (#S0710-1) was obtained from EM Science. Immobilized trypsin (#20230), sodium phosphate dibasic anhydrous (#S374-500), LC/MS-grade formic acid (#A117-50), acetonitrile (#A998-4), and water (#W7-4) were purchased from Fisher Scientific.

4.2.2. DEPC labeling and proteolytic digestion

DEPC-CL/MS of antibodies has been described previously.[31] Briefly, DEPC stock solutions were prepared in acetonitrile and DEPC labeling reactions were completed in MOPS buffer, with antibody:antigen concentrations of 1 µM mAb:1.2 µM TNFα and a total volume of 500 µL. TNFα is a trimer, and molar excesses of the mAbs were used to ensure ~100% complexation of the trimer. To ensure comparable amounts of labelable residues between control and experimental conditions, control experiments involved the addition of the non-binding mAb rituximab. Labeling was conducted at a DEPC:protein molar ratio of 1000:1 at 37 °C for 5 min. The DEPC concentration was chosen to avoid over labeling using a predictive method described previously.[32] After 5 minutes of reaction time, imidazole was added to quench the reaction at a 1:50 DEPC:imidazole molar ratio. For each mAb three replicates were performed. After the reaction mixtures were quenched, the proteins were denatured and digested with trypsin overnight. The samples were centrifuged at 14,000 rpm to remove trypsin, and the supernatant containing the peptides was collected. The supernatant was then concentrated using a speed vacuum from 500 µL to 100 µL. Samples were analyzed immediately after concentration.

4.2.3. LC/MS/MS of CL samples

Online LC/MS/MS analyses were completed with a Dionex UltiMate 3000 RSCL capillary LC system (Thermo Scientific). Separation was carried out with an Acclaim Pepmap RSLC column (300 µm x 15 cm, C18, 2 µM, Thermo Scientific) with LC/MS grade water and 0.1% formic acid as solvent A and acetonitrile as solvent B. A linear

gradient from 5% B to 50% B over 55 min was used. A Thermo Scientific Orbitrap Fusion mass spectrometer with tandem mass spectrometry (MS/MS) and collision-induced dissociation (CID) on a linear quadrupole ion trap was used to acquire mass spectra. An inclusion list of possible labeled and unlabeled TNFα tryptic peptides and an exclusion list of antibody peptides was used.

4.2.4. CL/MS data analysis

A custom software pipeline designed specifically for protein DEPC CL/MS experiments was used and has been described previously.[33] Briefly, CID tandem mass spectra were searched against a database consisting of TNFα and the common repository of adventitious proteins (http://www.thegpm.org/crap/index.html) for peptide mapping and labeled site identification. For semi-quantitation of modification extent, peak areas of labeled and unlabeled species obtained from reconstructed ion chromatograms of each species are used to calculate percent labeling at each labeled site.

4.2.5. HDX procedure

Stock solutions of 20 μM mAb and 16 μM TNFα were prepared by diluting mAbs from formulation with a 10 mM phosphate buffer. A ratio of 1:1.2 mAb:TNFα ratio was used to ensure binding. D_2O was prepared in a 10 mM phosphate buffer, and the pD was adjusted via a pH meter corrected by: pD = pH reading + 0.41.[34] The Leap HDX Automation Manager and Waters nanoACQUITY UPLC system (Waters Corporation, Milford, MA, USA) were used for the liquid handling of all HDX experiments.

3.0 µL aliquots of TNFα in complex with mAb or TNFα alone was diluted into 57.0 µL D_2O buffer, resulting in a final concentration of a 1 µM mAb:1.2 µM TNFα or 1.2 µTNFα respectively. The resulting solutions were incubated for seven different time points ranging from 10 s to 24 h at 10 °C. After incubation in deuterium, the reaction was quenched by adding the sample to a quenching buffer (1:1, v/v) at 1 °C for 5 min. This buffer contained 4 M GnHCl, 0.5 M TCEP, and 200 mM Na_2PO_4 in water (pH = 2.5). Once the reactions were quenched, the samples were injected into the Waters ACQUITY UPLC System. Each mAb:TNFα reaction was done in triplicate on different days.

4.2.6. LC/MS of HDX samples

A Waters ENZYMATE immobilized pepsin column (ID: 2.1 length: 30 mm) at high pressure (~11000 psi) and 10 °C was used to digest samples. The resulting proteolytic peptides were collected by a trap column (HSS T3 pre-column, 100 Å, 1.8 µm, 2.1 mm X 5 mm, Waters) for 4.5 min at 0 °C, and then the peptides were eluted into a Waters ACQUITY C18 column (2.1 x 50 mm, 1.8 µm). A binary solvent system was used for LC separation: solvent A was water with 0.1% formic acid at pH 2.5 and solvent B was acetonitrile with 0.1% formic acid and the separation was carried out at 0 °C. A linear gradient that increased from 5% B to 35% B over 7 min was used, followed by a column wash increasing from 35% B to 85% B in 1 min at a flow rate of 40 µL/min. Finally, analyte peptides were detected using a Waters SYNAPT G2Si mass spectrometer in MS^E mode over the m/z range of 50-2000.

4.2.7. HDX data analysis

The deuterium uptake level of each measured peptide at different exchange time points was manually inspected and calculated using the Waters DynamX 3.0 software. Final sequence coverage for all conditions was >90% (**Figure 4.1**). Averaged deuterium uptake values from triplicate experiments with propagated error are reported. The difference between the bound and the unbound state were calculated in Excel. Peptides that appeared in at least 2 out of 3 trials with at least four measured time points were included in our analysis. To determine which changes were statistically significant, volcano plots were generated as used previously by Weis and co-workers.[35,36] The pooled standard deviation was calculated over all time points and all conditions, and multiplied by four to determine the ΔHX cut off 0.295 Da. An error cutoff of $P > 0.001$ was used as well. These cutoffs were validated by comparing a TNFα alone run to a TNFα alone run on a different day, and no false positive were detected (**Figure 4.2**). Peptides were considered significantly different if there were three or more time points that met the cutoffs previously described.

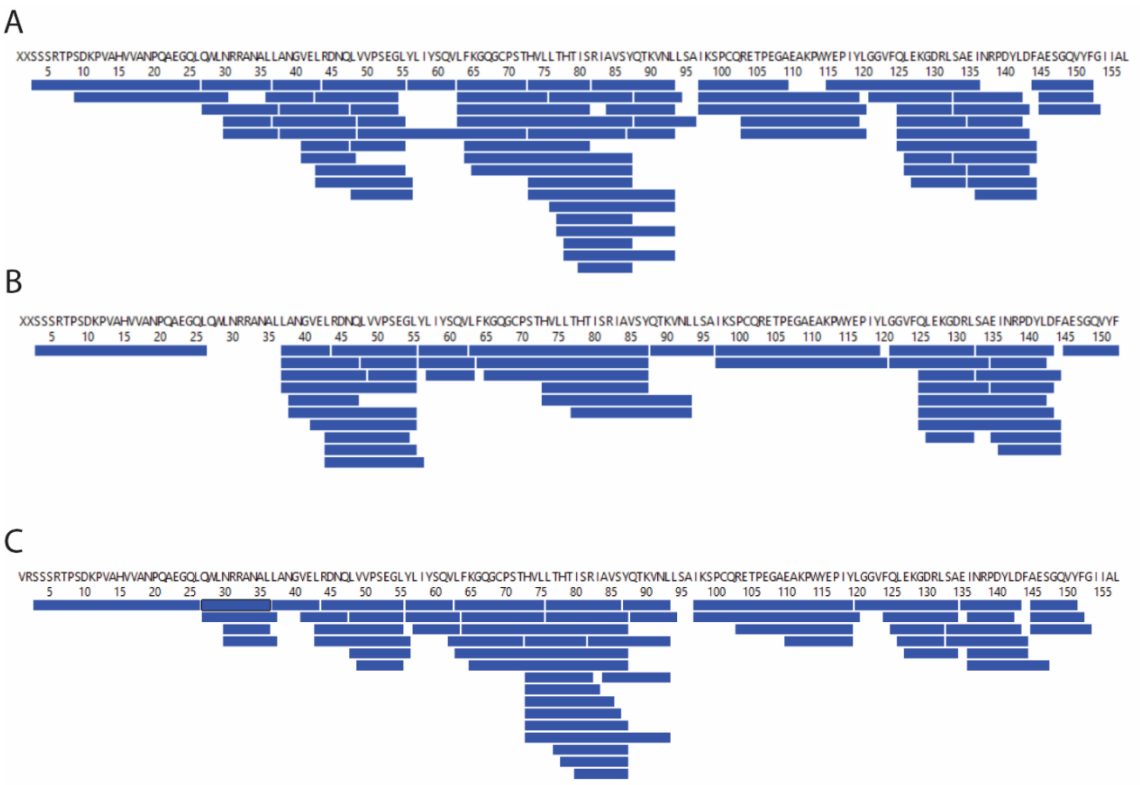

Figure 4.1: HDX sequence coverage for (A) adalimumab (B) Infliximab and (C) Golimumab.

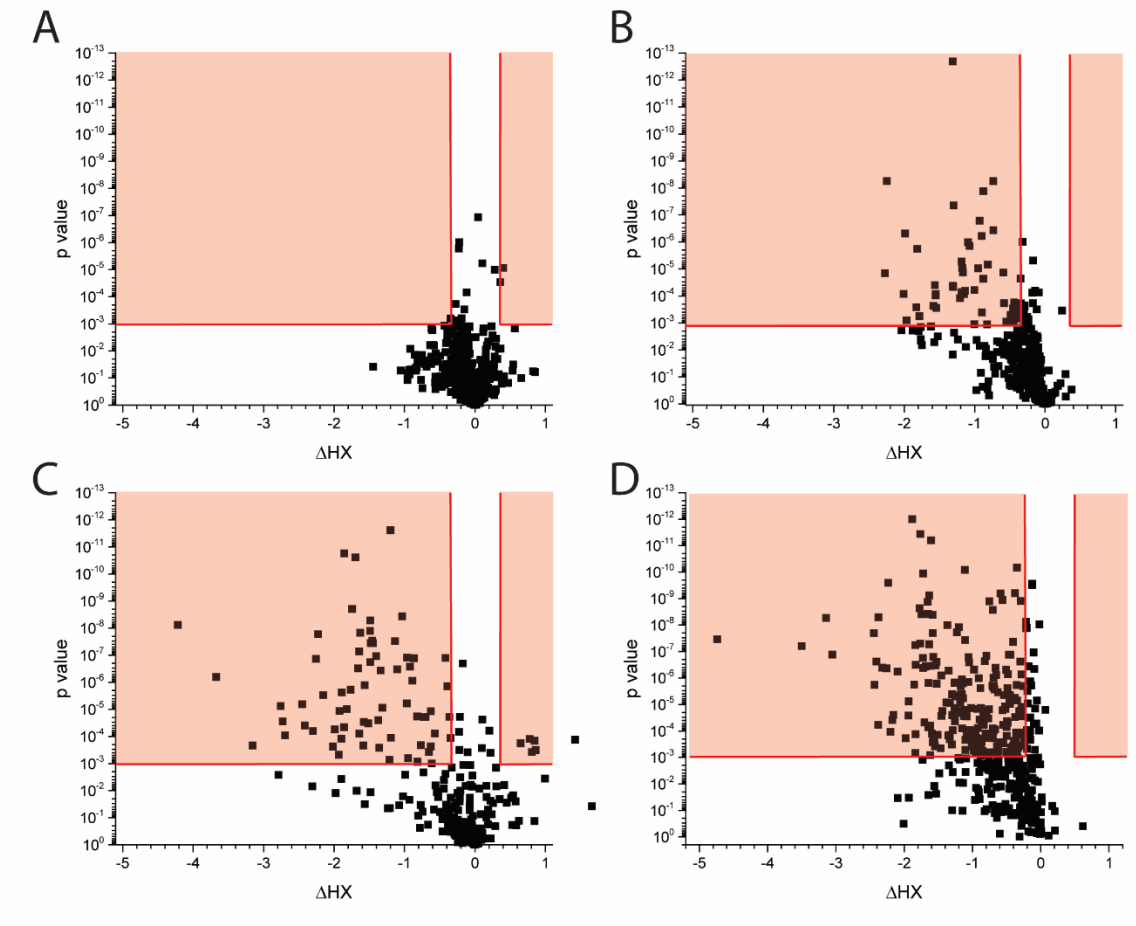

Figure 4.2: Volcano plots of HDX data for (A) free TNFα vs. free TNFα, (B) free TNFα vs. TNFα in complex with golimumab, (C) free TNFα vs. TNFα in complex with infliximab, (D) free TNFα vs. TNFα in complex with adalimumab. The x-axis is the ΔHX between the two states, while the y-axis is the p-value from the propagated error of the deuterium uptake values obtained from each HDX trial. Points that fall within the red regions are considered significant differences.

4.3. Results

4.3.1. DEPC-CL and HDX of TNFα in complex with Adalimumab

Adalimumab has the largest epitope of the three antibodies studied and stabilizes TNFα to the greatest extent. The TNFα epitope is made up of 25 residues, spanning two TNFα protomers in parts of the A-A', E-F, G-H, D-E loops and A, C, and D β-strands, covering ~2500 $Å^2$ (**Figure 4.3**).[37] Upon comparing the HDX/MS data of free TNFα and the adalimumab complex of TNFα, we find that half of the detected peptides undergo a significant decrease in deuterium uptake (**Figure 4.4** and **Table *C.1***), and these peptides span the entire protein sequence (**Figure 4.3**A). No peptides undergo a statistically significant increase in exchange. From CL/MS of the unbound and bound forms of TNFα, 29 residues are modified with six undergoing a decrease in labeling, 11 undergoing an increase, and 12 not changing (**Table *3.2***).

It is expected that regions of TNFα involved in epitope binding will undergo decreases in HDX and CL due to the loss of solvent exposure upon binding to adalimumab. Indeed, every peptide that contains one or more epitope residues decreases in deuterium uptake (**Figure 4.3**A and **Figure 4.4**). For example, the peptides ^{84}AVSYQTKVN^{93}L and ^{133}SAEINRPDYL^{143}D (**Figure 4.3**B) span epitope residues and significantly decrease in deuterium uptake even after 24 h of exchange. A similar decrease in HDX is seen for many other peptides from TNFα, as indicated by the horizontal blue lines in **Figure 4.3**A. Similarly, most DEPC modified residues that are present in, or immediately adjacent to, the epitope decrease in labeling extent. For example, Tyr141, Lys112, and Ser71 undergo significant decreases DEPC labeling upon adalimumab binding (**Figure 4.3**C). Interestingly, some Ser and Thr residues (i.e. Thr77,

Ser81, Thr89, and Ser147), which are adjacent to epitope regions and are only partially buried upon adalimumab binding, actually increase in DEPC labeling when adalimumab is present (**Figure 4.3**D). These residues undergo increased labeling because adalimumab binding creates nearby hydrophobic pockets that increases the local DEPC concentration, as has been previously suggested,[23,31,38,39] allowing these weakly nucleophilic residues to react more extensively than they do when exposed in unbound TNFα.

While all the peptides that span epitope residues undergo decreased exchange, several other peptides that do not include epitope residues also decrease in exchange upon adalimumab binding, which could lead to some ambiguity about identifying the epitope. Some examples include ^{30}NRRANAL^{37}L (**Figure 4.3**B) and ^{121}GGVFQLEKGDR^{132}L, which presumably decrease in exchange due to the stabilization of TNFα, which occurs upon adalimumab binding.[25,29] In some cases, these peptides are from regions of TNFα that do not contain any DEPC labelable residues (e.g., ^{30}NRRANAL^{37}L), so in the absence of known structural information, it might be difficult to conclude whether or not this protein region includes the epitope. In other cases, peptides do contain DEPC labelable residues that help clarify the HDX/MS data. As an example, the peptide ^{121}GGVFQLEKGDR^{132}L contains Lys128, which undergoes an increase in DEPC labeling extent, indicating that this region is unlikely to include the epitope and undergoes decreased HDX due to TNFα stabilization.

Often, protein regions that undergo binding-induced stabilization can be distinguished from epitope regions because the HDX/MS plots of peptides from the stabilized regions converge at longer exchange times, such as for the aforementioned peptide ^{30}NRRANAL^{37}L (**Figure 4.3**B). However, we find that some peptides that contain

epitope residues also converge at longer time points, such as the peptide ^{97}IKSPCQRETPEGAEAKPWYEPI^{119}Y (**Figure 4.3**B). This convergence at 24 h creates ambiguity about the actual epitope, as HDX data alone would been unable to definitively characterize this region as including the epitope. However, DEPC data reveal that Lys112 decreases significantly in labeling extent, strongly indicating that this part of the protein contains epitope residues.

As is sometimes the case, large peptides are measured during HDX/MS, making it difficult to fully resolve where and what kind of structural changes have occurred. For instance, the peptide ^{3}SSSRTPSDKPVAHVVANPQAEGQ^{26}L, includes a few epitope residues but mostly consists of non-epitope residues. This peptide decreases in HDX, but with the HDX/MS data alone identifying the epitope would be challenging. Fortunately, this protein region contains seven residues that are labeled by DEPC, and none undergo a decrease in labeling (**Figure 4.3**D and E), indicating that the region spanned by these residues is not involved in the epitope. Thus, DEPC-CL/MS effectively helps overcome the poor resolution that sometimes occurs in HDX/MS. A similar observation is made for several other long peptides such as ^{49}VVPSEGLYLIYSQVLFKGQGCPS^{72}T and ^{97}IKSPCQRETPEGAEAKPWYEPI^{119}Y, both of which contain DEPC labelable residues that complement the HDX/MS data.

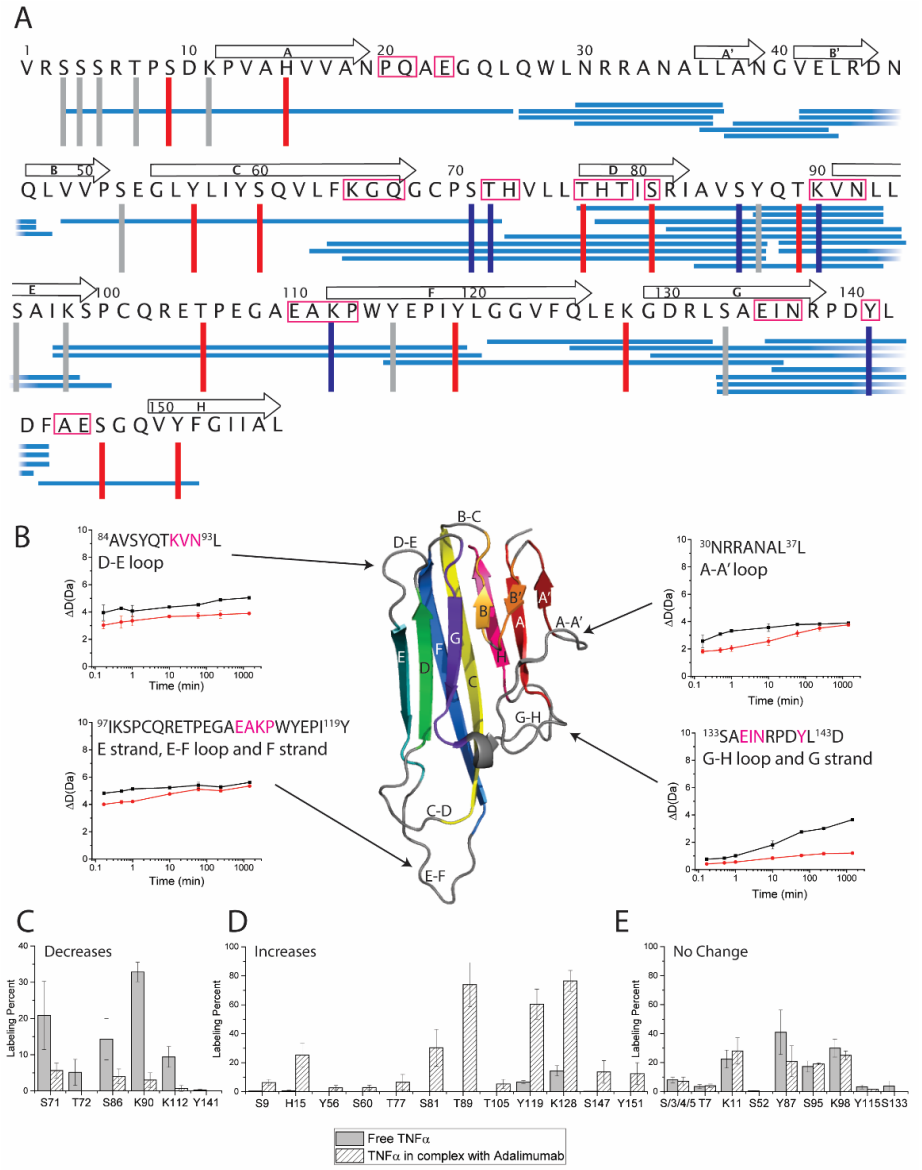

Figure 4.3: HDX/MS and DEPC-CL/MS results upon comparing the unbound and adalimumab-bound forms of TNFα. (A) Primary sequence of TNFα with peptides that decrease significantly in HDX indicated with blue horizontal lines. Residues involved in the epitope are indicated with magenta boxes. The vertical lines indicate residues that are labeled by DEPC but show no change in labeling extent (gray), increases in labeling extent (red), and decreases in labeling extent (blue). The β-strands of TNFα are indicated with arrows above the sequence. The sequence coverage during the HDX/MS experiments was 96% (**Figure 4.1**A), and the sequence coverage for the DEPC-CL/MS experiments was 100%. (B) Representative HDX/MS kinetic plots for select regions of TNFα. Residues in magenta are epitope residues. (C) DEPC-CL/MS results for residues that undergo decreased labeling upon binding to adalimumab. (D) DEPC-CL/MS results for residues that increase in labeling extent upon adalimumab binding (E) DEPC-CL/MS results for residues that do not significantly change in labeling extent upon adalimumab binding, according to a t-test at a 95% confidence interval.

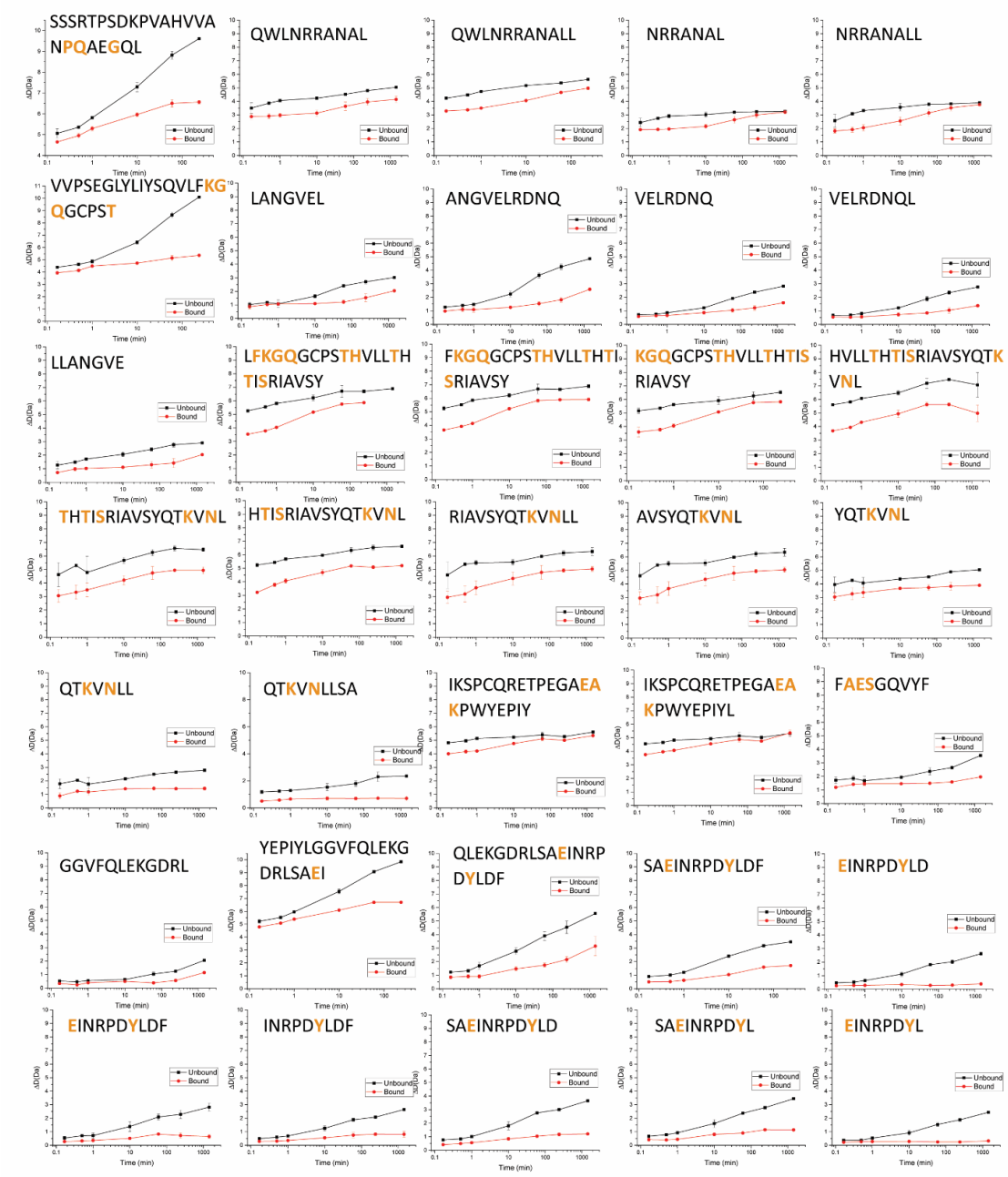

Figure 4.4: Deuterium uptake plots for all peptides that showed a significant difference from the free TNFα state to TNFα with adalimumab. The unbound state is plotted in black while the bound state is plotted in red. The peptide sequence is indicated about each plot with epitope residues indicated in orange.

4.3.2. DEPC-CL and HDX of TNFα in complex with infliximab

The infliximab epitope is smaller than adalimumab and stabilizes TNFα to a slightly lesser extent.[29] The epitope is made up 13 residues in parts of the C-D, G-H, and E-F loops and the C and D β-strands, covering 1,035 Å^2 (**Figure 4.5**).[30] There is some overlap between the infliximab and adalimumab epitopes, but adalimumab binds to the A-A' loops and D-E loops, which are not part of the infliximab epitope, and the C-D loop is important for infliximab binding but not adalimumab binding. Additionally, infliximab only binds one protomer of the homotrimer, while adalimumab binds two. When comparing the HDX/MS data of free TNFα to the infliximab complex, approximately one-third of the detected peptides decrease significantly in deuterium uptake, and one peptide increases significantly in deuterium uptake (**Figure 4.5**A, **Figure 4.6**, and **Table *C.2***). From CL/MS of the unbound and bound forms of TNFα, 26 residues are modified by DEPC, with four undergoing an increase in labeling extent, 10 undergoing a decrease, and 12 not changing (**Table *3.3***).

Of the 14 peptides that decrease significantly in deuterium uptake, 13 of them span epitope residues. For example, the peptides ^{64}FKGQGCPSTHVLLTHTISRIAVS^{87}Y and ^{133}SAEINRPDYLD^{144}F (**Figure 4.5**B) decrease in deuterium uptake at all time points. These peptides also contain DEPC labelable epitope residues (i.e., Ser71, Thr72, and Tyr141) that significantly decrease in labeling extent upon infliximab binding (**Figure 4.5**C). Such results are consistent with complete burial upon infliximab binding, as both methods indicate decreases. Additionally, several residues decrease in DEPC labeling extent due to their close proximity to the epitope (e.g. Lys112, **Figure 4.7**A) or loss of solvent exposure due to structural changes that occur upon infliximab binding (e.g.

Tyr87, **Figure 4.7**B). As was seen with adalimumab binding, a weakly nucleophilic residue at the edge of the epitope, Thr105 in this case, undergoes increased DEPC labeling due to the creation of hydrophobic pocket around this residue (**Figure 4.5**D).

Two peptides that are distant from the epitope undergo changes in HDX. One peptide, ^{9}SDKPVAHVVANPQAEGQLQWL^{30}N decreases in exchange (**Figure 4.5**B), yet this region contains three DEPC labelable residues that do not change in labeling extent (**Figure 4.5**E). The lack of labeling change for these residues is consistent with this region undergoing decreased HDX due to stabilization of the protein rather than burial due to antibody binding. The peptide ^{44}RDNQLVVPSEG^{55}L increases in deuterium uptake (**Figure 4.5**B) due to increased dynamics in this region. The one labelable residue within this region (i.e. Ser52) does not change in labeling extent, suggesting increased dynamics rather than complete unfolding upon infliximab binding.

Similar to the adalimumab data, some peptides containing epitope residues undergo the expected decrease in exchange upon binding, but after 24 h the exchange patterns of the infliximab-bound and unbound states converge. Typically, this HDX exchange behavior might suggest that this region is not part of the epitope but just undergoes changes in dynamics due to protein stabilization. An example is the peptide ^{97}IKSPCQRETPEGAEAKPWYEPI^{119}Y, which contains four epitope residues. This region of the protein also contains six labeled residues, five of which change in labeling extent. The decreases in DEPC-CL suggest that this region of the protein has decreased solvent exposure, presumably due to infliximab binding. Decreased labeling of Lys112 occurs because of the partial burial of this residue when infliximab binds. Labeling decreases at Lys98 and Tyr119 are more challenging to explain. Lys98 and Tyr119 are

both at the TNFα trimer interface, and stabilization of the trimer upon infliximab binding likely causes structural changes that influence the labeling of these residues. Thr105 and Ser99 increase in labeling extent. As mentioned above, Thr105 increases due to the increased hydrophobic microenvironment that is created around this residue upon infliximab binding (**Figure 4.7**C). Ser99 increases in labeling for similar reasons, as a hydrophobic pocket assembles around it due to nearby Phe28 from infliximab (**Figure 4.7**D).

Several long peptides are measured in the HDX/MS dataset, making it difficult to resolve exactly where structural changes are taking place solely using the HDX/MS. For instance, the peptides ^{64}FKGQGCPSTHVLLTHTISRIAVS^{87}Y and ^{125}QLEKGDRLSAEINRPDYL^{143}D decrease significantly in exchange. These peptides, however, both contain several DEPC labeled residues that help better pinpoint the epitope. Ser71 and Thr72 help narrow the epitope to the first part of the sequence of ^{64}FKGQGCPSTHVLLTHTISRIAVS^{87}Y, whereas the labeling data for Lys128 and Ser133, and the decreased labeling of Tyr141 help pinpoint the epitope to the latter part of ^{125}QLEKGDRLSAEINRPDYL^{143}D. While this latter peptide does have overlapping peptides in the HDX/MS dataset that help increase the structural resolution, the DEPC-CL/MS data further confirms the location of the epitope.

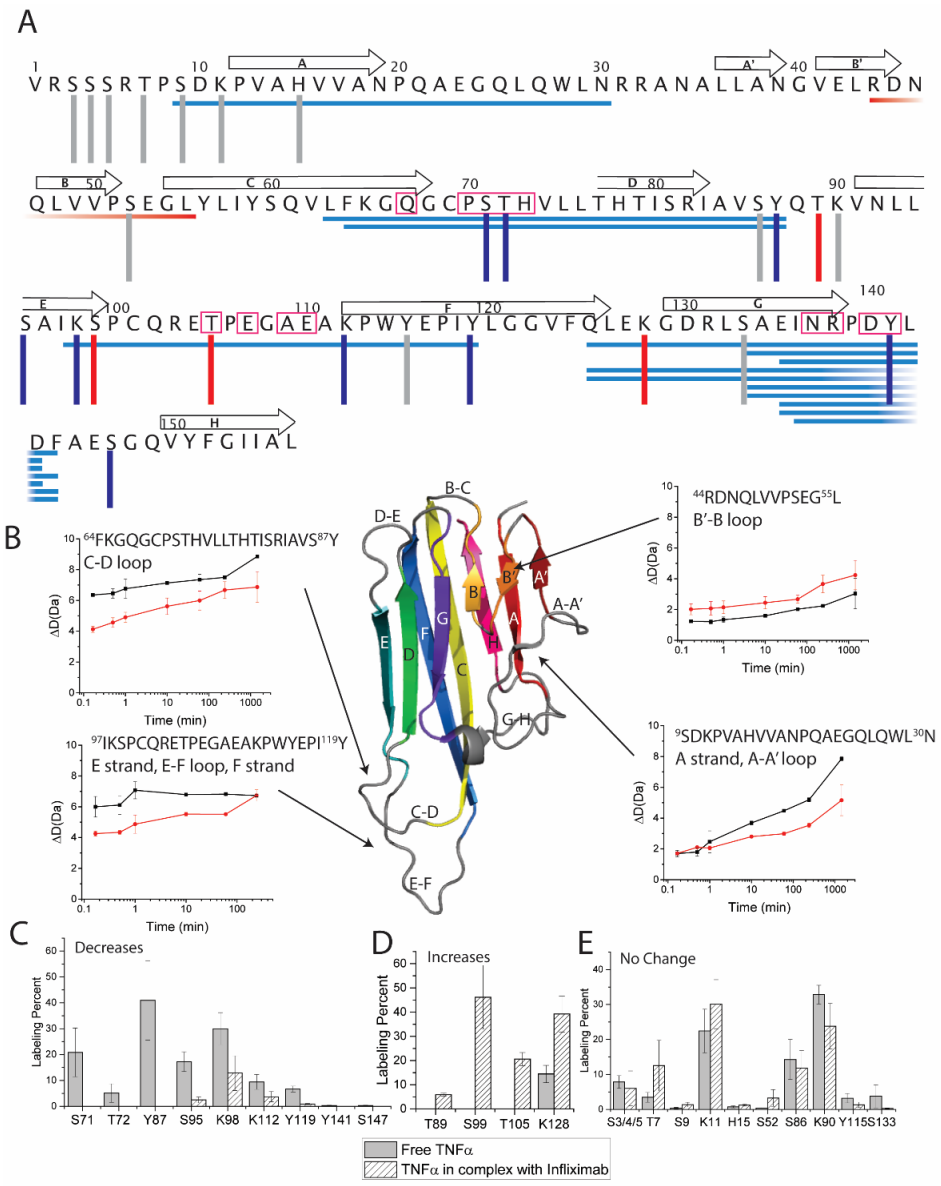

Figure 4.5: HDX/MS and DEPC-CL/MS results upon comparing the unbound and infliximab-bound forms of TNFα. (A) Primary sequence of TNFα with peptides that decrease significantly in HDX indicated with blue horizontal lines. Residues involved in the epitope are indicated with magenta boxes. The vertical lines indicate residues that are labeled by DEPC but show no change in labeling extent (gray), increases in labeling extent (red), and decreases in labeling extent (blue). The β-strands of TNFα are indicated with arrows above the sequence. The sequence coverage during the HDX/MS experiments was 92% (**Figure 4.1**B), and the sequence coverage for the DEPC-CL/MS experiments was 95%. (B) Representative HDX/MS kinetic plots for select regions of TNFα. Residues in magenta are epitope residues. (C) DEPC-CL/MS results for residues that undergo decreased labeling upon binding to infliximab. (D) DEPC-CL/MS results for residues that increase in labeling extent upon infliximab binding (E) DEPC-CL/MS results for residues that do not significantly change in labeling extent upon infliximab binding, according to a t-test at a 95% confidence interval.

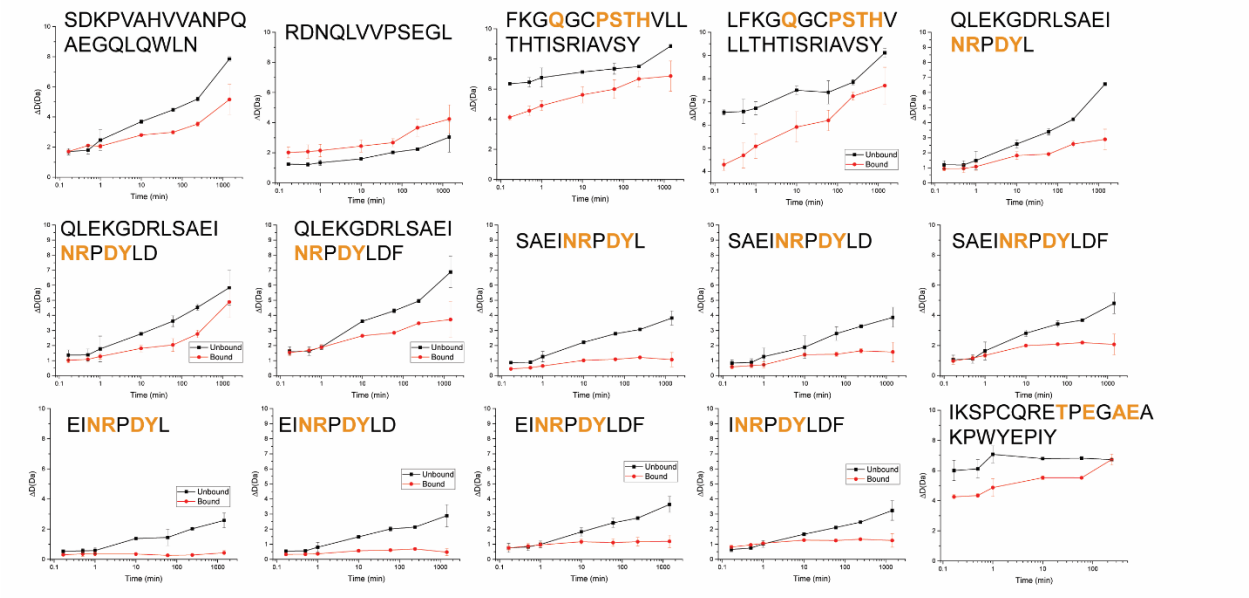

Figure 4.6: Deuterium uptake plots for all peptides that showed a significant difference from the free TNFα state to TNFα with infliximab. The unbound state is plotted in black while the bound state is plotted in red. The peptide sequence is indicated about each plot with epitope residues indicated in orange.

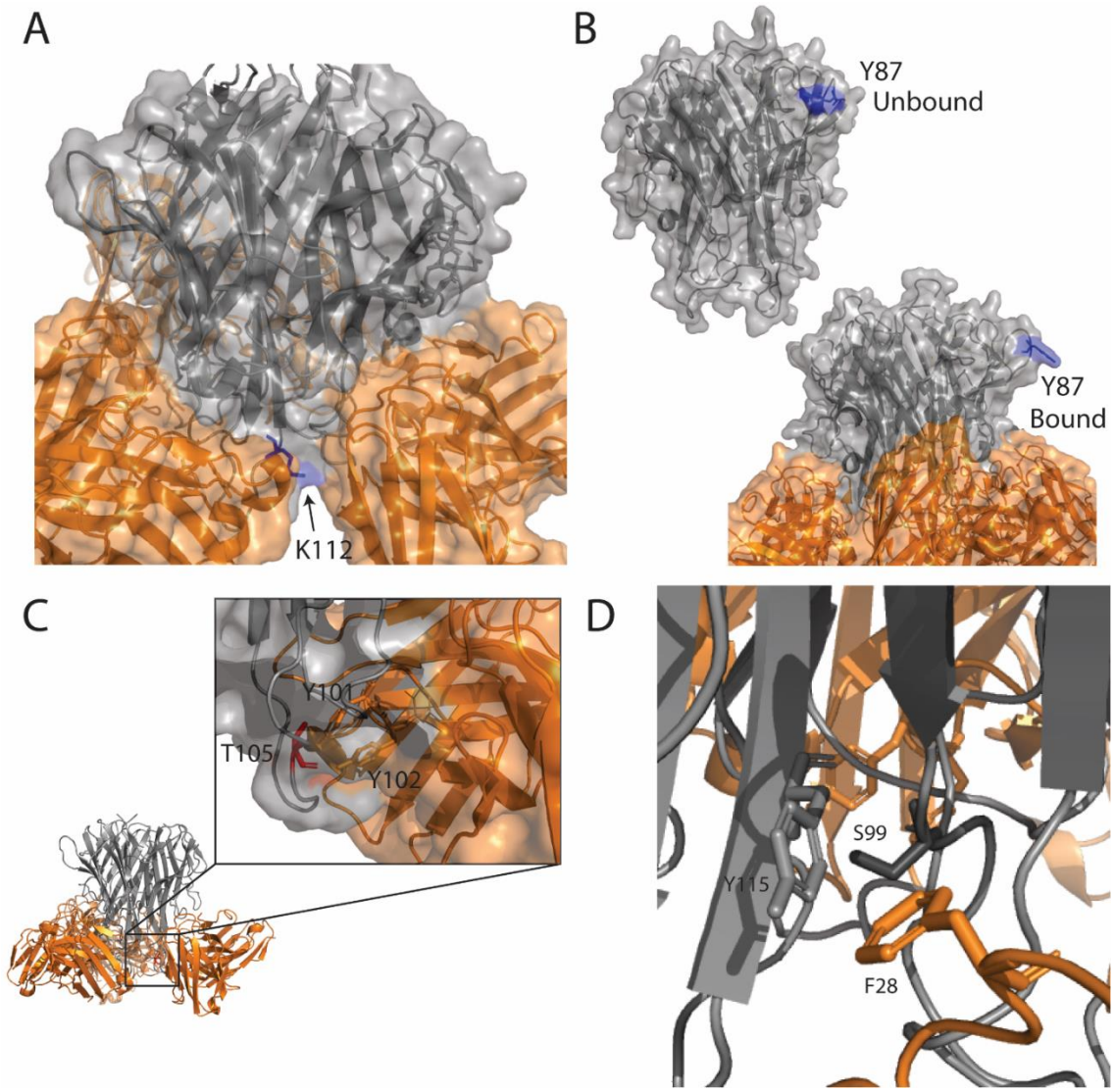

Figure 4.7:Surface view of TNFα in complex with infliximab (A) Residue Lys112 decreases in DEPC-CL due to partial burial by infliximab. (B) Residue Y87 undergoes a decrease in DEPC-CL presumably due to HOS shifts resulting in more solvent exposure upon infliximab binding. (C) While Thr 105 is an epitope residue, it increases in labeling as a result of an increase in hydrophobic microenvironment created by infliximab binding. (D) Residue Ser99 also increases in labeling due to an increase in hydrophobic microenvironment due to the proximity to Phe28.

4.3.3. DEPC-CL of TNFα in complex with Golimumab

Golimumab has the smallest epitope covering 905 $Å^2$ and stabilizes the trimer the least of the three mAbs studied.[29] The golimumab epitope is made up of 13 residues in parts of the A-A', C-D, E-F, and G-H loops and some residues in the C strand. The epitope overlaps with some of the same regions of the infliximab and adalimumab epitopes, such as the G-H and E-F loops. The HDX/MS data reveal that approximately one-fifth of the peptides detected have a significant decrease in deuterium uptake upon golimumab binding (**Figure 4.9**A, **Figure 4.8**, and **Table *C.3***). The DEPC-CL/MS data show 25 residues modified by DEPC, eight not changing in labeling extent upon binding, 11 decreasing, and six increasing (**Table *3.4***).

Similar to the adalimumab and infliximab HDX/MS data, the majority of peptides that contain epitope residues undergo a decrease in deuterium uptake upon binding to golimumab (**Figure 4.9**). For example, the peptides ^{62}VLFKGQGCPS^{72}T and ^{136}INRPDY^{142}L (**Figure 4.9**B) decrease in deuterium uptake. Likewise, DEPC labelable residues at the epitope (i.e., Ser71, Thr72, and Tyr141) decrease in labeling upon golimumab binding (**Figure 4.9**C). Together, these data are consistent with the expected effect of burial on the HDX/MS and CL/MS results. As was seen with adalimumab and infliximab binding, Thr105, a weakly nucleophilic residue at the edge of the epitope undergoes increased DEPC labeling due to the creation of hydrophobic pocket around this residue (**Figure 4.9**D).

While the majority of the peptides that undergo decreases in exchange include parts of the epitope, two protein regions have peptides that decrease in deuterium uptake but are distant from epitope. One of these peptides is ^{124}FQLEKGDRLS^{134}A, which

decreases in exchange at all time points (**Figure 4.9**B). The HDX/MS data alone might suggest that this span of residues contains the epitope, but increased DEPC labeling at Lys128 and no change in labeling at Ser133 indicates otherwise. The absence of DEPC-CL/MS decreases is consistent with this region being less dynamic rather than buried upon binding. Additionally, the peptide ^{73}HVLLTHTISR^{83}I decreases significantly in deuterium uptake at all time points (**Figure 4.9**B). DEPC-CL/MS data can aid in interpretation of this HDX/MS data because Thr77 and His78 increase in labeling. By considering both the HDX/MS and DEPC-CL/MS data, we can conclude that this region of the protein has experienced a change in dynamics, but not a loss in solvent exposure.

There are a few peptides containing epitope residues whose deuterium uptake converges after 24 hours, typically suggesting a change in dynamics. The peptide ^{64}FKGQGCPSTHVLLTHTISRIAVS^{87}Y, for example, converges after 24 hours, but contains four epitope residues (**Figure 4.8**). DEPC-CL/MS reveals that four residues in this protein region, Ser71, Thr72, Ser86, and Tyr87, decrease in labeling extent, thus indicating that the deuterium uptake decrease is likely due to a loss of solvent exposure rather than reduced dynamics. Indeed, residues Ser71 and Thr72 are epitope residues, and while Ser86 and Y87 are distant from the epitope, these decreases could also indicate a change in solvent exposure.

As is the case with the adalimumab and infliximab data, several long peptides are measured in the HDX/MS data, resulting in low spatial resolution. Fortunately, overlapping peptides make this poor resolution less of an issue for most protein regions in golimumab, except the N-terminus, which is spanned by one 23-residue peptide that does not change in deuterium uptake (**Figure 4.1**C). The DEPC-CL/MS data, however,

indicates there are a number of changes in this region. There are several residues, including Ser9, Thr7, Lys11, and His15, near the N-terminus of the protein and distant from the epitope that change in DEPC labeling extent (**Figure 4.9**C, D, and E). These results suggest that there is some side chain reorganization that takes place here that does not affect backbone dynamics.

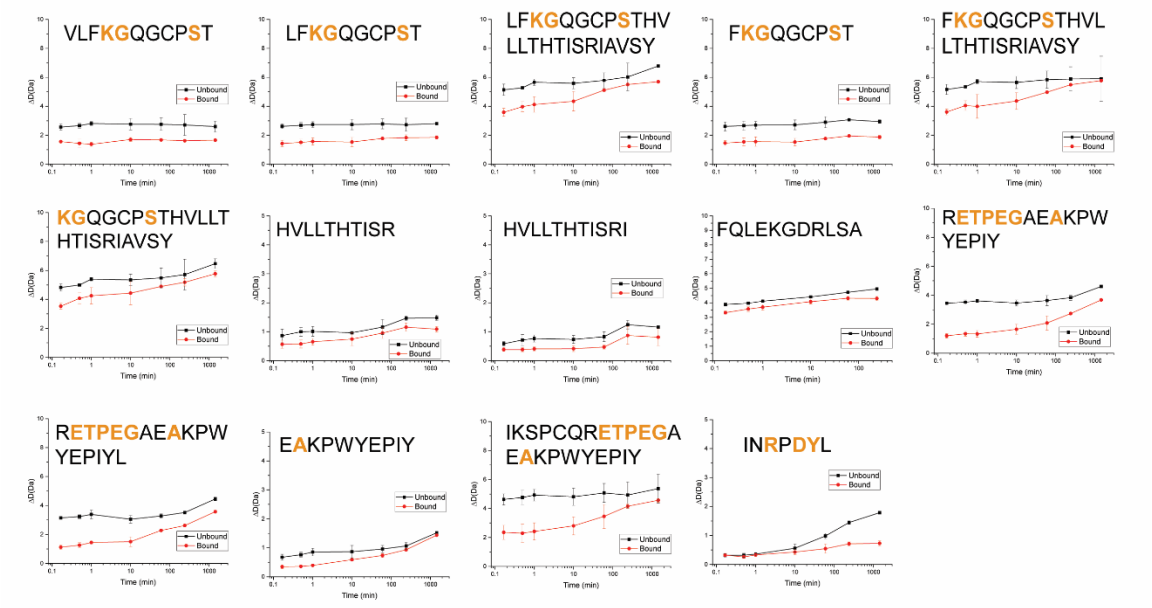

Figure 4.8: Deuterium uptake plots for all peptides that showed a significant difference from the free TNFα state to TNFα with golimumab. The unbound state is plotted in black while the bound state is plotted in red. The peptide sequence is indicated about each plot with epitope residues indicated in orange.

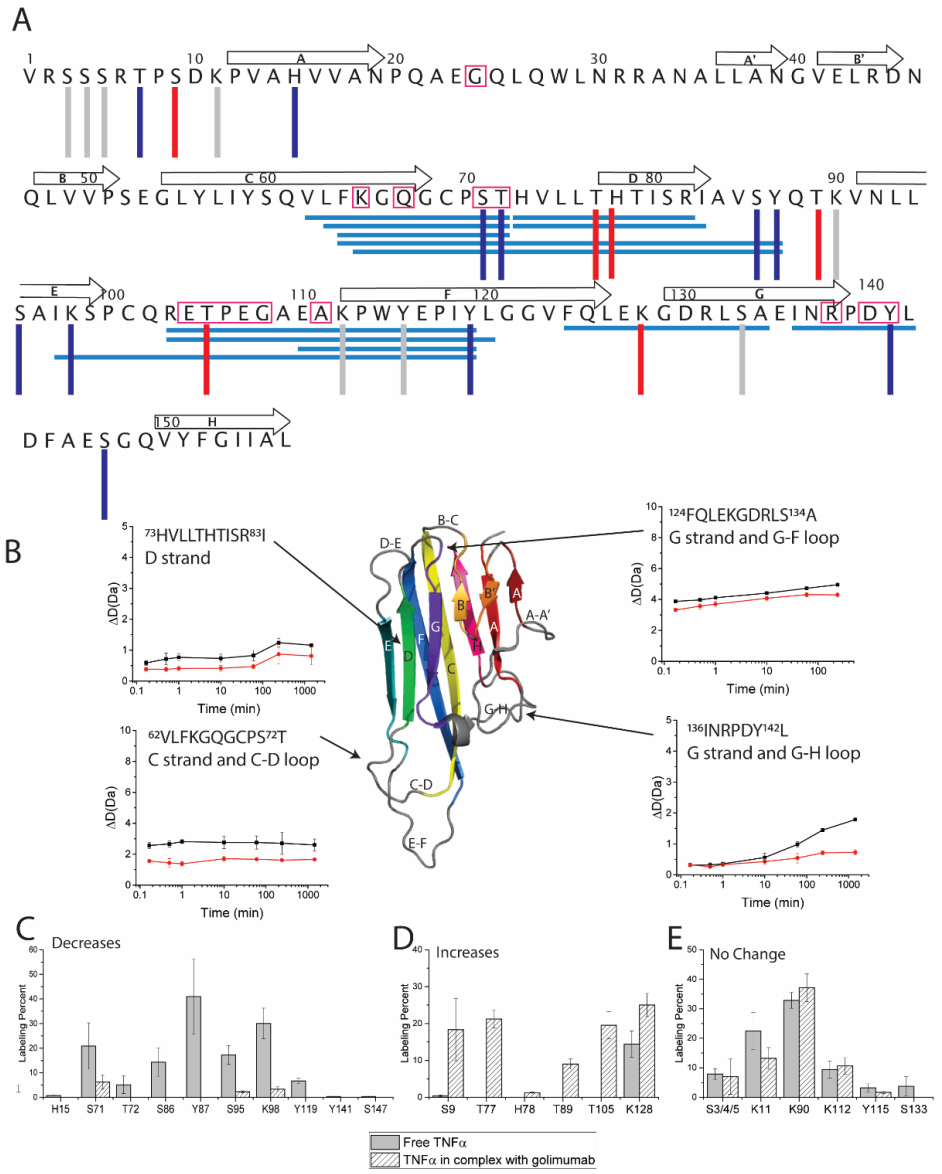

Figure 4.9: HDX/MS and DEPC-CL/MS results upon comparing the unbound and golimumab-bound forms of TNFα. (A) Primary sequence of TNFα with peptides that decrease significantly in HDX indicated with blue horizontal lines. Residues involved in the epitope are indicated with magenta boxes. The vertical lines indicate residues that are labeled by DEPC but show no change in labeling extent (gray), increases in labeling extent (red), and decreases in labeling extent (blue). The β-strands of TNFα are indicated with arrows above the sequence. The sequence coverage during the HDX/MS experiments was 92% (**Figure 4.1**C), and the sequence coverage for the DEPC-CL/MS experiments was 95%. (B) Representative HDX/MS kinetic plots for select regions of TNFα. Residues in magenta are epitope residues. (C) DEPC-CL/MS results for residues that undergo decreased labeling upon binding to golimumab. (D) DEPC-CL/MS results for residues that increase in labeling extent upon golimumab binding (E) DEPC-CL/MS results for residues that do not significantly change in labeling extent upon golimumab binding, according to a t-test at a 95% confidence interval.

4.4. Discussion

Here we investigate the type of HOS information can be obtained by comparing HDX with DEPC-CL/MS data for the purpose of studying antigen:antibody interactions. While other studies have used FPOP/MS in combination with HDX/MS to study such interactions, this is the first study to investigate DEPC-CL/MS in conjunction with HDX/MS for this purpose. Because FPOP takes place on the sub-millisecond time scale, it is affected by changes in side chain dynamics; however, DEPC-CL has a much slower intrinsic reaction rate and less sensitive to these changes. [23,24]. Our results suggest DEPC-CL/MS can be used to clarify ambiguous HDX/MS results. Additionally, due to difference in resolution (i.e., HDX/MS most often provides peptide-level resolution while DEPC-CL/MS provides residue level resolution), the two methods provide complementary information. Finally, in regions where there are changes in HDX that do not take place at the epitope, considering DEPC-CL/MS data can illuminate what types of structural changes have taken place.

4.4.1. DEPC-CL and HDX provide Complementary Information

DEPC-CL/MS reports on side chain solvent accessibility and microenvironment while HDX/MS measures solvent accessibility and backbone dynamics. As a result, the two methods can provide complementary information. Our data reveal that both methods generally report decreases in labeling and exchange at the epitope due to less solvent exposure upon mAb binding. For all three mAbs studied, most (76%) of the peptides that decrease significantly in deuterium uptake include epitope residues. Similarly, most (70%) of labelable epitope residues decrease in DEPC-CL, and the remaining 30% are

Ser, Thr, or Tyr residues that become newly labeled upon mAb binding because of the creation of a hydrophobic pocket that enables DEPC reactivity.[23,32,38,39] This complementarity between the two methods can be best observed with the TNFα complex with adalimumab. TNFα experiences decreases in HDX that span the majority of the protein sequence. By using solely HDX/MS data, one would not be able to definitively determine the location of the epitope. However, when the DEPC-CL/MS data is considered, the location of the epitope is narrowed down better (**Figure 4.10**).

Additional complementarity between the two methods stems from differences in resolution. In its most commonly used manner, HDX/MS provides peptide-level resolution. However, peptide lengths can range from 5 to 25 residues or sometimes even more. Thus, depending on which peptides are produced and detected, the spatial resolution can make it hard to pinpoint the parts of the peptide that are responsible for the decrease in deuterium uptake. While DEPC only labels ~30% of a protein's sequence, it provides residue level resolution, and therefore, it can often help pinpoint the parts of long peptides that are responsible for the observed decreases in deuterium uptake. For instance, in the adalimumab data the peptide ^{49}VVPSEGLYLIYSQVLFKGQGCPS^{72}T decreases in labeling extent, but its length makes it challenging to pinpoint the epitope. This region of the protein contains five labeled residues, three of which either increase or do not change in labeling extent while the other two, Ser71 and Thr72, decrease in labeling extent. When the DEPC-CL/MS data is considered together with the HDX/MS data, it is revealed that the C-terminal end of this peptide has likely decreased in solvent exposure and is responsible for the decrease in deuterium uptake while the N-terminal end is not likely responsible for the decrease.

This complementary is also observed in the infliximab data where there is a ~20 residue span from residues 65 to 87 that is covered by two different peptides that decrease in labeling extent. There are four labeled residues in this region, Ser71, Thr72, Ser86, and Tyr87. Ser71 and Thr72 are epitope residues, and both are prevented from labeling upon binding infliximab, while Ser86 does not change in labeling extent. Even though Tyr87 does decrease in labeling, changes to both Ser71 and Thr72 suggest that the N-terminal end of these peptides is more likely responsible for the decrease in solvent exposure and associated loss of deuterium uptake. By considering the data together a more confident conclusion about the epitope location can be made.

Additional complementarity for these two methods is observed in regions where one method cannot provide any information, either for lack of sequence coverage, or lack of labeling. For instance, there is one 36-residue span of TNFα from Val16 to Pro51 that contains no DEPC labelable residues, but the HDX/MS data contains several peptides that span this region. HDX/MS reveals that TNFα undergoes no structural or dynamical change upon binding golimumab, but it does undergo more complex structural changes upon binding adalimumab and infliximab. DEPC-CL/MS alone would not give any structural information regarding this section of TNFα, but HDX/MS clearly does. Additionally, despite the excellent sequence coverage in the HDX/MS dataset with golimumab, there is no coverage around Ser95. In contrast, DEPC-CL/MS data indicate that this residue decreases in labeling extent, suggesting a structural change in this region of the protein.

4.4.2. DEPC-CL can clarify ambiguous HDX results

Upon binding to a mAb, antigens can be stabilized, causing a decrease in backbone dynamics, such as is seen with TNFα. Decreases in backbone dynamics lead to less HDX, and decreases in solvent exposure due to binding also lead to less HDX. Both types of HDX decreases sometimes lead to ambiguous results. When the three different mAbs bind TNFα, different extents of stabilization occur, causing different extents of deuterium uptake. Decreases in HDX span more regions in adalimumab than infliximab or golimumab, and the trend follows the degree of TNFα stabilization that is known to occur with the three mAbs. DEPC-CL has a relatively slow reaction rate, as compared to HDX, and thus labeling by this reagent is not affected by protein dynamics that occur on the millisecond to second timescale. The slower reaction timescale of DEPC-CL allows the labeling results from this reagent to clarify ambiguous HDX/MS data. This effect is most prominent in the adalimumab data where decreases in HDX occur throughout the entire protein, whereas DEPC-CL decreases occur almost exclusively at the epitope (**Figure 4.3**A), but the effect is also seen in the infliximab (**Figure 4.5**A) and golimumab data (**Figure 4.9**A) as well.

Often the ambiguity in HDX data can be resolved by measuring exchange at much longer time periods where less dynamic regions have enough time to fully exchange while buried sites usually do not. For example, HDX of the peptide ^{30}NRRANAL^{37}L with and without adalimumab (**Figure 4.3**B) converges after 24 h of exchange, correctly indicating a decrease in backbone dynamics due to trimer stabilization. However, ^{97}IKSPCQRETPEGAEAKPWYEPI^{119}Y in the E-F loop also exhibits this exchange behavior (**Figure 4.3**B) even though it contains the largest region of the TNFα epitope.

Decreased DEPC labeling at residue Lys112, which is in the epitope, indicates a loss of solvent exposure, clarifying that binding is taking place in this region of the protein. A similar result is observed in the infliximab data for this peptide as well. HDX of this peptide with and without infliximab converges after 24 h, yet Lys112 decreases in DEPC labeling extent. Of course, Thr105, which is in this peptide and is part of the epitope, is newly labeled upon infliximab binding, which could add some ambiguity in the DEPC dataset. However, we consistently find that Ser, Thr, and Tyr residues that become newly labeled upon binding are present at or near the epitope. The hydrophobic pockets that are created when the antibody and antigen bind presumably increase the local DEPC concentration, allowing these weakly nucleophilic residues to be labeled. [23,32,38,39] Consequently, increased labeling of Ser, Thr, or Tyr residues, along with decreased labeling of nearby Lys and His residues, are probably best interpreted as binding regions. Overall, the DEPC labeling changes help resolve some of the ambiguity associated with the HDX/MS data.

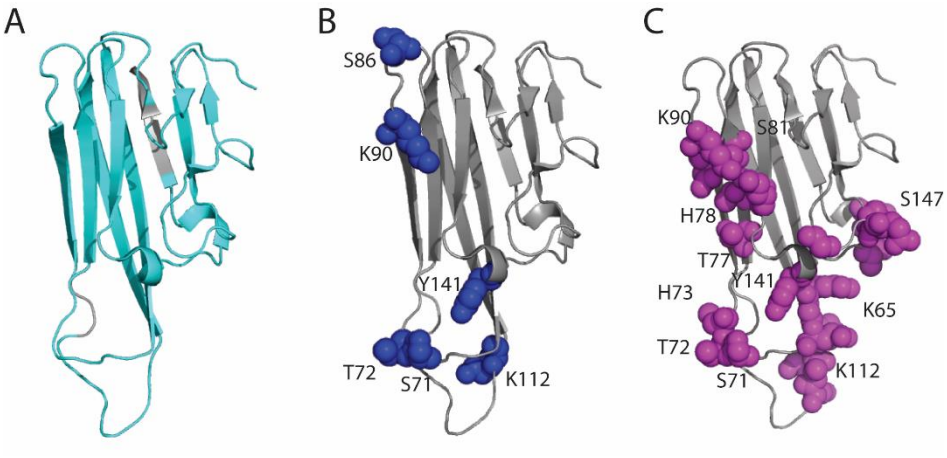

Figure 4.10: HDX decreases, DEPC-CL decreases, and epitope plotted on the TNFα structure (A) HDX decreases span the majority of the protein (B) DEPC-CL decreases are localized to regions where the (C) epitope is.

4.4.3. DEPC-CL and HDX can reveal HOS changes distant from the epitope

While the data provided about the epitope by HDX/MS and DEPC-CL/MS is valuable, also interesting is the HOS information obtained by these two methods at locations distant from the epitope. It is regions like this where the methods are synergistic, and the HOS obtained by combining the methods is greater than the sum of their parts. In the infliximab dataset, the peptide ^{9}SDKPVAHVVANPQAEGQLQWL^{30}N decreases in deuterium uptake. This protein region contains three labeled residues, none of which change in labeling extent. Thus, it can be concluded that the region from Ser9 to His15 experiences a decrease in dynamics, but not a corresponding decrease in solvent exposure or side chain microenvironment. Moreover, the two datasets confirm that this region is not part of the epitope.

Another example of the synergy of the two techniques are two overlapping peptides in the D strand from His73 to Ile83 that both decrease in deuterium uptake upon

golimumab binding, even though they do not span any epitope residues. There are two labeled residues in this region, Thr77 and H78, that increase in DEPC labeling extent. These DEPC increases suggest that the decrease in deuterium uptake is due to decreased protein dynamics and confirm that this peptide is not part of the epitope. Indeed, this region is important for trimer stabilization, not mAb binding.

Lastly, adalimumab and golimumab binding both result in peptides from residue 121 to 134 that decrease in HDX even though they are not involved in the epitope. This region contains residue Lys128 that increases in labeling extent and Ser133 that does not change. The lack of a DEPC-CL decrease in this region indicates a change in dynamics, but not a loss of solvent exposure. Together, the HDX/MS and DEPC-CL/MS data clarify that this protein region is not part of the epitope but undergoes a decrease in dynamics due to binding-induced stabilization.

4.5. Conclusions

DEPC-CL/MS and HDX/MS are complementary methods. HDX/MS reports on back bone solvent exposure and dynamics, while DEPC-CL/MS reports on side chain solvent exposure and microenvironment. Because HDX/MS provides data on both protein dynamics and solvent exposure, it can often lead to ambiguous results, especially in antibody:antigen systems. The HDX/MS data of TNFα in complex with adalimumab reveals decreases in deuterium uptake that span the entire protein. In contrast, DEPC-CL decreases primarily take place at the epitope, thus clarifying the HDX/MS data. The methods also complement in terms of structural resolution. HDX/MS data sometimes contains long peptides that make it difficult to identify epitope regions, while the single-residue resolution inherent in DEPC can pinpoint the residues involved in mAb binding.

On the other hand, sometimes large stretches of a protein are devoid of DEPC labelable residues yet can still undergo meaningful HDX. Finally, the two methods can provide synergistic information, especially when regions that decrease in HDX do not decreases in DEPC-CL. Such regions usually indicate decreased protein dynamics due to binding-induced stabilization. Neither DEPC-CL/MS nor HDX/MS alone confidently identify such regions, but the combination of the two methods allow this conclusion to be made confidently. Our results highlight the complementarity between these two techniques for study of epitopes and antibody:antigen interactions and suggest that they can be applied more broadly to other protein:protein systems. We predict the application of HDX/MS and DEPC-CL/MS together for studying HOS of protein therapeutics has the potential to aid and accelerate therapeutic protein development.

4.6. References

(1) Pettersson, I. Methods of Epitope Mapping. Mol. Biol. Rep. 1992, 16, 149–153.

(2) Opuni, K. F. M.; Al-Majdoub, M.; Yefremova, Y.; El-Kased, R. F.; Koy, C.; Glocker, M. O. Mass Spectrometric Epitope Mapping. Mass Spectrom. Rev. 2018, 37 (2), 229–241. https://doi.org/10.1002/mas.21516.

(3) Abbott, W. M.; Damschroder, M. M.; Lowe, D. C. Current Approaches to Fine Mapping of Antigen-Antibody Interactions. Immunology 2014, 142 (4), 526–535. https://doi.org/10.1111/imm.12284.

(4) Fiedler, W.; Borchers, C.; Macht, M.; Deininger, S. O.; Przybylski, M. Molecular Characterization of a Conformational Epitope of Hen Egg White Lysozyme by Differential Chemical Modification of Immune Complexes and Mass Spectrometric Peptide Mapping. Bioconjug. Chem. 1998, 9 (2), 236–241. https://doi.org/10.1021/bc970148g.

(5) Narang, D.; James, D. A.; Balmer, M. T.; Wilson, D. J. Protein Footprinting, Conformational Dynamics, and Core Interface-Adjacent Neutralization “Hotspots” in the SARS-CoV-2 Spike Protein Receptor Binding Domain/Human ACE2 Interaction. J. Am. Soc. Mass Spectrom. 2021. https://doi.org/10.1021/jasms.0c00465.

(6) Houde, D.; Berkowitz, S. A.; Engen, J. R. The Utility of Hydrogen/Deuterium Exchange Mass Spectrometry in Biopharmaceutical Comparability Studies. J. Pharm. Sci. 2011, 100 (6), 2071–2086. https://doi.org/10.1002/jps.22432.

(7) Hager-Braun, C.; Tomer, K. B. Determination of Protein-Derived Epitopes by Mass Spectrometry. Expert Rev. Proteomics 2005, 2 (5), 745–756. https://doi.org/10.1586/14789450.2.5.745.

(8) Sun, H.; Ma, L.; Wang, L.; Xiao, P.; Li, H.; Zhou, M.; Song, D. Research Advances in Hydrogen–Deuterium Exchange Mass Spectrometry for Protein Epitope Mapping. Anal. Bioanal. Chem. 2021, 413 (9), 2345–2359. https://doi.org/10.1007/s00216-020-03091-9.

(9) Pimenova, T.; Nazabal, A.; Roschitzki, B.; Seebacher, J.; Rinner, O.; Zenobi, R. Epitope Mapping on Bovine Prion Protein Using Chemical Cross-Linking and Mass Spectrometry. J. Mass Spectrom. 2008, 43 (2), 185–195. https://doi.org/10.1002/jms.1280.

(10) Masson, G. R.; Burke, J. E.; Ahn, N. G.; Anand, G. S.; Borchers, C.; Brier, S.; Bou-assaf, G. M.; Engen, J. R.; Englander, S. W.; Faber, J.; Garlish, R.; Griffin, P. R.; Gross, M. L.; Guttman, M.; Hamuro, Y.; Heck16, A. J. R.; Houde, D.; Iacob, R. E.; Jørgensen, T. J. D.; Kaltashov, I. A.; Klinman, J. P.; Konermann, L.; Man, P.; Mayne, L.; Pascal, B. D.; Reichmann, D.; Skehel, M.; Snijder, J.; Strutzenberg, T. S.; Underbakke, E. S.; Wagner, C.; Wales, T. E.; Walters, B. T.; Weis, D. D.; Wilson, D. J.; Wintrode, P. L.; Zhang, Z.; Zheng, J.; Schriemer, D. C.; Rand, K. D. Recommendations for Performing, Interpreting and Reporting Hydrogen Deuterium Exchange Mass

Spectrometry (HDX-MS) Experiments. Nat. Methods 2019, 16 (July), 595–602. https://doi.org/10.1038/s41592-019-0459-y.

(11) Huang, R. Y. C.; Iacob, R. E.; Sankaranarayanan, S.; Yang, L.; Ahlijanian, M.; Tao, L.; Tymiak, A. A.; Chen, G. Probing Conformational Dynamics of Tau Protein by Hydrogen/Deuterium Exchange Mass Spectrometry. J. Am. Soc. Mass Spectrom. 2018, 29 (1), 174–182. https://doi.org/10.1007/s13361-017-1815-8.

(12) Houde, D.; Arndt, J.; Domeier, W.; Berkowitz, S.; Engen, J. R. Characterization of IgG1 Conformation and Conformational Dynamics by Hydrogen / Deuterium Exchange Mass Spectrometry. Anal. Chem. 2009, 81 (7), 2644–2651. https://doi.org/10.1021/ac802575y.

(13) Rand, K. D.; Zehl, M.; Jensen, O. N.; Jørgensen, T. J. D. Protein Hydrogen Exchange Measured at Single-Residue Resolution by Electron Transfer Dissociation Mass Spectrometry. Anal. Chem. 2009, 81 (14), 5577–5584. https://doi.org/10.1021/ac9008447.

(14) Zehl, M.; Rand, K. D.; Jensen, O. N.; Jorgensen, T. J. D. Electron Transfer Dissociation Facilitates the Measurement of Deuterium Incorporation into Selectively Labeled Peptides with Single Residue Resolution. J. Am. Chem. Soc. 2008, 130 (51), 17453–17459. https://doi.org/10.1021/ja805573h.

(15) Huang, R. Y. C.; Kuhne, M.; Deshpande, S.; Rangan, V.; Srinivasan, M.; Wang, Y.; Chen, G. Mapping Binding Epitopes of Monoclonal Antibodies Targeting Major Histocompatibility Complex Class I Chain-Related A (MICA) with Hydrogen/Deuterium Exchange and Electron-Transfer Dissociation Mass Spectrometry. Anal. Bioanal. Chem. 2020, 412 (7), 1693–1700. https://doi.org/10.1007/s00216-020-02409-x.

(16) Li, J.; Wei, H.; Krystek, S. R.; Bond, D.; Brender, T. M.; Cohen, D.; Feiner, J.; Hamacher, N.; Harshman, J.; Huang, R. Y.; Julien, S. H.; Lin, Z.; Moore, K.; Mueller, L.; Noriega, C.; Sejwal, P.; Sheppard, P.; Stevens, B.; Chen, G.; Tymiak, A. A.; Gross, M. L.; Schneeweis, L. A. Mapping the Energetic Epitope of an Antibody/Interleukin-23 Interaction with Hydrogen/Deuterium Exchange, Fast Photochemical Oxidation of Proteins Mass Spectrometry, and Alanine Shave Mutagenesis. Anal. Chem. 2017. https://doi.org/10.1021/acs.analchem.6b03058.

(17) Cornwell, O.; Radford, S. E.; Ashcroft, A. E.; Ault, J. R. Comparing Hydrogen Deuterium Exchange and Fast Photochemical Oxidation of Proteins: A Structural Characterisation of Wild-Type and ΔN6 B2-Microglobulin. J. Am. Soc. Mass Spectrom. 2018, 29, 2413–2426. https://doi.org/10.1007/s13361-018-2067-y.

(18) Zhang, M. M.; Huang, R. Y. C.; Beno, B. R.; Deyanova, E. G.; Li, J.; Chen, G.; Gross, M. L. Epitope and Paratope Mapping of PD-1/Nivolumab by Mass Spectrometry-Based Hydrogen-Deuterium Exchange, Cross-Linking, and Molecular Docking. Anal. Chem. 2020, 92 (13), 9086–9094. https://doi.org/10.1021/acs.analchem.0c01291.

(19) Mendoza, V. L.; Vachet, R. W. Protein Surface Mapping Using Diethylpyrocarbonate with Mass Spectrometric Detection. Anal. Chem. 2008, 80 (8), 2895–2904. https://doi.org/10.1021/ac701999b.

(20) Limpikirati, P. K.; Zhao, B.; Pan, X.; Eyles, S. J.; Vachet, R. W. Covalent Labeling/Mass Spectrometry of Monoclonal Antibodies with Diethylpyrocarbonate: Reaction Kinetics for Ensuring Protein Structural Integrity. J. Am. Soc. Mass Spectrom. 2020, 31 (6), 1223–1232. https://doi.org/10.1021/jasms.0c00067.

(21) Yamamoto, R.; Wang, A.; Vitt, C. R.; Lin, L. S. Histidine-15: An Important Role in the Cytotoxic Activity of Human Tumor Necrosis Factor. Protein Eng. Des. Sel. 1989, 2 (7), 553–558. https://doi.org/10.1093/protein/2.7.553.

(22) Limpikirati, P.; Liu, T.; Vachet, R. W. Covalent Labeling-Mass Spectrometry with Non-Specific Reagents for Studying Protein Structure and Interactions. Methods 2018, 144, 79–93. https://doi.org/10.1016/j.ymeth.2018.04.002.

(23) Tremblay, C. Y.; Limpikirati, P.; Vachet, R. W. Complementary Structural Information for Stressed Antibodies from Hydrogen − Deuterium Exchange and Covalent Labeling Mass Spectrometry. 2021, 32 (5), 1237–1248. https://doi.org/10.1021/jasms.1c00072.

(24) Liu, T.; Limpikirati, P.; Vachet, R. W. Synergistic Structural Information from Covalent Labeling and Hydrogen − Deuterium Exchange Mass Spectrometry for Protein − Ligand Interactions. Anal. Chem. 2019, 91, 15248–15254. https://doi.org/10.1021/acs.analchem.9b04257.

(25) Daub, H.; Traxler, L.; Ismajli, F.; Groitl, B.; Itzen, A.; Rant, U. The Trimer to Monomer Transition of Tumor Necrosis Factor-Alpha Is a Dynamic Process That Is Significantly Altered by Therapeutic Antibodies. Sci. Rep. 2020, 10 (9265), 1–10. https://doi.org/10.1038/s41598-020-66123-5.

(26) Ono, M.; Horita, S.; Sato, Y.; Nomura, Y.; Iwata, S.; Nomura, N. Structural Basis for Tumor Necrosis Factor Blockade with the Therapeutic Antibody Golimumab. Protein Sci. 2018, 27 (6), 1038–1046. https://doi.org/10.1002/pro.3407.

(27) Kim, M. S.; Lee, S. H.; Song, M. Y.; Yoo, T. H.; Lee, B. K.; Kim, Y. S. Comparative Analyses of Complex Formation and Binding Sites between Human Tumor Necrosis Factor-Alpha and Its Three Antagonists Elucidate Their Different Neutralizing Mechanisms. J. Mol. Biol. 2007, 374 (5), 1374–1388. https://doi.org/10.1016/j.jmb.2007.10.034.

(28) Hu, S.; Liang, S.; Guo, H.; Zhang, D.; Li, H.; Wang, X.; Yang, W.; Qian, W.; Hou, S.; Wang, H.; Guo, Y.; Lou, Z. Comparison of the Inhibition Mechanisms of Adalimumab and Infliximab in Treating Tumor Necrosis Factor α-Associated Diseases from a Molecular View. J. Biol. Chem. 2013, 288 (38), 27059–27067. https://doi.org/10.1074/jbc.M113.491530.

(29) Van Schie, K. A.; Ooijevaar-De Heer, P.; Dijk, L.; Kruithof, S.; Wolbink, G.; Rispens, T. Therapeutic TNF Inhibitors Can Differentially Stabilize Trimeric TNF by Inhibiting Monomer Exchange. Sci. Rep. 2016, 6, 32747. https://doi.org/10.1038/srep32747.

(30) Liang, S.; Dai, J.; Hou, S.; Su, L.; Zhang, D.; Guo, H.; Hu, S.; Wang, H.; Rao, Z.; Guo, Y.; Lou, Z. Structural Basis for Treating Tumor Necrosis Factor α (TNFα)-

Associated Diseases with the Therapeutic Antibody Infliximab. J. Biol. Chem. 2013, 288 (19), 13799–13807. https://doi.org/10.1074/jbc.M112.433961.

(31) Limpikirati, P.; Hale, J. E.; Hazelbaker, M.; Huang, Y.; Jia, Z.; Yazdania, M.; Grabanb, E. M.; Vaughan, R. C.; Vachet, R. W. Covalent Labeling and Mass Spectrometry Reveal Subtle Higher Order Structural Changes for Antibody Therapeutics. MAbs 2019, 11 (3), 463–476. https://doi.org/10.1080/19420862.2019.1565748.

(32) Pan, X.; Limpikirati, P.; Chen, H.; Liu, T.; Vachet, R. W. Higher-Order Structure Influences the Kinetics of Diethylpyrocarbonate Covalent Labeling of Proteins. J. Am. Soc. Mass Spectrom. 2020, 31 (3), 658–665. https://doi.org/10.1021/jasms.9b00132.

(33) Borotto, N. B.; Zhou, Y.; Hollingsworth, S. R.; Hale, J. E.; Graban, E. M.; Vaughan, R. C.; Vachet, R. W. Investigating Therapeutic Protein Structure with Diethylpyrocarbonate Labeling and Mass Spectrometry. Anal. Chem. 2015. https://doi.org/10.1021/acs.analchem.5b03180.

(34) Krezel, A.; Bal, W. A Formula for Correlating PKa Values Determined in D2O and H2O. J. Inorg. Biochem. 2004, 98, 161–166. https://doi.org/10.1016/j.jinorgbio.2003.10.001.

(35) Hageman, T. S.; Weis, D. D. Reliable Identification of Significant Differences in Differential Hydrogen Exchange-Mass Spectrometry Measurements Using a Hybrid Significance Testing Approach. Anal. Chem. 2019, 91 (13), 8008–8016. https://doi.org/10.1021/acs.analchem.9b01325.

(36) Weis, D. D. Recommendations for the Propagation of Uncertainty in Hydrogen Exchange-Mass Spectrometric Measurements. 2021. https://doi.org/10.1021/jasms.0c00475.

(37) Hu, S.; Liang, S.; Guo, H.; Zhang, D.; Li, H.; Wang, X.; Yang, W.; Qian, W.; Hou, S.; Wang, H.; Guo, Y.; Lou, Z. Comparison of the Inhibition Mechanisms of Adalimumab and Infliximab in Treating Tumor Necrosis Factor α-Associated Diseases from a Molecular View. J. Biol. Chem. 2013, 288 (38), 27059–27067. https://doi.org/10.1074/jbc.M113.491530.

(38) Limpikirati, P.; Pan, X.; Vachet, R. W. Covalent Labeling with Diethylpyrocarbonate: Sensitive to the Residue Microenvironment, Providing Improved Analysis of Protein Higher Order Structure by Mass Spectrometry. Anal. Chem. 2019, 91 (13), 8516–8523. https://doi.org/10.1021/acs.analchem.9b01732.

(39) Biehn, S. E.; Limpikirati, P.; Vachet, R. W.; Lindert, S. Utilization of Hydrophobic Microenvironment Sensitivity in Diethylpyrocarbonate Labeling for Protein Structure Prediction. Anal. Chem. 2021, 93 (23), 8188–8195. https://doi.org/10.1021/acs.analchem.1c00395.

Chapter 5

Summary and Future Directions

5.1. Summary

This dissertation has focused on the use of diethylpyrocarbonate (DEPC) covalent labeling (CL) and hydrogen deuterium exchange (HDX), each combined with mass spectrometry (MS) to characterize the higher-order structure (HOS) of protein therapeutics. Both DEPC-CL and HDX characterize protein HOS by encoding the structure into the mass of the protein. Due to the differences in mechanism and experimental set up, the use of these two methods together provides a synergistic picture of protein structure. DEPC is a simple to use, commercially available CL reagent that reacts with nucleophilic residues to reveal a protein's structural properties with residue level resolution. HDX is a well-established technique that not only reports on solvent accessibility but is uniquely suited to detect protein dynamics. Characterizing therapeutic protein HOS, and specifically mAb HOS, is notoriously difficult, however is necessary for development of protein therapeutics. This dissertation aims to address the need in pharmaceutical industry for robust and high throughput methods of HOS characterization. Here we describe how DEPC can be used to study antibody-antigen interactions and how the use of HDX and DEPC-CL together can give a great depth of structure information than the sum of their parts for heat stressed mAbs and antibody-antigen interactions.

In **Chapter 2**, we investigated the use of HDX and DEPC-CL for studying HOS perturbations caused by heat stress. Using rituximab as a model mAb we find that DEPC-CL is more sensitive to subtle HOS perturbations caused by low levels of heat stress (i.e.,

45°C and 55°C). However, we also demonstrate that at high heat stress conditions (i.e., 65°C) HDX and DEPC-CL together provide information about the complex structural changes that take place in the protein. We show that there are changes to side chain orientation that result in changes in labeling extent, but that these changes do not necessarily correspond to changes in protein dynamics. Additionally, we hypothesize that regions where both methods show decreases are likely sources of aggregation, which is supported by aggregation prediction software. By considering the complementary data provided by each method, we show that more confident conclusions about complex HOS perturbations can be revealed. To the best of our knowledge, this is the first report of DEPC-CL/MS in parallel with HDX to study subtle HOS changes of a therapeutic mAb at the temperature below the antibody melting temperature.

In **Chapter 3**, we explored the use of DEPC-CL for studying antigen-antibody interactions. The model system used was TNFα in complex with three different mAbs. The labeling extent of residues on free and bound TNFα were compared to determine DEPC's utility for studying epitopes and antigen HOS changes. CL/MS using DEPC offers some advantages over other MS-based techniques for revealing protein-protein interfaces, such as the TNFα epitope. DEPC labeling reports on side chains, thereby providing a direct indication of binding interfaces. Decreased labeling at specific residues can be used to elucidate the binding interfaces because protein aggregation and ligand binding decrease the solvent accessibility of the side chains involved in the epitope. We found that generally, DEPC decreases were located at epitope residues and increases were often a result of changes in microenvironment to weakly nucleophilic residues.

Changes in labeling extent that do not fall into either of the previously mentioned categories often are a result of more complicated quaternary HOS.

In **Chapter 4**, we again apply DEPC-CL and HDX in parallel, this time to investigate antibody- antigen interactions. The same model system in chapter 3 of TNFα in complex with three different therapeutic mAbs was used. The benefit of this system over the previous heat stressed rituximab system is that the crystal structures of TNFα in complex with each of these antibodies is available. Thus, we can be more confident with the conclusions we make about the HOS perturbations that take place upon mAb binding. We find that by using the two methods together we can clearly determine locations of dynamics changes versus changes in solvent exposure. In the TNFα:adalimumab condition, DEPC can clearly clarify ambiguous HDX results. HDX decreases span the majority of the protein while decreases in DEPC-CL are localized to the epitope. The TNFα:infliximab condition highlights that HDX information can provide dynamics information that cannot be obtained from crystal structure data. A peptide increases in HDX meaning it become more dynamic upon antibody binding. All together the data from the three mAbs demonstrates the synergistic information that can be provided by the two methods.

As a result of the growing importance of protein therapeutics and the necessity to characterize their structure, robust methods to study protein HOS are needed. Here, we demonstrate that as a result of differences in intrinsic reaction rate, reaction mechanism, and experimental set up, HDX/MS and DEPC-CL/MS are complementary, and sometimes synergistic, methods for studying protein therapeutic structure. Previous work has shown DEPC-CL/MS and HDX/MS can provide complementary information about

protein-ligand interactions, but this work is the first instance of DEPC-CL/MS and HDX/MS being used together to study mAb HOS perturbations caused by heat stress. The data presented here suggests these methods can be applied more broadly to study mAb stability and HOS perturbations. Additionally, the application of DEPC-CL/MS and HDX/MS is used for the first time to study antigen:antibody interactions. Our results indicate that DEPC-CL/MS and HDX/MS together should be applicable to a variety of protein:protein systems, providing accurate information about binding sites and binding-induced structural changes. Moreover, the methods are valuable tools for epitope identification and can be used to garner a deeper understanding of mAb mechanisms of action.

5.2. Future Directions

The following sections discuss possible future applications of combining DEPC-CL/MS and HDX/MS as well as possible future improvements to the methods and data interpretation.

5.2.1. Other CL reagents for epitope mapping

While DEPC is capable of mapping ~30% of the sequence of the average protein there is a likelihood that the residues of interest may not be labelable by DEPC. For the work with TNFα, out of 25 epitope residues for adalimumab, only 10 are labelable by DEPC. Expanding the labeling reagents used could provide higher resolution and could provide further clarification about which changes are a result of loss of solvent exposure, and which changes are a result of changes in microenvironment. A promising new reagent currently being explored is an α, β-unsaturated carbonyl scaffold (ABUC).

ABUC can react with up to 13 different residues and thus provides a higher resolution than DEPC. While ABUC is promising, is not compatible with reducing agents such as TCEP and DTT meaning it is not a good reagent to study the structure of any protein with disulfides. Other reagents such as GEE, or HNSB may provide further information that could be helpful. Ideally reagents that have relatively slow intrinsic reaction rates are best for combination with HDX because they provide the most synergistic information. Methods like FPOP or carbene labeling provide information more similar to HDX as they react much faster and can report on dynamic changes.

5.2.2. Molecular modeling

Molecular modeling, or molecular dynamics (MD) simulates the movements of atoms or molecules in a protein. While additional labeling reagents may provide higher structural resolution, molecular modeling of protein systems will add an additional layer of HOS information that neither HDX nor CL could provide. By combining the data from all three methods it will be possible to get a clearer picture of protein HOS. Previous work in other groups has demonstrated the utility of MD simulations combined with HDX for data interpretation of which HOS perturbations are likely taking place.[87,88] The addition of MD data began to be explored in the TNFα data with modeling of TNFα alone and TNFα in complex with a single F_v fragment of adalimumab. This data was able to clarify some of the labeling data that was inconsistent with previous understandings of the DECP mechanism. For instance, MD shows that while some lysine and histidine residues may appear buried in the static crystal structure, they do have a significant amount of solvent exposure when their dynamics is revealed. Information from MD will also provide insight into microenvironment of residues such as serine, threonine, and

tyrosine, highlighting changes in side chain orientation that may lead to labeling extent changes. Future work incorporating MD with HDX and CL will inform over labeling studies, give greater insight into protein interfaces, and clarify ambiguous data.

5.2.3. Paratope mapping and investigating the HOS changes of mAbs upon antigen binding

The work in this dissertation around antigen-antibody interactions focused mainly on the HOS changes of the antigen upon mAb binding and epitope mapping. However, investigating the HOS changes of the antibody and paratope mapping is just as valuable. Due to the nature of HDX and DEPC-CL experiments, the HOS data of the antibody is in the mass spectra that has already been acquired and needs to be extracted and analyzed. While methods were optimized for TNFα analysis, there is still a significant amount of mAb data that can be processed. By processing this data, we could learn about the HOS of mAbs upon binding with TNFα. The HDX data would show changes in dynamics and solvent exposure while the DEPC-CL data could show changes in microenvironment and solvent exposure. A larger DEPC-CL data set might also help to interpret the data from Chapter 3 investigating TNFα with DEPC alone.

APPENDICES

APPENDIX A

A. CLEAVAGE PROFILE OF PROTEIN SUBSTRATES BY CLPXP REVEALS DELIBERATE STARTS AND PAUSES

Majority of this appendix part of a journal article published as: Catherine Y. Tremblay, Robert H. Vass, Richard W. Vachet, and Peter Chien, Cleavage profile of protein substrates by ClpXP reveals deliberate starts and pauses, *Biochemistry* **2020** *59* (44), 4294-4301

A.1. Introduction:

AAA+ proteases are required in all kingdoms of life during both normal growth and stress responses. In bacteria, the highly conserved ClpXP system is responsible for degradation of hundreds of substrates,[1,2] including products of stalled translation through the tmRNA-mediated trans-translation system.[1,2] ClpX consumes ATP to power recognition and unfolding of a target substrate, gripping proteins with a series of pore-loops, and translocating the unfolded polypeptides through a central pore to the chambered ClpP peptidase, where the protein is hydrolyzed to small peptides.[1,2] ClpXP is able to degrade proteins of diverse sequence and structural composition, without particular selectivity once substrate degradation is initiated. [1,2] Unfolded substrates are degraded more rapidly than folded substrates, but the relationship between target structure and unfolding is principally dependent on unraveling of local kinetically stable elements rather than global thermodynamic stability.[3] Importantly, how these parameters translate into the peptide products of degradation is less clear.

Initial studies have shown that the ClpP family of proteases produces peptides that range from 8-12 residues in length.[4-6] Structural and biochemical studies[7] reveal dynamic

pores that circumscribe the ClpP barrel and prevent larger peptides from exiting the chamber. Peptide product identity has been far less explored than other parameters of the ClpXP processing cycle as ClpP is relatively nonspecific based on preferences established with short peptide reporters.[5] Interestingly, during proteotoxic conditions, peptides released from the mitochondria ClpP trigger activation of the mitochondria unfolded protein response[8] suggesting that release of specific peptides could be a 'canary in the coalmine' signal for cells to respond to stress. Therefore, understanding what constraints drive peptide cleavage in the ClpP-family of proteases may aid in our discovery of these signals.

Here, we use a series of structurally distinct substrates and high-resolution mass spectrometry to determine the specific sites and patterns of substrate cleavage. We find that translocation speed, recognition efficiency, or number of active catalytic sites have negligible effects on product peptide identities. Rather, local structural constraints and product length superimposed on intrinsic peptide site preferences are the major drivers for where cleavage ultimately occurs. Interestingly, we also find a substrate-independent enrichment of peptides with a 12-residue average periodic cleavage pattern. In light of recent structural and single molecule studies, we interpret this 12-residue preference as the existence of a pause during ClpXP degradation of the *Caulobacter crescentus* species, driven by resetting of the ClpX ring and cleavage of the polypeptide extended into the ClpP chamber at sites constrained by primary sequence preference.

A.2. Results and Discussion

A.2.1. Cleavage preference is unaffected by substrate extrinsic reaction parameters.

Three proteins, GFP, RcdA, and β2m, that differ in size and secondary structure were expressed with an ssrA tag on the C-terminus and subjected to *in vitro* degradation by ClpXP. The peptides that are produced upon degradation of GFPSsrA, RcdAssrA, and disulfide-reduced β2mssrA were identified by LC/MS/MS (**Figure A.1A**). Sequence coverages ranging from 92-100%, with an average of 96% ± 3% (n=14), were obtained under standard degradation conditions. This high sequence coverage provides unprecedented insight into how substrates are digested by ClpXP. From these experiments, we find that cleavage is preferred when Leu, Met, Ser, or Ala residues are directly adjacent to the cleave site in the n-terminal direction, or the P1 position, while other positions show no obvious cleavage specificity (**Figure A.1**B). When each protein substrate is considered separately, the preference for the hydrophobic residues, Leu and Met, at the P1 position persists (**Figure A.1C, D, E**).

While this method of data analysis indicates preferred residues at cleavage sites, it does not clearly represent nonpreferred residues nor does it account for how often each residue appears in the sequence of the protein. To address these issues, the frequency with which a residue appears at the C-terminus of a peptide fragment was normalized to the frequency with which it is found in the protein sequence. **Figure A.1**F, G and H depict this normalized data, where values greater than zero indicate a preference for cleavage at the P1 position, values less than zero indicate that cleavage at a given residue is disfavored, and a value of zero indicates that cleavage at this residue is as likely as random chance. From this analysis, we find a preference for cleavage at Leu and Met

residues but also at Ala, Gly, Ser, and Asn residues. These cleavage preferences persist across the studied substrates, with 81% agreement (Pearson correlation) between reduced β2m and GFP and 77% agreement between RcdA and GFP for cleavage preference at the P1 position. The intrinsic preference of ClpXP for hydrophobic residues at the P1 position is consistent with previous work in which Gersch and coworkers found general cleavage preferences at Met, Ser, Leu, and Ala at the P1 position for human ClpP, *Escherichia coli* ClpP, and *Staphylococcus aureus* ClpP upon digestion of both endogenous substrates and peptide libraries.[5] Our data with a fourth species, *Caulobacter crescentus* ClpP, demonstrates that the preference is conserved across all these species. It is possible that differences observed in peptide products from ClpXP originating in different species could be a result of differences in dynamics or sequence of each unique species.

We next considered the length of produced peptides and found average peptide lengths of 13 ± 5, 13 ± 5, and 15 ± 6 residues for GFP, β2m, and RcdA, respectively, based on at least three replicate experiments for each protein. Peptide distributions are skewed towards higher molecular weights with peptides up to 28 amino acids observed in some cases (**Figure A.2**). When the distribution of peptides is weighted by their mass spectral intensities, we observe that the average lengths for GFP, reduced β2m, and RcdA are 11 ± 3, 12 ± 3, and 12 ± 4 residues, respectively. A similar MS-based analysis from Sieber and co-workers showed peptide product length distributions ranging from 8-12 residues derived from protein degradation by ClpXP,[589] largely consistent with what we find.

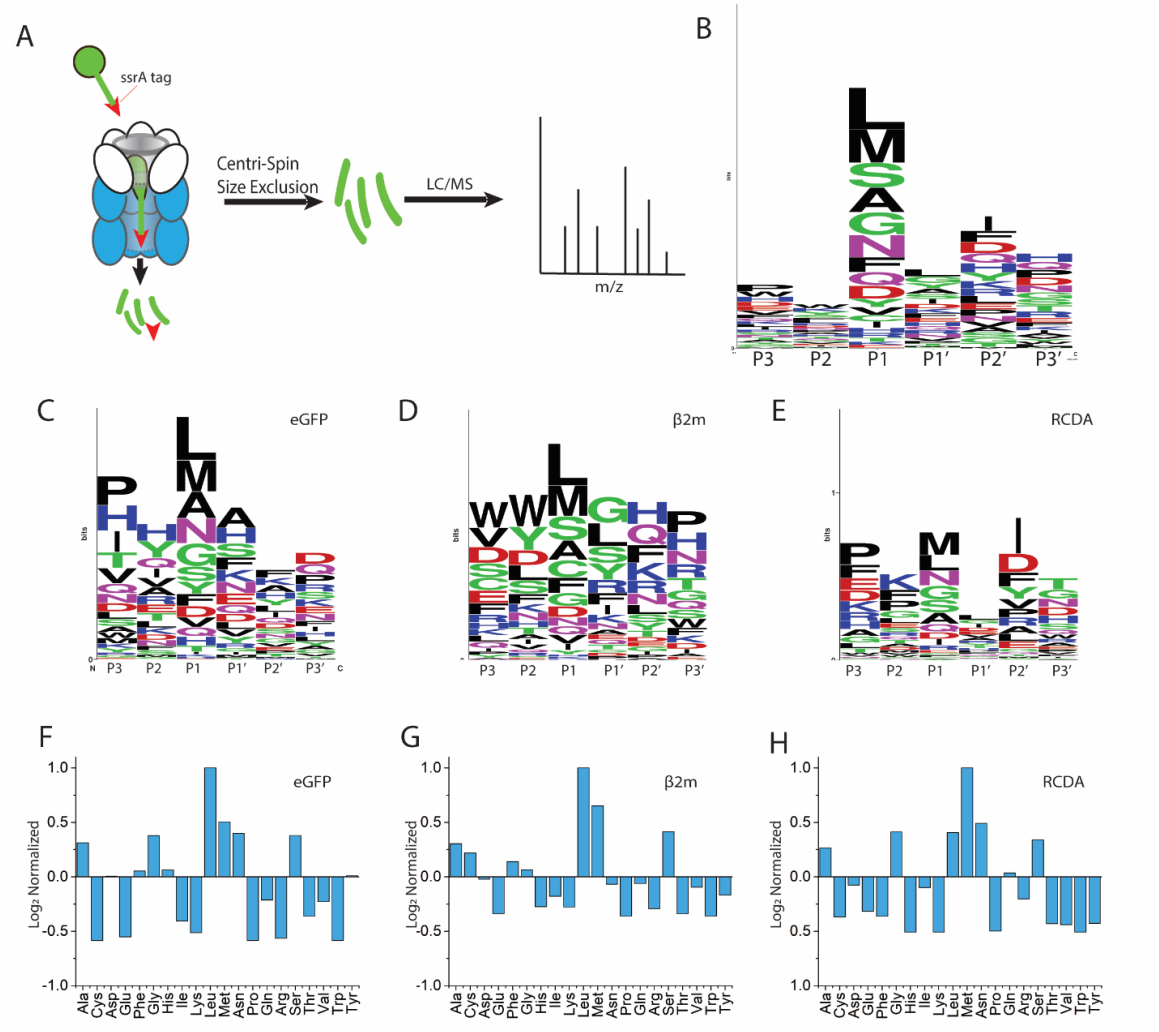

Figure A.1: Primary structure cleavage specificity of ClpXP. (A) Schematic depiction of tagged protein digestion, separation, and analysis. Residues directly adjacent to the cleavage site in the N-terminal direction are indicated as P1, P2 and P3, and residues directly adjacent to the cleavage site in the c-terminal direction are indicated as P1', P2' and P3', numerically increasing as they are further from the cleavage site. Weblogo representation of cleavage preferences for all substrates (B), GFP (C), reduced β2m (D), and RcdA (E). Amino acid preferences at the P1 position normalized to presence in the given protein for GFP (F), reduced β2m (G), and RcdA (H).

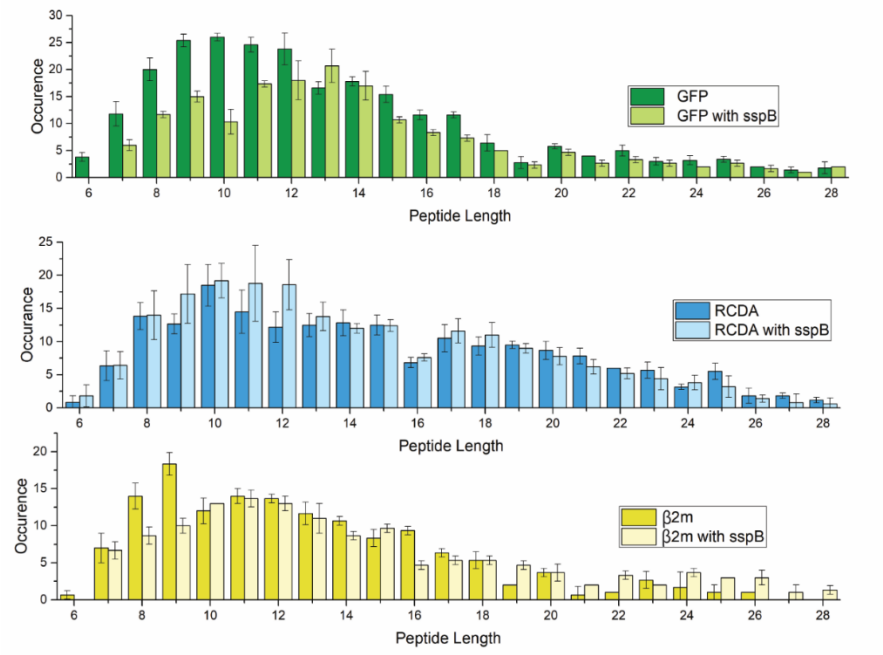

Figure A.2: Peptide length histogram for standard digestion of ClpXP and digestion with the sspB adapter. (A) GFP, (B) RcdA, and (C) disulfide reduced β2m.

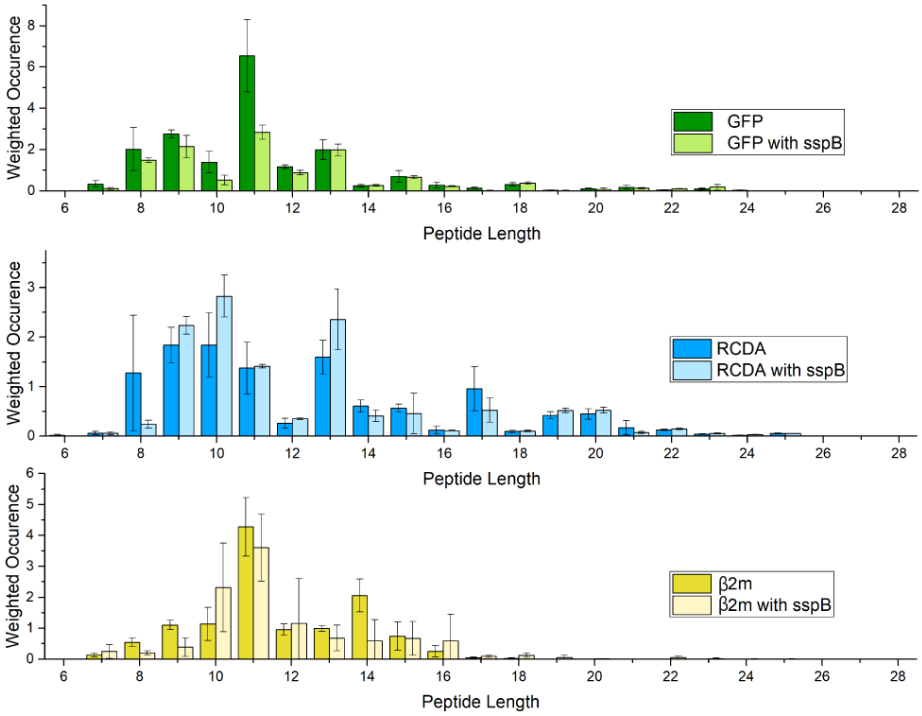

Figure A.3: Peptide length histogram weighted for mass spectral intensity for standard digestion of ClpXP and digestion with the sspB adapter. (A) GFP, (B) RcdA, and (C) disulfide reduced β2m

Having determined that cleavage specificity or length is not substrate dependent, we investigated if degradation rate influences these parameters. For example, slowing proteolysis may increase the dwell time a substrate spends within the barrel of ClpXP which may affect cleavage specificity or product length. Using GFPSsrA, we first investigated changes in ATP concentration as ATP hydrolysis affects degradation rate. By using sufficiently low ATP concentrations ranging from 7 to 31 μM, we could adjust the degradation rates substantially as monitored by loss of fluorescence (**Figure A.5A**). It is worth noting that at 7 μM ATP virtually no loss of full-length protein is observed by the fluorescence assay, but peptides are still generated and detected by MS, highlighting the sensitivity of our measurements. Overall, there is no significant difference in peptide length or cleavage specificity as compared to saturating ATP concentrations (**Figure A.4**). An analysis of the cleavage specificity of protease under optimal cleavage conditions compared with low ATP levels indicates greater than 97% agreement (Pearson correlation) for the preferred residues in the P1 position (**Table A.1**). The fact that peptide distributions are the same regardless of ATP concentration further supports our understanding that ClpXP is a highly processive protease and once engaged with a substrate will fully degrade that target. We note that this effect could also be contributed by ClpP itself given prior work suggesting that peptide bond hydrolysis alone may be sufficient to power processive degradation.[9]

ClpP degradation rate was also reduced by inhibiting active sites with the protease inhibitor diisopropyl fluorophosphate (DFP). DFP inhibits ClpP activity in a dose-dependent manner (**Figure A.5B**) by binding covalently and irreversibly to the active site

serine. Previous studies have shown that degradation of substrates by DFP-treated ClpP results in release of partially processed intermediates.[10] We speculated that by inhibiting some active sites, longer peptides with different cleavage specificities might be produced as there are fewer active sites available to cleave the protein. However, digestion of GFP in the presence of 5, 25, and 100-fold molar excesses of DFP resulted in both peptide length and cleavage specificity that were very similar to control experiments without DFP (i.e. >93% similar; see **Table A.1**). These results indicate that inhibiting active sites does not change cleavage preference or distribution of final peptide products, even though overall proteolysis is slowed.

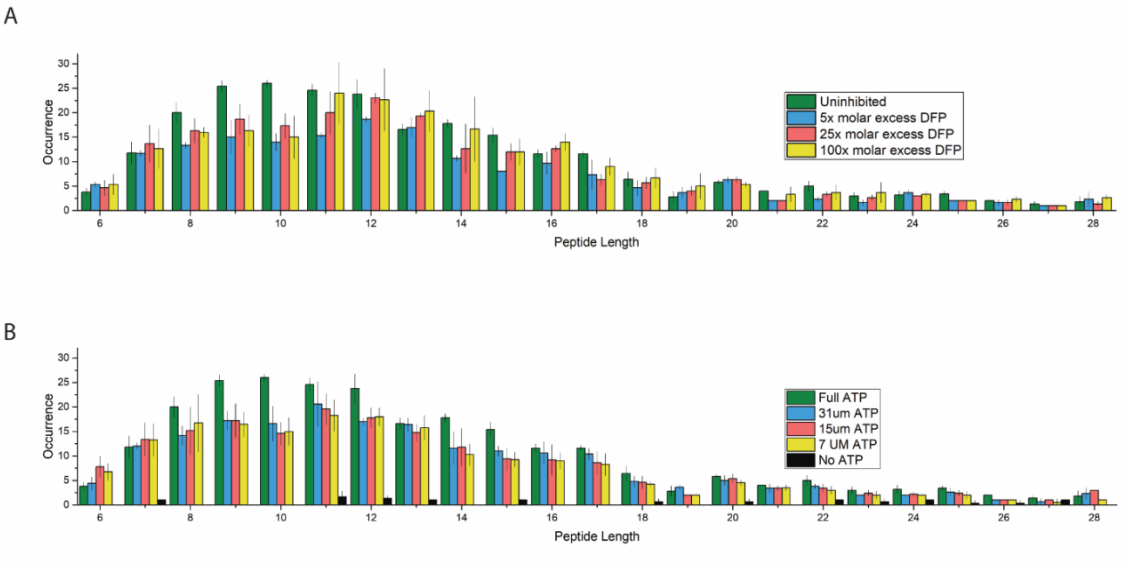

Figure A.4: peptides length histogram for digestion of GFP under (A) DFP inhibited degradation and (B) ATP limited degradation

We also increased degradation rates by using the SspB adaptor, which delivers ssrA-tagged substrates more effectively to ClpXP (**Figure A.5C**). Similar to slowing the reaction, accelerating the reaction has little effect on cleavage specificity or the resulting peptide length distribution (**Figure A.2** and **Table A.1).** The primary sequence cleavage

specificity and the peptide length distributions were >92% and >89% correlated, respectively, to GFP degradation under standard conditions (**Table A.1**). Together, our data show that the fundamental distribution of cleavage sites within a substrate degraded by ClpXP is mostly unaffected by energy consumption, number of peptide hydrolysis sites, or efficiency of substrate recognition, as summarized in **Figure A.5E** and **Table A.1**.

Table A.1: A summary of the Pearson correlations of primary sequence cleavage specificity and peptide length distribution as compared to native GFPSsrA degradation under standard conditions

	Primary sequence cleavage in P1 position	Peptide length distribution	Cleavage location on sequence
RcdA	77%	86%	
Reduced β2m	81%	93%	
β2m	75%	92%	
GFP +7μM ATP	98%	95%	97%
GFP +15μM ATP	98%	95%	96%
GFP +30μM ATP	97%	97%	97%
GFP +5X DFP	93%	93%	82%
GFP +25X DFP	97%	95%	86%
GFP +100XDFP	97%	93%	87%
GFP +sspB	92%	89%	91%

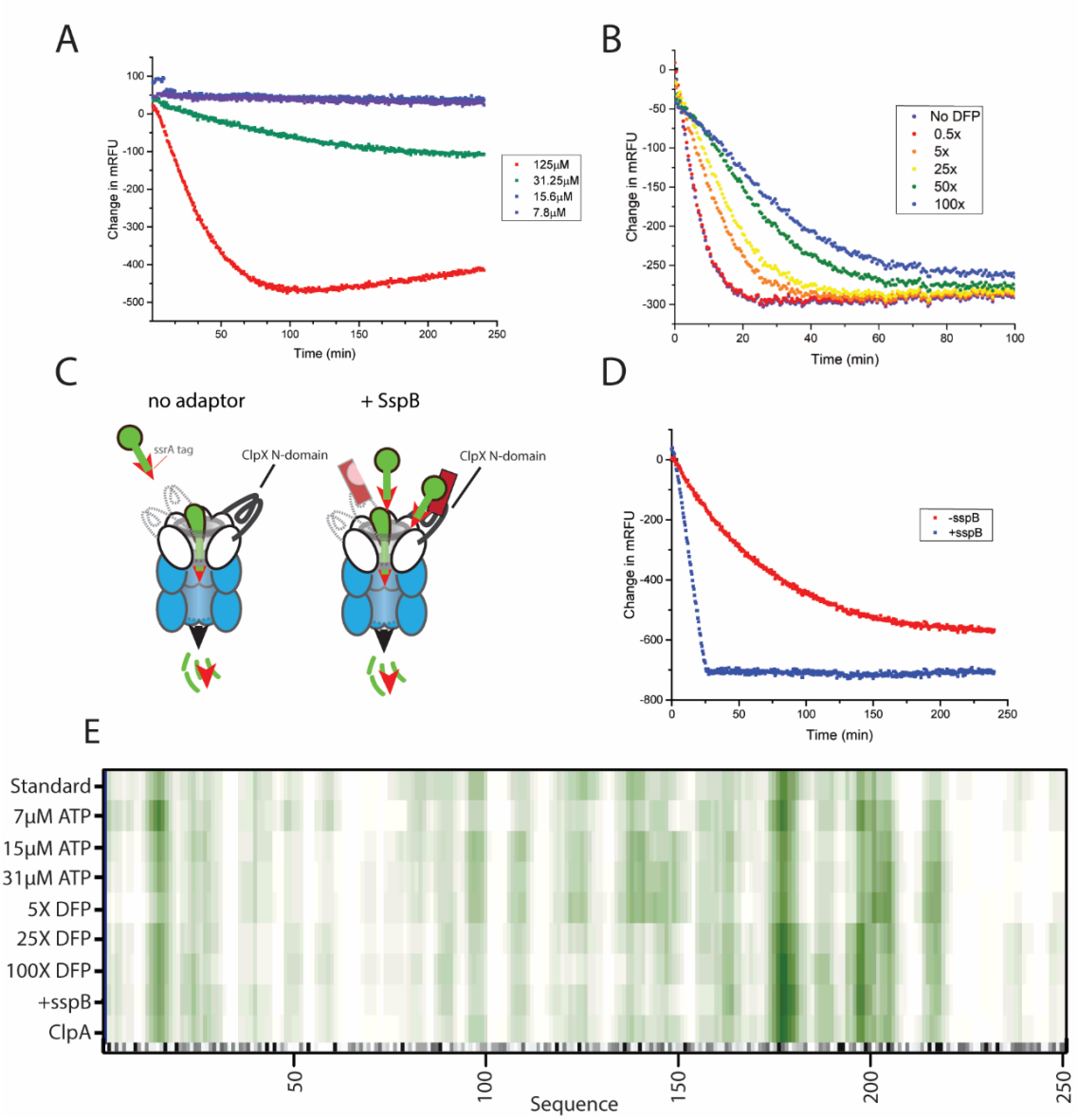

Figure A.5: Altered reaction conditions and rates do not change ClpXP cleavage specificities. (A) GFP degradation rate at varying ATP concentrations; 125 μM ATP (red) 31.25 μM (green), 15.6 μM (blue), and 7.8 μM (purple). (B) GFP degradation rate at 0.5, 5, 25, 50, and 100-fold molar excesses of the inhibitor DFP. (C) Cartoon depiction of the sspB adapter facilitating substrate orientation. (D) GFP degradation rate in the presence(blue) and absence(red) of the sspB adapter. (E) Heat map that summarizes the GFP cleavage locations under various reaction conditions. A darker shade of green indicates a higher incidence of cleavage, while white indicates a low incidence of cleavage. At the bottom of the plot, the gray scale indicates the cleavage specificity derived from Figure 1F with darker colors corresponding to amino acids that are more preferred in the P1 position.

A.2.2. Cleavage specificity is constrained by position

Interestingly, the preferences shown in the heatmaps of **Figure A.5E** suggest that there is positional specificity in the cleavage products of ClpXP. When mass spectral weighted cleavage sites are plotted as a function of substrate length for all substrates (**Figure A.9**), it becomes clear that there are "hot spots" that are not solely correlated to sites most likely to be cleaved based exclusively on primary sequence preference (**Figure A.9** and **Figure A.1F**). The average amino acid spacing between each peak in **Figure A.6** is 12 ± 3 (GFP), 12 ± 3 (β2m), and 13 ± 6 (RcdA), consistent with the peptide length distributions shown previously. Moreover, a power spectral analysis of the plots in **Figure A.6**, from a Fast Fourier Transform, reveals defined frequency components for the cleavage of each substrate, while no such defined frequency components are observed when the same analysis is done on the sequence preference (**Figure A.10**). These defined frequency components presumably correspond to discrete cleavage step sizes. Cleavage patterns also deviate when comparing the C-terminus (which would be the first to enter the ClpP chamber). In particular, near the initiation site at the C-terminus, cleavage site seems mostly driven by amino acid identity until a structured region is encountered, then cleavage appears to occur at regular intervals thereafter (**Figure A.7**). This observation suggests that upon initiation, cleavage of the pioneering sequence entering the ClpP chamber is random (resulting in no significant accumulation of a particular site), but once structured regions are being translocated, there are deliberate pauses in the processive degradation which result in enrichment of cleavage sites spaced 10-13 residues apart (**Figure A.6**).

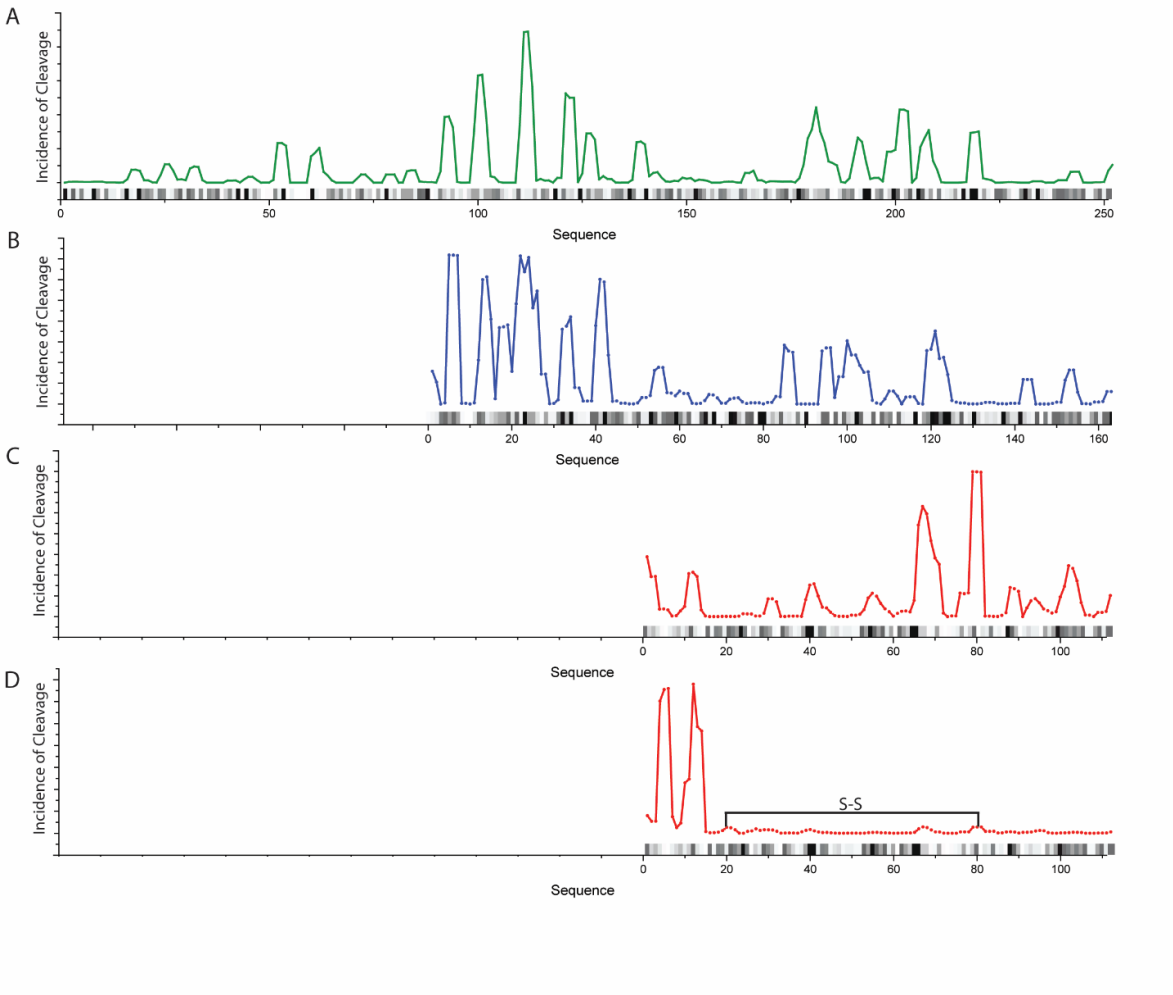

Figure A.6: Cleavage incidence locations on the studied substrates weighted for mass spectral intensity. (A) GFP, (B) RcdA, (C) reduced β2m and (D) oxidized β2m. The location of the disulfide bond is depicted as a black line. Data were subject to a moving average smoothing over 3 data points. The black and gray bars on each graph represent primary sequence cleavage specificity, where darker colors indicate higher likelihood of cleavage.

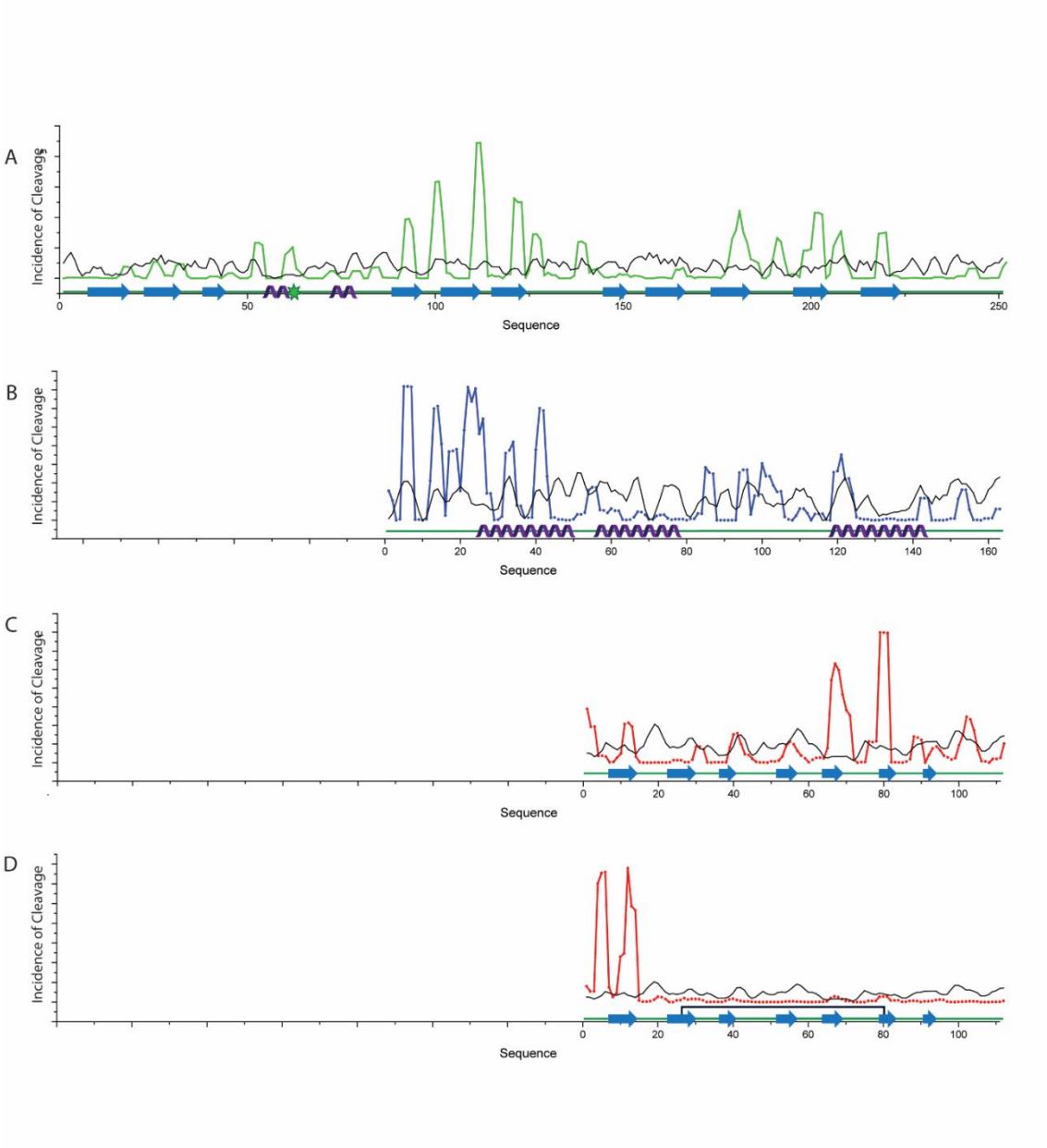

Figure A.7: Cleavage incidence locations on the studied substrates weighted for mass spectral intensity. (A) GFP, (B) RcdA, (C) reduced β2m and (D) oxidized β2m. Secondary structure is indicated underneath with blue arrows representing beta sheets, purple helices representing alpha helices and the chromophore of GFP represented as a star. The location of the disulfide bond is depicted as a black line. Data was subject to a moving average smoothing over 3 data points. The black line on each graph represents primary sequence cleavage specificity.

A.2.3. Disulfide effects on positional cleavage specificity

To further investigate the effect of protein higher order structure on ClpXP cleavage patterns, we examined the peptide products of the ssrA-tagged disulfide-bonded form of β2m. Peptides resulting from digestion of β2m with an intact disulfide bond are notably different than peptides produced from the reduced form of the protein (Figures 3C and 3D), with only a 55% correlation in the cleavage locations. This difference is even more apparent when the observed cleavage sites are weighted for mass spectral intensity (**Figure A.6D**). Considered in this way, there is a preference for cleavage at residues 66 and 78-80 in the reduced form but a preference at residues 4 and 12 for the oxidized form. We do not observe a significant difference in the degradation efficiency of between oxidized and reduced β2m, nor do we observe any aggregation of either form of this substrate. Because ClpX is known to accommodate a disulfide-bond linked polypeptide,[11] this suggests that the translocation of this more structured region results in a reset of cleavage site preference.

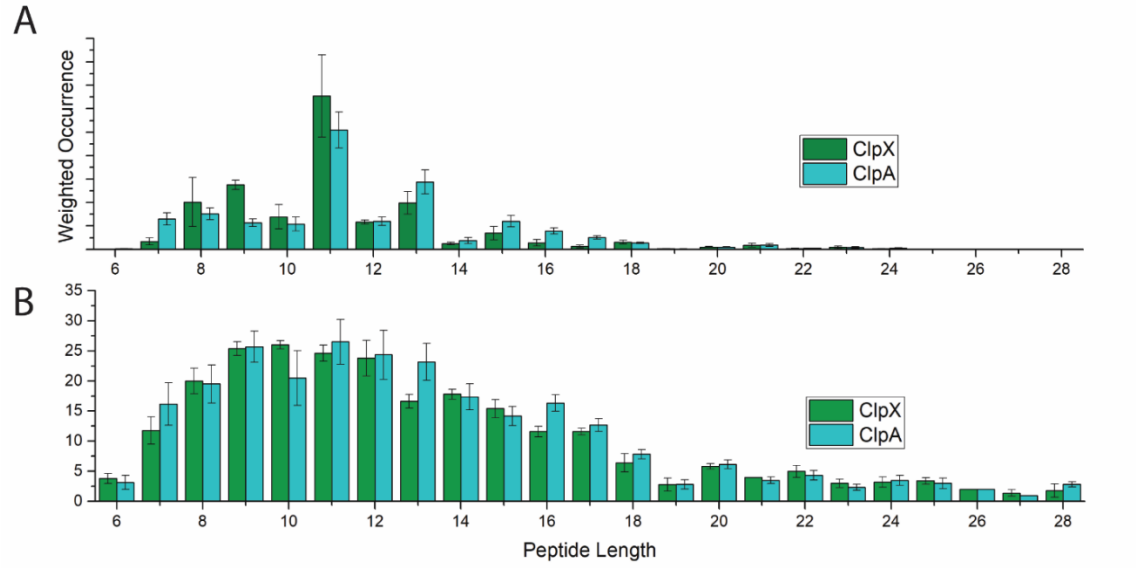

Figure A.8: Peptide length distribution for ClpA degradation compared to ClpX, (A) weighted for mass spectral intensity and (B) unweighted.

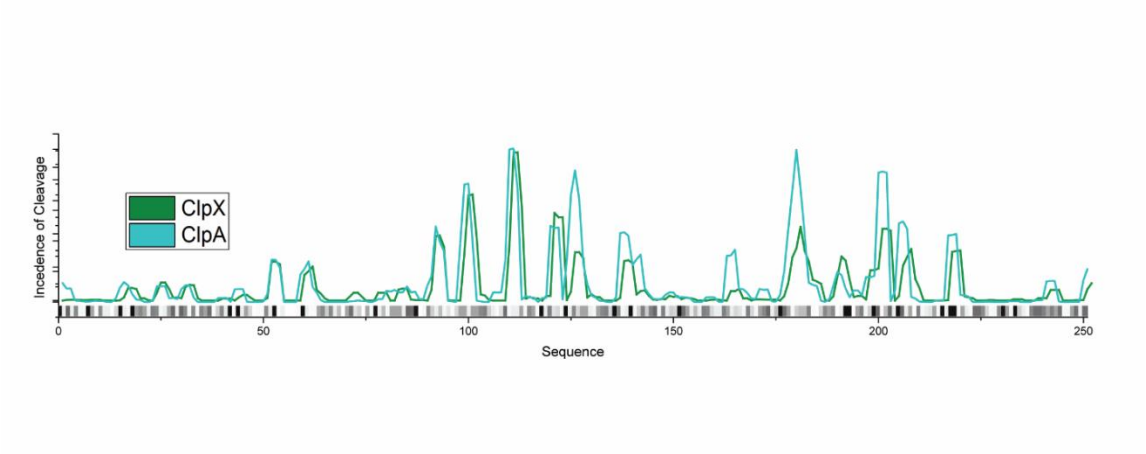

Figure A.9: Cleavage incidence locations on the GFP weighted for mass spectral intensity for ClpX and ClpA. Data were subject to a moving average smoothing over 3 data points. The black and gray bars on each graph represent primary sequence cleavage specificity, where darker colors indicate higher likelihood of cleavage.

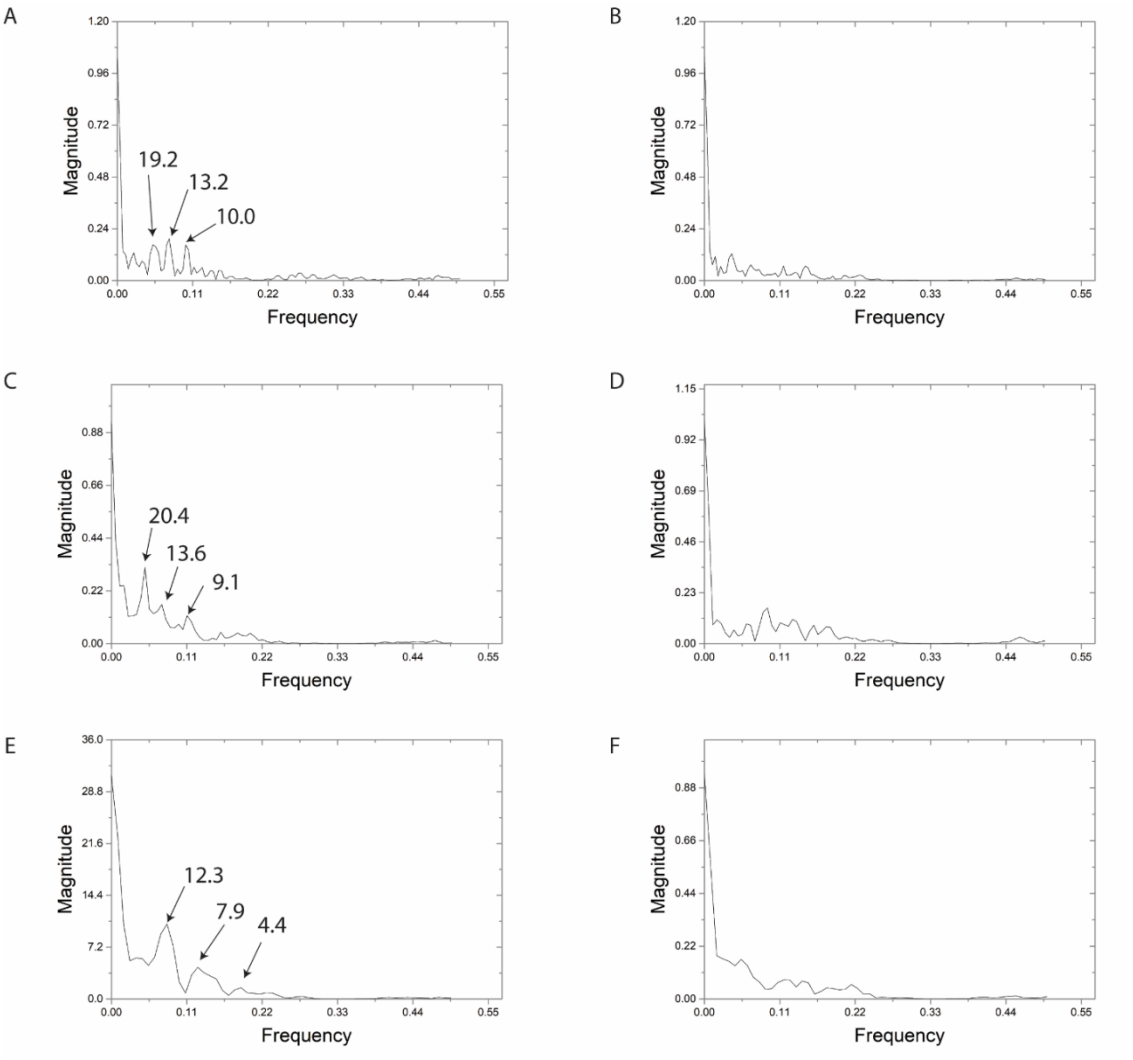

Figure A.10: Fast Fourier transform (FFT) of cleavage incidence of (A) GFP observed cleavage locations, (B) GFP amino acid sequence preference, (C) RcdA observed cleavage locations, (D) RcdA amino acid sequence preference and (E) reduced β2m overserved cleavage locations, and (F) β2m amino acid sequence preference. FFT analysis was done using the Origin FFT function with default setting with the exception of the blackman window which was used to exclude the C-terminus. FFT analysis confirms periodicity in cleave location of each substrate that does not exist if simply the primary sequence is considered. Peptide length values were calculated using the reciprocal of the frequency.

A.3. Discussion

Rather than a simple two-step process of recognition and degradation, our data indicate additional steps occur after the initial translocation during the degradation process of *C. cresentus* ClpXP that are influenced by the tertiary structure of the substrate (**Figure A.6D**). We propose that initiation of degradation is followed by several cycles of translocation and a defined pause such that unfolded substrates dwell in the peptidase chamber and those preferred sites most accessible to the ClpP active sites can be cleaved, while others remain out of reach (**Figure A.11**). Indeed, prior work shows that while ClpP is highly specific for certain residues when degrading small peptides, larger polypeptides show less discrimination in their products.[5] Given the high measured sequence coverage we obtain in our study, we predict that this difference in stringent selectivity stems from the position dependent cleavages we describe here.

We consider a possible model which explains our results based on recent structural and single molecule experiments. Recent cryo-electron microscopy studies of ClpXP bound to substrate show that subunits of ClpX form a shallow right-handed spiral, resulting in a grip that easily spans 10-13 residues (**Figure A.11**).[7,12] In the continuous spiral portion of these static structures, the pore loops of each subunit grip the substrate two residues away from the comparable position of the neighboring subunit. Given the hexameric nature of ClpX, our 12-residue average spacing between cleavage sites is consistent with a pause that occurs after all subunits in the ring has hydrolyzed ATP (6 ATP x 2 residues). During this pause, the unfolded polypeptide dangles into the ClpP chamber for a sufficient time to rapidly degrade at cleavage sites most favored by the intrinsic specificity of ClpP but is constrained by the hold of ClpX on the upstream sequence. After the ring is reset, hydrolysis begins again to start another cycle**.** This

model is also consistent with several recent optical trapping based single molecule experiments that demonstrate bursts of translocation that generally report 1-2 nm (or 6-12 aa) runs of translocation, followed by a brief pause.[13-15] Therefore, both static structural and dynamic solution experiments are consistent with our proposal that cycling of translocation and pausing results in dangling of substrates to yield defined substrate cleavage positions and spacing.

Interestingly, structures of ClpA, another hexameric unfoldase, have revealed similar processive translocation steps[16] and we observe similar peptide distributions with that enzyme (**Figure A.8** and **Figure A.9**). Indeed, prior biochemical studies with ClpAP using low resolution HPLC data forecasted a translocation/proteolysis pausing mechanism[90] similar to what we describe here with ClpXP. This is also in line with ClpAP 'step sizes' of 1-2 nm seen with single molecule studies using optical traps[17] or 5-14 residues seen with single-turnover population measurements.[18,19] Collectively, our data suggest that AAA+ proteases capture a series of ATP hydrolysis events collectively across all subunits to facilitate a run of translocation, followed by a pause for degradation. This pause would allow for more complete degradation of substrates to prevent the release of improperly sized products.

Regardless of the specific source of the pausing, our primary result is that we observe enrichment of specific periodically spaced peptides, which supports our hypothesis that ClpXP degradation has a defined start and fixed spacing in cleavage afterwards. Our main point (as illustrated in **Figure A.6**) is that not all highly preferred cleavage sites are used (e.g., region 60-80 in RcdA), but rather there is a defined spacing consistent with processive translocation of substrates into the cleavage chamber. Moreover, residues that

are not the most preferred seem to still result in cleavage (e.g., region 90-110 in GFP). The specific pattern of peptides therefore seems to be a combination of inherent primary chemical preference and a restriction on spacing that we propose is driven by translocation. This observation implies that peptides arising from ClpXP processing are not randomly distributed across a given protein and reasons that that specific peptides can be deliberately generated. This leads to a tempting hypothesis that peptides generated during a particular response, such as toxic stress, could be used as signaling molecules for the cell to respond to this damage.

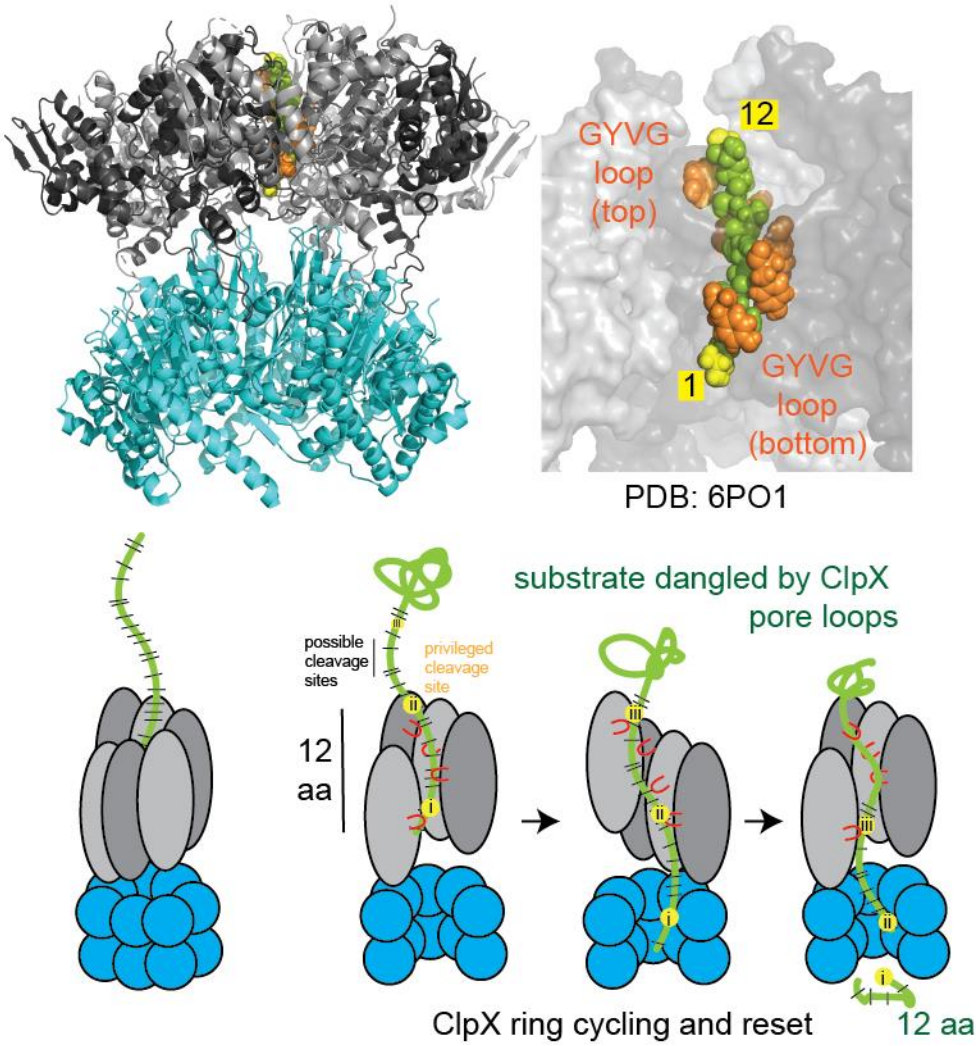

Figure A.11: Depiction of ClpXP degradation mechanism. Upper: the ClpXP structure (PDB 6PO1) can accommodate a 12-residue span of peptide in its grip. Lower: After initial engagement of the substrate, ClpX enters the processive state of degradation where two residues are translocated for every ATP hydrolyzed. After a complete cycle, ClpX pauses to reset. During this time, the dangled substrate is cleaved by the ClpP peptidase, at the sites most accessible to the catalytic active sites.

A.4. Materials and Methods:

A.4.1. Protein expression/purification

ClpX, ClpP-his, eGFPSsrA, and SspB were purified as before.[20,21] ClpX and ClpP are from the *C. Crescentus* species. HisSUMO tagged RcdA and β2m were appended with a

C-terminal ssrA tag (AANDNFAEEFAVAA) using appropriate oligonucleotides, expressed and purified as other similar constructs.[20] For β2mssrA, purified protein was also reduced with 2 mM tris(2-carboxyethyl)phosphine (TCEP) and the free cystines were then alkylated with 4 mM iodoacetamide (IAM) unless otherwise specified.

A.4.2. Fluorescence eGFPSsrA experiments

Adaptor, ATP and DFP (di-isopropyl fluorophosphate) concentration-based changes in ClpXP activity were experimentally determined by monitoring the fluorescence loss of model substrate eGFPSsrA over time in 20 µL reactions using a Spectramax fluorescence plate reader. All reactions used 1 µM $ClpX_6$, 2 µM $ClpP_{14}$ and 10 µM of substrate in 20 mM MOPS pH 7.5, 100 mM KCl, 10 mM $MgCl_2$, 10 % glycerol and an ATP regeneration mixture (4 mM ATP, 16 mM creatine phosphate, 0.75 µg/ml creatine kinase) unless otherwise described. ATP limiting conditions: ATP provided in the regeneration mixture was titrated as shown in Figure 2A. Adaptor based reactions: Initially a titration of adaptor SspB was performed to determine maximal adaptor activity, adaptor:unfoldase molar ratio. No significant inhibition was observed at the highest concentrations used here. This molar ratio was preserved for all other adaptor-substrate experiments. DFP analysis: 0-100 fold molar excess of DFP was preincubated with ClpP alone in H-buffer for 1 h at 30 °C prior to substrate digestion.

A.4.3. Degradation Preparation and Peptide Recovery

Degradation of substrates for peptide recovery took place in a 50 µL reaction volume with 20 mM MOPS buffer, 100 mM KCl, 10 mM $MgCl_2$, and 5 mM ATP. Concentrations of substrate, ClpX, and ClpP were 10 µM, 1 µM, and 2 µM, respectively. These ratios were used to guarantee a proper ClpX to ClpP ratio, as well as to ensure an excess of substrate

to facilitate degradation and thus peptide production. ATP was the last constituent added, and once added, the reaction was incubated at 30 °C for 1 h. SDS-PAGE separation and Coomassie staining was used to validate substrate depletion. After 1 h, the remaining proteins were separated from peptides by a Centri-Spin-10 size exclusion column. Columns were preequilibrated in water. Two spin downs were performed, the first to remove substances over 5 kDa, such as intact substrate or ClpXP, while retaining peptide fragments. The remaining peptides were eluted from the spin column with 50 µL of 50/50 ACN/H_2O. The 5 kDa cut off mass was determined to be acceptable as peptides above 30 mers were rarely detected. The peptide mixture was dried down with a speedVac for 1 h at 45 °C to remove the organic solvent and subsequently resuspend in HPLC grade H_2O. Peptides produced from di-sulfide intact β2m were reduced with 2 mM TCEP and the free cystines were then alkylated with 4 mM IAM.

A.4.4. Liquid Chromatography and Mass Spectrometry

LC/MS/MS analyses were carried out with a Thermo Scientific EASY-nLC 1200 System (Thermo Fisher Scientific) coupled to a Thermo Fisher Orbitrap Fusion mass spectrometer. A 20 mm by 75 µm Thermo Acclaim Pepmap trap column was used preceding a 150 mm by 75 µm Thermo Acclaim Pepmap RSCL analytical column packed with 2 µm particles. Solvent A and B were HPLC grade water with 0.1% formic acid and HPLC grade ACN with 0.1% formic acid, respectively. Separation was achieved with gradients 0 to 60% B in 60 minutes at 300 nL/min, with a 30-minute hold at 95% B as a post separation wash. A 30-minute blank was run between each injection to ensure no peptide carry over. 2 µL of sample were injected for all methods. The electrospray voltage was set to 1900-2100 V with the ion transfer tube temperature at 300 °C. Full mass range

scans were performed with a m/z range of 200 to 5000 with a resolution of 60,000. Collision-induced dissociation was performed on ions with an intensity of 5000 counts or higher with a collision energy of 35 eV and a 10 ms activation time.

A.4.5. Data Analysis

Peptide detection data processing was performed with Proteome Discoverer. Because nonspecific cleavage events were included in the search, a larger false positive discovery rate is expected. Consequently, only peptides detected with high confidence under strict validation criteria were considered for subsequent analysis. Peptides were analyzed for cleavage location, structural cleavage preference, and length. All structural results are normalized to the occurrence of that structure in the protein.

A.5. References

(1) Mahmoud, S. A.; Chien, P. Regulated Proteolysis in Bacteria. Annu. Rev. Biochem. 2018, 87, 677–696. https://doi.org/https://doi.org/10.1146/annurev-biochem-062917-012848.

(2) Sauer, R. T.; Baker, T. A. AAA + Proteases : ATP-Fueled Machines of Protein Destruction. Annu. Rev. Biochem. 2011, 80, 587–612. https://doi.org/10.1146/annurev-biochem-060408-172623.

(3) Lee, C.; Schwartz, M. P.; Prakash, S.; Iwakura, M.; Matouschek, A. ATP-Dependent Proteases Degrade Their Substrates by Processively Unraveling Them from the Degradation Signal. Mol. Cell 2001, 7 (3), 627–637. https://doi.org/10.1016/S1097-2765(01)00209-X.

(4) Choi, K.; Licht, S. Control of Peptide Product Sizes by the Energy-Dependent Protease ClpAP †. Biochemistry 2005, 44 (42), 13921–13931. https://doi.org/10.1021/bi0505060.

(5) Gersch, M.; Stahl, M.; Poreba, M.; Dahmen, M.; Dziedzic, A.; Drag, M.; Sieber, S. A. Barrel-Shaped ClpP Proteases Display Attenuated Cleavage Specificities. ACS Chem. Biol. 2016, 11 (2), 389–399. https://doi.org/10.1021/acschembio.5b00757.

(6) Sprangers, R.; Gribun, A.; Hwang, P. M.; Houry, W. A.; Kay, L. E. Quantitative NMR Spectroscopy of Supramolecular Complexes: Dynamic Side Pores in ClpP Are

Important for Product Release. Proc. Natl. Acad. Sci. U. S. A. 2005, 102 (46), 16678–16683. https://doi.org/10.1073/pnas.0507370102.

(7) Ripstein, Z. A.; Vahidi, S.; Houry, W. A.; Rubinstein, J. L.; Kay, L. E. A Processive Rotary Mechanism Couples Substrate Unfolding and Proteolysis in the ClpXP Degradation Machinery. Elife 2020, 9, 1–25. https://doi.org/10.7554/eLife.52158.

(8) Haynes, C. M.; Yang, Y.; Blais, S. P.; Neubert, T. A.; Ron, D. The Matrix Peptide Exporter HAF-1 Signals a Mitochondrial Unfolded Protein Response by Activating the Transcription Factor ZC376.7 in C. Elegans. Mol. Cell 2011, 37 (4), 529–540. https://doi.org/10.1016/j.molcel.2010.01.015.

(9) Jennings, L. D.; Lun, D. S.; Médard, M.; Licht, S. ClpP Hydrolyzes a Protein Substrate Processively in the Absence of the ClpA ATPase: Mechanistic Studies of ATP-Independent Proteolysis. Biochemistry 2008, 47 (44), 11536–11546. https://doi.org/10.1021/bi801101p.

(10) Thompson, M. W.; Singh, S. K.; Maurizi, M. R. Processive Degradation of Proteins by the ATP-Dependent Clp Protease from Escherichia Coli. Requirement for the Multiple Array of Active Sites in ClpP but Not ATP Hydrolysis. J. Biol. Chem. 1994, 269 (27), 18209–18215.

(11) Bolon, D. N.; Grant, R. A.; Baker, T. A.; Sauer, R. T. Nucleotide-Dependent Substrate Handoff from the SspB Adaptor to the AAA ClpXP Protease. Mol. Cell 2004, 16, 343–350.

(12) Fei, X.; Bell, T. A.; Jenni, S.; Stinson, B. M.; Baker, T. A.; Harrison, S. C.; Sauer, R. T. Structures of the ATP-Fueled ClpXP Proteolytic Machine Bound to Protein Substrate. Elife 2020, 9, 1–22. https://doi.org/10.7554/eLife.52774.

(13) Maillard, R. A.; Chistol, G.; Sen, M.; Righini, M.; Tan, J.; Kaiser, C. M.; Hodges, C.; Martin, A.; Bustamante, C. ClpX(P) Generates Mechanical Force to Unfold and Translocate Its Protein Substrates. Cell 2011, 145 (3), 459–469. https://doi.org/10.1016/j.cell.2011.04.010.

(14) Aubin-Tam, M.-E.; Olivares, A. O.; Sauer, R. T.; Baker, T. A.; Lang, M. J. Single-Molecule Protein Unfolding and Translocation by an ATP- Fueled Proteolytic Machine. Cell 2011, 145 (2), 257–267. https://doi.org/10.1038/jid.2014.371.

(15) Rodriguez-Aliaga, P.; Ramirez, L.; Kim, F.; Bustamante, C.; Martin, A. Substrate-Translocating Loops Regulate the Mechanochemical Coupling and Power Production in a AAA+ Protease. Nat Struct Mol Biol 2016, 23 (11), 974–981. https://doi.org/10.1038/nsmb.3298.

(16) Lopez, K. E.; Rizo, A. N.; Tse, E.; Lin, J. B.; Scull, N. W.; Thwin, A. C.; Lucius, A. L.; Shorter, J.; Southworth, D. R. Conformational Plasticity of the ClpAP AAA+ Protease Couples Protein Unfolding and Proteolysis. Nat. Struct. Mol. Biol. 2020, 27 (5), 406–416. https://doi.org/10.1038/s41594-020-0409-5.

(17) Olivares, A. O.; Nager, A. R.; Iosefson, O.; Sauer, R. T.; Baker, T. A. Mechanochemical Basis of Protein Degradation by a Double-Ring AAA+ Machine Adrian. Nat Struct Mol Biol 2014, 21 (10), 871–875. https://doi.org/10.1038/nsmb.2885.

(18) Miller, J. M.; Lin, J.; Li, T.; Lucius, A. L. E. Coli ClpA Catalyzed Polypeptide Translocation Is Allosterically Controlled by the Protease ClpP Justin. J. Mol. Biol. 2013, 425 (15), 2795–2812. https://doi.org/10.1038/jid.2014.371.

(19) Rajendar, B.; Lucius, A. L. Molecular Mechanism of Polypeptide Translocation Catalyzed by the Escherichia Coli ClpA Protein Translocase. J. Mol. Biol. 2010, 399 (5), 665–679. https://doi.org/10.1016/j.jmb.2010.03.061.

(20) Bhat, N. H.; Vass, R. H.; Stoddard, P. R.; Shin, D. K.; Chien, P. Identification of ClpP Substrates in Caulobacter Crescentus Reveals a Role for Regulated Proteolysis in Bacterial Development. Mol. Microbiol. 2013, 88 (6), 1083–1092. https://doi.org/10.1111/mmi.12241.

(21) Chien, P.; Perchuk, B. S.; Laub, M. T.; Sauer, R. T.; Baker, T. A. Direct and Adaptor-Mediated Substrate Recognition by an Essential AAA+ Protease. Proc. Natl. Acad. Sci. U. S. A. 2007, 104 (16), 6590–6595. https://doi.org/10.1073/pnas.0701776104.

APPENDIX B

B. DEPC MODIFICATION PERCENTAGES FOR INDIVIDUAL RESIDUES

Table B.1: DEPC-CL modification percentages for each labelable residue of rituximab under native conditions and under heat stress conditions (45 °C for 4 h). A difference was considered significant if the p-value, calculated by performing an unpaired T-test, was less than 0.05 (corresponding to a 95% confidence level, n = 4). Errors shown in the table are standard deviations.

Residue	Native	Stressed 45 °C 4 h	Significant?
Light Chain			
S 5	0.03% ± 0.02%	0.03% ± 0.01%	No
S 7			
S 12	0.07% ± 0.02%	0.05% ± 0.03%	No
S 14	1.5% ± 0.7%	0.6% ± 0.3%	No
K 18	0.2% ± 0.1%	0.09% ± 0.09%	No
T 20			
T 22			
S 26			
S 27	0.2% ± 0.1%	0.2% ± 0.3%	No
S 28	0.04% ± 0.04%	0.1% ± 0.1%	No
S 30			
Y 31	0.2% ± 0.1%	0.3% ± 0.3%	No
H 33	0.5% ± 0.4%	0.1% ± 0.1%	No
K 38	0.10% ± 0.06%	0.15% ± 0.08%	No
S 41	0.01% ± 0.02%	0.01% ± 0.01%	No
S 42	0.03% ± 0.02%	0.01% ± 0.01%	No
K 44	0.13% ± 0.06%	0.13% ± 0.05%	No
Y 48	0.05% ± 0.03%	0.07% ± 0.04%	No
T 50	0.11% ± 0.05%	0.09% ± 0.07%	No
S 51	0.05% ± 0.03%	0.03% ± 0.02%	No
S 55	0.02% ± 0.02%	0.01% ± 0%	No
S 62	3% ± 3%	2% ± 1%	No
S 64	2 % ± 2%	1.2% ± 1%	No
S 66	1% ± 1%	0.8% ± 0.3%	No
T 68	1% ± 1%	0.8% ± 0.3%	No
S 69	0.02% ± 0.02%	0.02% ± 0.01%	No
Y 70	0.02% ± 0.02%	0.02% ± 0.01%	No
S 71	50% ± 7%	30% ± 20%	No
T 73	8% ± 5%	5% ± 4%	No
S 75	8% ± 5%	6% ± 5%	No
T 84	0.08% ± 0.04%	0.07% ± 0.04%	No
Y 85			

Y 86			
T 91			
S 92	1.7% ± 0.8%	4% ± 4%	No
T 96	1.9% ± 0.8%	4% ± 4%	No
T 101			
K 102	0% ± 0%	0% ± 0%	No
K 106			
T 108			
S 113	0.02% ± 0.01%	0.1% ± 0.1%	No
S 120			
K 125			
S 126	0.1% ± 0.1%	0.02% ± 0.01%	No
T 128			
S 130			
Y 139			
K 144			
K 148	1% ± 2%	1.3% ± 0.8%	No
S 155	5% ± 2%	9% ± 4%	Yes
S 158	4% ± 2%	9% ± 4%	Yes
S 161	4% ± 2%	9% ± 4%	Yes
T 163	0.6% ± 0.6%	0.9% ± 0.5%	No
S 167	0.6% ± 0.6%	1.0% ± 0.6%	No
K 168			
S 170			
T 171			
Y 172			
S 173			
S 175			
S 176			
T 177			
T 179	0.5% ± 1%	0.06% ± 0.06%	No
S 181	1.0% ± 0.5%	0.31% ± 0.06%	Yes
K 182	16% ± 3%	8% ± 5%	No
Y 185			
K 187	90% ± 4%	92% ± 4%	No
H 188	78% ± 9%	90% ± 10%	No
K 189	77% ± 9%	86% ± 9%	No
Y 191	3% ± 1%	6% ± 5%	No
T 196	3% ± 2%	5% ± 1%	No
H 197	4% ± 2%	5% ± 0.9%	No
S 201			
S 202			
T 205			
K 206	0.9% ± 0.4%	1.3% ± 0.6%	No
S 207			

Heavy Chain			
K 13	3% ± 2%	3% ± 1%	No
S 17	2% ± 2%	3% ± 1%	No
K 19	0.20% ± 0.06%	0.22% ± 0.07%	No
S 21			
K 23	0.8% ± 0.7%	3% ± 3%	No
S 25			
Y 27	43% ± 1%	44% ± 4%	No
T 28	41% ± 2%	44% ± 3%	No
T 30	21% ± 8%	17% ± 8%	No
S 31	0.3% ± 0.4%	0.5% ± 0.3%	No
Y 32	0.3% ± 0.4%	0.5% ± 0.3%	No
H 35	90% ± 5%	84% ± 7%	No
K 38	56% ± 20%	57% ± 10%	No
T 40			
Y 52	0.3% ± 0.1%	0.3% ± 0.2%	No
T 58			
S 59			
Y 60			
K 63	1.6% ± 0.6%	1.1% ± 0.6%	No
K 65			
K 67	80% ± 10%	82% ± 20%	No
T 69	4% ± 2%	25% ± 20%	No
T 71	26% ± 5%	39% ± 20%	No
K 74	32% ± 5%	36% ± 20%	No
S 75			
S 76	26% ± 7%	7% ± 4%	Yes
S 77	14% ± 4%	2% ± 2%	Yes
T 78	0.5% ± 0.5%	0.5% ± 0.4%	No
Y 80	1.1% ± 1%	1.4% ± 0.6%	No
S 84	2.5% ± 0.4%	3% ± 6%	No
S 85			
T 87			
S 88	3.6% ± 0.8%	4% ± 2%	No
S 91			
Y 94	0.13% ± 0.08%	0.2% ± 0.1%	No
Y 95	3% ± 2%	3% ± 2%	No
S 99			
T 100			
Y 101			
Y 102			
Y 107			
T 115	0.1% ± 0.2%	0.6% ± 0.9%	No
T 116	0.1% ± 0.2%	0.6% ± 0.9%	No
T 118			

S 120	8% ± 4%	2.7% ± 0.9%	N
S 123	10% ± 2%	6% ± 5%	No
T 124	14% ± 4%	8% ± 6%	No
K 125	42% ± 10%	25% ± 20%	No
S 128	0.01% ± 0.01%	0.05% ± 0.03%	No
S 135	0.05% ± 0.02%	0.3% ± 0.2%	No
S 136	0.04% ± 0.02%	0.03% ± 0.02%	No
K 137	0.05% ± 0.02%	0.2% ± 0.1%	Yes
S 138	1.4% ± 0.9%	1.3% ± 0.7%	No
T 139	0.03% ± 0.02%	0.02% ± 0.02%	No
S 140	0.3% ± 0.2%	0.06% ± 0.03%	Yes
T 143	0.3% ± 0.2%	0.07% ± 0.04%	Yes
K 151			
Y 153	0.01% ± 0%	0.01% ± 0.01%	No
T 159	5% ± 3%	3% ± 1%	No
S 161	1.8% ± 0.5%	0.7% ± 0.8%	No
S 164	14% ± 4%	8% ± 5%	No
T 168	8% ± 4%	5% ± 3%	No
S 169	0.4% ± 0.6%	0.5% ± 0.3%	No
H 172	35% ± 4%	35% ± 8%	No
T 173			
S 180	8% ± 2%	10% ± 10%	No
S 181	7% ± 2%	9% ± 10%	No
Y 184			
S 185			
S 187	0.9% ± 0.9%	1% ± 1%	No
S 188	1% ± 1%	1% ± 1%	No
T 191	1.5% ± 0.8%	0.4% ± 0.5%	No
S 194	0.04% ± 0.02%	0.2% ± 0.1%	Yes
S 195	1.4% ± 0.7%	0.8% ± 0.5%	No
S 196	2% ± 1%	0.9% ± 0.5%	No
T 199			
T 201	0.6% ± 0.4%	2% ± 4%	No
Y 202	0.6% ± 0.4%	2% ± 4%	No
H 208	1.5% ± 0.2%	1.0% ± 0.7%	No
K 209	8% ± 3%	6% ± 3%	No
S 211	0% ± 0%	0% ± 0%	No
T 213			
K 214	0.3% ± 0.3%	0.2% ± 0.2%	No
K 217			
K 218			
K 222	100% ± 0%	100% ± 0%	No
S 223	0.8% ± 0.6%	1.3% ± 0.8%	No
K 226	39% ± 10%	73% ± 20%	Yes
T 227	0.07% ± 0.07%	0.1% ± 0.1%	No

H 228	16% ± 8%	14% ± 3%	No
T 229	16% ± 8%	14% ± 3%	No
S 243	0.06% ± 0.05%	0.04% ± 0.03%	No
K 250			
K 252	100% ± 0%	100% ± 0%	No
T 254			
S 258			
T 260			
T 264	0.04% ± 0.03%	0.03% ± 0.02%	No
S 271	5% ± 3%	4% ± 2%	No
H 272	5% ± 2%	4% ± 2%	No
K 278	0.13% ± 0.07%	0.16% ± 0.07%	No
Y 282	0.08% ± 0.07%	0.06% ± 0.02%	No
H 289	0.06% ± 0.05%	0.04% ± 0.01%	No
K 292	0.01% ± 0.01%	0.01% ± 0.01%	No
T 293	7% ± 3%	23% ± 10%	Yes
K 294	7% ± 3%	23% ± 10%	Yes
Y 300			
S 302	83% ± 4%	75% ± 20%	No
T 303	83% ± 4%	75% ± 20%	No
Y 304			
S 308			
T 311	1.6% ± 0.5%	1.2% ± 0.7%	No
H 314	0.3% ± 0.1%	0.3% ± 0.2%	No
K 321	5% ± 2%	3% ± 2%	No
Y 323			
K 324	94% ± 5%	92% ± 3%	No
K 326			
S 328			
K 330	100% ± 0%	100% ± 0%	No
K 338	0.5% ± 0.1%	0.5% ± 0.3%	No
T 339			
S 341	27% ± 3%	22% ± 8%	No
K 342			
K 344			
Y 353	27% ± 20%	39% ± 20%	No
T 354	0.01% ± 0%	0.01% ± 0.01%	No
S 358	0.11% ± 0.05%	0.17% ± 0.08%	No
T 363	0.12% ± 0.06%	0.19% ± 0.08%	No
K 364	0.11% ± 0.05%	0.17% ± 0.09%	No
S 368	0.03% ± 0.03%	0.04% ± 0.03%	No
T 370	8% ± 1%	14% ± 4%	Yes
K 374	8% ± 1%	14% ± 4%	Yes
Y 377	0.6% ± 0.3%	0.7% ± 0.2%	No
S 379			

S 387			
Y 395			
K 396	0.2% ± 0.1%	0.05% ± 0.02%	Yes
T 397			
T 398	10% ± 4%	6% ± 3%	No
S 404	9% ± 4%	6% ± 3%	No
S 407	1.6% ± 0.4%	1% ± 1%	No
Y 411			
S 412			
K 413			
T 415			
K 418			
S 419			
S 428	0.13% ± 0.06%	0.14% ± 0.1%	
S 430	6% ± 0.8%	5.2% ± 1%	
H 433	13% ± 3%	15% ± 2%	
H 437	14% ± 2%	11% ± 2%	
H 439	1.4% ± 0.6%	1.4% ± 0.3%	
Y 440	0% ± 0%	0.05% ± 0.04%	
T 441			
K 443	1.1% ± 0.6%	1.3% ± 0.7%	
S 444			
S 446			
S 448	17% ± 2%	26% ± 4%	
K 451			

Table B.2: DEPC-CL modification percentages for each labelable residue of rituximab under native conditions and under heat stress conditions (55 °C for 4 h). A difference was considered significant if the p-value, calculated by performing an unpaired T-test, was less than 0.05 (corresponding to a 95% confidence level, n = 3). Errors shown in the table are standard deviations.

Residue	Native	Stressed 55 °C 4 h	Significant?
Light Chain			
S 5	0.03% ± 0.01%	0.04% ± 0.00%	No
S 7			
S 12	0.03% ± 0.01%	0.02% ± 0.01%	No
S 14			
K 18	0.56% ± 0.06%	0.7% ± 0.2%	No
T 20	17% ± 4%	8% ± 2%	Yes

T 22			
S 26			
S 27			
S 28			
S 30			
Y 31			
H 33	0.08% ± 0.02%	0.21% ± 0.02%	Yes
K 38	0.15% ± 0.05%	0.24% ± 0.02%	No
S 41	0.04% ± 0.01%	0.02% ± 0.02%	No
S 42			
K 44	0.06% ± 0.02%	0.15% ± 0.01%	Yes
Y 48	0.09% ± 0.04%	0.13% ± 0.01%	No
T 50	0.03% ± 0.03%	0.05% ± 0.01%	No
S 51			
S 55			
S 62			
S 64			
S 66	18% ± 4%	15% ± 2%	No
T 68	18% ± 4%	15% ± 2%	No
S 69			
Y 70	14% ± 5%	11% ± 4%	No
S 71			
T 73	53% ± 10%	86% ± 3%	Yes
S 75	53% ± 10%	86% ± 3%	Yes
T 84	1.3% ± 0.2%	2.6% ± 0.5%	Yes
Y 85	1.3% ± 0.2%	2.6% ± 0.5%	Yes
Y 86			
T 91	0.03% ± 0.02%	0.10% ± 0.01%	Yes
S 92	1.8% ± 0.6%	2.1% ± 0.6%	No
T 96	2% ± 0.6%	2.2% ± 0.6%	No
T 101	0.18% ± 0.01%	0.14% ± 0.02%	No
K 102	0.08% ± 0.02%	0.10% ± 0.01%	No
K 106			
T 108	1.3% ± 0.4%	1.1% ± 0.3%	No
S 113	1% ± 0.3%	0.8% ± 0.1%	No
S 120			
K 125			
S 126			
T 128	5.4% ± 1%	3.1% ± 0.3%	Yes
S 130	5.4% ± 1%	3.1% ± 0.3%	Yes
Y 139			
K 144			
K 148	7.2% ± 1.7%	9.7% ± 0.8%	No
S 155			
S 158			

S 161			
T 163	0% ± 0%	0.01% ± 0.01%	No
S 167			
K 168	0.5% ± 0.2%	0.5% ± 0.2%	No
S 170			
T 171			
Y 172			
S 173			
S 175			
S 176			
T 177			
T 179			
S 181			
K 182	5% ± 2%	19% ± 10%	No
Y 185	23.5% ± 0.3%	27% ± 2%	Yes
K 187	85% ± 3%	86% ± 4%	No
H 188	55% ± 2%	64% ± 3%	Yes
K 189	60% ± 3%	66% ± 3%	No
Y 191	0.74% ± 0.09%	1.0% ± 0.3%	No
T 196			
H 197	0.11% ± 0.03%	0.16% ± 0.03%	No
S 201			
S 202			
T 205			
K 206	0.4% ± 0.1%	0.4% ± 0.1%	No
S 207	4% ± 2%	3% ± 2%	No
Heavy Chain			
K 13	2.7% ± 0.5%	3.7% ± 0.3%	Yes
S 17			
K 19	3.5% ± 0.7%	4.5% ± 0.4%	No
S 21	24% ± 4%	11% ± 4%	Yes
K 23	86% ± 5%	92% ± 4%	No
S 25			
Y 27			
T 28			
T 30			
S 31			
Y 32	0.05% ± 0.03%	0.4% ± 0.3%	No
H 35	23% ± 3%	4% ± 1%	Yes
K 38	30% ± 2%	22% ± 3%	Yes
T 40			
Y 52	1.1% ± 0.2%	1.3% ± 0.2%	No
T 58	0.12% ± 0.01%	0.15% ± 0.02%	No
S 59	0.09% ± 0.01%	0.09% ± 0.03%	No
Y 60	0.09% ± 0.01%	0.09% ± 0.03%	No

K 63			
K 65			
K 67	23% ± 7%	33% ± 2%	No
T 69			
T 71			
K 74	79% ± 4%	87% ± 1%	Yes
S 75			
S 76	2.4% ± 0.2%	1.5% ± 0.2%	Yes
S 77	0.01% ± 0.01%	0.01% ± 0.01%	No
T 78	0.3% ± 0.1%	0.3% ± 0.2%	No
Y 80			
S 84	1.8% ± 0.7%	1.4% ± 0.6%	No
S 85	0.32% ± 0.06%	0.3% ± 0.1%	No
T 87			
S 88	0.02% ± 0.01%	0.01% ± 0.01%	No
S 91	0.25% ± 0.04%	0.23% ± 0.09%	No
Y 94	0.25% ± 0.04%	0.23% ± 0.09%	No
Y 95			
S 99			
T 100			
Y 101			
Y 102			
Y 107			
T 115	14% ± 4%	12% ± 1%	No
T 116			
T 118	71% ± 3%	59% ± 7%	Yes
S 120	84% ± 2%	70% ± 7%	Yes
S 123	1.2% ± 0.3%	1.6% ± 0.2%	No
T 124			
K 125			
S 128	0.9% ± 0.4%	1% ± 1%	No
S 135	1.1% ± 0.5%	1% ± 1%	No
S 136			
K 137			
S 138			
T 139	0.13% ± 0.07%	0.12% ± 0.04%	No
S 140	0.03% ± 0.02%	0.02% ± 0.01%	No
T 143	0.01% ± 0.01%	0.01% ± 0.01%	No
K 151			
Y 153	0.02% ± 0.02%	0.07% ± 0.05%	No
T 159			
S 161	1.8% ± 0.2%	2.2% ± 0.4%	No
S 164	0.002% ± 0.001%	0.016% ± 0.005%	Yes
T 168	1.3% ± 0.4%	2% ± 1%	No
S 169	0.2% ± 0.1%	0.35% ± 0.1%	No

H 172	0.2% ± 0.1%	0.35% ± 0.1%	No
T 173	1.1% ± 0.2%	2.2% ± 0.7%	No
S 180			
S 181			
Y 184			
S 185			
S 187	10% ± 3%	11% ± 2%	No
S 188	10% ± 3%	10% ± 2%	No
T 191	5% ± 1%	4.3% ± 0.7%	No
S 194			
S 195			
S 196	0.01% ± 0%	0.05% ± 0.03%	No
T 199	0.01% ± 0%	0.05% ± 0.03%	No
T 201			
Y 202			
H 208	0.00% ± 0.00%	0.00% ± 0.00%	No
K 209	6% ± 2%	8.0% ± 0.9%	No
S 211	0.00% ± 0.00%	0.00% ± 0.00%	No
T 213			
K 214	0.5% ± 0.38%	0.4% ± 0.1%	No
K 217			
K 218			
K 222	99% ± 1%	100% ± 0%	No
S 223	0.06% ± 0.04%	0.04% ± 0%	No
K 226	33% ± 7%	72% ± 5%	Yes
T 227	1.4% ± 0.8%	2% ± 1%	No
H 228	36% ± 7%	40% ± 20%	No
T 229	36% ± 7%	40% ± 10%	No
S 243			
K 250			
K 252	100% ± 0	100% ± 0	No
T 254			
S 258	5% ± 2%	3.1% ± 0.8%	No
T 260	0.7% ± 0.6%	0.8% ± 0.3%	No
T 264	11% ± 2%	16% ± 10%	No
S 271	10% ± 1%	15% ± 10%	No
H 272	0.26% ± 0.08%	0.24% ± 0.06%	No
K 278	0.16% ± 0.1%	0.28% ± 0.07%	No
Y 282	0.39% ± 0.02%	0.33% ± 0.04%	No
H 289	0.5% ± 0.1%	0.41% ± 0.03%	No
K 292			
T 293	38% ± 6%	85% ± 8%	Yes
K 294			
Y 300	50% ± 1%	56% ± 7%	No
S 302	38% ± 3%	16% ± 6%	Yes

T 303			
Y 304			
S 308			
T 311			
H 314	0.24% ± 0.08%	0.23% ± 0.06%	No
K 321	0.29% ± 0.04%	0.28% ± 0.01%	No
Y 323			
K 324			
K 326			
S 328			
K 330	100% ± 0%	100% ± 0%	No
K 338	2% ± 2%	4.4% ± 0.5%	No
T 339			
S 341			
K 342			
K 344			
Y 353	0.4% ± 0.6%	14% ± 2%	Yes
T 354			
S 358			
T 363	0.006% ± 0.002%	0.012% ± 0.003%	Yes
K 364	0.15% ± 0.07%	0.3% ± 0.2%	No
S 368	0.02% ± 0.02%	0.18% ± 0.01%	Yes
T 370			
K 374	4% ± 2%	8% ± 2%	No
Y 377	11% ± 2%	12% ± 7%	No
S 379	13% ± 2%	13% ± 7%	No
S 387	11% ± 2%	12% ± 7%	No
Y 395	2.2% ± 0.8%	2% ± 1%	No
K 396	0.82% ± 0.2%	0.6% ± 0.3%	No
T 397	0.87% ± 0.3%	1.0% ± 0.2%	No
T 398	12% ± 1%	17% ± 3%	No
S 404	5% ± 1%	5% ± 2%	No
S 407	15% ± 4%	30% ± 6%	Yes
Y 411	8% ± 5%	20% ± 4%	Yes
S 412			
K 413			
T 415			
K 418	29% ± 20%	46% ± 4%	No
S 419	19% ± 20%	33% ± 2%	No
S 428	0.86% ± 0.08%	1.2% ± 0.4%	No
S 430	7% ± 2%	12% ± 2%	No
H 433	15% ± 2%	13% ± 4%	No
H 437	6% ± 3%	7.4% ± 0.9%	No
H 439	5.4% ± 0.9%	4% ± 3%	No
Y 440	0.02% ± 0.01%	0.02% ± 0.01%	No

T 441			
K 443	05% ± 0.2%	0.35% ± 0.07%	No
S 444			
S 446			
S 448	71% ± 10%	92% ± 4%	Yes
K 451	41% ± 20%	79% ± 7%	Yes

Table B.3: DEPC-CL modification percentages for each labelable residue of rituximab under native conditions and under heat stress conditions (65 °C for 4 h). A difference was considered significant if the p-value, calculated by performing an unpaired T-test, was less than 0.05 (corresponding to a 95% confidence level, n = 3). Errors shown in the table are standard deviations.

Residue	Native	Stressed 65 °C 4 h	Significant?
Light Chain			
S 5	0.03% ± 0.01%	0.01% ± 0.01%	Yes
S 7			
S 12	0.03% ± 0.01%	0.01% ± 0.01%	No
S 14			
K 18	0.56% ± 0.06%	0.3% ± 0.3%	No
T 20	17% ± 4%	13% ± 8%	No
T 22			
S 26			
S 27			
S 28			
S 30			
Y 31			
H 33	0.08% ± 0.02%	0.6% ± 0.5%	No
K 38	0.15% ± 0.05%	0.22% ± 0.06%	No
S 41	0.04% ± 0.01%	0.12% ± 0.04%	No
S 42			
K 44	0.06% ± 0.02%	0.09% ± 0.04%	No
Y 48	0.09% ± 0.04%	0.06% ± 0.01%	No
T 50	0.03% ± 0.03%	0.00% ± 0.00%	No
S 51			
S 55			
S 62			
S 64			
S 66	18% ± 4%	12% ± 4%	No
T 68	18% ± 4%	12% ± 4%	No
S 69			
Y 70	14% ± 5%	2% ± 2%	Yes

S 71			
T 73	50% ± 10%	70% ± 10%	No
S 75	50% ± 10%	70% ± 10%	No
T 84	1.3% ± 0.2%	3% ± 1%	No
Y 85	1.3% ± 0.2%	3% ± 1%	No
Y 86			
T 91	0.03% ± 0.02%	0.01% ± 0.01%	No
S 92	1.8% ± 0.6%	4% ± 2%	No
T 96	2.0% ± 0.6%	4% ± 2%	No
T 101	0.18% ± 0.01%	0.07% ± 0.05%	Yes
K 102	0.08% ± 0.02%	0.04% ± 0.02%	No
K 106			
T 108	1.3% ± 0.4%	0.7% ± 0.3%	No
S 113	1.0% ± 0.3%	0.5% ± 0.3%	No
S 120			
K 125			
S 126			
T 128	5% ± 1%	3% ± 2%	No
S 130	5% ± 1%	3% ± 2%	No
Y 139			
K 144			
K 148	7% ± 2%	5% ± 1%	No
S 155			
S 158			
S 161			
T 163	0.00% ± 0.00%	0.00% ± 0.00%	No
S 167			
K 168	0.5% ± 0.2%	0.4% ± 0.2%	No
S 170			
T 171			
Y 172			
S 173			
S 175			
S 176			
T 177			
T 179			
S 181			
K 182	5% ± 2%	13% ± 8%	No
Y 185	23.5% ± 0.3%	25% ± 4%	No
K 187	85% ± 3%	78% ± 4%	No
H 188	55% ± 2%	62% ± 8%	No
K 189	60% ± 3%	65% ± 6%	No
Y 191	0.74% ± 0.09%	1% ± 0.2%	No
T 196			
H 197	0.11% ± 0.03%	0.6% ± 0.2%	Yes

S 201			
S 202			
T 205			
K 206	0.4% ± 0.1%	0.6% ± 0.2%	No
S 207	4% ± 2%	2.7% ± 0.6%	No
Heavy Chain			
K 13	2.7% ± 0.5%	4% ± 1%	No
S 17			
K 19	3.5% ± 0.7%	3% ± 2%	No
S 21	24% ± 4%	12% ± 8%	No
K 23	86% ± 5%	96% ± 5%	No
S 25			
Y 27			
T 28			
T 30			
S 31			
Y 32	0.05% ± 0.03%	0.3% ± 0.2%	No
H 35	23% ± 3%	11% ± 3%	Yes
K 38	30% ± 2%	38% ± 10%	No
T 40			
Y 52	1.1% ± 0.2%	1.4% ± 0.2%	No
T 58	0.12% ± 0.01%	0.2% ± 0.2%	No
S 59	0.09% ± 0.01%	0.2% ± 0.2%	No
Y 60	0.09% ± 0.01%	0.2% ± 0.2%	No
K 63			
K 65			
K 67	23% ± 7%	70% ± 20%	Yes
T 69			
T 71			
K 74	79% ± 4%	52% ± 8%	Yes
S 75			
S 76	2.4% ± 0.2%	4% ± 1%	No
S 77	0.01% ± 0.01%	0.03% ± 0.01%	Yes
T 78	0.3% ± 0.1%	0.16% ± 0.09%	No
Y 80			
S 84	1.8% ± 0.7%	1.3% ± 0.5%	No
S 85	0.32% ± 0.06%	0.26% ± 0.09%	No
T 87			
S 88	0.02% ± 0.01%	0.03% ± 0.01%	No
S 91	0.25% ± 0.04%	0.21% ± 0.06%	No
Y 94	0.25% ± 0.04%	0.21% ± 0.06%	No
Y 95			
S 99			
T 100			
Y 101			

Y 102			
Y 107			
T 115	14% ± 4%	14% ± 5%	No
T 116			
T 118	71% ± 3%	55% ± 5%	Yes
S 120	84% ± 2%	69% ± 4%	Yes
S 123	1.2% ± 0.3%	1.2% ± 0.2%	No
T 124			
K 125			
S 128	0.9% ± 0.4%	0.3% ± 0.2%	No
S 135	1.1% ± 0.5%	0.4% ± 0.3%	No
S 136			
K 137			
S 138			
T 139	0.13% ± 0.07%	0.2% ± 0.1%	No
S 140	0.03% ± 0.02%	0.05% ± 0.01%	No
T 143	0.01% ± 0.01%	0.02% ± 0.01%	No
K 151			
Y 153	0.02% ± 0.02%	0.01% ± 0.01%	No
T 159			
S 161	1.8% ± 0.2%	1.2% ± 0.2%	Yes
S 164	0.00% ± 0.00%	0.02% ± 0.02%	No
T 168	1.3% ± 0.4%	2% ± 1%	No
S 169	0.2% ± 0.1%	0.2% ± 0.2%	No
H 172	0.2% ± 0.1%	0.2% ± 0.2%	No
T 173	1.1% ± 0.2%	1.9% ± 0.9%	No
S 180			
S 181			
Y 184			
S 185			
S 187	10% ± 3%	11% ± 2%	No
S 188	10% ± 3%	11% ± 2%	No
T 191	5% ± 1%	4.4% ± 0.1%	No
S 194			
S 195			
S 196	0.01% ± 0.00%	0.08% ± 0.02%	Yes
T 199	0.01% ± 0.00%	0.05% ± 0.02%	Yes
T 201			
Y 202			
H 208	0.00% ± 0.00%	0.04% ± 0.01%	Yes
K 209	6.4% ± 2.0%	4.0% ± 1.0%	No
S 211	0.00% ± 0.00%	0.21% ± 0.02%	Yes
T 213			
K 214	0.5% ± 0.4%	0.2% ± 0.1%	No
K 217			

K 218			
K 222	99% ± 1%	98% ± 2%	No
S 223	0.06% ± 0.04%	0.05% ± 0.01%	No
K 226	33% ± 7%	39% ± 17%	No
T 227	1.4% ± 0.8%	1.2% ± 0.8%	No
H 228	36% ± 7%	40% ± 10%	No
T 229	36% ± 7%	40% ± 10%	No
S 243			
K 250			
K 252	100% ± 0%	100% ± 0%	No
T 254			
S 258	5% ± 2%	1% ± 1%	Yes
T 260	0.7% ± 0.6%	0.2% ± 0.1%	No
T 264	11% ± 2%	10% ± 2%	No
S 271	10% ± 1%	9% ± 2%	No
H 272	0.26% ± 0.08%	0.2% ± 0.1%	No
K 278	0.2% ± 0.1%	0.24% ± 0.03%	No
Y 282	0.39% ± 0.02%	0.39% ± 0.08%	No
H 289	0.5% ± 0.1%	0.3% ± 0.2%	No
K 292			
T 293	38% ± 6%	82% ± 30%	No
K 294			
Y 300	50% ± 1%	30% ± 10%	No
S 302	38% ± 3%	10% ± 10%	Yes
T 303			
Y 304			
S 308			
T 311			
H 314	0.24% ± 0.08%	0.20% ± 0.03%	No
K 321	0.29% ± 0.04%	0.37% ± 0.06%	No
Y 323			
K 324			
K 326			
S 328			
K 330	100% ± 0%	100% ± 0%	No
K 338	2% ± 2%	1.5% ± 0.4%	No
T 339			
S 341			
K 342			
K 344			
Y 353	0.4% ± 0.6%	0.00% ± 0.00%	No
T 354			
S 358			
T 363	0.006% ± 0.002%	0.002% ± 0.001%	Yes
K 364	0.15% ± 0.07%	0.10% ± 0.08%	No

S 368	0.02% ± 0.02%	0.00% ± 0.00%	No
T 370			
K 374	4% ± 2%	4% ± 2%	No
Y 377	11% ± 2%	9% ± 5%	No
S 379	13% ± 2%	10% ± 5%	No
S 387	11% ± 2%	9% ± 5%	No
Y 395	2.2% ± 0.8%	2.3% ± 0.3%	No
K 396	0.8% ± 0.2%	0.7% ± 0.2%	No
T 397	0.9% ± 0.3%	1.0% ± 0.2%	No
T 398	12% ± 1%	16% ± 10%	No
S 404	5% ± 1%	5% ± 3%	No
S 407	15% ± 4%	23% ± 10%	No
Y 411	8% ± 5%	13% ± 6%	No
S 412			
K 413			
T 415			
K 418	29% ± 20%	36% ± 20%	No
S 419	19% ± 20%	25% ± 20%	No
S 428	0.86% ± 0.08%	0.4% ± 0.2%	Yes
S 430	7% ± 2%	8% ± 5%	No
H 433	15% ± 2%	16% ± 3%	No
H 437	6% ± 3%	5.2% ± 0.9%	No
H 439	5.4% ± 0.9%	2.5% ± 0.3%	Yes
Y 440	0.02% ± 0.01%	0.01% ± 0.01%	Yes
T 441			
K 443	0.5% ± 0.2%	0.3% ± 0.2%	No
S 444			
S 446			
S 448	71% ± 10%	47% ± 9%	No
K 451	41% ± 20%	5% ± 5%	Yes

APPENDIX C

C. HDX PEPTIDES DETECTED FOR TNFα IN COMPELIX WITH ANTIBODIES

Table C.1: List of detected peptides for TNFα in complex with Adalimumab

Start	End	Sequence	Significant?
3	26	SSSRTPSDKPVAHVVANPQAEGQL	Yes - Decrease
9	30	SDKPVAHVVANPQAEGQLQWLN	
27	36	QWLNRRANAL	Yes - Decrease
27	37	QWLNRRANALL	Yes - Decrease
30	36	NRRANAL	Yes - Decrease
30	37	NRRANALL	Yes - Decrease
36	42	LLANGVE	Yes - Decrease
37	43	LANGVEL	Yes - Decrease
37	48	LANGVELRDNQL	
38	47	ANGVELRDNQ	Yes - Decrease
38	48	ANGVELRDNQL	
41	47	VELRDNQ	Yes - Decrease
41	48	VELRDNQL	Yes - Decrease
43	54	LRDNQLVVPSEG	
43	55	LRDNQLVVPSEGL	
43	56	LRDNQLVVPSEGLY	
44	55	RDNQLVVPSEGL	
48	54	LVVPSEG	
48	55	LVVPSEGL	
48	56	LVVPSEGLY	
49	55	VVPSEGL	
49	72	VVPSEGLYLIYSQVLFKGQGCPST	Yes - Decrease
56	62	YLIYSQV	
63	72	LFKGQGCPST	
63	75	LFKGQGCPSTHVL	
63	81	LFKGQGCPSTHVLLTHTIS	
63	87	LFKGQGCPSTHVLLTHTISRIAVSY	Yes - Decrease

64	81	FKGQGCPSTHVLLTHTIS	
64	87	FKGQGCPSTHVLLTHTISRIAVSY	Yes - Decrease
65	87	KGQGCPSTHVLLTHTISRIAVSY	Yes - Decrease
73	81	HVLLTHTIS	
73	86	HVLLTHTISRIAVS	
73	87	HVLLTHTISRIAVSY	
73	93	HVLLTHTISRIAVSYQTKVNL	Yes - Decrease
76	87	LTHTISRIAVSY	
76	93	LTHTISRIAVSYQTKVNL	
77	87	THTISRIAVSY	
77	93	THTISRIAVSYQTKVNL	Yes - Decrease
78	87	HTISRIAVSY	
78	93	HTISRIAVSYQTKVNL	Yes - Decrease
80	87	ISRIAVSY	
82	93	RIAVSYQTKVNL	Yes - Decrease
84	93	AVSYQTKVNL	Yes - Decrease
87	93	YQTKVNL	Yes - Decrease
88	94	QTKVNLL	Yes - Decrease
88	96	QTKVNLLSA	Yes - Decrease
97	109	IKSPCQRETPEGA	
97	119	IKSPCQRETPEGAEAKPWYEPIY	Yes - Decrease
97	120	IKSPCQRETPEGAEAKPWYEPIYL	Yes - Decrease
103	119	RETPEGAEAKPWYEPIY	
103	120	RETPEGAEAKPWYEPIYL	
115	136	YEPIYLGGVFQLEKGDRLSAEI	Yes - Decrease
121	132	GGVFQLEKGDRL	Yes - Decrease
125	132	QLEKGDRL	
125	134	QLEKGDRLSA	
125	143	QLEKGDRLSAEINRPDYLD	
125	144	QLEKGDRLSAEINRPDYLDF	Yes - Decrease
126	132	LEKGDRL	
126	134	LEKGDRLSA	
127	134	EKGDRLSA	
133	142	SAEINRPDYL	Yes - Decrease
133	143	SAEINRPDYLD	Yes - Decrease
133	144	SAEINRPDYLDF	Yes - Decrease
135	142	EINRPDYL	Yes - Decrease
135	143	EINRPDYLD	Yes - Decrease
135	144	EINRPDYLDF	Yes - Decrease
136	144	INRPDYLDF	Yes - Decrease
144	152	FAESGQVYF	Yes - Decrease
145	152	AESGQVYF	
145	153	AESGQVYFG	

Table C.2: List of detected peptides for HDX/MS of TNFα in complex with Infliximab

Start	End	Sequence	Significant?
3	26	SSSRTPSDKPVAHVVANPQAEGQL	
9	30	SDKPVAHVVANPQAEGQLQWLN	Yes - Decrease
37	43	LANGVEL	
37	47	LANGVELRDNQ	
37	48	LANGVELRDNQL	
37	55	LANGVELRDNQLVVPSEGL	
38	47	ANGVELRDNQ	
38	55	ANGVELRDNQLVVPSEGL	
41	55	VELRDNQLVVPSEGL	
43	54	LRDNQLVVPSEG	
43	55	LRDNQLVVPSEGL	
43	56	LRDNQLVVPSEGLY	
44	55	RDNQLVVPSEGL	Yes - Increase
48	55	LVVPSEGL	
49	55	VVPSEGL	
56	62	YLIYSQV	
56	63	YLIYSQVL	
57	63	LIYSQVL	
63	87	LFKGQGCPSTHVLLTHTISRIAVSY	Yes - Decrease
64	87	FKGQGCPSTHVLLTHTISRIAVSY	Yes - Decrease
65	87	KGQGCPSTHVLLTHTISRIAVSY	
73	87	HVLLTHTISRIAVSY	
73	93	HVLLTHTISRIAVSYQTKVNL	
77	93	THTISRIAVSYQTKVNL	
88	96	QTKVNLLSA	
97	119	IKSPCQRETPEGAEAKPWYEPIY	Yes - Decrease
97	120	IKSPCQRETPEGAEAKPWYEPIYL	
121	132	GGVFQLEKGDRL	
121	134	GGVFQLEKGDRLSA	
125	132	QLEKGDRL	
125	134	QLEKGDRLSA	
125	142	QLEKGDRLSAEINRPDYL	Yes - Decrease

125	143	QLEKGDRLSAEINRPDYLD	Yes - Decrease
125	144	QLEKGDRLSAEINRPDYLDF	Yes - Decrease
126	132	LEKGDRL	
133	143	SAEINRPDYLD	Yes - Decrease
133	144	SAEINRPDYLDF	Yes - Decrease
133	142	SAEINRPDYL	Yes - Decrease
135	142	EINRPDYL	Yes - Decrease
135	143	EINRPDYLD	Yes - Decrease
135	144	EINRPDYLDF	Yes - Decrease
136	144	INRPDYLDF	Yes - Decrease
145	152	AESGQVYF	

Table C.3: List of detected peptides for HDX/MS of TNFα in complex with golimumab

Start	End	Sequence	Significant?
3	26	SSSRTPSDKPVAHVVANPQAEGQL	
27	36	QWLNRRANAL	
27	37	QWLNRRANALL	
30	36	NRRANAL	
30	37	NRRANALL	
37	43	LANGVEL	
41	47	VELRDNQ	
43	55	LRDNQLVVPSEGL	
43	56	LRDNQLVVPSEGLY	
44	55	RDNQLVVPSEGL	
48	55	LVVPSEGL	
48	56	LVVPSEGLY	
49	55	VVPSEGL	
56	62	YLIYSQV	
56	63	YLIYSQVL	
57	63	LIYSQVL	
62	72	VLFKGQGCPST	Yes - Decrease
63	72	LFKGQGCPST	Yes - Decrease
63	87	LFKGQGCPSTHVLLTHTISRIAVSY	Yes - Decrease
64	72	FKGQGCPST	Yes - Decrease
64	87	FKGQGCPSTHVLLTHTISRIAVSY	Yes - Decrease
65	87	KGQGCPSTHVLLTHTISRIAVSY	Yes - Decrease
73	81	HVLLTHTIS	
73	82	HVLLTHTISR	Yes - Decrease

73	83	HVLLTHTISRI	Yes - Decrease
73	85	HVLLTHTISRIAV	
73	86	HVLLTHTISRIAVS	
73	87	HVLLTHTISRIAVSY	
73	93	HVLLTHTISRIAVSYQTKVNL	
76	86	LTHTISRIAVS	
76	87	LTHTISRIAVSY	
77	87	THTISRIAVSY	
78	87	HTISRIAVSY	
80	87	ISRIAVSY	
82	93	RIAVSYQTKVNL	
84	93	AVSYQTKVNL	
87	93	YQTKVNL	
88	94	QTKVNLL	
97	119	IKSPCQRETPEGAEAKPWYEPIY	Yes - Decrease
97	120	IKSPCQRETPEGAEAKPWYEPIYL	
103	119	RETPEGAEAKPWYEPIY	Yes - Decrease
103	120	RETPEGAEAKPWYEPIYL	Yes - Decrease
110	119	EAKPWYEPIY	Yes - Decrease
120	134	LGGVFQLEKGDRLSA	
124	134	FQLEKGDRLSA	Yes - Decrease
125	132	QLEKGDRL	
126	132	LEKGDRL	
127	134	EKGDRLSA	
133	143	SAEINRPDYLD	
133	144	SAEINRPDYLDF	
135	143	EINRPDYLD	
136	142	INRPDYL	Yes - Decrease
136	144	INRPDYLDF	
136	147	INRPDYLDFAES	
145	151	AESGQVY	
145	152	AESGQVYF	
145	153	AESGQVYFG	

BIBLIOGRAPHY

Abbott, W. M.; Damschroder, M. M.; Lowe, D. C. Current Approaches to Fine Mapping of Antigen-Antibody Interactions. Immunology 2014, 142 (4), 526–535. https://doi.org/10.1111/imm.12284.

Andersen, C. B.; Manno, M.; Rischel, C.; Thorolfsson, M.; Martorana, V. Aggregation of a Multidomain Protein : A Coagulation Mechanism Governs Aggregation of a Model IgG1 Antibody under Weak Thermal Stress. Protein Sci. 2010, 19, 279–290. https://doi.org/10.1002/pro.309.

Arden, B. G.; Borotto, N. B.; Burant, B.; Warren, W.; Akiki, C.; Vachet, R. W. Measuring the Energy Barrier of the Structural Change That Initiates Amyloid Formation. Anal. Chem. 2020, 92 (7), 4731–4735. https://doi.org/10.1021/acs.analchem.0c00368.

Artigues, A.; Nadeau, O. W.; Rimmer, M. A.; Villar, M. T.; Du, X.; Fenton, A. W.; Carlson, G. M. Protein Structural Analysis via Mass Spectrometry-Based Proteomics. Adv. Exp. Med. Biol. 2016, 919, 397–431. https://doi.org/10.1007/978-3-319-41448-5.

Aubin-Tam, M.-E.; Olivares, A. O.; Sauer, R. T.; Baker, T. A.; Lang, M. J. Single-Molecule Protein Unfolding and Translocation by an ATP- Fueled Proteolytic Machine. Cell 2011, 145 (2), 257–267. https://doi.org/10.1038/jid.2014.371.

Baerga-Ortiz, A.; Hughes, C. A.; Mandell, J. G.; Komives, E. A. Epitope Mapping of a Monoclonal Antibody against Human Thrombin by H/D-Exchange Mass Spectrometry Reveals Selection of a Diverse Sequence in a Highly Conserved Protein. Protein Sci. 2002, 11 (6), 1300–1308. https://doi.org/10.1110/ps.4670102.

Beck, A.; Goetsch, L.; Dumontet, C.; Corvaïa, N. Strategies and Challenges for the next Generation of Antibody–Drug Conjugates. Nat. Publ. Gr. 2017, 16 (5), 315–337. https://doi.org/10.1038/nrd.2016.268.

Beck, A.; Sanglier-Cianférani, S.; Van Dorsselaer, A. Biosimilar, Biobetter, and Next Generation Antibody Characterization by Mass Spectrometry. Anal. Chem. 2012, 84 (11), 4637–4646. https://doi.org/10.1021/ac3002885.

Beneta, L. Z.; Hoseya, C. M.; Ursub, O.; Opreab, T. I. BDDCS, the Rule of 5 and Drugability Leslie. Adv. Drug Deliv. Rev. 2016, 101, 89–98. https://doi.org/10.1016/j.addr.2016.05.007.BDDCS.

Berkowitz, S. A.; Engen, J. R.; Mazzeo, J. R.; Jones, G. B. Analytical Tools for Characterizing Biopharmaceuticals and the Implications for Biosimilars. Nature 2012, 11, 527–540. https://doi.org/10.1038/nrd3746.

Berkowitz, S. A.; Engen, J. R.; Mazzeo, J. R.; Jones, G. B. Analytical Tools for Characterizing Biopharmaceuticals and the Implications for Biosimilars. Nat. Rev. Drug Discov. 2012, 11, 527–540. https://doi.org/10.1038/nrd3746.

Bhat, N. H.; Vass, R. H.; Stoddard, P. R.; Shin, D. K.; Chien, P. Identification of ClpP Substrates in Caulobacter Crescentus Reveals a Role for Regulated Proteolysis in Bacterial Development. Mol. Microbiol. 2013, 88 (6), 1083–1092. https://doi.org/10.1111/mmi.12241.

Biehn, S. E.; Limpikirati, P.; Vachet, R. W.; Lindert, S. Utilization of Hydrophobic Microenvironment Sensitivity in Diethylpyrocarbonate Labeling for Protein Structure Prediction. Anal. Chem. 2021, 93 (23), 8188–8195. https://doi.org/10.1021/acs.analchem.1c00395.

Biemann, K. Contributions of Mass Spectrometry to Peptide and Protein Structure. Biomed. Environ. Mass Spectrom. 1988, 16, 99–111.

Bolon, D. N.; Grant, R. A.; Baker, T. A.; Sauer, R. T. Nucleotide-Dependent Substrate Handoff from the SspB Adaptor to the AAA ClpXP Protease. Mol. Cell 2004, 16, 343–350.

Borotto, N. B.; Zhou, Y.; Hollingsworth, S. R.; Hale, J. E.; Graban, E. M.; Vaughan, R. C.; Vachet, R. W. Investigating Therapeutic Protein Structure with Diethylpyrocarbonate Labeling and Mass Spectrometry. Anal. Chem. 2015. https://doi.org/10.1021/acs.analchem.5b03180.

Borotto, N. B.; Zhou, Y.; Hollingsworth, S. R.; Hale, J. E.; Graban, E. M.; Vaughan, R. C.; Vachet, R. W. Investigating Therapeutic Protein Structure with Diethylpyrocarbonate Labeling and Mass Spectrometry. Anal. Chem. 2015, 87, 10627–10634. https://doi.org/10.1021/acs.analchem.5b03180.

Chen, K.; Long, D. S.; Lute, S. C.; Levy, M. J.; Brorson, K. A.; Keire, D. A. Simple NMR Methods for Evaluating Higher Order Structures of Monoclonal Antibody Therapeutics with Quinary Structure. J. Pharm. Biomed. Anal. 2016, 128, 398–407. https://doi.org/10.1016/j.jpba.2016.06.007.

Chien, P.; Perchuk, B. S.; Laub, M. T.; Sauer, R. T.; Baker, T. A. Direct and Adaptor-Mediated Substrate Recognition by an Essential AAA+ Protease. Proc. Natl. Acad. Sci. U. S. A. 2007, 104 (16), 6590–6595. https://doi.org/10.1073/pnas.0701776104.

Choi, K.; Licht, S. Control of Peptide Product Sizes by the Energy-Dependent Protease ClpAP †. Biochemistry 2005, 44 (42), 13921–13931. https://doi.org/10.1021/bi0505060.

Conchillo-Solé, O.; de Groot, N. S.; Avilés, F. X.; Vendrell, J.; Daura, X.; Ventura, S. AGGRESCAN: A Server for the Prediction and Evaluation of "Hot Spots" of Aggregation in Polypeptides. BMC Bioinformatics 2007, 8. https://doi.org/10.1186/1471-2105-8-65.

Contreras, M. A.; Macaya, L.; Neira, P.; Camacho, F.; González, A.; Acosta, J.; Montesino, R.; Toledo, J. R.; Sánchez, O. New Insights on the Interaction Mechanism of RhTNFα with Its Antagonists Adalimumab and Etanercept. bioRxiv Prepr. 2020. https://doi.org/10.1101/2020.06.21.163824.

Cornwell, O.; Ault, J. R.; Bond, N. J.; Radford, S. E.; Ashcroft, A. E. Investigation of D76N β 2 - Microglobulin Using Protein Footprinting and Structural Mass Spectrometry. J Am Soc Mass Spectrom 2021. https://doi.org/10.1021/jasms.0c00438.

Cornwell, O.; Radford, S. E.; Ashcroft, A. E.; Ault, J. R. Comparing Hydrogen Deuterium Exchange and Fast Photochemical Oxidation of Proteins: A Structural Characterisation of Wild-Type and ΔN6 B2-Microglobulin. J. Am. Soc. Mass Spectrom. 2018, 29, 2413–2426. https://doi.org/10.1007/s13361-018-2067-y.

Corti, A.; Fassina, G.; Marcucci, F.; Barbanti, E.; Cassani, G. Oligomeric Tumour Necrosis Factor α Slowly Converts into Inactive Forms at Bioactive Levels. Biochem. J. 1992, 284 (3), 905–910. https://doi.org/10.1042/bj2840905.

Cragg, M. S.; Bayne, M. B.; Tutt, A. L.; French, R. R.; Beers, S.; Glennie, M. J.; Illidge, T. M. A New Anti-Idiotype Antibody Capable of Binding Rituximab on the Surface of Lymphoma Cells. Blood 2004, 104 (8), 2540–2542. https://doi.org/10.1182/blood-2004-05-1733.

Dass, C. Mass Spectrometry : Structure Determination of Proteins and Peptides; 2010.

Daub, H.; Traxler, L.; Ismajli, F.; Groitl, B.; Itzen, A.; Rant, U. The Trimer to Monomer Transition of Tumor Necrosis Factor-Alpha Is a Dynamic Process That Is Significantly Altered by Therapeutic Antibodies. Sci. Rep. 2020, 10 (9265), 1–10. https://doi.org/10.1038/s41598-020-66123-5.

Deng, B.; Lento, C.; Wilson, D. J. Hydrogen Deuterium Exchange Mass Spectrometry in Biopharmaceutical Discovery and Developm .... Anal. Chim. Acta 2016, 940 (October 2017), 8–20. https://doi.org/10.1016/j.aca.2016.08.006.

Deng, B.; Zhu, S.; Macklin, A. M.; Xu, J.; Lento, C.; Sljoka, A.; Wilson, D. J. Suppressing Allostery in Epitope Mapping Experiments Using Millisecond Hydrogen / Deuterium Exchange Mass Spectrometry. MAbs 2017, 0862. https://doi.org/10.1080/19420862.2017.1379641.

Deperalta, G.; Alvarez, M.; Bechtel, C.; Dong, K.; Mcdonald, R.; Ling, V. Structural Analysis of a Therapeutic Monoclonal Antibody Dimer by Hydroxyl Radical Footprinting. MAbs 2013, 5 (1), 86–101.

Ecker, D. M.; Jones, S. D.; Levine, H. L. The Therapeutic Monoclonal Antibody Market. MAbs 2015, 7 (1), 9–14. https://doi.org/http://dx.doi.org/10.4161/19420862.2015.989042.

Edgeworth, M. J.; Phillips, J. J.; Lowe, D. C.; Kippen, A. D.; Higazi, D. R.; Scrivens, J. H. Global and Local Conformation of Human IgG Antibody Variants Rationalizes Loss of Thermodynamic Stability. Angew. Chemie - Int. Ed. 2015, 54 (50), 15156–15159. https://doi.org/10.1002/anie.201507223.

Edgeworth, M. J.; Phillips, J. J.; Lowe, D. C.; Kippen, A. D.; Higazi, D. R.; Scrivens, J. H. Global and Local Conformation of Human IgG Antibody Variants

Rationalizes Loss of Thermodynamic Stability. Angew. Chemie - Int. Ed. 2015, 54 (50), 15156–15159. https://doi.org/10.1002/anie.201507223.

Elgundi, Z.; Reslan, M.; Cruz, E.; Sifniotis, V.; Kayser, V. The State-of-Play and Future of Antibody Therapeutics. Adv. Drug Deliv. Rev. 2017, 122, 2–19. https://doi.org/10.1016/j.addr.2016.11.004.

Engen, J. R.; Botzanowski, T.; Peterle, D.; Georgescauld, F.; Wales, T. E. Developments in Hydrogen/Deuterium Exchange Mass Spectrometry. Anal. Chem. 2021, 93 (1), 567–582. https://doi.org/10.1021/acs.analchem.0c04281.

Englander, S. W.; Sosnickt, T. R.; Englander, J. J.; Maynet, L. Mechanisms and Uses of Hydrogen Exchange. Curr. Opin. Struct. Biol. 1996.

Fast, C. S.; Vahidi, S.; Konermann, L. Changes in Enzyme Structural Dynamics Studied by Hydrogen Exchange-Mass Spectrometry: Ligand Binding E Ff Ects or Catalytically Relevant Motions? Anal. Chem. 2017. https://doi.org/10.1021/acs.analchem.7b03506.

Fei, X.; Bell, T. A.; Jenni, S.; Stinson, B. M.; Baker, T. A.; Harrison, S. C.; Sauer, R. T. Structures of the ATP-Fueled ClpXP Proteolytic Machine Bound to Protein Substrate. Elife 2020, 9, 1–22. https://doi.org/10.7554/eLife.52774.

Fernandez-Escamilla, A. M.; Rousseau, F.; Schymkowitz, J.; Serrano, L. Prediction of Sequence-Dependent and Mutational Effects on the Aggregation of Peptides and Proteins. Nat. Biotechnol. 2004, 22 (10), 1302–1306. https://doi.org/10.1038/nbt1012.

Fiedler, W.; Borchers, C.; Macht, M.; Deininger, S. O.; Przybylski, M. Molecular Characterization of a Conformational Epitope of Hen Egg White Lysozyme by Differential Chemical Modification of Immune Complexes and Mass Spectrometric Peptide Mapping. Bioconjug. Chem. 1998, 9 (2), 236–241. https://doi.org/10.1021/bc970148g.

FINUCANE, M. D.; JARDETZKY, O. The PH Dependence of Hydrogen-Deuterium Exchange in Trp Repressor: The Exchange Rate of Amide Protons in Proteins Reflects Tertiary Interactions, Not Only Secondary Structure. Protein Sci. 1996, 653–662.

Fraczkiewicz, R.; Braun, W. Exact and Efficient Analytical Calculation of the Accessible Surface Areas and Their Gradients for Macromolecules. J. Comput. Chem. 1998, 19 (3), 319–333. https://doi.org/10.1002/(SICI)1096-987X(199802)19:3<319::AID-JCC6>3.0.CO;2-W.

Frokjaer, S.; Otzen, D. Protein Drug Stability: A Formulation Challenge. Nat. Rev. Drug Discov. 2005, 4 (May), 298–306. https://doi.org/10.1038/nrd1695.

Gersch, M.; Stahl, M.; Poreba, M.; Dahmen, M.; Dziedzic, A.; Drag, M.; Sieber, S. A. Barrel-Shaped ClpP Proteases Display Attenuated Cleavage Specificities. ACS Chem. Biol. 2016, 11 (2), 389–399. https://doi.org/10.1021/acschembio.5b00757.

Glocker, M. O.; Kalkum, M.; Yamamoto, R.; Schreurs, J. Selective Biochemical Modification of Functional Residues in Recombinant Human Macrophage Colony-Stimulating Factor β (RhM-CSF β): Identification by Mass Spectrometry. Biochemistry 1996, 35 (46), 14625–14633. https://doi.org/10.1021/bi961199o.

Glocker, M. O.; Nock, S.; Sprinzl, M.; Przybylski, M. Characterization of Surface Topology and Binding Area in Complexes of the Elongation Factor Proteins EF-Ts and EF-Tu·GDP from Thermus Thermophilus: A Study by Protein Chemical Modification and Mass Spectrometry. Chem. - A Eur. J. 1998, 4 (4), 707–715.

Gramlich, M.; Hays, H. C. W.; Crichton, S.; Kaiser, P. D.; Heine, A.; Schneiderhan-Marra, N.; Rothbauer, U.; Stoll, D.; Maier, S.; Zeck, A. Hdx/MS for Epitope Characterization of a Therapeutic Antibody Candidate on the Calcium-Binding Protein Annexin-A1. Antibodies 2021, 10 (11), 1–12. https://doi.org/10.3390/antib10010011.

Hageman, T. S.; Weis, D. D. Reliable Identification of Significant Differences in Differential Hydrogen Exchange-Mass Spectrometry Measurements Using a Hybrid Significance Testing Approach. Anal. Chem. 2019, 91 (13), 8008–8016. https://doi.org/10.1021/acs.analchem.9b01325.

Hager-Braun, C.; Tomer, K. B. Determination of Protein-Derived Epitopes by Mass Spectrometry. Expert Rev. Proteomics 2005, 2 (5), 745–756. https://doi.org/10.1586/14789450.2.5.745.

Hampson, G.; Ward, T. H.; Cummings, J.; Bayne, M.; Tutt, A. L.; Cragg, M. S.; Dive, C.; Illidge, T. M. Validation of an ELISA for the Determination of Rituximab Pharmacokinetics in Clinical Trials Subjects. J. Immunol. Methods 2010, 360 (1–2), 30–38. https://doi.org/10.1016/j.jim.2010.05.009.

Hamuro, Y.; Coales, S. J.; Southern, M. R.; Nemeth-Cawley, J. F.; Stranz, D. D.; Griffin, P. R. Rapid Analysis of Protein Structure and Dynamics by Hydrogen/Deuterium Exchange Mass Spectrometry. J. Biomol. Tech. 2003, 14 (3), 171–182.

Hawe, A.; Christina, J.; Friess, W.; Jiskoot, W. Structural Properties of Monoclonal Antibody Aggregates Induced by Freeze – Thawing and Thermal Stress. Eur. J. Pharm. Sci. 2009, 38, 79–87. https://doi.org/10.1016/j.ejps.2009.06.001.

Haynes, C. M.; Yang, Y.; Blais, S. P.; Neubert, T. A.; Ron, D. The Matrix Peptide Exporter HAF-1 Signals a Mitochondrial Unfolded Protein Response by Activating the Transcription Factor ZC376.7 in C. Elegans. Mol. Cell 2011, 37 (4), 529–540. https://doi.org/10.1016/j.molcel.2010.01.015.

Hondal, R. J.; Ma, S.; Caprioli, R. M.; Hill, K. E.; Burk, R. F. Heparin-Binding Histidine and Lysine Residues of Rat Selenoprotein P. J. Biol. Chem. 2001, 276 (19), 15823–15831. https://doi.org/10.1074/jbc.M010405200.

Houde, D.; Arndt, J.; Domeier, W.; Berkowitz, S.; Engen, J. R. Characterization of IgG1 Conformation and Conformational Dynamics by Hydrogen / Deuterium Exchange Mass Spectrometry. Anal. Chem. 2009, 81 (7), 2644–2651. https://doi.org/10.1021/ac802575y.

Houde, D.; Berkowitz, S. A.; Engen, J. R. The Utility of Hydrogen/Deuterium Exchange Mass Spectrometry in Biopharmaceutical Comparability Studies. J. Pharm. Sci. 2011, 100 (6), 2071–2086. https://doi.org/10.1002/jps.22432.

Hu, S.; Liang, S.; Guo, H.; Zhang, D.; Li, H.; Wang, X.; Yang, W.; Qian, W.; Hou, S.; Wang, H.; Guo, Y.; Lou, Z. Comparison of the Inhibition Mechanisms of Adalimumab and Infliximab in Treating Tumor Necrosis Factor α-Associated Diseases from a Molecular View. J. Biol. Chem. 2013, 288 (38), 27059–27067. https://doi.org/10.1074/jbc.M113.491530.

Hu, S.; Liang, S.; Guo, H.; Zhang, D.; Li, H.; Wang, X.; Yang, W.; Qian, W.; Hou, S.; Wang, H.; Guo, Y.; Lou, Z. Comparison of the Inhibition Mechanisms of Adalimumab and Infliximab in Treating Tumor Necrosis Factor α-Associated Diseases from a Molecular View. J. Biol. Chem. 2013, 288 (38), 27059–27067. https://doi.org/10.1074/jbc.M113.491530.

Huang, R. Y. C.; Iacob, R. E.; Sankaranarayanan, S.; Yang, L.; Ahlijanian, M.; Tao, L.; Tymiak, A. A.; Chen, G. Probing Conformational Dynamics of Tau Protein by Hydrogen/Deuterium Exchange Mass Spectrometry. J. Am. Soc. Mass Spectrom. 2018, 29 (1), 174–182. https://doi.org/10.1007/s13361-017-1815-8.

Huang, R. Y. C.; Krystek, S. R.; Felix, N.; Graziano, R. F.; Srinivasan, M.; Pashine, A.; Chen, G. Hydrogen/Deuterium Exchange Mass Spectrometry and Computational Modeling Reveal a Discontinuous Epitope of an Antibody/TL1A Interaction. MAbs 2018, 10 (1), 95–103. https://doi.org/10.1080/19420862.2017.1393595.

Huang, R. Y. C.; Kuhne, M.; Deshpande, S.; Rangan, V.; Srinivasan, M.; Wang, Y.; Chen, G. Mapping Binding Epitopes of Monoclonal Antibodies Targeting Major Histocompatibility Complex Class I Chain-Related A (MICA) with Hydrogen/Deuterium Exchange and Electron-Transfer Dissociation Mass Spectrometry. Anal. Bioanal. Chem. 2020, 412 (7), 1693–1700. https://doi.org/10.1007/s00216-020-02409-x.

Huang, R. Y. C.; Wang, Y.; Jhatakia, A. D.; Deng, A. X.; Bee, C.; Deshpande, S.; Rangan, V. S.; Bezman, N.; Gudmundsson, O.; Chen, G. Higher-Order Structure Characterization of NKG2A/CD94 Protein Complex and Anti-NKG2A Antibody Binding Epitopes by Mass Spectrometry-Based Protein Footprinting Strategies. J. Am. Soc. Mass Spectrom. 2021. https://doi.org/10.1021/jasms.0c00399.

Huang, R. Y.; Chen, G. Higher Order Structure Characterization of Protein Therapeutics by Hydrogen/Deuterium Exchange Mass Spectrometry. Anal Bioanal Chem 2014, 406, 6541–6558. https://doi.org/10.1007/s00216-014-7924-3.

Iacob, R. E.; Bou-assaf, G. M.; Makowski, L. E. E.; Engen, J. R.; Berkowitz, S. A.; Houde, D. Investigating Monoclonal Antibody Aggregation Using a Combination of H / DX/MS and Other Biophysical Measurements. J. Pharm. Sci. 2013, 102, 4315–4329. https://doi.org/10.1002/jps.23754.

Jennings, L. D.; Lun, D. S.; Médard, M.; Licht, S. ClpP Hydrolyzes a Protein Substrate Processively in the Absence of the ClpA ATPase: Mechanistic Studies of ATP-Independent Proteolysis. Biochemistry 2008, 47 (44), 11536–11546. https://doi.org/10.1021/bi801101p.

Jones, L. M.; Sperry, J.; Carroll, J.; Gross, M. L. Fast Photochemical Oxidation of Proteins (FPOP) for Epitope Mapping. Anal. Chem. 2011, 83 (20), 7657–7661. https://doi.org/10.1021/ac2007366.Fast.

Kant, R. Van Der; Karow-zwick, A. R.; Durme, J. Van; Blech, M.; Gallardo, R.; Seeliger, D.; Aßfalg, K.; Baatsen, P.; Compernolle, G.; Gils, A.; Studts, J. M.; Schulz, P.; Garidel, P.; Schymkowitz, J.; Rousseau, F. Prediction and Reduction of the Aggregation of Monoclonal Antibodies. J. Mol. Biol. 2017, 429 (8), 1244–1261. https://doi.org/10.1016/j.jmb.2017.03.014.

Kattat, V.; Chit, B. T. Hydrogen / Deuterium Exchange Electrospray Ionization Mass Spectrometry : A Method for Probing Protein Conformational Changes in Solution. J. Am. Chem. Soc. 1993, No. 13, 4–8. https://doi.org/10.1021/ja00067a054.

Kaur, P.; Tomechko, S. E.; Kiselar, J.; Shi, W.; Deperalta, G.; Wecksler, A. T.; Gokulrangan, G.; Ling, V.; Chance, M. R. Characterizing Monoclonal Antibody Structure by Carboxyl Group Footprinting. MAbs 2015, 7 (3), 540–552.

Kim, M. S.; Lee, S. H.; Song, M. Y.; Yoo, T. H.; Lee, B. K.; Kim, Y. S. Comparative Analyses of Complex Formation and Binding Sites between Human Tumor Necrosis Factor-Alpha and Its Three Antagonists Elucidate Their Different Neutralizing Mechanisms. J. Mol. Biol. 2007, 374 (5), 1374–1388. https://doi.org/10.1016/j.jmb.2007.10.034.

Konermann, L. Heavy Lessons in Protein Allostery. Nat. Publ. Gr. 2016, 23 (6), 511–512. https://doi.org/10.1038/nsmb.3234.

Konermann, L.; Pan, J.; Liu, Y.-H. Hydrogen Exchange Mass Spectrometry for Studying Protein Structure and Dynamics. R. Soc. Chem. 2011, 1224–1234. https://doi.org/10.1039/c0cs00113a.

Kong, L.; Lee, D. E.; Kadam, R. U.; Liu, T.; Giang, E.; Nieusma, T.; Garces, F.; Tzarum, N.; Woods, V. L.; Ward, A. B.; Li, S.; Wilson, I. A.; Law, M. Structural Flexibility at a Major Conserved Antibody Target on Hepatitis C Virus E2 Antigen. Proc. Natl. Acad. Sci. U. S. A. 2016, 113 (45), 12768–12773. https://doi.org/10.1073/pnas.1609780113.

Krezel, A.; Bal, W. A Formula for Correlating PKa Values Determined in D2O and H2O. J. Inorg. Biochem. 2004, 98, 161–166. https://doi.org/10.1016/j.jinorgbio.2003.10.001.

Krissinel, E.; Henrick, K. Inference of Macromolecular Assemblies from Crystalline State. J. Mol. Biol. 2007, 372 (3), 774–797. https://doi.org/10.1016/j.jmb.2007.05.022.

Leader, B.; Baca, Q. J.; Golan, D. E. Protein Therapeutics: A Summary and Pharmacological Classification. Nat. Rev. 2008, 7 (january), 21–39.

Lee, C.; Schwartz, M. P.; Prakash, S.; Iwakura, M.; Matouschek, A. ATP-Dependent Proteases Degrade Their Substrates by Processively Unraveling Them from the Degradation Signal. Mol. Cell 2001, 7 (3), 627–637. https://doi.org/10.1016/S1097-2765(01)00209-X.

Leitner, A. Cross-Linking and Other Structural Proteomics Techniques : How Chemistry Is Enabling Mass Spectrometry Applications in Structural Biology. Chem. Sci. 2016, 7, 4792–4803. https://doi.org/10.1039/C5SC04196A.

Lewis, E. Protein Dynamics from NMR. Biochem. Cell Biol. 1998.

Li, J.; Wei, H.; Krystek, S. R.; Bond, D.; Brender, T. M.; Cohen, D.; Feiner, J.; Hamacher, N.; Harshman, J.; Huang, R. Y.; Julien, S. H.; Lin, Z.; Moore, K.; Mueller, L.; Noriega, C.; Sejwal, P.; Sheppard, P.; Stevens, B.; Chen, G.; Tymiak, A. A.; Gross, M. L.; Schneeweis, L. A. Mapping the Energetic Epitope of an Antibody/Interleukin-23 Interaction with Hydrogen/Deuterium Exchange, Fast Photochemical Oxidation of Proteins Mass Spectrometry, and Alanine Shave Mutagenesis. Anal. Chem. 2017. https://doi.org/10.1021/acs.analchem.6b03058.

Li, J.; Wei, H.; Krystek, S. R.; Bond, D.; Brender, T. M.; Cohen, D.; Feiner, J.; Hamacher, N.; Harshman, J.; Huang, R. Y.; Julien, S. H.; Lin, Z.; Moore, K.; Mueller, L.; Noriega, C.; Sejwal, P.; Sheppard, P.; Stevens, B.; Chen, G.; Tymiak, A. A.; Gross, M. L.; Schneeweis, L. A. Mapping the Energetic Epitope of an Antibody/Interleukin-23 Interaction with Hydrogen/Deuterium Exchange, Fast Photochemical Oxidation of Proteins Mass Spectrometry, and Alanine Shave Mutagenesis. 2017. https://doi.org/10.1021/acs.analchem.6b03058.

Li, K. S.; Chen, G.; Mo, J.; Huang, R. Y.; Deyanova, E. G.; Beno, B. R.; O'Neil, S. R.; Tymiak, A. A.; Gross, M. L. Orthogonal Mass Spectrometry-Based Footprinting for Epitope Mapping and Structural Characterization: The IL-6 Receptor upon Binding of Protein Therapeutics. Anal. Chem. 2017, 89, 7742–7749. https://doi.org/10.1021/acs.analchem.7b01748.

Li, K. S.; Schaper Bergman, E. T.; Beno, B. R.; Huang, R. Y. C.; Deyanova, E.; Chen, G.; Gross, M. L. Hydrogen-Deuterium Exchange and Hydroxyl Radical Footprinting for Mapping Hydrophobic Interactions of Human Bromodomain

with a Small Molecule Inhibitor. J. Am. Soc. Mass Spectrom. 2019, 30 (12), 2795–2804. https://doi.org/10.1007/s13361-019-02316-1.

Li, K. S.; Shi, L.; Gross, M. L. Mass Spectrometry-Based Fast Photochemical Oxidation of Proteins (FPOP) for Higher Order Structure Characterization. Acc. Chem. Res. 2018, 51, 736–744. https://doi.org/10.1021/acs.accounts.7b00593.

Liang, S.; Dai, J.; Hou, S.; Su, L.; Zhang, D.; Guo, H.; Hu, S.; Wang, H.; Rao, Z.; Guo, Y.; Lou, Z. Structural Basis for Treating Tumor Necrosis Factor α (TNFα)-Associated Diseases with the Therapeutic Antibody Infliximab. J. Biol. Chem. 2013, 288 (19), 13799–13807. https://doi.org/10.1074/jbc.M112.433961.

Limpikirati, P. K.; Zhao, B.; Pan, X.; Eyles, S. J.; Vachet, R. W. Covalent Labeling/Mass Spectrometry of Monoclonal Antibodies with Diethylpyrocarbonate: Reaction Kinetics for Ensuring Protein Structural Integrity. J. Am. Soc. Mass Spectrom. 2020, 31 (6), 1223–1232. https://doi.org/10.1021/jasms.0c00067.

Limpikirati, P.; Hale, J. E.; Hazelbaker, M.; Huang, Y.; Jia, Z.; Yazdania, M.; Grabanb, E. M.; Vaughan, R. C.; Vachet, R. W. Covalent Labeling and Mass Spectrometry Reveal Subtle Higher Order Structural Changes for Antibody Therapeutics. MAbs 2019, 11 (3), 463–476. https://doi.org/10.1080/19420862.2019.1565748.

Limpikirati, P.; Liu, T.; Vachet, R. W. Covalent Labeling-Mass Spectrometry with Non-Specific Reagents for Studying Protein Structure and Interactions. Methods 2018, 144, 79–93. https://doi.org/10.1016/j.ymeth.2018.04.002.

Limpikirati, P.; Pan, X.; Vachet, R. W. Covalent Labeling with Diethylpyrocarbonate: Sensitive to the Residue Microenvironment, Providing Improved Analysis of Protein Higher Order Structure by Mass Spectrometry. Anal. Chem. 2019, 91 (13), 8516–8523. https://doi.org/10.1021/acs.analchem.9b01732.

Linding, R.; Schymkowitz, J.; Rousseau, F.; Diella, F.; Serrano, L. A Comparative Study of the Relationship between Protein Structure and β-Aggregation in Globular and Intrinsically Disordered Proteins. J. Mol. Biol. 2004, 342 (1), 345–353. https://doi.org/10.1016/j.jmb.2004.06.088.

Liu, T.; Limpikirati, P.; Vachet, R. W. Synergistic Structural Information from Covalent Labeling and Hydrogen − Deuterium Exchange Mass Spectrometry for Protein − Ligand Interactions. Anal. Chem. 2019, 91, 15248–15254. https://doi.org/10.1021/acs.analchem.9b04257.

Liu, T.; Marcinko, T. M.; Kiefer, P. A.; Vachet, R. W. Using Covalent Labeling and Mass Spectrometry To Study Protein Binding Sites of Amyloid Inhibiting Molecules. Anal. Chem. 2017, 89, 11583–11591. https://doi.org/10.1021/acs.analchem.7b02915.

Liu, X. R.; Zhang, M. M.; Gross, M. L. Mass Spectrometry-Based Protein Footprinting for Higher-Order Structure Analysis: Fundamentals and Applications. Chem. Rev. 2020, 120, 4355–4454. https://doi.org/10.1021/acs.chemrev.9b00815.

Lopez, K. E.; Rizo, A. N.; Tse, E.; Lin, J. B.; Scull, N. W.; Thwin, A. C.; Lucius, A. L.; Shorter, J.; Southworth, D. R. Conformational Plasticity of the ClpAP AAA+ Protease Couples Protein Unfolding and Proteolysis. Nat. Struct. Mol. Biol. 2020, 27 (5), 406–416. https://doi.org/10.1038/s41594-020-0409-5.

Lu, R.; Hwang, Y.; Liu, I.; Lee, C.; Tsai, H.; Li, H.; Wu, H. Development of Therapeutic Antibodies for the Treatment of Diseases. J. Biomed. Sci. 2020, 27 (1), 1–30. https://doi.org/https://doi.org/10.1186/s12929-019-0592-z.

Mahmoud, S. A.; Chien, P. Regulated Proteolysis in Bacteria. Annu. Rev. Biochem. 2018, 87, 677–696. https://doi.org/https://doi.org/10.1146/annurev-biochem-062917-012848.

Maillard, R. A.; Chistol, G.; Sen, M.; Righini, M.; Tan, J.; Kaiser, C. M.; Hodges, C.; Martin, A.; Bustamante, C. ClpX(P) Generates Mechanical Force to Unfold and Translocate Its Protein Substrates. Cell 2011, 145 (3), 459–469. https://doi.org/10.1016/j.cell.2011.04.010.

Majumdar, R.; Middaugh, C. R.; Weis, D. D.; Volkin, D. B. Hydrogen – Deuterium Exchange Mass Spectrometry as an Emerging Analytical Tool for Stabilization and Formulation Development of Therapeutic Monoclonal Antibodies. J. Pharm. Sci. 2015, 104 (2), 327–345. https://doi.org/10.1002/jps.24224.

Manikwar, P.; Majumdar, R.; Hickey, J. M.; Thakkar, S. V; Samra, H. S.; Sathish, H. A.; Bishop, S. M.; Middaugh, C. R.; Weis, D. D.; Volkin, D. B. Correlating Excipient Effects on Conformational and Storage Stability of an IgG1 Monoclonal Antibody with Local Dynamics as Measured by Hydrogen / Deuterium-Exchange Mass. J. Pharm. Sci. 2013, 102 (7), 2136–2151. https://doi.org/10.1002/jps.23543.

Marciano, D. P.; Dharmarajan, V.; Griffin, P. R. HDX/MS Guided Drug Discovery: Small Molecules and Biopharmaceuticals. Curr. Opin. Struct. Biol. 2014, 28, 105–111. https://doi.org/10.1016/j.sbi.2014.08.007.

Marcsisin, S. R.; Engen, J. R. Hydrogen Exchange Mass Spectrometry: What Is It and What Can It Tell Us? Sean. Anal Bioanal Chem 2011, 397 (3), 967–972. https://doi.org/10.1007/s00216-010-3556-4.Hydrogen.

Mark, R.; Aitken, M. L.; Berndt, E. R. Characterizing Markets for Biopharmaceutical Innovations : Do Biologics Differ from Small Molecules ? Forum Health Econ. Policy 2010, 13 (1).

Masson, G. R.; Burke, J. E.; Ahn, N. G.; Anand, G. S.; Borchers, C.; Brier, S.; Bou-assaf, G. M.; Engen, J. R.; Englander, S. W.; Faber, J.; Garlish, R.; Griffin, P. R.; Gross, M. L.; Guttman, M.; Hamuro, Y.; Heck16, A. J. R.; Houde, D.; Iacob, R. E.; Jørgensen, T. J. D.; Kaltashov, I. A.; Klinman, J. P.; Konermann, L.; Man, P.; Mayne, L.; Pascal, B. D.; Reichmann, D.; Skehel, M.; Snijder, J.; Strutzenberg, T. S.; Underbakke, E. S.; Wagner, C.; Wales, T. E.; Walters, B. T.; Weis, D. D.; Wilson, D. J.; Wintrode, P. L.; Zhang, Z.; Zheng, J.;

Schriemer, D. C.; Rand, K. D. Recommendations for Performing, Interpreting and Reporting Hydrogen Deuterium Exchange Mass Spectrometry (HDX/MS) Experiments. Nat. Methods 2019, 16 (July), 595–602. https://doi.org/10.1038/s41592-019-0459-y.

Mcallister, R. G.; Konermann, L. Challenges in the Interpretation of Protein H/D Exchange Data: A Molecular Dynamics Simulation Perspective. Biochemistry 2015, No. 1. https://doi.org/10.1021/acs.biochem.5b00215.

Mendoza, V. L.; Baro, M. A.; Blanco, C.; Vachet, R. W. Structural Insights into the Pre-Amyloid Tetramer of β -2- Microglobulin from Covalent Labeling and Mass Spectrometry. Biochemistry 2011, 50, 6711–6722.

Mendoza, V. L.; Vachet, R. W. Probing Protein Structure by Amino Acid-Specific Covalent Labeling and Mass Spectrometry. Mass Spectrom. Rev. 2010, 28 (5), 785–815. https://doi.org/10.1002/mas.20203.Probing.

Mendoza, V. L.; Vachet, R. W. Protein Surface Mapping Using Diethylpyrocarbonate with Mass Spectrometric Detection. Anal. Chem. 2008, 80 (8), 2895–2904. https://doi.org/10.1021/ac701999b.

Miller, J. M.; Lin, J.; Li, T.; Lucius, A. L. E. Coli ClpA Catalyzed Polypeptide Translocation Is Allosterically Controlled by the Protease ClpP Justin. J. Mol. Biol. 2013, 425 (15), 2795–2812. https://doi.org/10.1038/jid.2014.371.

Mitoma, H.; Horiuchi, T.; Tsukamoto, H.; Ueda, N. Molecular Mechanisms of Action of Anti-TNF-α Agents – Comparison among Therapeutic TNF-α Antagonists. Cytokine 2018, 101, 56–63. https://doi.org/https://doi.org/10.1016/j.cyto.2016.08.014.

Narang, D.; James, D. A.; Balmer, M. T.; Wilson, D. J. Protein Footprinting, Conformational Dynamics, and Core Interface-Adjacent Neutralization “Hotspots” in the SARS-CoV-2 Spike Protein Receptor Binding Domain/Human ACE2 Interaction. J. Am. Soc. Mass Spectrom. 2021. https://doi.org/10.1021/jasms.0c00465.

Nelson, A. L.; Dhimolea, E.; Reichert, J. M. Development Trends for Human Monoclonal Antibody Therapeutics. Nat. Rev. Drug Discov. 2010, 9, 767–774. https://doi.org/10.1038/nrd3229.

Olivares, A. O.; Nager, A. R.; Iosefson, O.; Sauer, R. T.; Baker, T. A. Mechanochemical Basis of Protein Degradation by a Double-Ring AAA+ Machine Adrian. Nat Struct Mol Biol 2014, 21 (10), 871–875. https://doi.org/10.1038/nsmb.2885.

Ono, M.; Horita, S.; Sato, Y.; Nomura, Y.; Iwata, S.; Nomura, N. Structural Basis for Tumor Necrosis Factor Blockade with the Therapeutic Antibody Golimumab. Protein Sci. 2018, 27 (6), 1038–1046. https://doi.org/10.1002/pro.3407.

Opuni, K. F. M.; Al-Majdoub, M.; Yefremova, Y.; El-Kased, R. F.; Koy, C.; Glocker, M. O. Mass Spectrometric Epitope Mapping. Mass Spectrom. Rev. 2018, 37 (2), 229–241. https://doi.org/10.1002/mas.21516.

Padlan, E. A. Anatomy of the Antibody Molecule. Mol. Immunol. 1994, 31 (3), 169–217.

Pan, J.; Zhang, S.; Chou, A.; Borchers, C. H. Higher-Order Structural Interrogation of Antibodies Using Middle-down Hydrogen/Deuterium Exchange Mass Spectrometry. Chem. Sci. 2016, 7 (2), 1480–1486. https://doi.org/10.1039/c5sc03420e.

Pan, J.; Zhang, S.; Chou, A.; Hardie, D. B.; Borchers, C. H. Fast Comparative Structural Characterization of Intact Therapeutic Antibodies Using Hydrogen − Deuterium Exchange and Electron Transfer Dissociation. Anal. Chem. 2015. https://doi.org/10.1021/ac504809r.

Pan, L. Y.; Salas-Solano, O.; Valliere-Douglass, J. F. Localized Conformational Interrogation of Antibody and Antibody-Drug Conjugates by Site- Specific Carboxyl Group Footprinting. MAbs 2017, 9 (2), 307–318. https://doi.org/10.1080/19420862.2016.1268306.

Pan, X.; Limpikirati, P.; Chen, H.; Liu, T.; Vachet, R. W. Higher-Order Structure Influences the Kinetics of Diethylpyrocarbonate Covalent Labeling of Proteins. J. Am. Soc. Mass Spectrom. 2020, 31 (3), 658–665. https://doi.org/10.1021/jasms.9b00132.

Pan, Y.; Piyadasa, H.; O'Neil, J. D.; Konermann, L. Conformational Dynamics of a Membrane Transport Protein Probed by H/D Exchange and Covalent Labeling: The Glycerol Facilitator. J. Mol. Biol. 2012, 416 (3), 400–413. https://doi.org/10.1016/j.jmb.2011.12.052.

Pettersson, I. Methods of Epitope Mapping. Mol. Biol. Rep. 1992, 16, 149–153.

Pimenova, T.; Nazabal, A.; Roschitzki, B.; Seebacher, J.; Rinner, O.; Zenobi, R. Epitope Mapping on Bovine Prion Protein Using Chemical Cross-Linking and Mass Spectrometry. J. Mass Spectrom. 2008, 43 (2), 185–195. https://doi.org/10.1002/jms.1280.

Pisupati, K.; Tian, Y.; Okbazghi, S.; Benet, A.; Ackermann, R.; Ford, M.; Saveliev, S.; Hos, C. M.; Urh, M.; Carlson, E.; Becker, C.; Tolbert, T. J.; Schwendeman, S. P.; Ruotolo, B. T.; Schwendeman, A. A Multidimensional Analytical Comparison of Remicade and the Biosimilar Remsima. Anal. Chem. 2017. https://doi.org/10.1021/acs.analchem.6b04436.

Preamyloid Dimer of β-2-Microglobulin from Covalent Labeling and Mass Spectrometry. Biochemistry 2010, 49, 1522–1532. https://doi.org/10.1021/bi901748h.

Rajendar, B.; Lucius, A. L. Molecular Mechanism of Polypeptide Translocation Catalyzed by the Escherichia Coli ClpA Protein Translocase. J. Mol. Biol. 2010, 399 (5), 665–679. https://doi.org/10.1016/j.jmb.2010.03.061.

Rand, K. D.; Zehl, M.; Jensen, O. N.; Jørgensen, T. J. D. Protein Hydrogen Exchange Measured at Single-Residue Resolution by Electron Transfer Dissociation Mass Spectrometry. Anal. Chem. 2009, 81 (14), 5577–5584. https://doi.org/10.1021/ac9008447.

Reichert, J. M. Monoclonal Antibodies as Innovative Therapeutics. Curr. Pharm. Biotechnol. 2008, 423–430.

Reichert, J. M.; Valge-archer, V. E. Development Trends for Monoclonal Antibody Cancer Therapeutics. Nat. Rev. 2007, 6 (May), 349–356.

Ripstein, Z. A.; Vahidi, S.; Houry, W. A.; Rubinstein, J. L.; Kay, L. E. A Processive Rotary Mechanism Couples Substrate Unfolding and Proteolysis in the ClpXP Degradation Machinery. Elife 2020, 9, 1–25. https://doi.org/10.7554/eLife.52158.

Rodriguez-Aliaga, P.; Ramirez, L.; Kim, F.; Bustamante, C.; Martin, A. Substrate-Translocating Loops Regulate the Mechanochemical Coupling and Power Production in a AAA+ Protease. Nat Struct Mol Biol 2016, 23 (11), 974–981. https://doi.org/10.1038/nsmb.3298.

Rogstad, S.; Faustino, A.; Ruth, A.; Keire, D.; Boyne, M.; Park, J. Retrospective Evaluation of the Use of Mass Spectrometry in FDA Biologics License Applications. Am. Soc. Mass Spectrom. 2017, 28, 786–794. https://doi.org/10.1007/s13361-016-1531-9.

Rousseau, F.; Schymkowitz, J.; Serrano, L. Protein Aggregation and Amyloidosis: Confusion of the Kinds? Curr. Opin. Struct. Biol. 2006, 16 (1), 118–126. https://doi.org/10.1016/j.sbi.2006.01.011.

Saleem, R.; Cantin, G.; Wikström, M.; Bolton, G.; Kuhns, S.; McBride, H. J.; Liu, J. Analytical and Functional Similarity Assessment of ABP 710, a Biosimilar to Infliximab Reference Product. Pharm. Res. 2020, 37 (6). https://doi.org/10.1007/s11095-020-02816-w.

Sauer, R. T.; Baker, T. A. AAA + Proteases : ATP-Fueled Machines of Protein Destruction. Annu. Rev. Biochem. 2011, 80, 587–612. https://doi.org/10.1146/annurev-biochem-060408-172623.

Schmidt, C.; Robinson, C. V. Dynamic Protein Ligand Interactions - Insights from MS. FEBS J. 2014, 281 (8), 1950–1964. https://doi.org/10.1111/febs.12707.

Sowole, M. A.; Simpson, S.; Skovpen, Y. V; Palmer, D. R. J.; Konermann, L. Evidence of Allosteric Enzyme Regulation via Changes in Conformational Dynamics: A Hydrogen/Deuterium Exchange Investigation of Dihydrodipicolinate Synthase. Biochemistry 2016. https://doi.org/10.1021/acs.biochem.6b00764.

Sprangers, R.; Gribun, A.; Hwang, P. M.; Houry, W. A.; Kay, L. E. Quantitative NMR Spectroscopy of Supramolecular Complexes: Dynamic Side Pores in ClpP Are Important for Product Release. Proc. Natl. Acad. Sci. U. S. A. 2005, 102 (46), 16678–16683. https://doi.org/10.1073/pnas.0507370102.

Suckau, D.; Köhl, J.; Karwath, G.; Schneider, K.; Casaretto, M.; Bitter-Suermann, D.; Przybylski, M. Molecular Epitope Identification by Limited Proteolysis of an Immobilized Antigen-Antibody Complex and Mass Spectrometric Peptide Mapping. Proc. Natl. Acad. Sci. U. S. A. 1990, 87 (24), 9848–9852. https://doi.org/10.1073/pnas.87.24.9848.

Sun, H.; Ma, L.; Wang, L.; Xiao, P.; Li, H.; Zhou, M.; Song, D. Research Advances in Hydrogen–Deuterium Exchange Mass Spectrometry for Protein Epitope Mapping. Anal. Bioanal. Chem. 2021, 413 (9), 2345–2359. https://doi.org/10.1007/s00216-020-03091-9.

Thompson, M. W.; Singh, S. K.; Maurizi, M. R. Processive Degradation of Proteins by the ATP-Dependent Clp Protease from Escherichia Coli. Requirement for the Multiple Array of Active Sites in ClpP but Not ATP Hydrolysis. J. Biol. Chem. 1994, 269 (27), 18209–18215.

Tian, Y.; Huang, L.; Ruotolo, B. T.; Wang, N. Hydrogen/Deuterium Exchange-Mass Spectrometry Analysis of High Concentration Biotherapeutics: Application to Phase-Separated Antibody Formulations. MAbs 2019, 11 (4), 779–788. https://doi.org/10.1080/19420862.2019.1589850.

Trabjerg, E.; Nazari, Z. E.; Rand, K. D. Conformational Analysis of Complex Protein States by Hydrogen/Deuterium Exchange Mass Spectrometry (HDX/MS): Challenges and Emerging Solutions. TrAC - Trends Anal. Chem. 2018, 106, 125–138. https://doi.org/10.1016/j.trac.2018.06.008.

Tremblay, C. Y.; Limpikirati, P.; Vachet, R. W. Complementary Structural Information for Stressed Antibodies from Hydrogen − Deuterium Exchange and Covalent Labeling Mass Spectrometry. 2021, 32 (5), 1237–1248. https://doi.org/10.1021/jasms.1c00072.

Trikha, M.; Yan, L.; Nakada, M. T. Monoclonal Antibodies as Therapeutics in Oncology. Curr. Opin. Biotechnol. 2002, 609–614.

Van Schie, K. A.; Ooijevaar-De Heer, P.; Dijk, L.; Kruithof, S.; Wolbink, G.; Rispens, T. Therapeutic TNF Inhibitors Can Differentially Stabilize Trimeric TNF by Inhibiting Monomer Exchange. Sci. Rep. 2016, 6, 32747. https://doi.org/10.1038/srep32747.

Walsh, I.; Seno, F.; Tosatto, S. C. E.; Trovato, A. PASTA 2.0: An Improved Server for Protein Aggregation Prediction. Nucleic Acids Res. 2014, 42 (W1), 301–307. https://doi.org/10.1093/nar/gku399.

Wecksler, A. T.; Kalo, M. S.; Deperalta, G. Mapping of Fab-1:VEGF Interface Using Carboxyl Group Footprinting Mass Spectrometry. J. Am. Soc. Mass Spectrom. 2015, 26 (12), 2077–2080. https://doi.org/10.1007/s13361-015-1273-0.

Wei, H.; Ahn, J.; Yu, Y. Q.; Tymiak, A.; Engen, J. R.; Chen, G. Using Hydrogen/Deuterium Exchange Mass Spectrometry to Study Conformational Changes in Granulocyte Colony Stimulating Factor upon PEGylation Hui. J

Am Soc Mass Spectrom 2012, 23 (3), 498–504. https://doi.org/10.1007/s13361-011-0310-x.

Wei, H.; Mo, J.; Tao, L.; Russell, R. J.; Tymiak, A. A.; Chen, G.; Iacob, R. E.; Engen, J. R. Hydrogen / Deuterium Exchange Mass Spectrometry for Probing Higher Order Structure of Protein Therapeutics : Methodology and Applications. Drug Discov. Today 2014, 19 (1), 95–102. https://doi.org/10.1016/j.drudis.2013.07.019.

Wei, H.; Mo, J.; Tao, L.; Russell, R. J.; Tymiak, A. A.; Chen, G.; Iacob, R. E.; Engen, J. R. Hydrogen/Deuterium Exchange Mass Spectrometry for Probing Higher Order Structure of Protein Therapeutics: Methodology and Applications. Drug Discov. Today 2015, 19 (1), 95–102. https://doi.org/10.1016/j.drudis.2013.07.019.Hydrogen/Deuterium.

Weiner, L. M.; Surana, R.; Wang, S. Monoclonal Antibodies : Versatile Platforms for Cancer Immunotherapy. Nat. Publ. Gr. 2010, 10 (5), 317–327. https://doi.org/10.1038/nri2744.

Wilson, D. J.; Brown, K. A. Bottom-up Hydrogen Deuteriumexchange Mass Spectrometry: Data Analysis and Interpretation. R. Soc. Chem. 2017, 2874–2886. https://doi.org/10.1039/c7an00662d.

Yamamoto, R.; Wang, A.; Vitt, C. R.; Lin, L. S. Histidine-15: An Important Role in the Cytotoxic Activity of Human Tumor Necrosis Factor. Protein Eng. Des. Sel. 1989, 2 (7), 553–558. https://doi.org/10.1093/protein/2.7.553.

Yip, K. M.; Fischer, N.; Paknia, E.; Chari, A.; Stark, H. Atomic-Resolution Protein Structure Determination by Cryo-EM. Nature 2020, 587 (7832), 157–161. https://doi.org/10.1038/s41586-020-2833-4.

Zehl, M.; Rand, K. D.; Jensen, O. N.; Jorgensen, T. J. D. Electron Transfer Dissociation Facilitates the Measurement of Deuterium Incorporation into Selectively Labeled Peptides with Single Residue Resolution. J. Am. Chem. Soc. 2008, 130 (51), 17453–17459. https://doi.org/10.1021/ja805573h.

Zhang, H.; Song, L.; Ye, H.; Hu, L.; Liang, W.; Liu, D. Characterization of a Novel Humanized Anti-CD20 Antibody with Potent Anti-Tumor Activity against Non-Hodgkin's Lymphoma. Cell. Physiol. Biochem. 2013, 32 (3), 645–654. https://doi.org/10.1159/000354468.

Zhang, M. M.; Huang, R. Y. C.; Beno, B. R.; Deyanova, E. G.; Li, J.; Chen, G.; Gross, M. L. Epitope and Paratope Mapping of PD-1/Nivolumab by Mass Spectrometry-Based Hydrogen-Deuterium Exchange, Cross-Linking, and Molecular Docking. Anal. Chem. 2020, 92 (13), 9086–9094. https://doi.org/10.1021/acs.analchem.0c01291.

Zhang, Q.; Yang, J.; Bautista, J.; Badithe, A.; Olson, W.; Liu, Y. Epitope Mapping by HDX/MS Elucidates the Surface Coverage of Antigens Associated with High Blocking Efficiency of Antibodies to Birch Pollen Allergen. Anal. Chem. 2018, 90 (19), 11315–11323. https://doi.org/10.1021/acs.analchem.8b01864.

Zheng, X.; Wintrode, P. L.; Chance, M. R. Complementary Structural Mass Spectrometry Techniques Reveal Local Dynamics in Functionally Important Regions of a Metastable Serpin. Cell Press 2008, 16 (January), 38–51. https://doi.org/10.1016/j.str.2007.10.019.